

Extraction of Bio-based Organic Acids using Supported Liquid Membranes with Novel Solvents

A thesis submitted to
The University of Manchester for the degree of
Doctor of Philosophy
in the Faculty of Science and Engineering

2022

Pablo López-Porfiri

Department of Chemical Engineering

'Blank page'

Table of contents

| | |
|---|-----------|
| Table of contents | 3 |
| List of figures | 7 |
| List of tables | 13 |
| Notation | 15 |
| Abstract | 19 |
| Declaration | 21 |
| Copyright statement | 21 |
| Acknowledgements | 22 |
| Funding source | 22 |
| About the author | 23 |
| Formation | 23 |
| Education..... | 23 |
| Experience | 23 |
| Achievements..... | 25 |
| On PhD project | 25 |
| On other projects | 26 |
| Honours & awards..... | 27 |
| Chapter 1. Introduction | 29 |
| 1.1 Motivation and scope | 31 |
| 1.2 Aims and objectives..... | 32 |
| 1.2.1 General..... | 32 |
| 1.2.2 Specifics | 32 |
| 1.3 Thesis outline..... | 33 |
| Chapter 2. Background | 35 |
| 2.1 Bio-based organic acids..... | 35 |
| 2.2 Novel green solvents | 39 |
| 2.2.1 Ionic liquids..... | 40 |
| 2.2.2 Eutectic solvents | 43 |
| 2.2.3 Bio-based solvents..... | 46 |
| 2.3 Thermodynamic modelling..... | 47 |
| 2.4 Membrane separation technology | 50 |
| Chapter 3. Green solvents selection guide for bio-based organic acids recovery | 53 |
| 3.1 Foreword..... | 54 |

| | | |
|---|--|------------|
| 3.2 | Abstract..... | 56 |
| 3.3 | Introduction | 57 |
| 3.4 | Experimental section | 59 |
| 3.4.1 | Materials | 59 |
| 3.4.2 | Preparation of eutectic solvents | 60 |
| 3.4.3 | Experimental extraction procedure | 60 |
| 3.4.4 | COSMO-RS Approach..... | 62 |
| 3.5 | Results and discussion | 63 |
| 3.5.1 | Experimental extraction yields..... | 63 |
| 3.5.2 | Solvent family performance..... | 64 |
| 3.5.3 | Effect of organic acid structure..... | 66 |
| 3.5.4 | Effect of extraction conditions | 67 |
| 3.5.5 | Validation of COSMO-RS methodology | 69 |
| 3.5.6 | Thermodynamic analysis using COSMO-RS | 71 |
| 3.5.7 | Screening of green solvents for extraction of bio-organic acids..... | 75 |
| 3.5.8 | Green solvent selection guide..... | 80 |
| 3.6 | Conclusions..... | 82 |
| | | |
| Chapter 4. Solubility study and thermodynamic modelling of succinic acid and fumaric acid in bio-based solvents..... | | 83 |
| 4.1 | Foreword | 84 |
| 4.2 | Abstract..... | 85 |
| 4.3 | Introduction | 86 |
| 4.4 | Materials and methods..... | 88 |
| 4.4.1 | Materials | 88 |
| 4.4.2 | Experimental procedure..... | 89 |
| 4.4.3 | Solubility correlations..... | 90 |
| 4.4.4 | COSMO-RS approach..... | 92 |
| 4.5 | Results and discussion | 93 |
| 4.5.1 | Methodology validation..... | 93 |
| 4.5.2 | Experimental organic acid solubilities | 93 |
| 4.5.3 | Correlation of organic acid solubility data | 95 |
| 4.5.4 | Thermodynamic analysis of organic acid – solvent systems using COSMO-RS..... | 97 |
| 4.5.5 | Energies of solution of organic acid – solvent systems..... | 100 |
| 4.6 | Conclusions..... | 104 |
| | | |
| Chapter 5. Liquid membrane technology for sustainable separations..... | | 106 |
| 5.1 | Foreword | 107 |
| 5.2 | Introduction to liquid membrane (LM) technology..... | 108 |
| 5.2.1 | Components of a liquid membrane | 110 |

| | | |
|------------------------|--|------------|
| 5.2.2 | Liquid membrane configurations | 112 |
| 5.3 | Fundamental aspects of liquid membranes | 119 |
| 5.3.1 | Theoretical background..... | 119 |
| 5.3.2 | Transport mechanisms in liquid membranes | 124 |
| 5.3.3 | Extraction and recovery efficiencies | 126 |
| 5.3.4 | Liquid membrane stability..... | 128 |
| 5.3.5 | Compounds interaction within liquid membranes..... | 131 |
| 5.4 | Sustainable separations with liquid membranes | 133 |
| 5.4.1 | Recovery of biomolecules in bio-refinery | 134 |
| 5.4.2 | Amino acid recovery..... | 140 |
| 5.4.3 | Environmental and wastewater treatment..... | 142 |
| 5.4.4 | Metal ion recovery and heavy metal removal | 146 |
| 5.4.5 | Nuclear waste treatment | 152 |
| 5.4.6 | Rare-earth recovery..... | 156 |
| 5.5 | Conclusions and perspectives..... | 159 |
| | | |
| Chapter 6. | Green supported liquid membranes: the permeability activity-based linear operation (PABLO) method | 161 |
| 6.1 | Foreword..... | 162 |
| 6.2 | Abstract | 164 |
| 6.3 | Introduction..... | 165 |
| 6.4 | Permeability activity-based model..... | 168 |
| 6.5 | Bio-organic acid recovery with green-SLM | 171 |
| 6.5.1 | Materials | 171 |
| 6.5.2 | Preparation of green-SLMs..... | 172 |
| 6.5.3 | Methodology for the extractions with SLMs..... | 173 |
| 6.5.4 | Modelling procedure | 173 |
| 6.5.5 | Results and discussion..... | 175 |
| 6.6 | Cascade extraction process theoretical design | 178 |
| 6.6.1 | Graphical activity-based process design | 180 |
| 6.6.2 | Required green-SLM area estimation..... | 185 |
| 6.6.3 | Temperature-driven green SLM extraction..... | 187 |
| 6.7 | Conclusions..... | 190 |
| | | |
| Chapter 7. | Thesis conclusions and further research | 192 |
| 7.1 | Conclusions..... | 192 |
| 7.2 | Further research | 195 |
| 7.2.1 | On green solvents..... | 195 |
| 7.2.2 | On supported liquid membranes..... | 196 |
| 7.2.3 | On extraction process feasibility | 197 |
| 7.3 | Closing words..... | 197 |
| | | |
| References..... | | 198 |

| | |
|---|------------|
| Appendix A. SI: Green solvents selection guide for bio-based organic acids recovery | 219 |
| Structures of bio-organic acids | 219 |
| Physical characterization of solvents..... | 219 |
| Experimental extraction results..... | 220 |
| pKa and pH-values of bio-based organic acids | 221 |
| Molecular interaction analysis..... | 222 |
| Solvent-water affinity analysis | 224 |
| Green solvent selection guide methodology | 226 |
| Appendix B. SI: Solubility study and thermodynamic modelling of succinic acid and fumaric acid in bio-based solvents | 227 |
| Methodology validation..... | 227 |
| Experimental uncertainty..... | 228 |
| Experimental solubility data..... | 231 |
| Correlation relative deviations..... | 232 |
| Computed organic acid activity coefficients | 233 |
| Saturated organic acid - bio-based solvent excess mixing energies..... | 234 |
| Energies of solution uncertainties estimation | 235 |
| Appendix C. SI: Green supported liquid membranes: the permeability activity-based linear operation (PABLO) method | 237 |
| Eutectic solvent (ES) preparation..... | 237 |
| Supported liquid membranes (SLM) preparation and characterization... | 237 |
| Solute activity coefficients fitting algorithm | 239 |
| pH effect on the organic acids' activity coefficient..... | 241 |
| Experimental succinic acid extraction with green-SLM data | 242 |
| Activity gradient logarithmic mean derivation | 244 |

Word count: 62935.-

List of figures

- Figure 2.1.** Comparison between the chemical production routes from petroleum-based and bio-based raw materials..... 35
- Figure 2.2.** a) Schematic phase diagram of a eutectic mixture of two components (10). The molecular interactions of the solids A and B with their respective melting points (Mp / T) cause a decrease in the temperature of fusion (ΔT_f) compared to the ideal mixture; b) Example of eutectic solvent formation from a mixture of two solid compounds to a homogenous liquid. 43
- Figure 2.3.** Representation of the COSMO-RS σ - surfaces (left) and σ - profiles (right) of water and representative bio-based organic acids. 49
- Figure 3.1.** Evaluation flow diagram of green solvents for bio-based organic acids recovery from aqueous solution. 54
- Figure 3.2.** Screening results of the main descriptors for bio-based organic acids recovery from aqueous solution with green solvents. a) Solvent performance, $\ln(K_i)$; b) solvent-water affinity, $\ln(\gamma_w^\infty)$; and c) thermodynamic spontaneity, G^{ex} . Results distribution was modelled using the Kernel smooth density estimation method (123)..... 55
- Figure 3.3.** Experimental organic acid extraction yields at a temperature of 25 °C and solvent:feed ratio of 1 using various green solvents. 64
- Figure 3.4.** Experimental response surface plots representing the effect of temperature and solvent:feed ratio on the extraction yield of organic acids using the green solvents [C₄mim][Tf₂N], DL-menthol:OctA (1:1), and 2-MeTHF. 68
- Figure 3.5.** a) σ - Profile of succinic acid (in green); levulinic acid (in red); fumaric acid (in purple); and water (in blue). b) Examples of σ - Profile conformers: Levulinic acid showing internal hydrogen bonding (in red); levulinic acid showing non-internal hydrogen bonding (in black). 70
- Figure 3.6.** Correlation between experimental extraction yield, %Ex, at 25 °C and solvent:feed ratio of 1, and partition coefficients computed with COSMO-RS at 25 °C, of organic acids using green solvents, $r^2 = 0.7$ 71
- Figure 3.7.** Excess enthalpy (H^{ex}) contributions and excess entropy ($-TS^{ex}$) of binary systems composed of organic acid-solvent and water-solvent mixtures at 25 °C, as computed by the COSMO-RS method, including a) succinic acid + solvent, b) levulinic acid + solvent, c) fumaric acid + solvent, and d) water + solvent systems. 74
- Figure 3.8.** Screening of green solvents for extraction of organic acids in terms of solute partition coefficients, $\ln(K_i)$: succinic acid (in blue); levulinic acid (in

red); fumaric acid (in purple); malic acid (in green); itaconic acid (in yellow); and lactic acid (in orange), as computed with COSMO-RS at 25 °C.....77

Figure 3.9. a) Partition coefficients, $\ln(K_i)$, dependence of organic acid chemical potential on the screened solvents at infinite dilution, $\mu_i^{s,\infty}$; b) Relationship between organic acid partition coefficients, $\ln(K_i)$, with the screened solvents and: organic acid-solvent excess free energy, G^{ex} , on the x -axis; organic acid-solvent excess enthalpy, H^{ex} , on the y -axis; and organic acid-solvent excess entropy ($-TS^{ex}$) which are proportional to marker size. Succinic acid (in blue); levulinic acid (in red); fumaric acid (in purple); malic acid (in green); itaconic acid (in yellow); and lactic acid (in orange), computed with COSMO-RS at 25 °C.....78

Figure 4.1. Schematic representation of the experimental results and the charge density profiles used to perform the thermodynamic modelling of the mixtures of succinic acid and fumaric acid in bio-based solvents.84

Figure 4.2. Molecular structures of the bio-based solvents and organic acids studied in this work.89

Figure 4.3. Experimental and literature (147,160,176–183,167,169–175) solubilities of organic acids in water and bio-based solvents at temperatures ranging [283 – 313] K: a) Succinic acid; b) Fumaric acid. Average combined expanded uncertainty of measurement $U_{Comb,95\%}(x_1) = 5.2 \cdot 10^{-4} \text{ mol mol}^{-1}$ 94

Figure 4.4. Representation of the σ – surfaces (left) and σ – profiles (right) of the bio-based solvents and organic acids studied in this work..... 97

Figure 4.5. Natural logarithm activity coefficient, $\ln(\gamma_1)$, of saturated succinic acid (solid lines) and fumaric acid (dash lines) in water and bio-based solvents computed by COSMO-RS method within the experimental temperature range of each [organic acid (1) + solvent (2)] system. 98

Figure 4.6. Analysis of the excess mixing energies of saturated organic acid – bio-based solvent systems computed by the COSMO-RS method at 293.15 K. a) Excess Gibbs free energy ($G^E / \text{kJ mol}^{-1}$), Excess enthalpy ($H^E / \text{kJ mol}^{-1}$), and Excess entropy ($-TS^E / \text{kJ mol}^{-1}$); b) Excess enthalpy contributions (kJ mol^{-1}): electrostatic energy (MF), hydrogen bonding (HB), and van der Waals forces (vdW). 99

Figure 4.7. Schematic representation of energies of solution estimation from the solubility experimental data in the van't Hoff plot modified by Krug et al. (185,186). The free energy of solution, $\Delta G_{\text{soln}} / \text{kJ mol}^{-1}$, is proportional to the function intercept, i.e., the function evaluated at $T = T_{\text{hm}}$, the enthalpy of solution, $\Delta H_{\text{soln}} / \text{kJ mol}^{-1}$, to the function slope. The entropy of solution is obtained from the Gibbs free energy relationship: $\Delta G = \Delta H - T\Delta S$ 101

Figure 4.8. Enthalpy-entropy compensation effect for organic acids in water and bio-based solvents at a mean harmonic temperature of $T_{\text{hm}} = 299 \text{ K}$ and

$T_{hm} = 300$ K for succinic acid and fumaric acid. Dotted lines represent the linear regression for each organic acid..... 103

Figure 5.1. Fields where liquid membranes (LMs) are applied and main features..... 109

Figure 5.2. Liquid membrane system scheme..... 110

Figure 5.3. Main liquid membranes configurations. (a) Bulk liquid membrane; (b) Emulsion liquid membrane; (c) Supported liquid membrane..... 113

Figure 5.4. Other liquid membrane arrangement schemes: (a) Taylor flow LM; (b) ELM operating into a spray column; (c) Hollow fibre SLM; (d) Hollow fibre renewal liquid membrane; (e) Pseudo-emulsion hollow fibre strip dispersion membrane..... 119

Figure 5.5. Solute chemical potential, $\mu_i / \text{kJ}\cdot\text{mol}^{-1}$, profile through a liquid membrane..... 121

Figure 5.6. Solute concentration, $C_i / \text{mol}\cdot\text{m}^{-3}$, profile through a liquid membrane..... 122

Figure 5.7. Transport mechanisms in liquid membrane: (a) simple transport; (b) stripping phase reaction reaction-facilitated transport; (c) carrier-facilitated transport; (d) couple-facilitated transport; (e) couple-counter-facilitated transport. 126

Figure 5.8. Schematic typical behaviour in the LM extraction process: (a) phase concentration profile; (b) extraction efficiency parameters. 127

Figure 5.9. Total liquid membrane publications number per year given by the search engine Google Scholar using the keywords “*bulk liquid membranes*”, “*emulsion liquid membranes*”, and “*supported liquid membranes.*” 133

Figure 6.1. Green SLM development is presented in this work. Under an activity-based approach, suitable design methods can be proposed that allow for better process evaluations..... 162

Figure 6.2. Maturity of the separation process technology. Technological sophistication as the patent activity wane (x -axis); Use maturity as the antiquity in the last century (y -axis). Reconstructed from Vision 2020: 2000 Separation Roadmap, Center for Waste Reduction Technologies of the AIChE, 2000 (19). 167

Figure 6.3. Schematic comparison of the liquid membrane behaviour predicted from a concentration-based approach (Eq. 6.1) and an activity-based approach (Eq. 6.5). I) Ideal trajectories for the solute concentration with the same affinity with the feed and stripping phases; II) Concentration profile obtained from the concentration-based approach; III) Activity trajectories for the solute concentration with different affinity with the feed and stripping

phases; IV) Concentration profile obtained from the activity-based approach. a-point: initial feed concentration; b-point: initial stripping concentration; c-point: final ideal feed and ideal stripping concentration; d-point: final activity-based feed concentration; e-point: final activity-based stripping concentration..... 171

Figure 6.4. Experimental setup used in this work for the succinic acid recovery with green-SLMs. I) SLM prepared by immersing a PVDF porous support in a green solvent; II) Diffusion cell and SLM module..... 172

Figure 6.5. Experimental, ideal (Eq. 6.1), and fitted permeability activity-based (Eq. 6.5) models concentration profile and extraction yields (E_x) for succinic acid extraction with a eucalyptol-based green-SLM and three different stripping solutions. I) pure water; II) 0.1 M NaOH; III) 0.5 M NaOH. The same behaviour is observed for all green-SLM studied in this work. 176

Figure 6.6. I) Succinic acid activity coefficient in water and alkaline solutions predicted by the COSMO-RS method at 20 °C and fitted to the experimental extraction data with green-SLM and the permeability activity-based model proposed in this work; II) Root mean squared deviation comparison of the ideal and fitted permeability activity-based models. The goodness of the models is also evaluated through the root mean squared deviations of the experimental uncertainty with a confidence level of 95%..... 177

Figure 6.7. Succinic acid permeability ($m \cdot s^{-1}$) for the green-SLM studied in this work with water and two alkaline aqueous solutions (0.1 and 0.5 M NaOH) as stripping phase obtained from the ideal and fitted permeability activity-based models. Error bars considered the value uncertainties with a confidence level of 95%..... 178

Figure 6.8. Cascade green-SLM extraction process in a countercurrent flow diagram. F , feed stream; S , stripping stream; R , raffinate stream; E , extract stream; N , total stages number; n , stage number; C_F , initial solute concentration in the feed stream; C_S , initial solute concentration in the stripping stream; $C_{R,n}$, solute concentration in the raffinate for stage n ; $C_{E,n}$, solute concentration in the extract for stage n ; C_R , final solute concentration in the raffinate stream; C_E , final solute concentration in the extract stream. 180

Figure 6.9. Solute (succinic acid) recovery as a function of the number of stages in a countercurrent cascade at operating conditions listed in Table 6.2 (analytical resolution). The solute recovery converges to an upper limit given by the system thermodynamic equilibrium. To reach a target final concentration $C_E = 67 \text{ g l}^{-1}$, a five-stage extraction process is required..... 182

Figure 6.10. Green-SLM countercurrent cascade extraction process graphical algorithm (PABLO) to determinate the number of stages required to reach the target final concentration by the permeability activity-based linear operation. I) Activities trajectories of the solute in the feed and stripping phases as well as the operating line obtained from the respective solute activity coefficient in

each phase and the process operating conditions through Eq. 6.15 to Eq. 6.17; II) Stage number determination procedure: vertically descending from the initial feed concentration, C_F , to the operation line, then spitted horizontally towards the feed, C_{Rn} , and stripping, C_E , lines. Repeat the procedure from, C_{Rn} , until reaching the final concertation in the raffinate, C_R ; II) Total number stages as the step number required to reach the final raffinate concentration, obtained under the operational condition listed in Table 6.2. 184

Figure 6.11. I) Activity profile and II) concentration profile of the succinic acid throughout a countercurrent cascade five-stages green-SLM extraction obtained from the permeability activity-based model proposed in this work. A solution of 0.5 M NaOH is used as stripping phase. *F*: feed stream; *S*: stripping stream; *R*: raffinate stream; *E*: extract steam. Lines were included to guide the eye. 185

Figure 6.12. Estimated total and by stage mass transfer area for the extraction of succinic acid in a five-stage countercurrent cascade extraction process using an alkaline aqueous solution (0.5 M NaOH) as the stripping phase and four different green-SLM. 187

Figure 6.13. I) Succinic acid activity dependence with concentration and temperature computed with COSMO-RS method and represented by the NRTL model; II) Schematic two-stage countercurrent cascade extraction process with intermediate cooler/heater auxiliary processes. 189

Figure A0.1. Structures of bio-organic acids studied in this work. a) Succinic acid; b) Levulinic acid; c) Fumaric acid; d) Malic acid; e) Itaconic acid; and f) Lactic acid. 219

Figure A.0.2. Conformer weighting analysis in terms of the percentage of non-internal HB of organic acid in each solvent (above) and its difference with respect to the percentage in water (below), computed at 25 °C by COSMO-RS method. 222

Figure A.0.3. Relationship between organic acid partition coefficients, $\ln(K_i)$, and organic acid - solvent energies contributions: a) hydrogen bonding excess enthalpy contribution ($H^{\text{ex}}_{\text{HB}}$), $r^2 = 0.69$; b) electrostatic excess enthalpy contribution ($H^{\text{ex}}_{\text{MF}}$), $r^2 = 0.36$; c) van der Waals excess enthalpy contribution ($H^{\text{ex}}_{\text{vdW}}$) $r^2 = 0.02$; d) excess entropy ($-TS^{\text{ex}}$), $r^2 = 0.67$. Computed with COSMO-RS at 25 °C. 223

Figure A.0.4. Relationship between organic acid partition coefficients, $\ln(K_i)$, and water activity coefficient at infinite dilution, $\ln(\gamma^{\infty}_w)$, for screened solvents computed with COSMO-RS at 25 °C. $r^2 = 0.75$ 224

Figure A.0.5. Relationship between the organic acid partition coefficients computed considering pure green solvents, $\ln(K_i)$, (on *x*-axis) and the organic acid partition coefficients computed considering water saturated green solvents, $\ln(K_i)^*$, (on *y*-axis). Data was computed for the systems used for the

methodology validation, i.e., succinic, levulinic, and fumaric acids with [C₄mim][Tf₂N], [C₄pyrr][Tf₂N], [N₈₈₈₁][Tf₂N], DL-menthol:OctA, N₄₄₄₄Cl:OctA, DL-menthol:DecA, CPME, 2-MeTHF, 1,8-Cineol, and EtOAc. $r^2 = 0.90$225

Figure A.0.6. Quality matrix for green solvents recommendation assessment.226

Figure B.0.1. Percentage of the individual relative deviation from a) van't Hoff equation (Eq. 4.3); b) Modified Apelblat equation (eq. 4.4); and c) Buchowski-Ksiazaczak λh model (Eq. 4.5) for experimental organic acid solubility in water and bio-based solvents. Filled symbols: succinic acid; empty symbols: fumaric acid.....232

Figure C.0.1. Green-SLM stability in pure water test at 25 °C.....238

Figure C.0.2. Succinic acid permeability regression of ψ -values of mass balance integration of the extraction with DL-menthol:OctA in PVDF SLM and 0.1 M NaOH stripping solution. $r^2=1$240

Figure C.0.3. The algorithm developed for the solute activity coefficients fitting to the experimental green-SLM extractions data. In blue, experimental measurement stage; in red, COSMO-RS activity computation stage; in green, MatLab fitting routine stage.241

Figure C.0.4. Estimated activity coefficients of different bio-based organic acid in function on the aqueous phase pH-value before mixing for succinic acid (in blue), levulinic acid (in red), fumaric acid (in purple), malic acid (in green), itaconic acid (in yellow), and lactic acid (in orange), computed by COSMO-RS at 20 °C. The model solution is composed of the organic acid at 50 g l⁻¹ for all solutes except fumaric acid, with a concentration of 5 g l⁻¹.242

Figure C.0.5. Experimental concentrations (●, feed; ▲, stripping), ideal model prediction (---, feed; —, stripping), COSMO-RS model prediction (---, feed; —, stripping), and fitted permeability activity-based model (---, feed; —, stripping), concentration profiles for succinic acid extraction with the green-SLM studied in this work using three different alkaline stripping solutions: pure water; 0.1 M NaOH; 0.5 M NaOH. The same behaviour is observed for all systems.243

Figure C.0.6. I) Schematic countercurrent green-SLM extraction process. II) Solute activity profile along a countercurrent green-SLM extraction process. (→) Feed stream; (←) Stripping stream; (⇄) Transmembrane solute flow.....244

List of tables

| | |
|---|-----|
| Table 2.1. Summary of the main bio-based organic acids produced as building blocks for the bio-based industry (16)..... | 38 |
| Table 2.2. Examples of organic compounds recovery using ionic liquids. | 41 |
| Table 2.3. Examples of organic compounds recovery using ionic liquids, continuation. | 42 |
| Table 2.4. Examples of organic compounds recovery using eutectic solvents. | 44 |
| Table 2.5. Examples of organic compounds recovery using eutectic solvents, continuation. | 45 |
| Table 2.6. Examples of organic compounds recovery using bio-based solvents. | 47 |
| Table 3.1. Representative solvents studied in this work..... | 60 |
| Table 3.2. Green solvent selection guide for bio-based organic acids recovery. (●) Highly recommended; (●) Moderately recommended; (●) Lowly recommended. | 81 |
| Table 4.1. Properties of bio-based solvents and organic acids used in this work. | 89 |
| Table 4.2. Fitted values of parameters for the van't Hoff equation (Eq. 4.3), modified Apelblat equation (Eq. 4.4), and Buchowski-Ksiazaczak λh model (Eq. 4.5) for the organic acid solubilities in water and bio-based solvents..... | 96 |
| Table 4.3. Estimated Gibbs free energy (ΔG_{soln}), enthalpy (ΔH_{soln}), and entropy ($T_{\text{hm}} \cdot \Delta S_{\text{soln}}$) of solution, and their respective uncertainty with a confidence limit of 95% ($U_{\text{Comb},95\%}$), for succinic acid and fumaric acid in water and the bio-based solvents studied in this work. Estimations were performed following the methodology detailed in section 4.5.5 at $T_{\text{hm}}=299$ K. | 103 |
| Table 5.1. Strengths and limitations of the three main liquid membrane configurations. | 113 |
| Table 5.2. Summary of recent liquid membrane studies for the recovery of compounds in biorefinery..... | 135 |
| Table 5.3. Summary of recent liquid membrane studies for the recovery of amino acids. | 140 |
| Table 5.4. Summary of recent liquid membrane studies for wastewater treatment..... | 142 |

| | |
|--|-----|
| Table 5.5. Summary of recent liquid membrane studies for the removal of heavy metals and recovery of metal ions..... | 148 |
| Table 5.6. Summary of recent liquid membrane studies for nuclear waste treatment..... | 153 |
| Table 5.7. Summary of recent liquid membrane studies for the recovery of RE elements. | 157 |
| Table 6.1. Green-SLMs and their properties studied in this work. | 172 |
| Table 6.2. Operating conditions and target final concentrations for the succinic acid recovery with green-SLM in a countercurrent cascade process..... | 181 |
| Table A.0.1. Physical properties of green solvents at 25 °C..... | 220 |
| Table A.0.2. Experimental extraction yields of organic acids using green solvents at the temperature of 25 °C and feed:solvent ratio of 1..... | 220 |
| Table A.0.3. pKa-values of bio-based organic acids. | 221 |
| Table A.0.4. pH-values of the bio-based organic acid aqueous solutions used for the experimental extraction essays in this work..... | 221 |
| Table A.0.5. Quality scores for green solvents recommendation assessment. | 226 |
| Table B.0.1. Comparison of experimental and mean values found in the literature for aqueous solubility of succinic and fumaric acids for methodology validation. The estimated combined expanded uncertainty for the mean literature values: $U_{\text{comb},95\% \ln x_{1 \text{lit}}} = 0.10$ and 0.14 , for succinic and fumaric acids, respectively. | 227 |
| Table B.0.2. Estimation of the combined expanded uncertainty for the saturated organic acid mole fraction in bio-based solvents, $U_{\text{Comb},95\%}(x_1)$, based on the contributions of properties and variables measured and calculated. | 230 |
| Table B.0.3. Experimental saturated organic acid mole fraction ($x_1 / \text{mol} \cdot \text{mol}^{-1}$) in water and bio-based solvents and its combined expanded uncertainties. | 231 |
| Table B.0.4. Organic acid activity coefficients at the saturated liquid condition obtained from SLE computed by the COSMO-RS method within the experimental temperature range..... | 233 |
| Table B.0.5. Excess mixing energies of saturated organic acid – bio-based solvent systems and excess enthalpy contributions: electrostatic energy (MF), hydrogen bonding (HB), and van der Waals forces (vdW), computed by COSMO-RS method at 293.15 K..... | 234 |

Notation

Acronyms:

| | |
|----------|---|
| AARD | Average absolute relative deviation |
| ABE | Acetone – butanol – ethanol mixture |
| BFLM | Bulk flow liquid membrane |
| BLM | Bulk liquid membrane |
| BOLM | Bubbling organic liquid membrane |
| BS | Biobased solvent |
| CAGR | Compound annual growth rate |
| CL | Confidence level |
| CLM | Continuous liquid membrane |
| CMPO | Octyl-(phenyl)-N,N-diisobutyl carbamoyl methyl phosphine oxide |
| COSMO-RS | Conductor-like screening model for real solvents method |
| D2EHPA | Di(2-ethylhexyl)phosphoric acid |
| DES | Deep eutectic solvent |
| E | Extract stream |
| ELM | Emulsion liquid membrane |
| ES | Eutectic solvent |
| ESPLIM | Electrostatic pseudo-liquid membranes |
| F | Feed stream |
| FSM | Fixed site membrane |
| GS | Gas separation |
| HB | Hydrogen bonding contribution |
| HBA | Hydrogen bond acceptor |
| HBD | Hydrogen bond donor |
| HF | Hollow fibre |
| HFRLM | Hollow fibre renewal liquid membrane |
| HLB | Hydrophilic-lipophilic balance value |
| IEA | International energy agency |
| IF | Impact factor |
| IL | Ionic liquid |
| LC | Level of confidence |
| LLX | Liquid-liquid extraction |
| LM | Liquid membrane |
| MD | Membrane distillation |
| MF | Microfiltration / electrostatic interactions contribution (misfit energy) |
| MOF | Metal organic framework |
| NF | Nanofiltration |
| OF | Objective function |
| O/W/O | Oil in water in oil ELM |
| PABLO | Permeability activity-based linear operation method |
| PELM | Pickering emulsion liquid membrane |
| PEHFSD | Pseudo-emulsion hollow fibre strip dispersion |
| PES | Polyethylene sulfonize polymer |
| PIM | Polymer inclusion membrane |
| PP | Polypropylene polymer |
| PPM | Plasticized polymer membrane |
| PTFE | Polytetrafluoroethylene polymer |
| PV | Pervaporation |
| PVDF | Polyvinyl floured polymer |
| R | Raffinate stream |
| RE | Rare earth |
| RMSD | Root-mean-square deviation |
| RO | Reverse osmosis |

| | |
|-------|------------------------------------|
| S | Stripping stream |
| SDG | Sustainable development goal |
| SLM | Supported liquid membrane |
| TBA | Tributylamine |
| TBP | Tributylphosphate |
| TFLM | Taylor flow liquid membrane |
| TOA | Trioctylamine |
| TOMAC | Tri-n-octylmethylammonium chloride |
| TOPO | Trioctylphosphine oxide |
| UF | Ultrafiltration |
| vdW | van der Waals forces contribution |
| VOC | Volatile organic compound |
| W/O/W | Water in oil in water ELM |

Symbols:

| | |
|--------------------------|---|
| [acid] | Organic acid concentration ($\text{g} \cdot \text{L}^{-1}$) |
| Δa_m LM | Activity gradient logarithmic mean ($\text{mol} \cdot \text{m}^{-3}$) |
| ΔG_{fus} | Gibbs free energy of fusion ($\text{kJ} \cdot \text{mol}^{-1}$) |
| ΔG_{soln} | Gibbs free energy of solution ($\text{kJ} \cdot \text{mol}^{-1}$) |
| ΔH_m | Enthalpy of fusion ($\text{kJ} \cdot \text{mol}^{-1}$) |
| ΔH_{soln} | Enthalpy of solution ($\text{kJ} \cdot \text{mol}^{-1}$) |
| ΔS_{soln} | Entropy of solution ($\text{kJ} \cdot \text{mol}^{-1} \cdot \text{K}^{-1}$) |
| A | Area (m^2) |
| a | Molar activity ($\text{mol} \cdot \text{mol}^{-1}$) / Instrument resolution / Linear regression intercept |
| a_m | Activity ($\text{mol} \cdot \text{m}^{-3}$) |
| b | Linear regression slope |
| c | Solute molar fraction ($\text{mol} \cdot \text{mol}^{-1}$) |
| C | Solute concentration ($\text{mol} \cdot \text{m}^{-3}$) |
| D | Diffusion coefficient ($\text{m}^2 \cdot \text{s}^{-1}$) |
| E_a | Activation energy ($\text{J} \cdot \text{mol}^{-1}$) |
| E_f | Extraction factor |
| Ex | Overall extraction yield (%) |
| Ex_F | Extraction efficiency (%) |
| Ex_S | Stripping efficiency (%) |
| e | Interaction energy of a molecule |
| F/S | Solvent:feed ratio |
| G | Gibbs free energy ($\text{kJ} \cdot \text{mol}^{-1}$) |
| \bar{G} | Partial molar Gibbs free energy ($\text{kJ} \cdot \text{mol}^{-1}$) |
| H | Enthalpy ($\text{kJ} \cdot \text{mol}^{-1}$) |
| h | Enthalpic factor (p_2) in λh model ($\text{kJ} \cdot \text{mol}^{-1}$) |
| h | Convective heat transfer coefficient ($\text{kW} \cdot \text{m}^{-2} \cdot \text{K}^{-1}$) |
| J | Mass flux ($\text{mol} \cdot \text{m}^{-2} \cdot \text{s}^{-1}$) |
| K'_D | Solute distribution coefficient |
| K_i | Partition coefficient |
| k_{phase} | Mass transfer coefficients in each phase ($\text{m} \cdot \text{s}^{-1}$) |
| K_{phase} | Global mass transfer coefficient in each phase ($\text{m} \cdot \text{s}^{-1}$) |
| k | Thermal conductivity ($\text{kW} \cdot \text{m}^{-1} \cdot \text{K}^{-1}$) |
| k_L | Coverage factor |
| L | Membrane length (m) / proportional coefficient in membrane species transport |
| M_{solution} | Saturated supernatant plus the vial mass (g) |
| M_{vial} | Vial mass (g) |
| M_{wet} | Dry organic acid plus the vial mass (g) |
| MW | Molar weight ($\text{g} \cdot \text{mol}^{-1}$) |
| m | Solute distribution coefficient |

| | |
|-------------------|--|
| N | Total data/stage number |
| n | Solute mass (mol) |
| P | Permeability ($\text{m}\cdot\text{s}^{-1}$) |
| p | Fitted parameter i of solubility correlation |
| $p(\mu)$ | σ -potential |
| $p(\sigma)$ | σ -profile |
| Q | Heat transfer ($\text{kJ}\cdot\text{kg}^{-1}$) |
| q | Transported solute flow ($\text{mol}\cdot\text{s}^{-1}$) |
| r | Molecule radius (m) / Sample size |
| r^2 | Squared Pearson correlation coefficient |
| S | Entropy ($\text{J}\cdot\text{mol}^{-1}\cdot\text{K}^{-1}$) |
| $S_{a,b}$ | Membrane selectivity for the a -component respect the b -component |
| s | Parameter standard deviations of the least-squared linear regression method |
| $s_{Y/X}$ | Random errors in the y -direction of the least-squared linear regression method |
| T | Temperature (K) |
| T_b | Compound boiling point (K) |
| T_{hm} | Harmonic mean temperature (K) |
| t | Time (s) |
| $t_{(N-2)}$ | t -factor |
| u | Molecular mobility /Standard uncertainty |
| U_{comb} | Expanded combined uncertainty |
| V | Volume (m^3) |
| v | Degree of freedom |
| W | SLM weight |
| wt_w | Water content |
| X | Solute free-based concentration |
| X | Independent variable of the least-squared linear regression method |
| x | Saturated solute mole fraction ($\text{mol}\cdot\text{mol}^{-1}$) / x -axis length (m) |
| Y | Dependent variable of the least-squared linear regression method |
| y | y -axis length (m) |
| z | z -axis length (m) |

Constants:

| | |
|------------------------|---|
| $k_{\text{Boltzmann}}$ | Boltzmann constant = $1.38\cdot 10^{-23}$ ($\text{J}\cdot\text{K}^{-1}$) |
| pK_a | Acid dissociation constant |
| R | Gas constant = 8.314 ($\text{J}\cdot\text{mol}^{-1}\cdot\text{K}^{-1}$) |

Greek letters:

| | |
|------------|---|
| α | Phase |
| γ | Activity coefficient |
| δ | Membrane thickness (m) / Root mean squared deviation |
| ϵ | SLM impregnation ratio (%) / Relative deviation |
| η | Dynamic viscosity ($\text{Pa}\cdot\text{s}$) |
| λ | Non-ideality (p_1) in λh model |
| μ | Chemical potential ($\text{J}\cdot\text{mol}^{-1}$) |
| ρ | Density ($\text{mol}\cdot\text{m}^{-3}$) |
| σ | Molecular charge density ($e\cdot\text{nm}^{-2}$) |
| ψ | Solute activity coefficients fitting parameter |

Superscripts:

| | |
|----------|--------------------------|
| cal | Calculated |
| E / ex | Excess property |
| eq | Equilibrated state |
| exp | Experimental |
| F | Feed phase |
| lit | Literature average value |
| max | Maximum |
| op | Operating |
| p | Pure component |
| S | Stripping phase |
| s | Green solvent phase |
| st | Steady |
| std | Standard state |
| w | Aqueous phase |
| ∞ | Infinite dilution |
| * | Hypothetical |

Subscripts:

| | |
|-----|---|
| 0 | Initial |
| 1 | Organic acid |
| 2 | Bio-based green solvent |
| BF | Bulk feed phase |
| E | Extract |
| eff | Effective |
| F | Feed phase |
| Fi | Feed-membrane interface |
| f | Final |
| i | Component i / Individual data point i |
| int | Internal phase on ELM |
| j | Data-point j |
| k | Dataset k |
| LM | Liquid membrane phase |
| n | Stage n |
| S | Stripping phase |
| SB | Bulk stripping phase |
| Si | Membrane-stripping interface |
| T | Total |

Abstract

Novel green solvents and supported liquid membranes were studied for the recovery of bio-based organic acids from model fermentation broths. As fundamental building blocks for the chemical industry, the production of organic acids from renewable feedstock have been broadly developed. Among them, succinic acid, levulinic acid, and fumaric acid have been highlighted as leading representatives. Nevertheless, their downstream separation and purification still require further research to build a suitable green production route. This turns the development of environmentally-friendly extractants as well as efficient separation methods into priority key research areas for bio-separations.

The growing number of available green solvents, such as ionic liquids, eutectic solvents, and bio-based solvents, makes unbearable the experimental screening process to find the most appropriate extractant. In this work, the molecular interactions driving the overall extraction performance for the organic acids were systematically analysed. Experimental measurements of the liquid-liquid extraction and solid-liquid equilibria, as well as thermodynamic modelling using the quantum chemistry-based COSMO-RS method, were carried out. Organic acids extraction yields and solubilities, systems excess energies, activity coefficients, and energies of solutions are reported. The combination of structurally different acids and extraction solvents arise complex interactions; however, hydrogen bonding showed to determine the overall behaviour. As a result, a straightforward selection guide was developed based on the organic acids partition coefficients in the extractant/water system, $\ln(K)$, system's water affinity, $\ln(\gamma_s^w)$, and separation process spontaneity, ΔG . Furthermore, the dissolution process of the organic acids in green solvents displayed an endothermic and spontaneous process with an enthalpy-entropy compensation effect. The separation is driven by the new and stronger interactions formed, increasing the order of the systems.

The state-of-the-art on sustainable applications of liquid membrane technology was thoroughly reviewed. Despite its high potential to replace conventional liquid-liquid extraction processes, some operational issues must be overcome and better predictive models developed. The feasibility of green-supported liquid membranes for succinic acid recovery was explored. As suggested by previous results, the solvent-phase affinities became key in the extraction performance. Experimental extractions were carried out to assess the effect of the green solvents and receiving phase. Commercial polyvinylidene fluoride (PVDF) porous membranes were impregnated with four different green solvents: the eutectic solvents DL-menthol:OctA and N₄₄₄₄Cl:OctA, the bio-based solvents eucalyptol, and the ionic liquid [C₄pyrr][Tf₂N]. The acid recovery for all liquid membranes was 50%, 51% and 59% with pure water and alkaline aqueous solutions of 0.1M and 0.5M NaOH in the stripping phase, respectively. It was found that extraction yield indeed depends on the pH of the stripping phase and that the solute permeation rate depends on the extraction solvent. For the first time, a permeability model based on experimental data and activity coefficients computed using the COSMO-RS method was developed. Moreover, the novel Permeability Activity-Based Linear Operation (PABLO) method was developed and proposed to determine the theoretical stages number and mass transfer area in a countercurrent cascade extraction system.

Overall, this thesis comprehensively covers two research needs for the bioseparations of key building blocks. The contributions will certainly enhance the development and design of green production routes, boosting the next generation of sustainable chemicals and biorefinery industries.

Declaration

No portion of the work referred to in the thesis has been submitted in support of an application for another degree or qualification of this or any other university or other institute of learning.

Copyright statement

- i)* The author of this thesis (including any appendices and/or schedules to this thesis) owns certain copyright or related rights in it (the “Copyright”) and s/he has given The University of Manchester certain rights to use such Copyright, including for administrative purposes.
- ii)* Copies of this thesis, either in full or in extracts and whether in hard or electronic copy, may be made only in accordance with the Copyright, Designs and Patents Act 1988 (as amended) and regulations issued under it or, where appropriate, in accordance with licensing agreements which the University has from time to time. This page must form part of any such copies made.
- iii)* The ownership of certain Copyright, patents, designs, trademarks and other intellectual property (the “Intellectual Property”) and any reproductions of copyright works in the thesis, for example graphs and tables (“Reproductions”), which may be described in this thesis, may not be owned by the author and may be owned by third parties. Such Intellectual Property and Reproductions cannot and must not be made available for use without the prior written permission of the owner(s) of the relevant Intellectual Property and/or Reproductions.
- iv)* Further information on the conditions under which disclosure, publication and commercialisation of this thesis, the Copyright and any Intellectual Property and/or Reproductions described in it may take place is available in the University IP Policy (see <http://documents.manchester.ac.uk/DocuInfo.aspx?DocID=24420>), in any relevant Thesis restriction declarations deposited in the University Library, The University Library’s regulations (see <http://www.library.manchester.ac.uk/about/regulations/>) and in The University’s policy on Presentation of Theses.

Acknowledgements

Of the many people to whom I owe my gratitude, my parents Jaime and Viviana will always come in the first place. They have given everything to me and my sisters. I thank my family for their constant support, which was never limited in any way.

I must also recognize my wonderful supervisors. María, who trusted me since the very beginning of my research career and encouraged me to pursue my PhD. And Patricia, who constantly pushed me to reach the highest potential of my work. I've always appreciated their mentoring, dedication, and inspiration that allowed me to accomplish my formation. Thank you both for everything you taught me and, more than anything, for your immense caring.

Lastly, to my teammates from our lab group for giving me their friendship, collaboration, and good times on countless occasions. Everyone was a small step in this achievement. Thank you.

Funding source

This work was funded by the CONICYT PFCHA/ DOCTORADO BECAS CHILE/2017-72180306.

About the author

Formation

Education

Master of Science – MSc. Chemical Engineering

Universidad Técnica Federico Santa María. Valparaiso, Chile. 2015 – 2016

Thesis: *High-Pressure liquid-vapour Equilibria of Binary and Ternary Systems Containing CO₂ + Volatile Apple Aroma Compounds*. Grade 100/100.

Chemical Engineering

Universidad Técnica Federico Santa María. Valparaiso, Chile 2009 – 2016

Courses:

- Certified Peer Reviewer (2021) Elsevier Researcher Academy.
- Computational Fluid Phase Thermodynamics (2018) By Prof. Dr Andreas Klamt. University of Regensburg, Germany.
- Thermodynamics of Advanced Chemical Engineering (2016) By PhD. Juan H. Vera (McGill University – Canada). Universidad Santiago de Chile, Chile.

Experience

Postgraduate Researcher

The University of Manchester. Manchester, UK. 2018 - 2022

- UoM research project. *Combining novel solvents (renewable deep eutectic solvents, biocompatible ionic liquids, and bio-based solvents) and membrane separation technology as a sustainable alternative for downstream processes in the high-value biomolecules production.*
- LEGOCHIP Project 2020. *Developing nanoporous functionalized graphene-based membranes to be integrated into biosensors for early diagnosis of melanoma.*
- UoM – USM international collaboration. *Linking together phenomenological and scale-up Membrane Distillation technology to achieve a mature level for water and energy recovery in the lithium production industry.*

Project Engineer

Universidad Técnica Federico Santa María. Valparaiso, Chile. 2017 - 2018

- ANGLOAMERICAN, Los Bronces operation, Chile. *Operational sustainability consulting for the pulp, tailings, and recovered-water transport processes. An early-alerts and alarms strategy was developed based on historical operation data analysis and KPIs formulation.*
- Sales de Jujuy, Argentina. *Operational engineering consulting through processes conceptualization for lithium production.*
- Soprocal, Chile. *Operational engineering consulting for new product development and feasibility study based on sodium metabisulfite and soil conditioner.*

Research Assistant

Universidad Técnica Federico Santa María. Valparaiso, Chile. 2013 - 2017

- National Fund for Scientific and Technological Development. FONDECYT #1150822 – Chile. *Exploring relationships between chemical structure and solubility in supercritical CO₂ for solutes with pharmacological importance. An interdisciplinary approach using molecular simulation, chemical synthesis, and direct measurement of solubility.*
- National Fund for Scientific and Technological Development. FONDECYT #1111008 – Chile. *Reducing experimental work for screening, scale-up, and cost analysis of supercritical CO₂ extraction of high-value compounds from vegetable substrates.*

Invited Researcher

University of Notre Dame. Indiana, USA. 2015

- Research project. Giving a first approach to the physicochemical nature of the formation of deep eutectic solvents with potential uses in the production of biodiesel and other separation and reaction processes.

Teaching Assistant

Universidad Técnica Federico Santa María. Valparaiso, Chile. 2012 - 2016

- Assistant lecturer and assistants' group coordinator of the courses: *Thermodynamics for Chemical Engineering, Process Thermodynamics, and Chemical Reactor Design.*

Achievements

On PhD project

Publications:

| Title / Journal [<i>impact factor 2021</i>] | Role / Status | Ref. |
|--|------------------------------|------|
| 1. Green Supported Liquid Membranes: the Permeability Activity-Based Linear Operation (PABLO) Method. <i>Chem Eng J.</i> 2022 [16.744] | First author Published | (1) |
| 2. Liquid Membrane Technology for Sustainable Separations. Chapter in: <i>Sustainable Separation Engineering. First Edit.</i> Wiley. 2022 | First author Published | (2) |
| 3. Green Solvent Selection Guide for Biobased Organic Acid Recovery. <i>ACS Sustainable Chem. Eng.</i> 2020 [9.224] | First author Published | (3) |
| 4. Solubility Study and Thermodynamic Modelling of Succinic Acid and Fumaric Acid in Bio-based Solvents. | First author Under review | (4) |

Presentations and conference proceedings:

- i) **Supported Green Solvents Membranes for Bio-based Organic Acid Recover** (Poster). *Euromembrane Conference 2021. Copenhagen, Denmark. 28 Nov – 02 Dec 2021.*
- ii) **Thermodynamic Understanding of The Liquid-Liquid Extraction of Bio-based Organic Acids with Hydrophobic Ionic Liquids (ILs) and Eutectic Solvents (ESs)** (Lightning talk). *International Symposium on Solubility Phenomena and Related Equilibrium Processes 19. (ISSP 19). Online, 12-16 July 2021.*
- iii) **Thermodynamic Assessment of ILs and DESs for Bio-based Organic Acids Recovery through COSMO-RS and Experiments** (Oral presentation). *6th Iberoamerican Meeting on Ionic Liquids 2021 (IMIL 2021). Online, 24-26 May 2021.*
- iv) **Supported Liquid Membranes (SLM) using green solvents for bio-based organic acids extraction** (Oral presentation). *7th Network Young Membranes Meeting 2020 (NYM 2020) Online, 3-4 Dec 2020.*

v) **Bio-organic acids extraction using hydrophobic Ionic Liquids and Deep Eutectic Solvents** (Poster). *4th International Conference on ionic Liquids in Separation & Purification Technology 2019 (ILSEPT 2019)*. Sitges, Spain. 8-11 Sept 2019.

vi) **Extraction of bio-based organic acids using novel solvents** (Poster). *CEAS PGR conference 2019. Manchester, UK. 17 May 2019*.

On other projects

Publications:

| Title / Journal [impact factor 2021] | Role / Status | Ref. |
|---|------------------------------|------|
| 1. The Missing Link in the Technological Maturity of Membrane Distillation. | First author Under review | (5) |
| 2. Hydrogen Bond Donor and Alcohol Chain Length Effect on The Physicochemical Properties of Choline Chloride Based Deep Eutectic Solvents Mixed with Alcohols. <i>J Mol Liq.</i> 2022 [6.633] | Co-author Published | (6) |
| 3. High-pressure vapor+ liquid equilibria for the binary system CO₂+(E)-2-hexenal. <i>J Supercrit Fluids.</i> 2020 [4.514] | Co-author Published | (7) |
| 4. Vapour pressure and vaporisation enthalpy for two key apple odorants, ethyl butyrate and ethyl hexanoate, at pressures from (15 to 105) kPa. <i>J Chem Thermodyn.</i> 2020 [3.269] | Co-author Published | (8) |
| 5. High-pressure (vapor+ liquid) equilibria for binary systems containing carbon dioxide and key apple odorants, hexanal and ethyl-2-methylbutyrate. <i>J Chem Thermodyn.</i> 2017 [3.269] | First author Published | (9) |
| 6. Excess Molar Enthalpies of Deep Eutectic Solvents Composed of Quaternary Ammonium Salts and Glycerol or Ethylene Glycol. <i>J Chem Eng Data.</i> 2016 [3.119] | First author Published | (10) |
| 7. High-pressure (vapour+ liquid) equilibria for ternary systems composed by {(E)-2-hexenal or hexanal+ carbon dioxide+ water}: Partition coefficient measurement. <i>J Chem Thermodyn.</i> 2015 [3.269] | Co-author Published | (11) |

Presentations and conference proceedings:

- i) Excess Molar Enthalpies of Deep Eutectic Solvents (DESS) Composed of Quaternary Ammonium Salts and Glycerol or Ethylene Glycol (Poster).** *14th International Conference on Properties and Phase Equilibria for Product and Process Design (PPEPPD 2016). Porto, Portugal. 22-26 May 2016.*
- ii) High-Pressure Vapor + Liquid Equilibria for Binary Systems CO₂ + Hexanal and CO₂ + Ethyl 2-Methylbutyrate (Poster).** *14th International Conference on Properties and Phase Equilibria for Product and Process Design (PPEPPD 2016). Porto, Portugal. 22-26 May 2016.*
- iii) Coeficientes de Partición CO₂/Agua de Aromas de Manzana a Alta Presión (Oral presentation).** *XIX Congreso Chileno de Ingeniería Química (CCHIQ 2014). Concepción, Chile. 15-17 Oct, 2014.*

Honours & awards

- i) Becas Chile - Scholarships for postgraduate studies (2017)** *Chilean National Agency for Research and Development. Chile. Financial scholarship awarded by ANID in the Advance Human Capital Program to study a PhD Chemical Engineering at The University of Manchester in the United Kingdom. Ranking 95 among 360 selected applicants.*
- ii) Program of Incentives to the Scientific Initiation (2016)** *Universidad Técnica Federico Santa María. Chile. Financial grant awarded by Direction of Research and Postgraduate for the realization of a scientific research project.*
- iii) CONICYT's scholarship for short stays in foreign (2015)** *National Commission for Scientific and Technological Research – Chile. Financial scholarship awarded by CONICYT for a research internship at the University of Notre Dame, USA.*
- iv) UTFSM Scholarships for Studies of Scientific Master (2015)** *Universidad Técnica Federico Santa María. Chile. Fee and financial scholarship awarded by Direction of Research and Postgraduate for the Master of Sciences in Engineering Chemical program.*

Part I

The bottleneck and opportunities in the biorefinery industry
development.

"I am looking for someone to share in an adventure..."

— J.R.R. Tolkien, *The Hobbit*

Chapter 1. Introduction

Nowadays societal challenges have driven a shift in the chemical industries towards the twelve principles of green chemistry (12). The need to establish clean and safe production routes and lessen the fossil resources dependency has opened the gates for the biorefinery industry as a biomass valorisation vehicle. In the words of the International Energy Agency (IEA), biorefining is "*the sustainable processing of biomass into a spectrum of marketable products and energy*" (13). The interest in the conversion of biomass into energy, fuels, chemicals and materials is also driven by the world's economic and social sustainability urges, being climate change the main concern (14).

The product-driven biorefinery is dedicated to biomaterials and biochemicals production as key industrial platforms. In 2020, the global production of bio-based products was estimated to be 90 million tonnes and, adding biofuels, could mean revenue of US\$ 10 billion (15). The top high-value biomolecules targeted by the US DOE Office of Energy Efficiency and Renewable Energy are succinic acid, levulinic acid, fumaric acid, malic acid, itaconic acid, glycerol, aspartic acid, glucaric acid, 2,5-furan dicarboxylic acid, 3-hydroxypropionic acid, glutamic acid, and 3-hydroxybutyrolactone (16). Those chemicals, and especially bio-organic acids, have shown a substantial increase in their demand, with a forecasted annual growth rate of 12.6% (17). Nevertheless, an acknowledged biorefinery weakness is that it remains in the research and concept development stage, far from reaching the real market (18).

Bioseparations have been featured as one of the highest priority key research needs for today's industry (19). Economic evaluations, new material and extractants, and a deep understanding of molecular chemistry are required to accomplish this goal. Exhaustive efforts have been made to build a feasible green industry based mainly on biorefinery as a sustainable chemical supplier. However, throughout the biomolecules production line, some stages are

misaligned with the original purpose. Specifically, the stages of separation and purification constitute the core component of biorefinery with a cost of 20–50% of the total production (20). Phase change-based processes, such as distillation or crystallization, are high energy demanding; while solvent-based techniques, such as liquid-liquid extraction or absorption, require a large amount of hazardous solvents.

There is growing research aiming to improve process sustainability giving a solid base to develop solutions for target applications. Production paths for eco-friendly substances and materials are constantly identified and characterized. Ionics liquids, eutectic solvents and bio-based solvents have been intensively studied as alternatives for conventional extractants. Computational quantum chemistry methods, such as COSMO-RS, are powerful tools that allow for property predictions and direct assessment of extract media alternatives. In addition, emergent technologies such as membrane-based separation methods promise to overcome conventional process limitations. Liquid membranes technology can exploit the benefits of novel green solvents and the simple operation of membrane separation, providing a twofold contribution to the process sustainability.

The assessment of novel technology proposals requires establishing evaluation criteria and design methods. It is known that the extraction performance of a target compound with a solvent candidate is governed by their molecular affinity. Such affinities are determined by molecular interactions, which can be estimated by thermodynamic modelling. Furthermore, liquid membranes allow for an efficient compound recovery with minimal solvent consumption. Focusing on sustainable extractants and membrane separation technology integration, the implementation of *green-supported liquid membranes* into the biomolecules production routes will boost the green industry development.

Based on experimental assays and thermodynamics assessments, the underlying patterns of extraction solvent performance and liquid membrane separation behaviours can be recognised. Then, this can be used to formulate proper guidelines and better predictive transport models. Ultimately, the extraction of bio-based organic acids using green-supported liquid membranes with novel solvents will allow the development of new approaches to propose practical industrial applications.

1.1 Motivation and scope

The road towards a green chemical industry needs to be paved with consecutive incremental contributions along the production process stages. From the renewable feedstock valorisation to the final product use as a substitute for petrochemical substances, these efforts must warrant a sustainable production of high-value molecules capable to compete with the conventional routes. The research work in this thesis is focused on the recovery of organic acids from their fermentation broths, by consolidating the basis of the feasibility assessment of neoteric extraction media and emergent separation technologies. The motivation of this project is to help build better and clean chemical industries. For this reason, the scope, discussion, and results implications are oriented toward an environmentally-friendly perspective. Under no circumstance, this work attempts to misuse popular terminologies, such as sustainability, green or other trending labels, falling into questionable research practices or what has been recently identified as "*Scholarly bullshit*" (21). By fulfilling these goals, this thesis will certainly contribute to the establishment of a strong bio-based industry.

1.2 Aims and objectives

1.2.1 General

The aim of this thesis is to develop guidelines and models for bio-organic acid recovery process design using green solvents coupled with liquid membrane technology. Understanding the underlying mechanisms of this novel separation process will ultimately promote novel bio-based production routes as competitive alternatives to meet some of the sustainable development goals (SDGs), e.g. Industry, innovation and infrastructure, Responsible consumption and production, and Climate action.

1.2.2 Specifics

- i)* Identifying the organic acid – green solvent molecular interactions through a thermodynamic assessment using the quantum chemical COSMO-RS method and experimental data.
- ii)* Reviewing the state-of-the-art and maturity of liquid membrane technology for sustainable separations.
- iii)* Evaluating the performance of green solvent-based supported liquid membranes to recover target organic acids.
- iv)* Proposing guidelines and design methods for the recovery process design.

1.3 Thesis outline

This thesis is structured in a *Journal Format*, i.e., a paper compendium submitted to peer-reviewed journals, according to the university's guiding principles. The thesis is composed of seven chapters and appendices grouped into five parts:

- i)* The bottleneck and opportunities in the biorefinery industry development. ([Chapter 1](#) & [Chapter 2](#))

Project background to complete the thesis narrative. The research problem, objectives, and relevant literature review are presented to support the context of the project and fulfil the storyline of the publications. This section summarizes the key tasks to address in the nowadays biorefinery bottlenecks: separation and purification stages are not completely environmentally-friendly, the literature is overflowed with solvent candidates for potential green processes, and novel separation technology alternatives remain at an immature level.

- ii)* The search for suitable green solvents for bio-based organic acids recovery. ([Chapter 3](#) & [Chapter 4](#))

The growing number of novel extraction media, such as ionic liquids, eutectic solvents, and bio-based solvents, available in the literature raise the need to establish tools for assessing their suitability for specific processes. This section develops the basis and guidelines for their selection as well as the basic thermodynamic properties needed for the separation and purification of bio-organic acids. Two publications were submitted on this topic:

- Scientific paper - Green solvents selection guide for bio-based organic acids recovery.
- Scientific paper - Solubility study and thermodynamic modelling of succinic acid and fumaric acid in bio-based solvents.

iii) Maturing the liquid membrane technology as a clean separation alternative. ([Chapter 5](#) & [Chapter 6](#))

Liquid membranes are an emerging technology for sustainable separations that can potentially replace liquid-liquid extraction. This section provides an in-depth overview of its applications, ranging from the recovery of high-value components to high-risk waste remediation, as well as their potential and limitations. Furthermore, a permeability model and conceptual process design method are developed to promote technology maturity. Two publications were submitted on this topic:

- Book chapter contribution - Liquid membrane technology for sustainable separations.
- Scientific paper - Green supported liquid membranes: the permeability activity-based linear operation (PABLO) method.

iv) Contribution to knowledge. ([Chapter 7](#))

The main conclusions of the thesis are summarized. Additionally, new research gaps derived from this work are proposed along with a roadmap to addressing them.

v) Appendices.

Supplementary information relative to the presented documents.

Chapter 2. Background

This chapter briefly outlines the context of this thesis and the publications derived from the research project.

2.1 Bio-based organic acids

Two production routes can be followed in the chemical industry, as depicted in Figure 2.1. First, the conventional path of petroleum-based routes starts from the fossil fuels refinery and compounds transformations into the final chemical products. This route works by depleting the raw materials and is subject to several environmental concerns, due to the risk that the intermediate substances pose. The second route is the bio-based route, which exploits biomass as renewable raw material to obtain fundamental building blocks. They are subsequently transformed into the desired chemical intermediates to be used in the final applications.

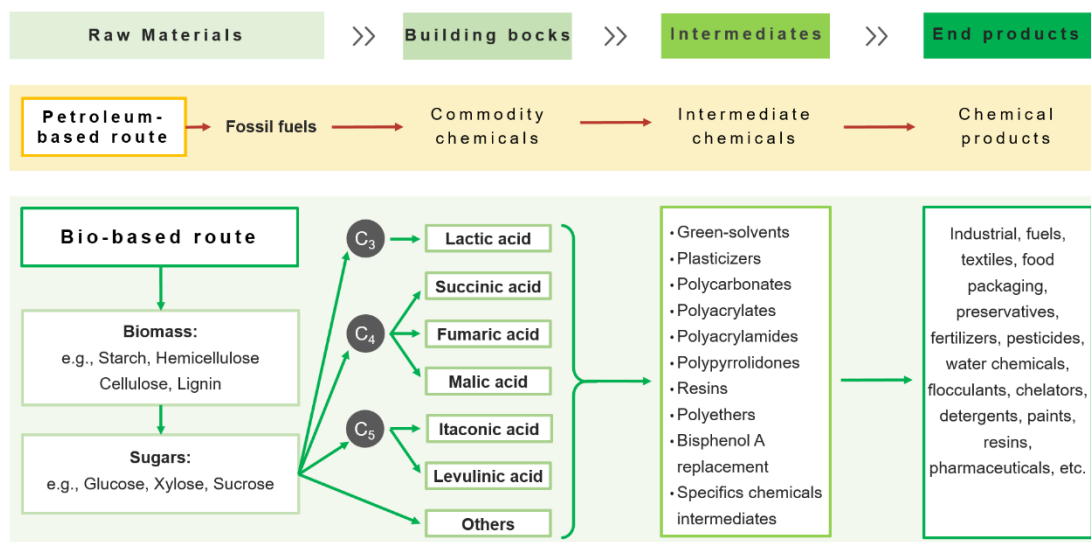


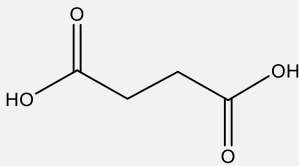
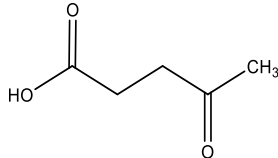
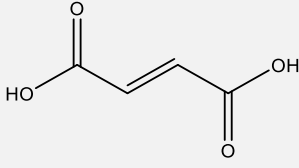
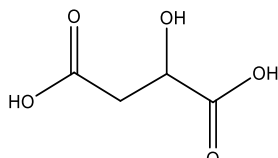
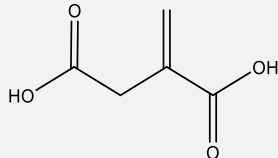
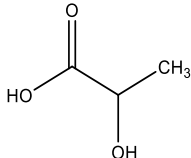
Figure 2.1. Comparison between the chemical production routes from petroleum-based and bio-based raw materials.

The most important bio-based organic acids for the bio-based chemical industry are summarized in [Table 2.1](#), along with their main applications and fermentation pathways to building blocks from sugars. For instance, succinic acid is used as starting material in the production of a wide range of commodities. Among them are 1,4-butanediol, γ -butyrolactone, tetrahydrofuran, and bio-based polymers such as butylene succinic acid. Depending on its fermentation path, it is possible to obtain bio-succinic acid from lactose, xylose, arabinose, cellobiose, or biomass such as whey, cane molasses, straw, corn fibre, crop stalk, wheat, and duckweed ([22–27](#)). Levulinic acid is widely used in solvents, biofuels, chemical intermediates, resins, and other applications, using monosaccharides, 5-hydroxymethylfurfural, furfural, polysaccharides or starch, and lignocellulosic biomass as raw material ([28–31](#)). Bio-fumaric acid can be produced from renewable materials such as molasses, starch or lignocellulosic substrates, and its uses include the production of resins, biopolymers, malic and aspartic acid ([32–35](#)).

One of the most used methods for the downstream separation of bio-based organic acids is precipitation and crystallization ([34](#)). Compounds separations based on phase change processes are well-known for their high energy consumption and associated greenhouse gas emissions. Likewise, liquid-liquid extraction is also broadly used for the extraction of carboxylic acids from aqueous solutions. Among the commonly used extracting media for this task are trioctylamine, tributyl phosphate, and trioctylphosphine oxide ([36,37](#)). These solvents are also used in mixtures with MIBK, toluene or other volatile organic nonpolar solvents, acting as complexing reactants. However, organophosphorus and aliphatic amines are toxic and pose several environmental risks.

Innovative technologies such as ion exchange, adsorption, or electro dialysis, have been proposed. Supercritical carbon dioxide has also been proposed as another environmentally-friendly solvent alternative for carboxylic acid extraction, yet low partition coefficients are obtained when no complexing reactants are used (38). Patented succinic acid recovery processes include crystallization by acidification and pH control, precipitation, solvent extraction with amines or other organic solvents, ion-exchange extractions, nanofiltration, electro dialysis, and esterification in reactive distillations (39). Different separation technologies have been proposed for levulinic acid recovery. Among them are vacuum distillation, steam stripping, absorption, solvent extraction, and more innovative ionic liquids extraction or membrane separation (28). After impurities precipitation and filtration, fumaric acid can be crystallized by cooling (34) or acidification to a pH value of 1 with sulphuric acid (40). Cao et al. (33) proposed a recovery process of fumaric acid based on different ion-exchange resins. A conceptual design of a dual reactive dividing wall column has also been explored for bio-lactic acid purification (41). Further research is still needed to ensure the sustainability of bio-based organic acid production. Overall, non-toxic and environmentally compatible extraction media, as well as low-energy separation methods, are the key research needs to achieve this goal.

Table 2.1. Summary of the main bio-based organic acids produced as building blocks for the bio-based industry (16).

| Bio-acid | Structure | Applications | Fermentation pathway |
|-----------|---|--|---|
| Succinic |  | Drop-in replacement for petrochemical succinic acid and adipic acid in some applications. Used in the production of resins, plasticizers and biodegradable polymers. | -Aerobic yeast or fungal/bacterial fermentation -Anaerobic bacterial fermentation -Bio-transformation |
| Levulinic |  | Used as a precursor for pharmaceuticals, new acrylate polymers, polycarbonate resins, gasoline and biodiesel additives. | -Chemical/catalytic transformation |
| Fumaric |  | Commonly used as a preservative in food and beverages, in the production of paints and coatings, as well as in the production of paper. | -Aerobic yeast or fungal/bacterial fermentations -Chemical/catalytic transformation |
| Itaconic |  | Used to produce rubber, resins for coatings, lubricants, thickeners, and some herbicides. | -Aerobic yeast or fungal fermentations |
| Malic |  | Flavour enhancer in the food industry. Can be converted into other chemical derivatives used for a variety of plastic, polymer and resin products. Replacement for maleic anhydride. | -Aerobic yeast or fungal/bacterial fermentation |
| Lactic |  | Broadly used in chemical, food, cosmetic, textile, bio-medical Industries, and as polymer precursor for bioplastics production. | -Aerobic yeast or fungal fermentations -Anaerobic yeast or fungal/bacterial fermentation |

2.2 Novel green solvents

There is no universal consensus on the exact characteristics that grant a compound the title of green solvent. However, academia and industry have started to build the concept based on the twelve principles of green chemistry (12). Stipulated in 1998 by Paul Anastas and John Warner as design rules to reach sustainability, the principles are:

- i) Prevention of waste.*
- ii) Atom economy to maximize inclusion of materials in the final product.*
- iii) Less hazardous chemical synthesis that poses little or no toxicity.*
- iv) Designing safer chemicals that reduce toxicity and preserve efficacy.*
- v) Safer solvents and auxiliaries, avoiding their use whenever possible.*
- vi) Design for energy efficiency to reduce environmental and economic impacts.*
- vii) Use of renewable feedstocks to avoid depleting raw materials whenever technically and economically feasible.*
- viii) Reduce derivatives to reduce the use of additional reagents and waste generated.*
- ix) Catalysis over stoichiometric reagents to perform chemical transformations.*
- x) Design for degradation to ensure the chemical break down into innocuous compounds at the end of the function.*
- xi) Real-time analysis for pollution prevention prior formation of hazardous substances*
- xii) Inherently safer chemistry for accident prevention to minimize chemical accidents.*

It is not always practicable to apply the principles all together to a given application. Nevertheless, following these rules as much as possible can help to substantially improve process sustainability towards a real green chemical industry. Likewise, it is not feasible to develop compounds of specific properties that meet such principles whatever the application (42). Thus, the category of green solvent depends on the component as well as the target process. In this context, selection guides and design methods to establish evaluation criteria are more important than ever.

The outlook of the green solvent adoption is determined by the need for sustainability but is subject to economic pressures (43). It is worth noting that stricter government regulations have caused an exponential growth of the research on biotechnology applications since the beginning of the century (44). Current trends in solvent-based separations are based on the replacement of conventional solvents with ionic liquids, eutectic solvents, or bio-based solvents in metal or hydrocarbons separations, carbon capture, food industry, and biorefinery (45–47). These neoteric solvents and their sustainable application are briefly reviewed in the following subsections.

2.2.1 Ionic liquids

During the last decades, ionic liquids (ILs) have been intensely studied due to their promising capacities as novel solvents for several industrial processes. Ionic liquids are organic salts with a melting point under 100 °C, which have attracted great interest due to their property tailoring capacity by carefully selecting their components (48). The combination of a pair of structurally different cations and anions results in specific thermophysical properties, from viscosity and density to heat capacity and thermal conductivity (49). The large quantity of available ions combination has boosted their application in several production fields, such as lubricating and corrosion-inhibitors additives, electrochemical applications, chemical and enzymatic reactions, and most importantly as extraction media (50). Other advanced applications of ILs include the manufacturing of supercapacitors for energy storage (51), biomass

fractionation (52), as well as drug solubilisation and delivery, biosensing, and protein stabilization in biomedicine (53).

Although ILs have been traditionally featured as eco-friendly solvents, there are concerns about if their synthesis, recycling and bio-degradability meet the twelve principles of green chemistry. This had led to questioning their production routes and life-cycle re-examination (54). Ionic liquid toxicity shows to increase with the hydrophobicity and instability, following an overall trend of cation type of: cholinium < piperidinium < pyrrolidinium < morpholinium < pyridinium/ imidazolium < ammonium < phosphonium (55). Meanwhile, possible toxic effects of the anions bis-(trifluoromethyl sulfonyl)imide and tris(pentafluoroethyl) trifluoro phosphate have been reported (56,57).

Nevertheless, ILs produced from biocompatible sources such as carboxylic acids, amino acids or glucose, have emerged as a new family of bio-ionic liquids (58). Several bioactive compound extractions have been achieved with ionic liquids (59). Among them are lipids, essential oils, carotenoids, saponins, amino acids, proteins, and drugs. More extraction studies on the recovery of organic compounds with ILs are summarized in Table 2.2 and Table 2.4.

Table 2.2. Examples of organic compounds recovery using ionic liquids.

| [Cation][Anion] | System type | Solute | Ref. |
|--|---|--|------|
| [C ₄ min][PF ₆] [C ₆ min][PF ₆] [C ₈ min][PF ₆] [C ₆ min][BF ₄] [C ₈ min][BF ₄] | Liquid-Liquid Extraction with hydrophobic ionic liquids | 3-indole butyric acid | (60) |
| [C ₄ min][Br] [C ₆ min][Br] [C ₈ min][Br] | IL-Based Aqueous biphasic systems | Proteins of bovine serum | (61) |
| [P ₆₆₆₁₄][Cl] [P ₆₆₆₁₄][Dec] [P ₆₆₆₁₄][Phos] | Liquid-Liquid Extraction with hydrophobic ionic liquids | Lactic, Malic, Succinic acids | (36) |
| [C ₄ mim][PF ₆] [C ₆ mim][PF ₆] [C ₈ mim][PF ₆] | Liquid-Liquid Extraction with hydrophobic ionic liquids | Acetic, glycolic, propionic, lactic, butyric and pyruvic | (62) |

Table 2.3. Examples of organic compounds recovery using ionic liquids, continuation.

| [Cation][Anion] | System type | Solute | Ref. |
|---|---|--|-------------|
| [C ₄ min][Br] [C ₆ min][Br] [C ₈ min][Br] | IL-Based Aqueous biphasic systems | Succinic acid | (63) |
| [C ₄ mim][PF ₆] | Liquid–Liquid Extraction with hydrophobic ionic liquid | Amino acids | (64) |
| [P ₄₄₄₁][Tf ₂ N] [N ₄₄₄₁][Tf ₂ N] [N ₈₈₈₁][Tf ₂ N] | Liquid–Liquid Extraction with hydrophobic ionic liquids | Tyrosol | (65) |
| [C ₂ mim][Tf ₂ N] [C ₄ mim][Tf ₂ N] [C ₆ mim][Tf ₂ N] | Liquid–Liquid Extraction of pesticides with hydrophobic ionic liquids | Imidacloprid, acetamiprid, nitenpyram and thiamethoxam | (66) |
| [S ₂₂₁][Tf ₂ N] [S ₂₂₂][Tf ₂ N] [N ₄₁₁₁][Tf ₂ N] [N ₁₈₈₈][Tf ₂ N] [P ₁₈₈₈][Tf ₂ N] | Other hydrophobic ionic liquids | Mutual solubility between water hydrophobic ionic liquids | (67) |
| [C ₆ min][FAP] [BMPL][FAP] [PH ₃ T][FAP] [HNH ₂ MPL][FAP] | Ultra-hydrophobic ionic liquids | Polycyclic Aromatic Hydrocarbons | (68) |
| [P ₆₆₆₁₄][DCA] [P ₆₆₆₁₄][Tf ₂ N] [P ₆₆₆₁₄][Cl] [P ₆₆₆₁₄][BF ₄] [P ₆₆₆₁₄][Tf ₂ N] | Liquid–Liquid Extraction with hydrophobic ionic liquids | Low-titre short chain volatile fatty acids from anaerobic fermentation | (69) |
| [N ₁₈₈₈][Tf ₂ N] [Chol][Tf ₂ N] [N ₄₁₁₁][Tf ₂ N] [Pmim][Tf ₂ N] [P ₄₄₄₁][Tf ₂ N] [Odecmin][Tf ₂ N] | Selective Liquid–Liquid Extraction with hydrophobic ionic liquids | Levulinic acid and formic acid | (70) |
| [C ₂ mim][Tf ₂ N] [C ₃ mim][Tf ₂ N] [C ₄ mim][Tf ₂ N] [C ₅ mim][Tf ₂ N] [C ₆ mim][Tf ₂ N] [C ₇ mim][Tf ₂ N] [C ₈ mim][Tf ₂ N] [C ₆ mim][Tf ₂ N] [C ₈ mim][Tf ₂ N] [C ₄ mim][Tf ₂ N] [C ₈ mim][Tf ₂ N] [C ₃ mpyrr][Tf ₂ N] [C ₃ mpyr][Tf ₂ N] [C ₃ mpip][Tf ₂ N] [C ₄ mpyrr][Tf ₂ N] [C ₄ mmim][Tf ₂ N] | Liquid–Liquid Extraction with hydrophobic ionic liquids | Tryptophan | (71) |

2.2.2 Eutectic solvents

Eutectic solvents (ESs), as well as deep eutectic solvents (DESs), are eutectic mixtures of different Lewis or Brønsted acids and bases. In the mixture, each component acts as a hydrogen bond acceptor and as a hydrogen bond donor. The mutual interaction between the molecules of the mixture promotes a charge delocalization through hydrogen bonding, causing a decrease in the melting point (72). Figure 2.2.a shows a schematic representation of this phenomenon. They show very similar properties to ionic liquids: low vapour pressure, wide liquid range, and non-flammability. Despite their similitudes, they have different chemical properties, resulting in different possible applications. Both solvent families are differentiated by the fact that eutectic solvents might be easily prepared from natural and biodegradable materials, meaning that they can be cheaper and more environmentally-friendly solvents. Commonly, quaternary ammonium salts are used as the acceptor component, but other compounds with functional groups such as hydroxyl can fulfil this role as well. Moreover, eutectic solvents might gain a hydrophobic nature by using fatty acids as the hydrogen bond donor component (73). ESs are prepared by mixing the hydrogen bond acceptor and donor components in their specific molar ratio. Then, the mixture is stirred in a heat bath until no solid is observed in the liquid fluid. Figure 2.2.b shows the phase behaviour along the preparation.

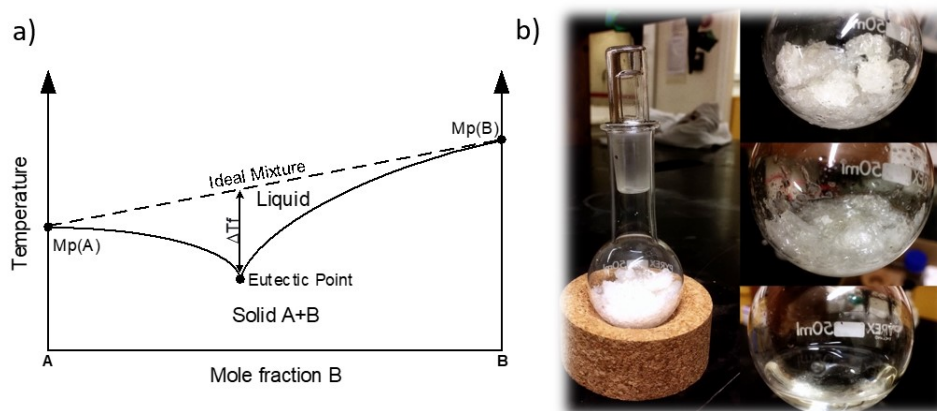


Figure 2.2. a) Schematic phase diagram of a eutectic mixture of two components (10). The molecular interactions of the solids A and B with their respective melting points (M_p / T) cause a decrease in the temperature of fusion (ΔT_f) compared to the ideal mixture; b) Example of eutectic solvent formation from a mixture of two solid compounds to a homogenous liquid.

ESs applications for process separation ranges from synthesis media and biotransformations to metal deposition or CO₂ adsorption, as well as biodiesel purification (10). They have been proposed as phase change materials in solar thermal power plants (74) and for battery manufacturing (75). In the bio-industry, eutectic solvents have been shown to improve lignocellulosic biomass fractionation (76) and fermentation systems (77). Other examples of studies of eutectic solvents for organic compounds recovery are summarized in Table 2.4 and Table 2.5

Table 2.4. Examples of organic compounds recovery using eutectic solvents.

| HBA:HBD | Ratio HBA:HBD | System type | Solute | Ref |
|----------------------------------|------------------|--|---|------|
| N ₈₈₈₁ -Cl:DecA | 1:2 | Liquid-Liquid Extraction with hydrophobic DESs | Acetic, propionic and butyric acids | (73) |
| N ₇₇₇₇ -Cl:DecA | 1:2 | | | |
| N ₈₈₈₈ -Cl:DecA | 1:2 | | | |
| N ₈₈₈₁ -Cl:DecA | 1:2 | | | |
| N ₈₈₈₈ -Br:DecA | 1:2 | | | |
| Lid:DecA | 1:2 | Liquid-Liquid Extraction with hydrophobic DESs | Alkali and transition metal ions | (78) |
| | 1:3 | | | |
| | 1:4 | | | |
| DL-Menthol:AceticA | 1:1 | Liquid-Liquid Extraction with hydrophobic DESs | Caffeine, tryptophan, isophthalic acid, and vanillin | (79) |
| DL-Menthol:PyruvicA | 2:1 | | | |
| DL-Menthol:LacticA | 2:1 | | | |
| DL-Menthol:LauricA | 1:2 | | | |
| Menthol:AceticA | 1:1 | | | |
| Menthol:LevulinicA | 1:1 | Liquid-Liquid Extraction of pesticides with hydrophobic DESs | Imidacloprid, acetamiprid, nitenpyram and thiamethoxam | (66) |
| Menthol:PyruvicA | 1:2 | | | |
| Menthol:ButyricA | 1:1 | | | |
| Menthol:HexanoicA | 1:1 | | | |
| Menthol:OctanoicA | 1:1 | | | |
| Menthol:DecA | 1:1 | | | |
| Menthol:DodecanoicA | 2:1 | | | |
| N ₄₄₄₄ -Cl:AceticA | 1:1 | | | |
| N ₄₄₄₄ -Cl:LevulinicA | 1:2 | | | |
| N ₄₄₄₄ -Cl:HexanoicA | 1:2 | | | |
| N ₄₄₄₄ -Cl:OctanoicA | 1:2 | | | |
| N ₄₄₄₄ -Cl:DecA | 1:2 | Liquid-Liquid Extraction with hydrophobic DESs | Synthetic pigments in beverage | (80) |
| N ₈₈₈₁ -Cl:DecA | 1:2 | | | |
| N ₈₈₈₁ -Cl:OctanoicA | 1:2 | | | |
| N ₈₈₈₁ -Cl:DecA | 1:2 | | | |
| N ₈₈₈₁ -Cl:OctanoicA | 1:2 | Liquid-Liquid Extraction | Vanilla-derived compounds | (81) |
| DL-Menthol:OctanoicA | 1:1 | | | |
| DL-Menthol:DecanoicA | 1:1 | | | |
| DL-Menthol:DodecanoicA | 2:1 | | | |

Table 2.5. Examples of organic compounds recovery using eutectic solvents, continuation.

| HBA:HBD | Ratio HBA:HBD | System type | Solute | Ref |
|---|------------------|-----------------|-----------------------|------|
| N ₈₈₈₁ -Cl:HexanoicA | 1:2 | | | |
| N ₈₈₈₁ -Cl:OctanoicA | 1:2 | | | |
| N ₈₈₈₁ -Cl:CapricA | 1:2 | | | |
| N ₈₈₈₁ -Cl:LauricA | 1:2 | | | |
| N ₈₈₈₁ -Cl:MyristicA | 1:1 | | | |
| N ₈₈₈₁ -Cl:PalmiticA | 1:1 | | | |
| N ₈₈₈₁ -Cl:cis-9-OctadecenoicA | 1:2 | | | |
| N ₈₈₈₁ -Cl:RicinoleicA | 1:2 | Solid-Liquid | Polyprenyl | |
| N ₈₈₈₁ -Cl:1-Propanol | 1:2 | Extraction with | acetates from | (82) |
| N ₈₈₈₁ -Cl:1-Butanol | 1:2 | hydrophobic | <i>Ginkgo biloba</i> | |
| N ₈₈₈₁ -Cl:Hexyl alcohol | 1:2 | DESs | leaves | |
| N ₈₈₈₁ -Cl:Capryl alcohol | 1:2 | | | |
| N ₈₈₈₁ -Cl:Decyl alcohol | 1:2 | | | |
| N ₈₈₈₁ -Cl:Dodecylalcohol | 1:1 | | | |
| N ₈₈₈₁ -Cl:1-Tetradecanol | 1:2 | | | |
| N ₈₈₈₁ -Cl:Hexadecanol | 1:2 | | | |
| N ₈₈₈₁ -Cl:Cyclohexanol | 1:2 | | | |
| N ₈₈₈₁ -Cl:DL-Menthol | 1:2 | | | |
| N ₈₈₈₁ -Cl:Ethylene glycol | 1:2 | | | |
| N ₈₈₈₁ -Cl:1-Propanol | 1:2 | | | |
| N ₈₈₈₁ -Cl:1,3-Propanediol | 1:2 | | | |
| N ₈₈₈₁ -Cl:Glycerol | 1:2 | | | |
| N ₈₈₈₁ -Cl:1-Butanol | 1:2 | | | |
| N ₈₈₈₁ -Cl:1,2-Butanediol | 1:2 | Solid-Liquid | Artemisinin | |
| N ₈₈₈₁ -Cl:Hexyl alcohol | 1:2 | Extraction with | from <i>Artemisia</i> | (83) |
| N ₈₈₈₁ -Cl:Capryl alcohol | 1:2 | hydrophobic | <i>annua</i> leaves | |
| N ₈₈₈₁ -Cl:Decyl alcohol | 1:2 | DESs | | |
| N ₈₈₈₁ -Cl:Dodecyl alcohol | 1:2 | | | |
| N ₈₈₈₁ -Cl:1-Tetradecanol | 1:2 | | | |
| N ₈₈₈₁ -Cl:Cyclohexanol | 1:2 | | | |
| N ₈₈₈₁ -Cl:DL-Menthol | 1:2 | | | |
| N ₈₈₈₁ -Cl:DL-Menthol | 1:2 | | | |
| N ₈₈₈₁ -Cl:OctanoicA | 1:1 | | | |
| N ₈₈₈₁ -Cl:DecanoicA | 1:2 | | | |
| N ₈₈₈₁ -Cl:DodecanoicA | 1:2 | | | |
| N ₄₄₄₄ -Br:DL-Menthol | 1:1 | | | |
| N ₄₄₄₄ -Br:OctanoicA | 1:1 | Solid-Liquid | Natural | |
| N ₄₄₄₄ -Br:DecanoicA | 1:1 | Extraction with | phenolic | (84) |
| N ₄₄₄₄ -Br:DodecanoicA | 1:1 | hydrophobic | antioxidants | |
| DL-Menthol:OctanoicA | 1:1 | DESs | from winery | |
| DL-Menthol:DecanoicA | 1:1 | | wastewater | |
| DL-Menthol:DodecanoicA | 2:1 | | | |
| OctanoicADecanoicA | 1:1 | | | |
| OctanoicA:DodecanoicA | 3:1 | | | |
| DecanoicA:DodecanoicA | 2:1 | | | |

2.2.3 Bio-based solvents

Following the biorefinery vision for sustainable chemical industry, the production of solvents from renewable sources and their inclusion in the process itself becomes a key task in the development of green production routes. As the biomolecules produced as building blocks, the bio-based solvents (BSs) are chemicals produced from biomass by fermentation, enzymatic processes, or esterification pathways (85). They have been considered a sustainable alternative to fossil-based solvents due to their biomass valorisation implications. It is worth noting that their suitability lies not only in their origin, but also in several other characteristics, such as biodegradability, low toxicity and ecotoxicity, and high boiling points (86). All together, these features mean important advantages of the BSs compared to the volatile organic compounds of petrochemical origin. Progress in biorefinery has also allowed for production routes replacement of conventional solvents. For instance, the production of ethyl acetate from ethanol and biomass has been recently demonstrated (87).

As BSs differ in their molecular structures, so do their properties, which expands their application range. It is possible to identify examples of compounds which have different natures, such as aprotic dipolar, apolar, amphiprotic, and polar protic (88). Recently, several BSs have been studied for the extraction of high-value biomolecules, such as lipids and carotenoids, as well as for biodiesel production applications (89). Table 2.6 lists examples of studies on the recovery of organic molecules with bio-based solvents.

Table 2.6. Examples of organic compounds recovery using bio-based solvents.

| Bio-solvent | System type | Solute | Ref. |
|---|---|--|------|
| CPME 2-MeTHF D-limonene | Liquid-Liquid Extraction | Vanilla-derived compounds from wastewater | (81) |
| CPME 2-MeTHF D-limonene | Liquid-Liquid Extraction for removal of phenolic acids | Hydroxybenzoic acids and hydroxycinnamic acids | (90) |
| CPME 2-MeTHF | Liquid-Liquid Extraction | Natural antioxidants from winery wastewater | (91) |
| CPME Ethyl lactate Isopropyl alcohol PEG 300 isopropyl acetate isopropyl acetate DMC MEK 2-MeTHF Ethyl acetate | Solid-Liquid Extraction | Limonene from orange peel waste | (92) |

2.3 Thermodynamic modelling

Phase equilibria in multicomponent systems can be modelled by equations of state or activity coefficient models. The equation of the state group aims to relate the volumetric properties of the systems (i.e., volume, temperature, and pressure) to describe their behaviour. One of the first equations of state was proposed by J. D. van der Waals in 1873. He considered two fundamental aspects: the effective volume where the molecules exist, without neglecting their own volume, and the interactions that they exhibit, which meant important progress in the description of complex systems. Since then, numerous modifications have been proposed to improve its accuracy, such as the Redlich-Kwong equation (93). Nowadays, their main representatives are the Soave-Redlich-Kwong (94) and Peng-Robinson (95) equations, which are available in most of the modern process simulation packages such as *ChemCAD*, *AspenPlus*, *Hysim*, and *PRO/II*. Based on the statistical associating fluid theory, a novel equation of state is the Perturbed-Chain-Statistical Associating Fluid Theory or PC-SAFT (96). It considers the complex molecular

interaction types, such as hard-chain, dispersion, association, polar, and ions. In the second group, the activity coefficients models allow for a direct estimation of the activities of the compounds and the excess free energies. Among them stand out the Non-Random Two Liquid model or NRTL (97), the Wilson model (98), the Universal Quasi-Chemical or UNIQUAC equation (99), and other hybrid excess free energy-based equations of state models (100).

Along with the advances in computational power, *ab initio* or “from first principles” quantum chemical methods have become a fundamental instrument in the calculation of thermochemical properties and molecular interactions understanding (101). Based on the quantum chemistry theory, several approaches have been developed to solve the wave function of quantum-mechanical systems by the electronic Schrödinger equation (102). Among them are the Quantum Structure–Property Relationship (103), the Volume-Based Thermodynamics (104), *ab initio*-Molecular Dynamics (105), and the COnductor-like Screening MOdel for Real Solvents (COSMO-RS) (106,107).

In particular, COSMO-RS combines the quantum chemistry models with dielectric continuum models, electrostatic surface interactions, and statistical thermodynamics. By screening the charge density, σ , on the molecular surface, it predicts fluid properties, essentially the chemical potential. In addition, this method is capable to model theoretical thermodynamics equilibria of liquid mixtures, even with complex interaction systems, such as those containing ionic liquids (108) or eutectics solvents (109,110). Moreover, COSMO-RS has been shown to be a valuable tool to assess the thermodynamic properties of green solvents (111) and to generate critical inputs for process simulations (112). The σ - profile of a compound is obtained from density functional theory methods that optimize the molecular geometry and electron density, illustrating key information about the nature of the compounds. As shown in Figure 2.3, the hydrogen bond donor and acceptor capacity are found in the areas at $\sigma < -0.82 \text{ e nm}^{-2}$ and $\sigma > 0.82 \text{ e nm}^{-2}$, respectively, while the non-polar region is within them.

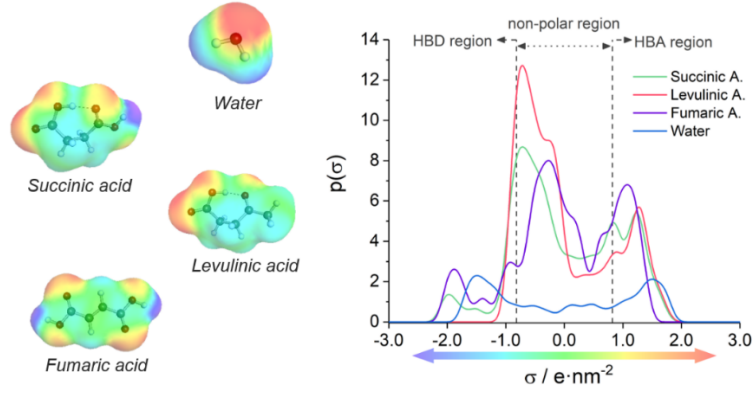


Figure 2.3. Representation of the COSMO-RS σ - surfaces (left) and σ - profiles (right) of water and representative bio-based organic acids.

The mixture σ - profile, $p_s(\sigma)$, is determined by Eq. 2.1 as the sum of the probability distribution of the surface segment charge density, $p_i(\sigma)$, pondered by the component mole fraction, x_i . The affinity of the mixture to a surface with a respective σ is quantified by the σ - potential, $\mu_s(\sigma)$, according to Eq. 2.2. Here, $e(\sigma, \sigma')$ is the total interaction energy of a molecule with charge density σ with another molecule with charge density σ' , in a surface segment a_{eff} . This energy is composed of electrostatic, hydrogen bonding, and van der Waals interactions, which are calculated by the method algorithms.

$$p_s(\sigma) = \sum_{i \in S} x_i p_i(\sigma) \quad (2.1)$$

$$\mu_s(\sigma) = -\frac{RT}{a_{eff}} \ln \left[\int p_s(\sigma') \cdot \exp \left(\frac{a_{eff}}{RT} (\mu_s(\sigma') - e(\sigma, \sigma')) \right) d\sigma' \right] \quad (2.2)$$

Finally, the chemical potential, μ_i , defined by the partial molar Gibbs free energy \bar{G}_i , is calculated by integrating the σ - potential of the compound i over the σ - profile surface plus a combinatorial contribution, $\mu_i^{C,S}$, according to Eq. 2.3. The combinatorial contribution term depends on the molecular volume, molecular area, and mole fraction, as well as three adjustable parameters, where the default values are contained in the COSMOtherm package software.

$$\mu_i^S = \bar{G}_i = \mu_i^{C,S} + \int p_i(\sigma) \mu_s(\sigma) d\sigma \quad (2.3)$$

2.4 Membrane separation technology

One of the main tasks of chemical engineering is to perform and optimize separation processes. However, conventional techniques might be not enough to accomplish the operation requirements of efficacy and efficiency. In this context, the use of membranes for molecular separations has gained industrial attention. Based on a thin semipermeable barrier, membranes can control the permeation rate of different chemical substances, giving a selective separation. This technology has an extensive heritage. First mentions of membrane phenomena date from the XVIII century, being used as laboratory tools late in the 1800s and starting their way to commercial applications in the middle of the twentieth century (113). Today, membrane science has widely spread to almost every production sector, such as the petrochemical industry (114), water treatment or desalination (115), energy production and storage (116), food processing (117), and pharmaceutical-biotechnology applications (118).

The driving force for the permeation phenomena in membranes is due to differences in the chemical potential of the species between both sides of the selective barrier. The species transport flux (J_i) is governed by a proportional coefficient (L_i) and the chemical potential gradient ($d\mu_i/dx$) across the membrane thickness, as shown in Eq. 2.4 (113). Nevertheless, depending on the target application, the chemical potential gradient might be induced by hydraulic pressure, compounds concentration, stream temperature, or electrical field. For instance, high pressure is used for reverse osmosis and nanofiltration while low pressure is applied in ultra/microfiltration. Concentration differences allow for naturally driven forward-osmosis processes. Equilibrium-based membrane distillation and pervaporation use thermal gradients. And lastly, electrodialysis exploits ion charges to accomplish their separation from the solution (119).

$$J_i = -L_i \frac{d\mu_i}{dx} \quad (2.4)$$

The semipermeable barrier is usually composed of polymers, such as cellulose, polyethersulfone, and poly(vinylidene difluoride), or inorganic materials, such as ceramic, glass, metal, and zeolites (120). However, new membrane materials are constantly proposed and tested to extend the technology's applicability. For instance, immobilized graphene oxide-based membranes have been demonstrated to improve the operation performance in desalination applications (121) and superglassy polymers of intrinsic microporosity enhance gas separation selectivity (122). The material to conform to the separation barrier can be a liquid matrix instead of a solid, in the so-called liquid membranes. Driven by differences in concentration, in this configuration, the permeability rate is controlled by the affinity of the solutes with the membrane to perform selective separation.

Although liquid membranes have also a relatively long history, no large-scale applications have been installed so far. An in-depth overview of the state-of-the-art is given in Chapter 5. Gaps in permeation models that correctly predict the experimental data, as well as process design methods, are among the causes of this technological delay.

Part II

The search for suitable green solvents for bio-based organic acids
recovery.

"I'm an optimist because I know what technology can accomplish and because I know what people can accomplish. I'm profoundly inspired by all the passion I see, especially among young people, for solving this problem. If we keep our eye on the big goal –getting to zero– and we make serious plans to achieve that goal, we can avoid a disaster."

— Bill Gates, How to Avoid a Climate Disaster

Chapter 3. Green solvents selection guide for bio-based organic acids recovery

This chapter discusses the performance of green solvents in the recovery of bio-based organic acids from fermentation broths. The broad range of solvent candidates constantly proposed in the literature evidence an important gap in their suitable selection for further studies. The presented paper (3) assesses key factors in the extraction of bio-based organic acids from aqueous matrices and establishes guidelines to serve as a roadmap to address the research on this topic.

| | |
|--------------------------------|---|
| Authors: | Pablo López-Porfiri Patricia Gorgojo María González-Miquel |
| Journal: | ACS Sustainable Chemistry & Engineering |
| Pages: | 8958–8969 |
| Volume (Issue): | 8 (24) |
| Status: | Published |
| Publication Date: | May 22, 2020 |
| DOI: | doi.org/10.1021/acssuschemeng.0c01456 |
| Supporting Information: | Appendix A, page 219 |

ACS
Sustainable
Chemistry & Engineering

pubs.acs.org/journal/acsceng

Research Article

Green Solvent Selection Guide for Biobased Organic Acid Recovery

Pablo López-Porfiri, Patricia Gorgojo, and Maria Gonzalez-Miquel*

Cite This: <https://dx.doi.org/10.1021/acssuschemeng.0c01456>

[Read Online](#)

ACCESS |

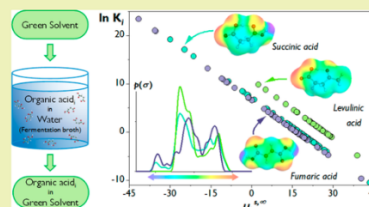
[Metrics & More](#)

[Article Recommendations](#)

[Supporting Information](#)

ABSTRACT: Biobased organic acids constitute an important group of building block chemicals that can be produced from renewable resources, becoming a sustainable alternative to conventional petrochemical-derived commodities. However, due to the growing number of green solvents emerging as extraction media, the proper solvent selection for biomolecule separation from fermentation broths has become a key challenge in the biorefinery industry. The overall aim of this work is to develop a roadmap to select and design green solvents for sustainable downstream processing of biobased organic acids. To this end, a wide range of neoteric solvents (ionic liquids, eutectic solvents, and biobased solvents) were systematically evaluated for the recovery of relevant bio-organic acids through a combination of experimental and COSMO-RS (conductor-like screening model for real solvents) molecular simulation methods. Comprehensive thermodynamic analyses evaluating the organic acid partition coefficients, excess enthalpy contributions, solvent–water affinity, and process spontaneity were performed to elucidate the main mechanism driving the separation process and to provide essential guidelines for further solvent development. On the basis of these findings, a rational screening approach was established to identify suitable solvents for the recovery of structurally different bio-organic acids. Ultimately, this paper provides a green solvent selection guide to design sustainable separation processes for biobased organic acids to serve as valuable platform chemicals to transition toward a biobased economy.

KEYWORDS: Organic acids, Ionic liquids, Eutectic solvents, Green solvents, Liquid–liquid extraction, COSMO-RS



3.1 Foreword

Finding appropriate substances for clean technology development is not a straightforward task. The literature is crowded with extraction media candidates backing their suitability in green separation processes by different criteria. However, testing every promising candidate becomes unfeasible at a research level. This work aims to contribute with a comprehensive evaluation approach by studying the underlying interactions in the liquid-liquid extraction of bio-based organic acids from model fermentation broths. Supported by experimental data and quantum chemical modelling, a selection guide of green solvents for organic acids recovery was developed. The selection criteria are based on system extractive capacity, selectivity towards water, and thermodynamic spontaneity as [Figure 3.1](#) outlines.

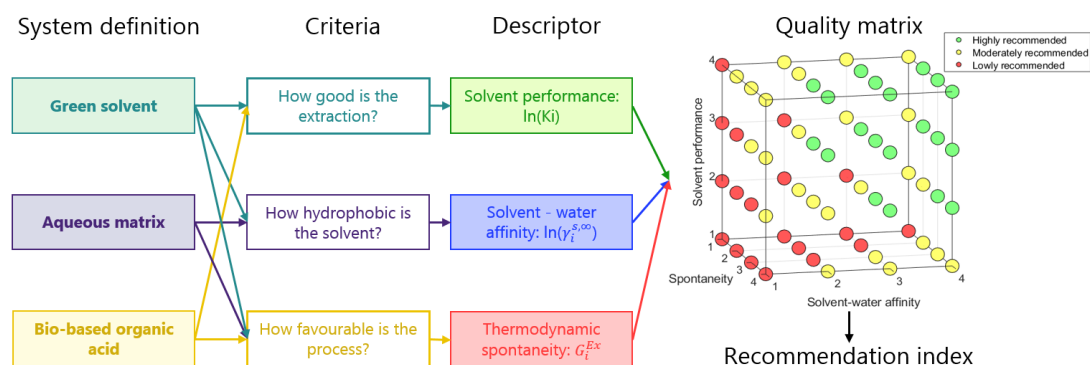


Figure 3.1. Evaluation flow diagram of green solvents for bio-based organic acids recovery from aqueous solution.

A set of 420 solute-solvent systems has been considered: six relevant bio-organic acids (succinic, levulinic, fumaric, malic, itaconic, and lactic acids), and a range of 70 hydrophobic green solvents (24 ILs, 11 ESs, 29 BSs, and 6 conventional solvents). The solvent recommendation is determined by evaluating the descriptor values, using as a reference the favourable theoretical values, i.e., $\ln(K_i) > 0$; $\ln(\gamma_w^\infty) > 0$; and $G^{ex} < 0$ and screening results as shown in [Figure 3.2](#).

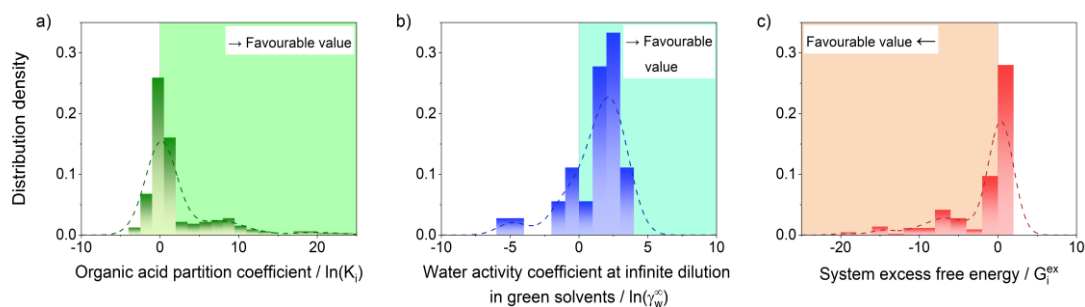


Figure 3.2. Screening results of the main descriptors for bio-based organic acids recovery from aqueous solution with green solvents. a) Solvent performance, $\ln(K_i)$; b) solvent–water affinity, $\ln(\gamma_w^\infty)$; and c) thermodynamic spontaneity, G^{ex} . Results distribution was modelled using the Kernel smooth density estimation method (123).

This study showed how the solvent-solute affinities become key in the system selection assessment, as attractive candidates might not meet the whole requirements. It is important to note that other selection criteria, e.g., toxicity, lifecycle, downstream compatibility, or techno-economics still need to be considered. These aspects depend on the specific process design and operational context. It is worth mentioning that this paper was highlighted by the *Expectations for Manuscripts Contributing to the Field of Solvents* editorial of the journal *ACS Sustainable Chemistry & Engineering*, as the appropriate way to approach evaluation studies of new extraction solvents (124). The research findings of this work will further support the development of advanced separation technologies, such as liquid membranes extraction, as it will show in the next chapters.

3.2 Abstract

Bio-based organic acids constitute an important group of building block chemicals that can be produced from renewable resources, becoming a sustainable alternative to conventional petrochemical-derived commodities. However, due to the growing number of green solvents emerging as extraction media, the proper solvent selection for biomolecule separation from fermentation broths has become a key challenge in the bio-refinery industry. The overall aim of this work is to develop a roadmap to select and design green solvents for sustainable downstream processing of biobased organic acids. To this end, a wide range of neoteric solvents (ionic liquids, eutectic solvents, and bio-based solvents) were systematically evaluated for the recovery of relevant bio-organic acids through combination of experimental and COSMO-RS molecular simulation methods. Comprehensive thermodynamic analyses evaluating the organic acid partition coefficients; excess enthalpy contributions, solvent-water affinity, and process spontaneity were performed to elucidate the main mechanism driving the separation process and to provide essential guidelines for further solvent development. Based on these findings, a rational screening approach was established to identify suitable solvents for the recovery of structurally different bio-organic acids. Ultimately, this paper provides a green solvent selection guide to design sustainable separation processes of biobased organic acids, as valuable platform chemicals transitioning towards a biobased economy.

3.3 Introduction

Currently, the need to reduce the consumption of non-renewable resources has boosted the development of biorefinery schemes and the establishment of a strong biobased industry (125). In fact, the chemical market based on a biobased platform is undergoing a dramatic increase as an alternative to petroleum-based chemicals in various consumer-goods industries, expecting to reach 22.75 billion USD by 2025, expanding at a compound annual growth rate (CAGR) of 12.6% (17). In this context, biobased organic acids have been recognized as important building blocks to be used as starting materials in the chemical industry. They can be utilized to manufacture commodity products and fine chemicals such as polymers, food, pharmaceuticals, cosmetics, solvents, and fuel additives, among others (126). The United States Department of Energy published a pivotal report entitled “*Top Value Added Chemicals from Biomass*” (16), identifying several organic acids (such as succinic, levulinic, fumaric, malic, itaconic, and lactic acids) as strategical platform chemicals that can be produced directly from carbohydrates and lignocellulose-derived sugars by fermentation (127). Recent studies considering sustainability metrics for organic acid production conclude that biobased alternatives present competitive costs with respect to their petrochemical counterparts (128); however, the authors point out the need to improve downstream steps in order to promote the biobased routes. In fact, efficient separation of bio-organic acids from fermentation broths has become a real challenge for process engineers, as their separation can demand more than two-thirds of the total cost (23). Currently, the recovery of bio-organic acids is carried out by precipitation or through liquid–liquid extraction, physical or reactive, using volatile organic compounds (VOCs) (129). Commonly used VOCs include organo-phosphorus compounds and aliphatic amines (34,37), which both are in opposition with initial green efforts. Furthermore, environmental regulations limiting the use of harmful solvents in the chemical industry (i.e., REACH, European Regulation on Registration, Evaluation, Authorisation and Restriction of Chemicals), coupled with

increasing consumer awareness and demand for more sustainable products (130), has boosted the search for alternative solvents with a more benign environmental, health and safety profile for biotechnological applications (44).

There is a rising number of greener solvent alternatives currently available, such as ionic liquids (ILs), eutectic solvents (ESs), and biobased solvents (BSs), displaying a wide range of inherent distinct physicochemical properties, which are key to the development of efficient separation processes (131-133). For this reason, fast computational tools are of chief importance to preliminarily evaluate and further develop neoteric solvents for sustainable downstream processing of target molecules. The conductor-like screening model for real solvents (COSMO-RS) is a quantum chemical method that allows for the prediction of chemical potentials and thermodynamic properties of fluid systems based on the structural information on the compounds (106). COSMO-RS has been proved a valuable method to model thermodynamic equilibria of complex novel systems such as those containing ionic liquids or eutectic solvents (108-110,134,135). Schöder et al. (136) successfully used COSMO-RS to predict the temperature-dependence solubility of carboxylic acids in water. Likewise, Zhou et al. (137) screened the mutual solubility between a wide range of ILs and water at 298.15 K, and results were successfully validated with experimental data. Moreover, COSMO-RS method has shown to be an accurate tool for the prediction of partition coefficients, mixing enthalpies and molecular interactions as key parameters to evaluate the affinity between target solutes and solvent systems (138,139).

The overall aim of this work is to provide a roadmap to select and design green solvents for the sustainable downstream processing of biobased organic acids. To this end, a wide range of neoteric solvents (ionic liquids, eutectic solvents, and biobased solvents) were systematically evaluated for the physical extraction (i.e., no reactive mechanisms involved) of relevant bio-organic acids through a combination of experimental and COSMO-RS molecular simulation methods. First, extraction experiments were performed for succinic, levulinic, and fumaric acids using representative solvents from

each family, including the optimization of the extraction conditions through the response surface methodology. Afterwards, partition coefficients of target solutes computed by the COSMO-RS method were successfully validated against the experimental extraction efficiencies. Detailed energetic contributions and molecular interaction analyses were performed to provide insights into the main mechanism driving the separation process. On the basis of these findings, a rational COSMO-RS screening was conducted over a broad range of structurally different neoteric solvents for the recovery of an extended set of bio-organic acids, helping to elucidate essential guidelines for suitable solvent development. Ultimately, this paper provides a comprehensive appraisal of green solvents for downstream processing of biobased platform chemicals to promote transitioning to a sustainable biobased economy.

3.4 Experimental section

3.4.1 Materials

Succinic, levulinic, and fumaric acids and the set of representative green solvents listed in [Table 3.1](#) were chosen as target systems for this work. Succinic acid ($\geq 99.0\%$ w/w), levulinic acid (99% w/w) and fumaric acid ($\geq 99.0\%$ w/w) were purchased from Sigma-Aldrich, as well as the ionic liquids [C₄mim][Tf₂N] ($\geq 98\%$ w/w), [C₄pyrr][Tf₂N] ($\geq 98.5\%$ w/w), [N₈₈₈₁][Tf₂N] ($\geq 99\%$ w/w). The bio-based solvents 2-MeTHF ($\geq 99.0\%$ w/w), 1,8-cineol (99% w/w), EtOAc (99% w/w) and CPME ($>99.9\%$ w/w) were purchased from Alfa Aesar. Eutectic solvents were prepared from octanoic acid ($\geq 98\%$ w/w), decanoic acid ($\geq 98.0\%$ w/w), and tetrabutylammonium chloride ($>98\%$ w/w) purchased from Sigma-Aldrich, and DL-menthol ($\geq 97.0\%$ w/w) purchased from Alfa Aesar. Reagents were used without further purification.

Table 3.1. Representative solvents studied in this work.

| Solvent | Abbreviation |
|---|--|
| <i>ILs: Ionic Liquids</i> | |
| 1-Butyl-3-methylimidazolium Bis(trifluoromethylsulfonyl)imide | [C ₄ mim][Tf ₂ N] |
| 1-Butyl-1-methylpyrrolidinium Bis(trifluoromethylsulfonyl)imide | [C ₄ pyrr][Tf ₂ N] |
| Methyl-trioctylammonium Bis(trifluoromethylsulfonyl)imide | [N ₈₈₈₁][Tf ₂ N] |
| <i>ESs: Eutectic Solvents (Molar ratio HBA : HBD)</i> | |
| DL-menthol : Octanoic acid (1:1) | DL-menthol:OctA |
| Tetrabutylammonium chloride : Octanoic acid (1:2) | N ₄₄₄₄ Cl:OctA |
| DL-menthol : Decanoic acid (1:1) | DL-menthol:DecA |
| <i>BSs: Bio-based Solvents</i> | |
| Cyclopentyl methyl ether | CPME |
| 2-Methyl tetrahydrofuran | 2-MeTHF |
| Eucalyptol | 1,8-Cineol |
| <i>Conventional Solvent</i> | |
| Ethyl acetate | EtOAc |

3.4.2 Preparation of eutectic solvents

ESs were prepared by mixing the hydrogen bond acceptor (HBA) with the hydrogen bond donor (HBD) components in its specific molar ratio. Compounds were weighted in a Mettler Toledo MS1045/01 analytical balance, with a corresponding standard uncertainty of $u(\text{mass}) = 10^{-4}$ g. The relative error on molar ratio were lower than 0.45%. The mixture was stirred in a heat bath at 50 °C until no solid was observed in the homogeneous liquid fluid.

3.4.3 Experimental extraction procedure

Model aqueous solutions were prepared to reproduce typical compositions reported in literature. Organic acids concentration in fermentation broths varied according to the substrate, fermentation path, and operational conditions. The average concentration of succinic acid in fermentation broths is about 51.9 g · L⁻¹, within a large variation range between 3.6 to 146 g · L⁻¹ (22). Levulinic acid fermentation broths usually present a mass fraction of target solute around 3–11%, equivalent to ~35–110 g · L⁻¹ approx. (37). Fumaric acid can be produced with an average concentration of 30–50 g · L⁻¹ (34). Aqueous

model solutions of organic acids were prepared by diluting the solid organic acid in Milli-Q water type 1. Initial concentrations, $[acid]_0$, were set at $50.00 \text{ g} \cdot \text{L}^{-1}$, $U_{comb}^{95.45\%}([acid]_0) \leq 0.17 \text{ g} \cdot \text{L}^{-1}$, for succinic and levulinic acids (near to the typical final broth concentrations) and $5.00 \text{ g} \cdot \text{L}^{-1}$, $U_{comb}^{95.45\%}([acid]_0) \leq 0.02 \text{ g} \cdot \text{L}^{-1}$, for fumaric acid (under saturation point at room temperature).

Physical characterization of solvents, i.e., density (ρ) and viscosity (η), were measured at $25 \text{ }^\circ\text{C}$ by using an Anton Paar DMA 4500 M density meter with a Lovis 2000 ME micro-viscometer. Likewise, the solvent saturated water content (wt_w) at $25 \text{ }^\circ\text{C}$ was measured by Karl Fisher titration using a Metrohm 899 coulometer.

Extractions were performed by mixing 4 mL of an aqueous solution with 4 mL of water-saturated solvent in a 14 mL plastic vial (solvent:feed ratio of 1:1). The vials were shaken in a Labnet Vortemp 1550 incubator for 2 h at 900 rpm at the constant temperature defined for each assay. Extraction conditions were previously optimized to ensure that the thermodynamic equilibrium was reached. Phase separation was carried out in a Labnet Spetrafuge 6C centrifuge at 6500 rpm for 1 h, and afterward, the vials were placed in a Labnet Accublock dry bath for 12 h at a constant temperature.

The extraction yield, $\%Ex$, is defined according to Eq. 3.1, where $[acid]_0$ and $[acid]_f$ correspond to the initial and final organic acid concentration in the aqueous phase, respectively.

$$\%Ex = \frac{[acid]_0 - [acid]_f}{[acid]_0} \quad (3.1)$$

All solvents were saturated with pure Milli-Q water type 1 before the extraction to ensure that the phase volumes remain constant, fulfilling the mass balance for the calculation of the extraction yield, $\%Ex$.

The final organic acid concentration in the aqueous phase was analysed by UV-Vis spectrophotometry performed in a Shimadzu UV-2700. Calibration curves were built at wavelengths of 230, 283, and 285 nm for succinic, levulinic,

and fumaric acids, respectively. All the experiments have been performed in triplicate. Experimental data reported include the respective uncertainty expressed as a confidence level of 95.45% ($CL_{95.45\%}$), which are calculated according to the directions of Chirico et al. (140) and Miller and Miller (141).

The effect of the operating conditions, i.e., temperature (T) and solvent:feed ratio (S/F), on the extraction performance was explored through response surfaces. The selected systems were composed of the best solvent candidates of each family (IL, ES, and BS) and succinic, levulinic, and fumaric acids. The extraction experiments were performed following the procedure described above, assuming the same uncertainty obtained on the extraction essays. Conditions were established as $T = 25, 40, \text{ and } 55 \text{ }^\circ\text{C}$ and $S/F = 0.5$ (2:4 mL), 1 (4:4 mL), and 1.5 (6:4 mL).

3.4.4 COSMO-RS Approach

The quantum chemical COnductor-like Screening Model for Real Solvents (COSMO-RS) method employs the screening charge density on the molecular surface, σ , to predict thermophysical fluid properties and thermodynamic phase equilibrium (107). Under phase equilibrium, extraction yields can be expressed as the organic acid partition coefficient ($K_i / \text{mol mol}^{-1}$) between the aqueous and solvent phases. At low solute concentration the partition coefficient can be predicted by modelling the organic acid activity coefficient at infinite dilution ($\gamma^{\alpha,\infty} / \text{mol mol}^{-1}$) (142) according to Eq. 3.2, where α correspond to the solvent phase, i.e., green solvent phase (s) or aqueous phase (w).

$$K_i = \frac{x_i^s}{x_i^w} = \frac{\gamma_i^w}{\gamma_i^s} \approx \frac{\gamma_i^{w,\infty}}{\gamma_i^{s,\infty}} \quad (3.2)$$

$\gamma^{\alpha,\infty}$ can be determined computing the chemical potentials, according to Eq. 3.3, where μ_i^a and μ_i^p correspond to the compound i chemical potential in the α -phase or as a pure substance, respectively. Therefore, the partition coefficient can be expressed according to Eq. 3.4:

$$RT \cdot \ln(\gamma_i^\alpha) = \mu_i^\alpha - \mu_i^p \quad (3.3)$$

$$\ln(K_i) \approx \frac{\mu_i^{w,\infty} - \mu_i^{s,\infty}}{RT} \quad (3.4)$$

On the other hand, attractive or repulsive interactions can be identified as a function of the free excess energy, G^{ex} according to Eq. 3.5, with more negative values (i.e., lower G^{ex} , lower H^{ex} , and lower $-TS^{ex}$), being related to more spontaneous phenomena.

$$G^{ex} = H^{ex} - TS^{ex} \quad (3.5)$$

The COSMO-RS method allows for the calculation of the activity coefficients and the excess energies, even specific interactions such as hydrogen bond (HB), electrostatics or misfit (MF), and van der Waals forces (vdW) can be determined through the excess enthalpy contribution (Eq. 3.6), providing a comprehensive description of the studied system.

$$H^{ex} = H_{HB}^{ex} + H_{MF}^{ex} + H_{vdW}^{ex} \quad (3.6)$$

Computational calculations were performed using the *COSMOtherm* software, version C30, release 18.0.2, at the parametrization BP_TZVP_18.

3.5 Results and discussion

3.5.1 Experimental extraction yields

Organic acid extraction yields were determined for a series of green solvents including ionic liquids (ILs), eutectic solvents (ESs) and bio-based solvents (BSs). EtOAc was also included as a conventional benchmark solvent for physical extraction. Experiments were performed at room temperature and solvent:feed ratio of 1:1. The results are shown in Figure 3.3. Estimated expanded combined uncertainties were $U_{comb}^{95.45\%}(\%Ex_{Succ}) \leq 2.6\%$, $U_{comb}^{95.45\%}(\%Ex_{Lev}) \leq 0.95\%$, and $U_{comb}^{95.45\%}(\%Ex_{Fum}) \leq 3.2\%$, for succinic, levulinic, and fumaric acid, respectively.

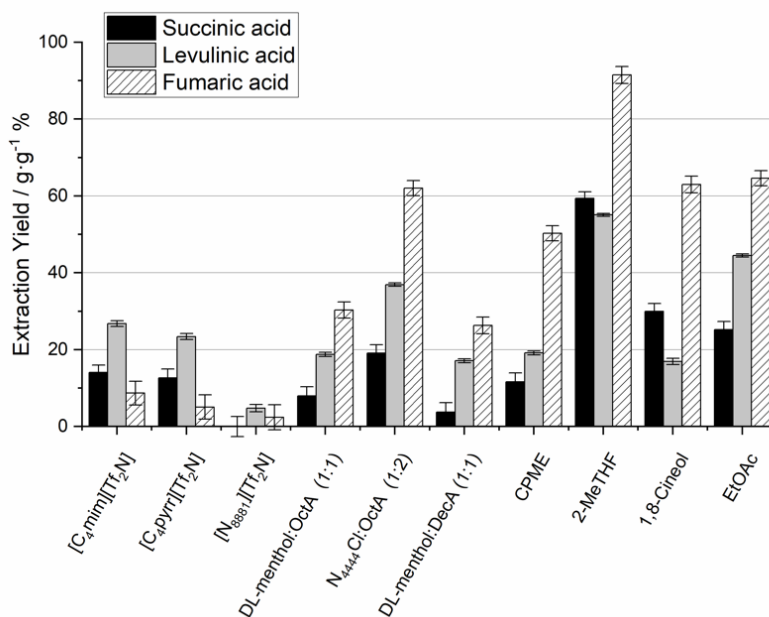


Figure 3.3. Experimental organic acid extraction yields at a temperature of 25 °C and solvent:feed ratio of 1 using various green solvents.

3.5.2 Solvent family performance

ILs show the lower extraction performance for the three organic acids, $\%Ex_{IL} \leq 26.8\%$, with all of them providing the higher recovery yields for levulinic acid. No significant differences are observed between 1-butyl-3-methylimidazolium [C₄mim]-based and 1-butyl-1-methylpyrrolidinium [C₄pyrr]-based ILs, which exhibit the same trend through organic acids recovery regardless of the aromatic or nonaromatic nature of the cation. Gonzalez et al. (143) reported consistent conclusions on their study focused on phenolic compounds extraction with aromatic, 1-hexyl-3-methylimidazolium [C₆mim], and nonaromatic, 1-hexyl-1-methylpyrrolidinium [C₆pyrr], cation-based ILs; such work suggested that the solute hydrophobicity seems to have a major effect than the aromatic cation nature on the extraction process. On the other hand, methyl-trioctylammonium [N₈₈₈₁]-based IL presented the lowest extraction yields. Experimental results indicate that the three large alkyl chains (C₈) impart the solvent a lower polarity and higher viscosity hindering solvent-solute interactions formation and limiting mass transfer. Extraction yields of succinic and fumaric acids with [N₈₈₈₁][Tf₂N] present no significant differences under the estimated uncertainty.

A comparative study on phenols and aromatic amides extraction capacities of different cation-based ILs was carried out by Egorov et al (144). The authors found higher recovery efficiencies using quaternary ammonium-based ILs, even better than those obtained using imidazolium-based ILs. This led them to conclude that dispersive forces between quaternary ammonium cations and those solutes are predominant over the π - π interactions between the aromatic group and the IL and that hydrogen bonding interactions may be present when using imidazolium cations. Nevertheless, the capability of some organic acids to interact through intramolecular hydrogen bonding, while lacking aromatic groups, could be the reason for the opposite trends observed in this work, as discussed in detail in a subsequent section.

All ESs show similar organic acid extraction performance trend: $\%Ex_{Succ} < \%Ex_{Lev} < \%Ex_{Fum}$. Menthol-based ESs show comparable extraction yields with no significant differences respect to the fatty acid alkyl chain length component (HBD), i.e., octanoic acid and decanoic acid. In addition, N₄₄₄₄Cl:OctA presents a better overall extraction performance; however, its high water content, $w_{t_w} = 0.1379 \text{ g} \cdot \text{g}^{-1}$, indicates an important hydrogen bond presence that may affect solvent selectivity. Florindo et al. (66) studied the stability of ES in water for several menthol-based and N₄₄₄₄Cl-based solvents by NMR analysis. In the case of the N₄₄₄₄Cl:OctA, the authors report a migration of the quaternary ammonium salt to the aqueous phase due to its hydrophilicity, while no leaching of DL-menthol:OctA was observed. Leaching of salt components from hydrophobic ESs has been reported before in the work of van Osch et al. (73), who observed a decrease in the salt loss for longer alkyl chain lengths. Likewise, Reyhanitash et al. (132) reported a significant amount of salt migration to the aqueous phase of [P₆₆₆₁₄]-based ILs during the extraction of acetic acid, attributed to an ion-exchange mechanism; however, the specific complexation mechanism strongly depends on the extracting solvent-acid interactions (145). Nonetheless, in this work, the solvent phase was visible throughout all extraction experiments. Despite the possibility of some salt leaching could bring disadvantage to real applications,

the better extraction efficiency provided by ES should be taken into account; hence, the solvent stability should be studied extensively to determine the prospects of this extraction technology.

The high extraction yields, $\%Ex_{BS} \leq 91.5\%$, and low water contents, $wt_w \leq 0.0448 \text{ g} \cdot \text{g}^{-1}$, of BSs show a better selectivity toward organic acid than the previous solvent families. Two distinct trends have been found in BSs results, including (1) for CPME, where the lower extraction is observed for succinic acid, and (2) for 2-MTHF and 1,8-cineol, where the succinic acid extraction yields are higher than for levulinic acid. However, in all cases, fumaric acid presents a higher extraction. Contrarily to ILs and ESs, BSs and conventional solvents are simple single-component systems with higher volatilities, which mean weaker like-molecule interactions. Consequently, the performance obtained is attributed to the hydrogen bonding interactions between the oxygen atom in the solvent and the organic acid. Additionally, BSs and EtOAc have a significantly lower viscosity, which improves the mass transfer process under the experimental conditions.

3.5.3 Effect of organic acid structure

In terms of the general trends for the three representative organic acids, succinic acid presents the poorest extraction yield for all four solvent families: $\%Ex_{Succ-IL} \leq 14.1\%$, $\%Ex_{Succ-ES} \leq 19.1\%$, $\%Ex_{Succ-BS} \leq 59.3\%$, and $\%Ex_{Succ-EtOAc} = 25.2\%$ for ILs, ESs, BSs, and EtOAc respectively. Oliveira et al. (36) studied organic acid extraction with phosphonium-based ILs at different initial concentrations, obtaining succinic acid extraction efficiencies higher than 73%. Nevertheless, the ILs ([P₆₆₆₁₄]-based ILs) used in the aforementioned work present lower hydrophobicity, $wt_w \leq 0.1600 \text{ g} \cdot \text{g}^{-1}$ at 25 °C (146), than the [Tf₂N]-based ILs, $wt_w \leq 0.0142 \text{ g} \cdot \text{g}^{-1}$, used in this work. The implications of this factor will be discussed later.

Only levulinic acid shows acceptable yields, $\%Ex_{Lev-IL} \geq 20\%$, with ILs as extractants. Moreover, it presents higher extraction yields than succinic acid for all solvents, except for 2-MeTHF and 1,8-cineol. The methyl group present

in levulinic acid imparts a less polar nature to this molecule in comparison to the carboxyl groups present in the other organic acids; thus, in the aqueous phase, the interactions are preferentially water–water over water–levulinic acid, enhancing the extraction.

Lastly, fumaric acid presents the highest recovery yield with ESs, BSs and EtOAc. Differently to the succinic and levulinic acids, fumaric acid has a lower water solubility, less than $6.95 \text{ g}\cdot\text{L}^{-1}$ at $25 \text{ }^\circ\text{C}$ (147); hence, the poor water affinity facilitates its extraction. Likewise, the carbon–carbon double bond does not allow the formation of internal hydrogen bonds, leaving the two carboxyl groups free to interact with the solvent functional groups. Nonetheless, ILs are not able to provide high fumaric acid extraction yields. This can be explained by considering the lower polarity of such solvents and their lower capacity to efficiently interact through hydrogen bonding with the solute.

3.5.4 Effect of extraction conditions

To evaluate the extraction behaviour of organic acids as a function of the operating conditions, response surfaces were built for a representative green solvent of each family (i.e., ionic liquids, eutectic solvents, and biobased solvents). The solvents chosen were those providing better overall organic acid extraction performance, i.e., IL, $[\text{C}_4\text{mim}][\text{Tf}_2\text{N}]$; ES, DL-menthol:OctA; and BS, 2-MeTHF. The results of response surface parameter variations for each organic acid + solvent system are illustrated in [Figure 3.4](#).

Extraction of succinic acid with $[\text{C}_4\text{mim}][\text{Tf}_2\text{N}]$ has no significant changes, $U_{\text{comb}}(\%EX_{\text{Succ}}) \leq 2.6\%$, neither with temperature nor solvent:feed ratio. Levulinic acid extraction shows a notable increase at higher S/F ratio values, in the range of 11–18%, and minor growths with increasing temperature, less than 6.6%. A different behaviour is observed for fumaric acid, as the yields barely vary with S/F and are reduced an average of 4.6% when the temperature is increased. ES based on DL-menthol:OctA shows minor organic acid recovery variations with the temperature, which tends to decrease at higher

temperatures. Moreover, at 55 °C, succinic acid recovery becomes not significant. On the other hand, the extraction capacity of the solvent DL-menthol:OctA increases by up to 6% for succinic acid, 14% for levulinic acid, and 19% for fumaric acids at higher *S/F* values. Extraction yields using 2-MeTHF have a significant increase when increasing *S/F*, showing increments of 12 to 32% for succinic acid, 17 to 36% for levulinic acid, and 1 to 25% for fumaric acid. Contrarily, the yields decrease up to 23, 15, and 26% with increasing temperature for succinic, levulinic, and fumaric acids, respectively. Overall, the solubility of organic acids increases faster in the aqueous phase than in the extraction solvent at higher temperatures, diminishing the recovery. Meanwhile, the probability to establish efficient hydrogen bonding interactions increases at higher solvent:feed ratios, hence improving the extraction.

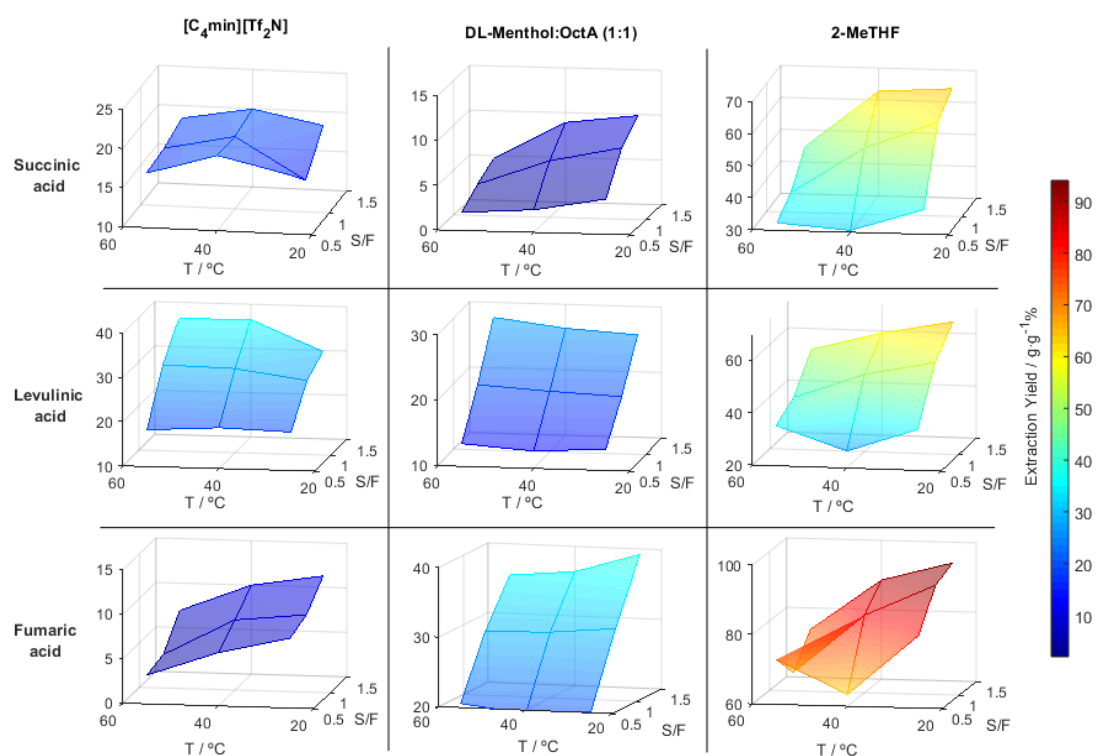


Figure 3.4. Experimental response surface plots representing the effect of temperature and solvent:feed ratio on the extraction yield of organic acids using the green solvents [C₄mim][Tf₂N], DL-menthol:OctA (1:1), and 2-MeTHF.

Another relevant aspect to consider for the extraction of biobased organic acids is the acidity of the fermentation broth. The overall mass transfer mechanism may be divided into the physical extraction stage, where the acid passes from the aqueous phase to the solvent phase that is conditioned to the extraction constant, and an acid–base equilibria stage, where the aqueous acid concentration in its molecular form is determined by the pK_a constant (129). Since physical extraction requires the solute to appear as a molecular form, i.e., nondissociated state, the pH value of the aqueous phase may be determinant.

The acid dissociation is determined by the Henderson–Hasselbalch equation (Eq. 3.7), where $[A^-]$ and $[AH]$ correspond to the dissociated and molecular acid concentration, respectively. Therefore, the acid recovery is improved at aqueous pH values lower than the corresponding pK_a values, i.e., when the acid equilibria is favoured toward the molecular state.

$$pH = pK_a + \log_{10} \frac{[A^-]}{[AH]} \quad (3.7)$$

Table A.0.3 and Table A.0.4 show the pK_a values of the biobased organic acids considered in this work and the measured pH values of the aqueous solutions prepared for the experimental extraction essays. Overall, it can be seen that the pH values of the organic acid aqueous solutions used in this work are lower than the pK_a values of the solutes, hence supporting that the organic acids were preferentially in their molecular form, facilitating the extraction.

3.5.5 Validation of COSMO-RS methodology

The probability distribution of a molecular surface segment having a specific charge density, i.e., the so-called σ – profile, is a valuable property to interpret key information about the nature of the compound. The hydrogen bond donor and acceptor capacity, at areas $\sigma < -0.82 \text{ e nm}^{-2}$ and $\sigma > 0.82 \text{ e nm}^{-2}$, respectively, and the non-polar region within, can be determine through this property. Figure 3.5a shows the σ – profile of water and the organic acids studied in this work. The COSMO-RS method also takes into consideration the conformer (stable molecular configurations) population for its calculation,

which is determined based on the free energy Boltzmann distribution. Some succinic and levulinic acid conformers may form intramolecular hydrogen bonds. This leads to the loss of its peak in the HBD region, [Figure 3.5b](#), and its capacity to interact through hydrogen bonding with other molecules, varying the global system behaviour. The competition of attractive hydrogen bonding interactions between like and unlike species in ES formation has been suggested before as a relevant effect on overall interactions within the system [\(10\)](#). Hence this effect becomes an important consideration for a more rigorous thermodynamic analysis.

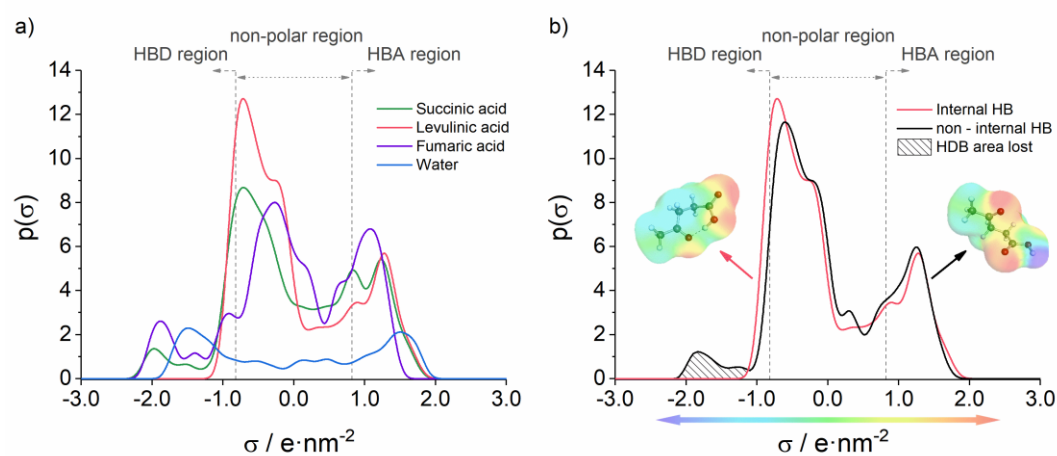


Figure 3.5. a) σ - Profile of succinic acid (in green); levulinic acid (in red); fumaric acid (in purple); and water (in blue). b) Examples of σ - Profile conformers: Levulinic acid showing internal hydrogen bonding (in red); levulinic acid showing non-internal hydrogen bonding (in black).

COSMO-RS calculations were corroborated with the experimental data through a statistically significant linear correlation of the extraction performance, $\%Ex$, versus the natural logarithm of the partition coefficient, $\ln(K_i)$, as shown in [Figure 3.6](#). The regression was weighted inversely by considering the experimental uncertainty of each data point to consider their variability. Consistent results are obtained between experimental and modelling methods in terms of qualitative trends of the solvents to recover organic acids from aqueous solutions. Thus, overall results support the validation of the proposed computational methodology as a useful tool to qualitatively predict the extraction ability of green solvents.

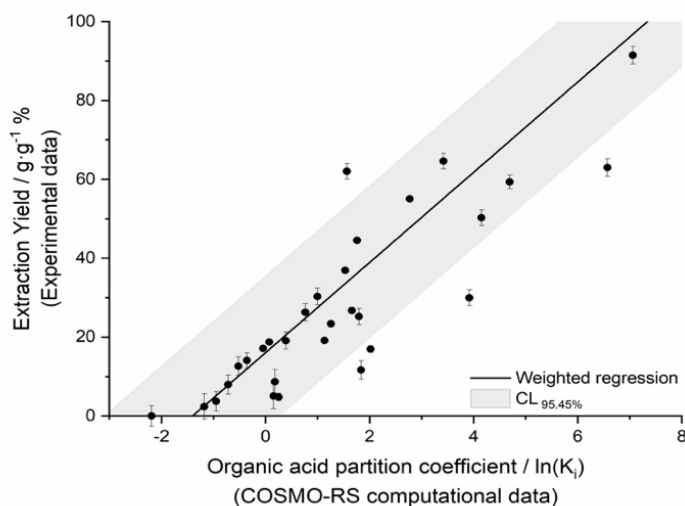


Figure 3.6. Correlation between experimental extraction yield, %*Ex*, at 25 °C and solvent:feed ratio of 1, and partition coefficients computed with COSMO-RS at 25 °C, of organic acids using green solvents, $r^2 = 0.7$.

3.5.6 Thermodynamic analysis using COSMO-RS

COSMO-RS allows providing insights into the thermodynamic behaviour of mixtures based on the excess enthalpy, H^{ex} , contributions (i.e., hydrogen bonding (HB), electrostatic interactions (MF), and van der Waals forces (vdW)) and excess entropy (expressed as $-TS^{ex}$). Computed interaction energies of binary systems composed of organic acid + solvents and water + solvents are summarized in [Figure 3.7](#). Succinic and levulinic acids conformers were divided into two groups: (i) internal HB, i.e., those forming intramolecular hydrogen bonds; and (ii) non-internal HB, i.e., those not forming intramolecular hydrogen bonds. A special case is fumaric acid, since the carbon-carbon double bond present in the middle of its structure avoids the internal HB formation. For each computed system, a conformer weighting analysis was considered in order to complement the study of the molecular interaction behaviour.

The poor solvent solubility in water is attributed to the so-called “hydrophobic effect”. In this effect, an entropic phenomenon plays an important role ([148](#)), in addition to the fact that the vdW interactions in water are weaker than HB ([149](#)). Moreover, water can form a complex interaction network, due to its ability to assume a tetrahedral distribution with a total of

four HB. Therefore, interactions with itself are stronger than with other nonpolar groups (150).

The aforementioned enthalpic effect is observed in water–IL interactions, [Figure 3.7d](#), showing a predominantly positive HB contribution, i.e., energy is needed to break the water–water HB in order to mix with the IL. This explains their low mutual affinity and the better extraction performance for levulinic acid over succinic and fumaric acid. The system for water + menthol-based ESs presents negative (favourable) HB and positive (repulsive) MF contributions, while the system for water + N₄₄₄Cl-based ESs shows a large negative excess enthalpy according to the contribution energies, supporting its high water content. The latter behaviour is also observed, at a lesser extent, for water + BSs. In those cases, a large positive excess entropy ($-TS^{\text{ex}}$) drives the hydrophobic effect, forming a complex order within the system for the interactions formed.

Excess enthalpies of organic acids in the aqueous phase are negative. The interactions are mainly HB, and only levulinic acid, [Figure 3.7b](#), has a significant MF and vdW contribution to the total enthalpy, attributed to its methyl group. Moreover, the conformer-weighting establishes that the most stable kind of configurations are the non-internal HB contributions, for both succinic and levulinic acids in water (approximately two-thirds and four-fifths of the total molecules, respectively). This denotes the organic acid affinity with water and suggests that the acids have a more stable configuration, forming HB with water molecules rather than with themselves when they are in an aqueous solution.

Succinic and levulinic acids show appreciable positive HB interactions with the ILs. Succinic acid conformer-weighting remains without significant changes with respect to water, while levulinic acid internal HB conformers increase from one-fifth to one-third, suggesting the preference of a molecule to form intramolecular HB over the IL solvents. Additionally, both succinic and levulinic acids exhibit positive excess entropies (negative $-TS^{\text{ex}}$),

suggesting a more spontaneous process despite their repulsive H^{ex} contribution energies. Instead, fumaric acid, [Figure 3.7c](#), shows weak interactions in all energetic contributions with ILs. Those effects may hinder the phase transfer and explain the low extraction efficiency values experimentally obtained for fumaric acid when using ILs.

Menthol-based ESs show positive, or nearly null, MF enthalpy contributions with the organic acids. This may cause a decrease in the extraction performance in comparison to $N_{4444}Cl$ -based ESs. $N_{4444}Cl:OctA$ shows the larger increment of non-internal HB conformers of succinic and levulinic acids, up to 20% more with respect to non-internal HB conformers in water. These increments agree with its large negative HB energy and positive $-TS^{ex}$ value in solution.

The analysis of interaction for BSs corroborates the trend observed in the experimental results: the large negative HB energy of organic acid + BS systems justifies the good extraction yields obtained. Levulinic and succinic acids show positive MF energy in CPME and 1,8-cineol, which proportionally decreases the extraction (see [Figure 3.3](#)). Due to the large HB interactions in BS, a significant increase of the non-internal HB conformer with respect to the aqueous solution is observed for succinic and levulinic acids. On the other hand, all energetic contributions are negative for the fumaric acid + BS system.

Energetic results suggest an entropic–enthalpic compensation throughout the studied systems. With the exception of organic acid + $N_{4444}Cl:OctA$ and succinic acid + DL-menthol:OctA systems, the excess entropy, $-TS^{ex}$, of all systems composed of organic acid + solvent are smaller than those of water + solvent systems. On the other hand, the systems with a more favourable enthalpic contribution display a better recovery performance. Consequently, it is possible to establish that the core driving force in the extraction process is the formation of strong interactions, mainly HB, giving the system a “higher order”. On the basis of the energetic analysis and molecular interactions discussed above, extraction results agree with the thermodynamics basis. The

recovery is improved for those systems that exhibit more negative excess enthalpies and greater excess entropies (lower $-TS^{\text{ex}}$) in the solvent phase, i.e., a more negative Gibbs free energy.

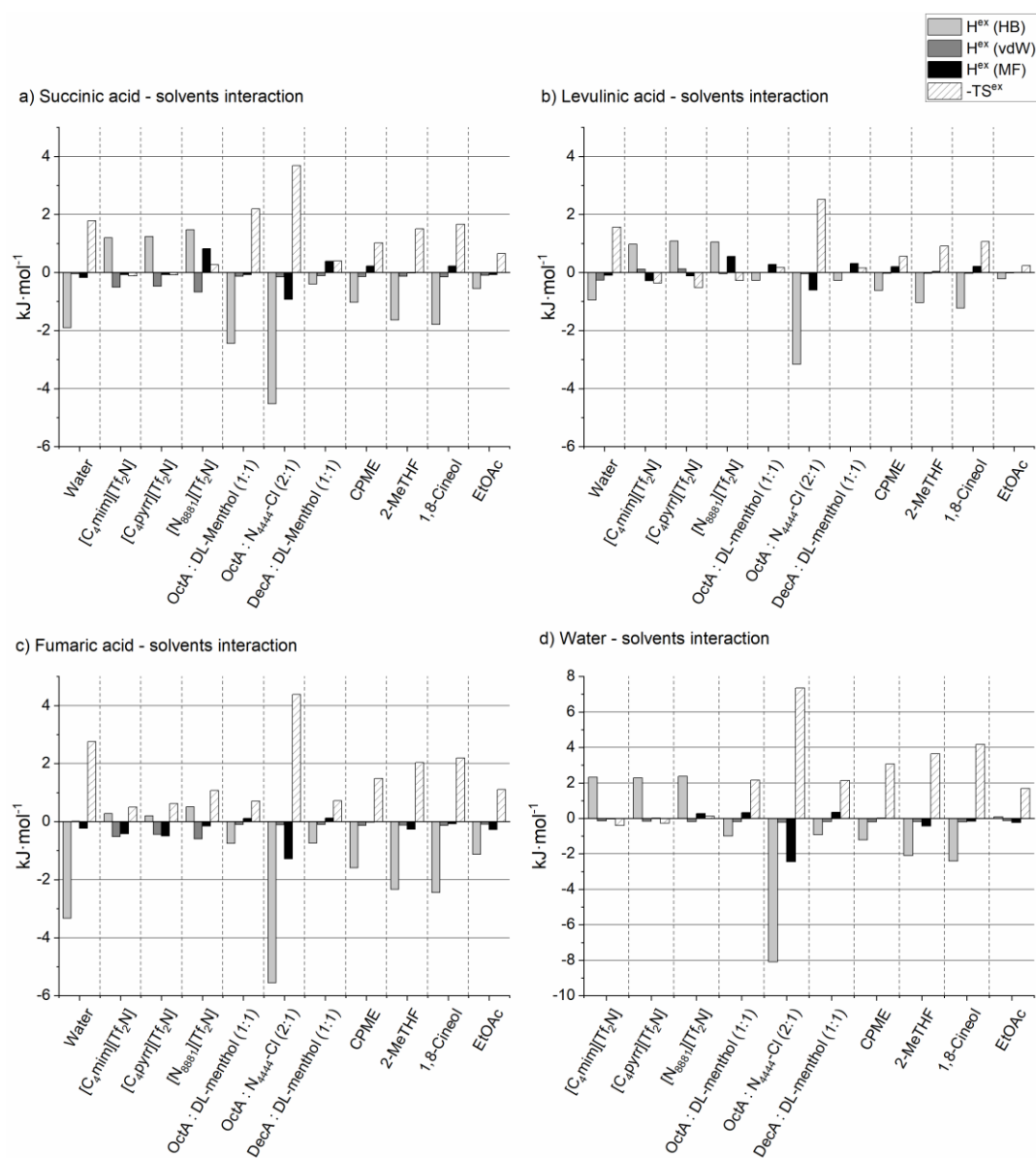


Figure 3.7. Excess enthalpy (H^{ex}) contributions and excess entropy ($-TS^{\text{ex}}$) of binary systems composed of organic acid-solvent and water-solvent mixtures at 25 °C, as computed by the COSMO-RS method, including a) succinic acid + solvent, b) levulinic acid + solvent, c) fumaric acid + solvent, and d) water + solvent systems.

3.5.7 Screening of green solvents for extraction of bio-organic acids

On the basis of the previous methodology and analyses, a COSMO-RS screening in terms of partition coefficients, $\ln(K_i)$, has been performed to evaluate the extraction efficiency for an extended set of 420 solute–solvent systems. To provide a compressive overview of potential green solvents for the recovery of biobased organic acids, six relevant bio-organic acids (i.e., succinic, levulinic, fumaric, malic, itaconic, and lactic acids) and a range of 70 hydrophobic solvents (24 ILs, 11 ESs, 29 BSs, and 6 conventional solvents) have been considered. The solvent selection includes ILs based on different cation–anion families (i.e., imidazolium-, phosphonium-, pyrrolidinium-, ammonium-, and sulfonium-based ILs paired with a variety of anions), ESs composed of hydrogen bond acceptor–donors of different nature (i.e., menthol, thymol, lidocaine, ammonium salts, and organic acids of increasing alkyl chain lengths), BSs covering renewable molecular biobased solvents showing distinct structures, and benchmark conventional solvents often used in physical and reactive extractions of organic acids from aqueous solutions. Solvent screening results for the extraction of relevant biobased organic acids are shown in [Figure 3.8](#).

ILs show a clear preference for both levulinic and itaconic acids, with partition coefficients several times higher than those of other organic acids, which can be attributed to their respective methyl and vinyl functional groups. On the other hand, fumaric acid does not seem to present a particular affinity toward ILs, contrasting with the results observed for others ESs or BSs. [Tf₂N]-based ILs show a better overall performance than [FAP]-based and [PF₆]-based ILs. In terms of cation effects, the alkyl chain length of the imidazolium components does not appear to play a significant role. However, hydroxyl-functionalized cations, i.e., [(OH)C₂C₁im]-cation and [(OH)C₂C₁pyrr]-cation, resulted in higher organic acid partition coefficients. Note that [P₆₆₆₁₄]-based ILs and [N₈₈₈₁:Dicyanamide] provide high organic acid partition coefficients, yet those solvents also present higher water affinities, hence decreasing the

selectivity during the extraction process, which will be discussed in detail later. ESs show positive $\ln(K_i)$ values for all organic acids, except for succinic and malic acids. According to their most stable conformers, those acids present higher capacity to form intramolecular hydrogen bonds. Therefore, considering that HB is the main interaction involving ES (72), the lack of available $-OH$ groups to form a bond with target solutes results in poor recovery. Charged-nature HBA compounds, i.e., quaternary ammonium salts, provide higher partition coefficients than noncharged HBA. Nonetheless, as was discussed above, those ESs may undergo salt leaching to the aqueous phase, compromising its stability. On the other hand, BSs show an overall consistent trend regarding their capacity to recover organic acids, where the solvents with favourable partition coefficients, i.e., $\ln(K_i) \leq 0$, show a good performance for all organic solutes under consideration. The wide range of results obtained for the six structurally different organic acid compounds illustrates the importance of the proper solvent selection. Typical nonpolar solvents found in the industry, such as hexane and other chlorinated compounds, have a poor affinity with the carboxyl groups of the organic acids; hence, the obtained partition coefficients are negligible, i.e., $\ln(K_i) \leq 0$. Nevertheless, the methyl group in levulinic acid enhances the partition coefficients with dichloromethane and chloroform. Contrarily, the organic solvents tributyl-phosphate and trioctylamine show excellent organic acid recoveries, with $\ln(K_i) > 1.8$ and 7.1 , respectively. These partition coefficients are in agreement with the extraction efficiencies of carboxylic compounds with organophosphorus and aliphatic amines that are reported in the literature (151–154). Tributyl-phosphate and trioctylamine are often used pure or as an additive with other nonpolar solvents in reactive extraction due to their capacity to form complexes.

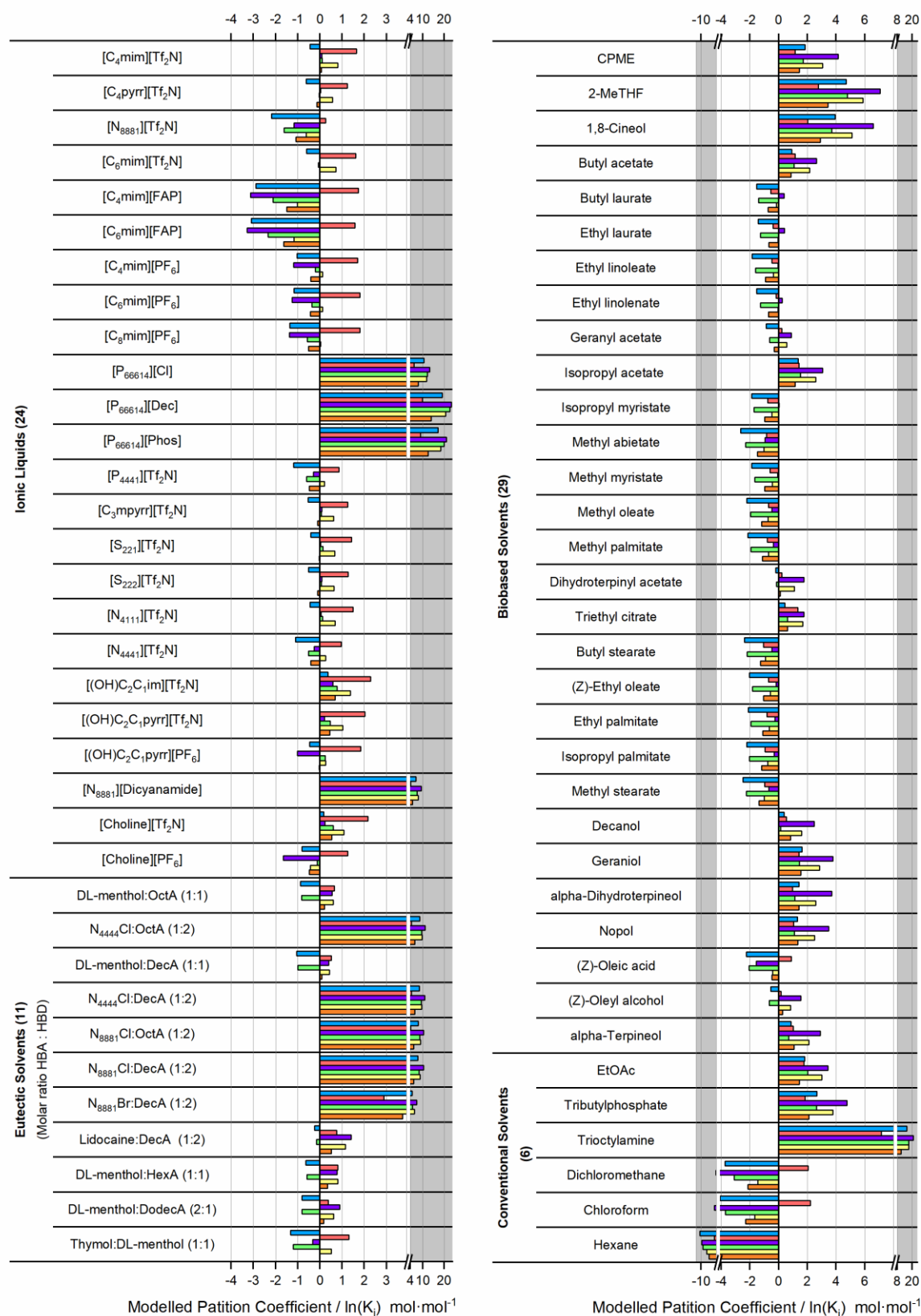


Figure 3.8. Screening of green solvents for extraction of organic acids in terms of solute partition coefficients, $\ln(K_i)$: succinic acid (in blue); levulinic acid (in red); fumaric acid (in purple); malic acid (in green); itaconic acid (in yellow); and lactic acid (in orange), as computed with COSMO-RS at 25 °C.

The modelled partition coefficients depend directly on the organic acid chemical potential in both phases. As [Figure 3.9a](#) shows, the linear relationship between $\ln(K_i)$ and $\mu_i^{s,\infty}$ (Eq. 2.4) explains the results observed on the screened solvents in terms of the mass transfer driving force within the phases. Despite its high water solubility, 743.1 g·L⁻¹ at 25 °C (147), the cases where levulinic acid shows the better extraction performance are due to its high chemical potential in water; while the larger partition coefficients are as a result of the lower chemical potential of the acid in the solvents. The relationship of the organic acid preference for the extraction solvent and its hydrophobicity has been reported in the literature (129).

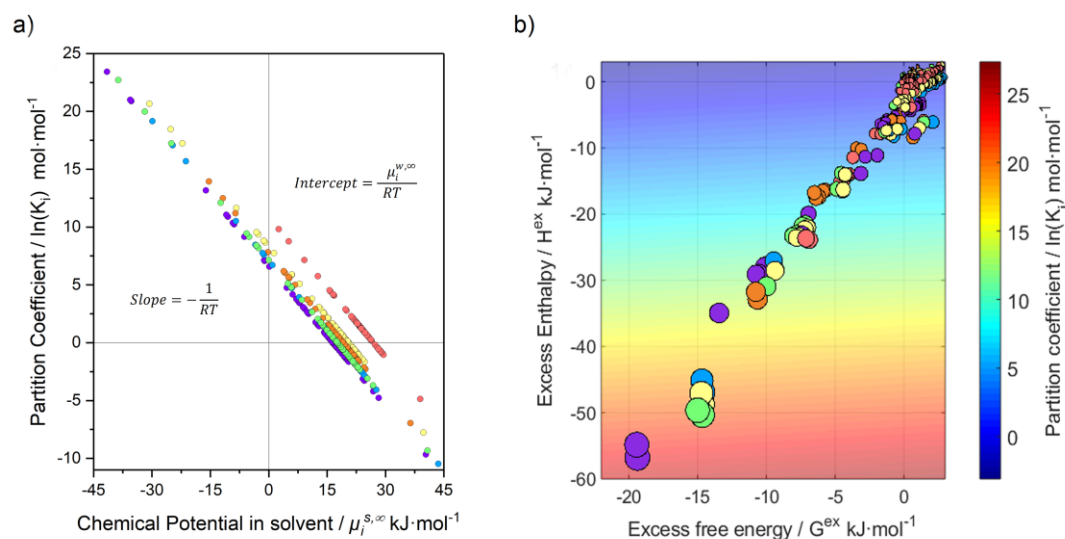


Figure 3.9. a) Partition coefficients, $\ln(K_i)$, dependence of organic acid chemical potential on the screened solvents at infinite dilution, $\mu_i^{s,\infty}$; b) Relationship between organic acid partition coefficients, $\ln(K_i)$, with the screened solvents and: organic acid–solvent excess free energy, G^{ex} , on the x -axis; organic acid–solvent excess enthalpy, H^{ex} , on the y -axis; and organic acid–solvent excess entropy ($-TS^{\text{ex}}$) which are proportional to marker size. Succinic acid (in blue); levulinic acid (in red); fumaric acid (in purple); malic acid (in green); itaconic acid (in yellow); and lactic acid (in orange), computed with COSMO-RS at 25 °C.

The energetic analysis of the screened solvents is summarized in [Figure 3.9b](#), where each organic acid + solvent system was located according to its respective excess free energy, G^{ex} , on the x -axis; excess enthalpy, H^{ex} , on the y -axis; and its excess entropy, $-TS^{\text{ex}}$, proportional to its marker size. The aforementioned properties were correlated to the partition coefficient, $\ln(K_i)$, through a response surface. As was discussed above, better extractions should be observed for those systems with lower excess free energy. Although it is

possible to see that the better extraction solvents are those systems displaying higher spontaneity (lower G^{ex}), the results show a clear trend related to excess enthalpy. At lower H^{ex} , the partition coefficients increase, while at lower G^{ex} and constant H^{ex} , there are no significant improvements. Furthermore, partition coefficients increase at greater $-TS^{\text{ex}}$ (more negative excess entropy). The consistent behaviour throughout all organic acids and extraction solvents agrees with the entropic–enthalpic compensation mentioned above. Therefore, the solvent extraction performance depends on its capacity to form strong interactions with the organic acids, which implies increasing the order within the system. However, the overall process is still spontaneous. This compensation keeps them on a uniform trend, confirming that the main driving force of the process is the new interactions formed between the solvent and the organic acids over the organic acid–water affinity.

Among the energy contributions, i.e., HB, MF, and vdW, toward these newly formed interactions, an energetic analysis shows that they are formed mainly through HB, while MF has a minor influence. Both contributions are shown to be correlated with the extraction performance, despite the organic acid analysed. Contrarily, the vdW forces do not appear to be a significant contribution to H^{ex} ; however, it depends on the specific organic acid. Nevertheless, the large dispersion on the vdW contribution with respect to the partition coefficients precludes the determination of its importance on the general trend.

Since the hydrogen bonding was identified as the main interaction between the organic acids and both solvent phases, the solvent–water affinity becomes a key factor in both the extraction performance and selectivity. The solvent–water affinity can be expressed as the water activity coefficient at infinite dilution in the green solvents, $\ln(\gamma_w^\infty)$. As previously observed in the experimental results, the computational values support that higher solvent–water affinities, i.e., lower $\ln(\gamma_w^\infty)$ values, can be related to higher organic acid partition coefficients. The hydrophobicity of ILs has been attributed to the length of the alkyl chain, to the temperature, and mainly to

the anion component (60,155). The hydrophobicity of the anions follows the trend: [FAP] > [Tf₂N] > [PF₆] > [BF₄] > halides (156). Moreover, the formation of reverse micelles within the hydrophobic IL-phase has been discussed in the literature (129), where small amounts of the aqueous phase, rich in organic acid, may provide higher $\ln(K_i)$ values but may compromise the selectivity. Likewise, ESs attribute their hydrophobicity to the fatty acid alkyl chain length (73). Consequently, a careful selection of the extraction solvent should be adopted to improve the organic acid recovery, considering the water absorption capacity and its potential implications on the process requirements.

3.5.8 Green solvent selection guide

Over the course of this work, three main descriptors to assess the suitability of green solvents for organic acids recovery had been identified: (i) solvent performance, $\ln(K_i)$; (ii) solvent–water affinity, $\ln(\gamma_w^\infty)$; and (iii) thermodynamic spontaneity, G^{ex} . On the basis of such descriptors, a green solvent selection guide has been developed, as illustrated in Table 3.2. The method employs a quality matrix, where a solvent recommendation index is determined by multiplying the quality score of each descriptor, using as a reference the favourable theoretical values, i.e., $\ln(K_i) > 0$; $\ln(\gamma_w^\infty) > 0$; and $G^{\text{ex}} < 0$. Subsequently, solvents are classified as highly recommended, moderately recommended, and lowly recommended for the recovery of each relevant bio-organic acid.

Table 3.2. Green solvent selection guide for bio-based organic acids recovery. (●) Highly recommended; (○) Moderately recommended; (●) Lowly recommended.

| Green solvent | Succinic acid | Levulinic acid | Fumaric acid | Malic acid | Itaconic acid | Lactic acid |
|---|---------------|----------------|--------------|------------|---------------|-------------|
| Ionic Liquids | | | | | | |
| [C ₄ mim][Tf ₂ N] | ● | ○ | ○ | ○ | ○ | ● |
| [C ₄ pyrr][Tf ₂ N] | ● | ○ | ○ | ○ | ○ | ● |
| [N ₈₈₈₁][Tf ₂ N] | ● | ○ | ○ | ○ | ○ | ● |
| [C ₆ mim][Tf ₂ N] | ● | ○ | ○ | ○ | ○ | ● |
| [C ₄ mim][FAP] | ● | ○ | ○ | ○ | ○ | ● |
| [C ₆ mim][FAP] | ● | ○ | ○ | ○ | ○ | ● |
| [C ₄ mim][PF ₆] | ● | ○ | ○ | ○ | ○ | ● |
| [C ₆ mim][PF ₆] | ● | ○ | ○ | ○ | ○ | ● |
| [C ₆ mim][PF ₆] | ● | ○ | ○ | ○ | ○ | ● |
| [P ₆₆₆₁₄][Cl] | ○ | ○ | ○ | ○ | ○ | ○ |
| [P ₆₆₆₁₄][Dec] | ○ | ○ | ○ | ○ | ○ | ○ |
| [P ₆₆₆₁₄][Phos] | ○ | ○ | ○ | ○ | ○ | ○ |
| [P ₄₄₄₁][Tf ₂ N] | ● | ○ | ○ | ○ | ○ | ● |
| [C ₃ pyrr][Tf ₂ N] | ● | ○ | ○ | ○ | ○ | ● |
| [S ₂₂₁][Tf ₂ N] | ● | ○ | ○ | ○ | ○ | ● |
| [S ₂₂₂][Tf ₂ N] | ● | ○ | ○ | ○ | ○ | ● |
| [N ₄₁₁₁][Tf ₂ N] | ● | ○ | ○ | ○ | ○ | ● |
| [N ₄₄₄₁][Tf ₂ N] | ● | ○ | ○ | ○ | ○ | ● |
| [(OH)C ₂ C ₁ im][Tf ₂ N] | ○ | ○ | ○ | ○ | ○ | ○ |
| [(OH)C ₂ C ₁ pyrr][Tf ₂ N] | ○ | ○ | ○ | ○ | ○ | ○ |
| [(OH)C ₂ C ₁ pyrr][PF ₆] | ● | ○ | ○ | ○ | ○ | ● |
| [N ₈₈₈₁][Dicyanamide] | ○ | ○ | ○ | ○ | ○ | ○ |
| [Choline][Tf ₂ N] | ○ | ○ | ○ | ○ | ○ | ○ |
| [Choline][PF ₆] | ● | ○ | ○ | ○ | ○ | ● |
| Eutectic Solvents (Molar ratio HBA : HBD) | | | | | | |
| DL-menthol:OctA (1:1) | ● | ○ | ○ | ○ | ○ | ● |
| N ₄₄₄₄ Cl:OctA (1:2) | ○ | ○ | ○ | ○ | ○ | ○ |
| DL-menthol:DecA (1:1) | ● | ○ | ○ | ○ | ○ | ● |
| N ₄₄₄₄ Cl:DecA (1:2) | ○ | ○ | ○ | ○ | ○ | ○ |
| N ₈₈₈₁ Cl:OctA (1:2) | ○ | ○ | ○ | ○ | ○ | ○ |
| N ₈₈₈₁ Cl:DecA (1:2) | ○ | ○ | ○ | ○ | ○ | ○ |
| N ₈₈₈₁ Br:DecA (1:2) | ○ | ○ | ○ | ○ | ○ | ○ |
| Lidocaine:DecA (1:2) | ● | ○ | ○ | ○ | ○ | ○ |
| DL-menthol:HexA (1:1) | ● | ○ | ○ | ○ | ○ | ○ |
| DL-menthol:DodecA (2:1) | ● | ○ | ○ | ○ | ○ | ○ |
| Thymol:DL-menthol (1:1) | ● | ○ | ○ | ○ | ○ | ○ |
| Biobased Solvents | | | | | | |
| CPME | ○ | ○ | ○ | ○ | ○ | ○ |
| 2-MeTHF | ○ | ○ | ○ | ○ | ○ | ○ |
| 1,8-Cineol | ○ | ○ | ○ | ○ | ○ | ○ |
| Butyl acetate | ○ | ○ | ○ | ○ | ○ | ○ |
| Butyl laurate | ○ | ○ | ○ | ○ | ○ | ○ |
| Ethyl laurate | ○ | ○ | ○ | ○ | ○ | ○ |
| Ethyl linoleate | ○ | ○ | ○ | ○ | ○ | ○ |
| Ethyl linolenate | ○ | ○ | ○ | ○ | ○ | ○ |
| Geranyl acetate | ○ | ○ | ○ | ○ | ○ | ○ |
| Isopropyl acetate | ○ | ○ | ○ | ○ | ○ | ○ |
| Isopropyl myristate | ○ | ○ | ○ | ○ | ○ | ○ |
| Methyl abietate | ○ | ○ | ○ | ○ | ○ | ○ |
| Methyl myristate | ○ | ○ | ○ | ○ | ○ | ○ |
| Methyl oleate | ○ | ○ | ○ | ○ | ○ | ○ |
| Methyl palmitate | ○ | ○ | ○ | ○ | ○ | ○ |
| Dihydroterpinyl acetate | ○ | ○ | ○ | ○ | ○ | ○ |
| Triethyl citrate | ○ | ○ | ○ | ○ | ○ | ○ |
| Butyl stearate | ○ | ○ | ○ | ○ | ○ | ○ |
| (Z)-Ethyl oleate | ○ | ○ | ○ | ○ | ○ | ○ |
| Ethyl palmitate | ○ | ○ | ○ | ○ | ○ | ○ |
| Isopropyl palmitate | ○ | ○ | ○ | ○ | ○ | ○ |
| Methyl stearate | ○ | ○ | ○ | ○ | ○ | ○ |
| Decanol | ○ | ○ | ○ | ○ | ○ | ○ |
| Geraniol | ○ | ○ | ○ | ○ | ○ | ○ |
| alpha-Dihydroterpineol | ○ | ○ | ○ | ○ | ○ | ○ |
| Nopol | ○ | ○ | ○ | ○ | ○ | ○ |
| (Z)-Oleic acid | ○ | ○ | ○ | ○ | ○ | ○ |
| (Z)-Oleyl alcohol | ○ | ○ | ○ | ○ | ○ | ○ |
| alpha-Terpineol | ○ | ○ | ○ | ○ | ○ | ○ |
| Conventional Solvents | | | | | | |
| EtOAc | ○ | ○ | ○ | ○ | ○ | ○ |
| Tributylphosphate | ○ | ○ | ○ | ○ | ○ | ○ |
| Trioctylamine | ○ | ○ | ○ | ○ | ○ | ○ |
| Dichloromethane | ○ | ○ | ○ | ○ | ○ | ○ |
| Chloroform | ○ | ○ | ○ | ○ | ○ | ○ |
| Hexane | ○ | ○ | ○ | ○ | ○ | ○ |

The solvent assessment developed in this work highlights the need to consider the relationships among different aspects related to the extraction phenomenon for the solvent selection. For instance, high extraction yields may be jeopardized by a lower selectivity from water, as in the case of [P₆₆₆₁₄]-based ILs; while the overall performance of highly hydrophobic solvents, e.g., [FAP]-based ILs and conventional solvents, strongly depends on the molecular structure of the organic acid, as indicated by the spontaneity values. Finally, it should be noted that recommendations are built from the methodology and analysis presented above, combining experimental results with computer-aided tools focused on thermodynamic aspects. Therefore, the final solvent selection must also consider nontechnical parameters such as the toxicity or operational cost among others inherent to the target process. Nevertheless, the guidelines established in this work entail a compressive framework for solvent selection in the early stages of process design for biobased organic acid recovery.

3.6 Conclusions

Identifying the underlying mechanisms driving extraction is key in developing sustainable downstream processes based on neoteric solvents. The appraisal of green solvents for the recovery of bio-organic acids performed in this work provides a fundamental understanding of the thermodynamic behaviour of such complex systems. The molecular structure of the solvents is a decisive factor affecting the overall extraction performance. Energetic effects related to enthalpy–entropy compensation, phase affinities, and competitive intramolecular/intermolecular interactions determine the solvent's capacity to effectively recover biobased organic acids from aqueous media. Overall, this paper allows the establishment of strategic guidelines and recommendations to select and design suitable solvents for the sustainable downstream processing of target biobased platform chemicals to support the development of biobased industries.

Chapter 4. Solubility study and thermodynamic modelling of succinic acid and fumaric acid in bio-based solvents

Specific solute-solvent interactions of organic acids in bio-based solvents are studied in this chapter. System affinities are identified from solubility measurement and solid-liquid equilibria modelling helping to understand the underlying mechanisms driving the dissolution phenomenon. This work has been submitted for publication and at the time of this thesis writing, it was under revision (4).

| | |
|--------------------------------|--|
| Authors: | Pablo López-Porfiri Patricia Gorgojo María González-Miquel |
| Journal: | - |
| Pages: | - |
| Volume (Issue): | - |
| Status: | Under review |
| Publication Date: | - |
| Doi: | - |
| Supporting Information: | Appendix B, page 227 |

Solubility Study and Thermodynamic Modelling of Succinic Acid and Fumaric Acid in Bio-based Solvents

Pablo López-Porfiri¹, Patricia Gorgojo^{1,2,3}, and María Gonzalez-Miquel^{1,4}*

¹Department of Chemical Engineering, Faculty of Science and Engineering, The University of Manchester, Manchester M13 9PL, UK.

²Nanoscience and Materials Institute of Aragón (INMA) CSIC-Universidad de Zaragoza, C/ Mariano Esquillor s/n, 50018 Zaragoza, Spain.

³Chemical and Environmental Engineering Department, Universidad de Zaragoza, C/ Pedro Cerbuna 12, 50009 Zaragoza, Spain.

⁴Departamento de Ingeniería Química Industrial y del Medioambiente, ETS Ingenieros Industriales, Universidad Politécnica de Madrid, C/ José Gutiérrez Abascal 2, Madrid, Spain.

*Corresponding author. E-mail: maria.gonzalezmiquel@upm.es

4.1 Foreword

After liquid-liquid extraction of bio-based organic acids from aqueous fermentation broths, they need to be purified in downstream processes. Organic acids are not simple solutes, as in their pure form are solid crystals, they dissociate in aqueous solutions, and might form strong interactions with solvents. This makes the phase change-based separation process highly energy-consuming, meaning a major obstacle in the establishment of green production routes. Optimal design is therefore required to reduce the impact of the operation. As evidenced in the previous chapter, the knowledge of solute-solvent interactions allows for a proper system performance evaluation in chemical processes. Furthermore, thermodynamic parameters, such as solubility and activity coefficients, are fundamental for process design.

The article's graphical abstract, depicted in [Figure 4.1](#), summarises the work presented in this chapter. The solid-liquid equilibria of organic acids in bio-based solvents were measured and modelled to offer a comprehensive overview of the molecular interactions. Succinic and fumaric acids were selected in this study due to their high melting point, while bio-based solvents were due to their volatility. Overall results provide insights into the mechanisms driving the dissolution process as well as the energies associated with this phenomenon.

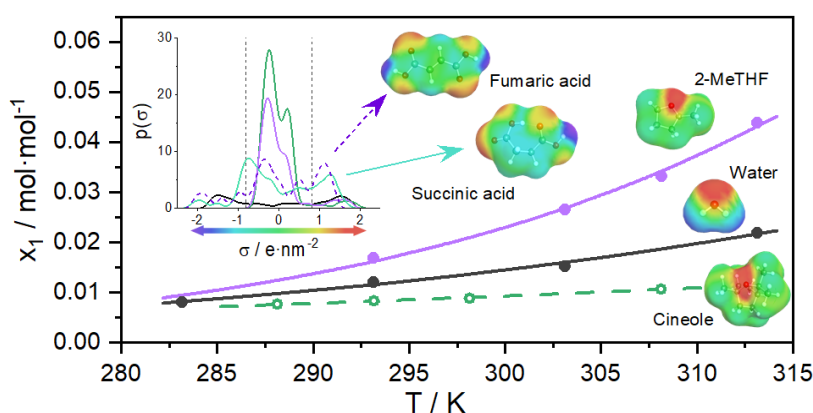


Figure 4.1. Schematic representation of the experimental results and the charge density profiles used to perform the thermodynamic modelling of the mixtures of succinic acid and fumaric acid in bio-based solvents.

4.2 Abstract

The solubility and thermodynamic behaviour of organic acids in green solvents are relevant to the design of sustainable biorefinery downstream processes. In this work, the solubility of two important bio-based organic acids such as succinic acid and fumaric acid, in water and four bio-based solvents (i.e., ethyl acetate, 1,8-cineole, cyclopentyl methyl ether, and 2-methyl tetrahydrofuran) were measured within a temperature range of [283 – 313] K. A gravimetric methodology was adopted, previously validated using the organic acid aqueous solubilities available in the literature. The reported data present an average estimated uncertainty of measurement, with a level of confidence of 95%, of $5.2 \cdot 10^{-4}$ mol mol⁻¹. Experimental results were correlated with the van't Hoff equation, the modified Apelblat equation, and the Buchowski- Ksiazaczak λh model, where the root mean squared deviations were less than $3.9 \cdot 10^{-4}$ for all systems. From the experimental data and the COSMO-RS molecular simulation method, the solid-liquid equilibria were modelled to estimate the excess energies and the solute activity coefficients of the saturated solutions. Excess enthalpy contribution analysis shows that attractive hydrogen-bonding interactions between the organic acids and the green solvents drive the dissolution phenomena. The magnitude of the hydrogen-bonding interactions increases with temperature for all systems, agreeing with the observed solubility trends. The organic acid energies of solution were estimated from the van't Hoff equation, demonstrating an enthalpy-entropy compensation effect. The energetic analysis shows that the dissolution phenomenon is an enthalpy-driven process for fumaric acid, whereas no predominant effect is observed for succinic acid.

4.3 Introduction

Nowadays, a global urge to reduce fossil fuel consumption along with the increasing governmental environmental regulations encourages green routes in chemical manufacturing (130). In this context, the production of bio-based molecules from renewable sources in the biorefinery industry is key to addressing such a challenge (125). Their use as chemical building blocks allows replacing petrochemical-based compounds in the production of solvents, food, textiles, cosmetics, pharmaceuticals, detergents, as well as other chemical commodities (126).

In particular, the United States Department of Energy has identified bio-based organic acids, among other target building blocks, as strategic platform chemicals (16). Succinic acid and fumaric acid are two bio-based organic acids that can be produced by fermentation starting from lignocellulose-derived sugars (22,34). However, despite being acknowledged as a competitive alternative to the petrochemical routes, there is still a need to improve its downstream recovery and purification processes (128). After fermentation, separation of the bio-based organic acids from the aqueous broths is usually carried out by liquid-liquid extraction (LLX) with volatile organic compounds, such as organophosphorus compounds or aliphatic amines, which is a clear mismatch with their green purpose (34,37). Moreover, the separation stage is critical, with a cost representing more than two-thirds of the total production cost (23).

Due to the aforementioned reasons, the search for alternative solvents presenting more benign environmental, health and safety features for biotechnological uses is receiving increasing attention (44). A large number of hydrophobic green novel solvents have been proposed and systematically evaluated to fulfil the current gap in bio-based organic acids recovery (3). Although several of them have proved their capacity for the extraction task, basic thermodynamic properties such the solute solubilities and solution energies are still needed to carry out proper separation and purification

process design. It is possible to find in the literature experimental studies on the solubility of succinic acid in several organic solvents, such as isopropanol (157); water-methanol and water-ethanol mixtures (158); binary mixtures of cyclohexanone, cyclohexanol, and cyclohexane (159); binary mixtures of methanol, ethanol, and propanol (160); as well as on the solubility of fumaric acid in n-propanol, isopropanol, ethanol and acetone (161). Nevertheless, most of the aforementioned solvents show polar nature, excluding them for LLX from aqueous matrices. Based on the molecular structural information, the quantum chemical COnductor-like Screening Model for Real Solvents (COSMO-RS) method is capable of predicting the chemical potential of the compounds and thereby further thermodynamics properties (106). COSMO-RS method has been shown to accurately predict the temperature-dependence of the solubility of carboxylic acids in water (136). Likewise, the method allows identifying solute-solvent affinities by computing mixing enthalpies and molecular interactions, as well as partition coefficient estimations, which have been used to evaluate solvents candidates for sustainable LLX (138,139). COSMO-RS predictions had been thoroughly assessed by contrasting with experimental data (162). The average absolute relative deviations (AARD) of infinite dilution activity coefficients resulted in 84.6% and 58.5% for the TZVP-COSMO and TZVPD-FINE and parametrization levels, respectively. Likewise, the infinite dilution partial excess enthalpy showed an AARD of 244% and 255% for the above parametrizations. On the other hand, COSMO-RS predictions of free energies of hydration showed an accuracy of approximately 0.5 kcal mol⁻¹ (163).

The objective of this work is to perform a solubility study of succinic acid and fumaric acid in aqueous solutions and target bio-based solvents. 1,8-Cineole, also known as eucalyptol (Cineole), cyclopentyl methyl ether (CPME), and 2-methyl tetrahydrofuran (2-MeTHF) have been selected based on their good performance towards the recovery of such organic acids, as shown in our previous work (3). We have also included ethyl acetate (EtOAc), a conventional solvent providing high organic acids extraction yields, which

has been recently demonstrated that can be also produced from renewable sources (87). The obtained experimental solubilities have been correlated with thermodynamic models including the van't Hoff equation, the modified Apelblat equation, and the Buchowski-Ksiazaczak λh model. The molecular interactions, in terms of excess energies, within the saturated mixture were modelled with the COSMO-RS method. In addition, the energies of solution have been estimated from the van't Hoff equation to better understand the organic acids dissolution process phenomenon. Overall, the results derived from this work will contribute to the development and design of green routes for bio-based organic acids recovery, promoting sustainable downstream processes in the biorefinery industry.

4.4 Materials and methods

4.4.1 Materials

Succinic acid ($\geq 99.0\%$ w/w, CAS: 110-15-6), fumaric acid ($\geq 99.0\%$ w/w, CAS: 110-17-8), cineole (99% w/w, CAS: 470-82-6), and 2-MeTHF ($\geq 99.0\%$ w/w, CAS: 96-47-9) were purchased from Sigma-Aldrich. EtOAc (99% w/w, CAS: 141-78-6) and CPME ($> 99.9\%$ w/w, CAS: 5614-37-9) were purchased from Alfa Aesar. Reagents were used without further purification. Both organic acids were kept in a desiccator to avoid water absorption due to hygroscopicity. High purity water (Milli-Q type 1) was produced in the laboratory. [Table 4.1](#) shows some of the relevant properties for the experimental and modelling procedures of the compounds used in this work, including the moisture content in the bio-based solvents measured using a Karl Fisher titrator prior to the experiments. The molecular structures of the compounds can be found in [Figure 4.2](#).

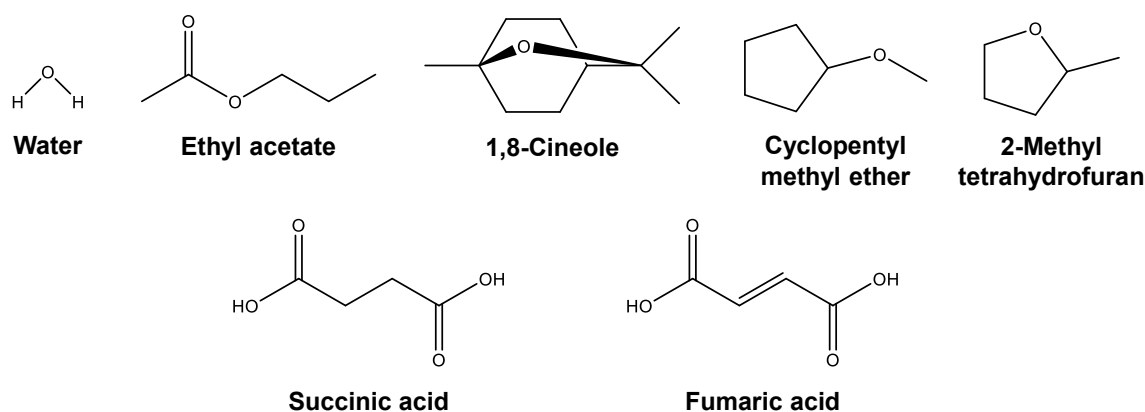
Table 4.1. Properties of bio-based solvents and organic acids used in this work.

| Compound | Abbreviation | MW | BP ^a | MP ^b | Water content ^c |
|--------------------------|--------------|---------------------|--------------------|--------------------|-------------------------------------|
| | | g mol ⁻¹ | T _b / K | T _m / K | wt _w / g g ⁻¹ |
| Water | - | 18.02 | 373.15 | - | - |
| Ethyl acetate | EtOAc | 88.11 | 350.15 | - | 0.0003 |
| 1,8-Cineole | Cineole | 154.25 | 449.15 | - | 0.0024 |
| Cyclopentyl methyl ether | CPME | 100.16 | 379.15 | - | 0.0005 |
| 2-Methyl tetrahydrofuran | 2-MeTHF | 86.13 | 351.15 | - | 0.0001 |
| Succinic acid | - | 118.09 | - | 455.2 | - |
| Fumaric acid | - | 116.07 | - | 562.55 | - |

^a Boiling point according to the suppliers.

^b Melting point (164).

^c Measured by Karl Fisher titration at 25 °C using a Metrohm 899 coulometer. Standard uncertainty for water content, $u(wt_w) \leq 10^{-7} \text{ g g}^{-1}$.

**Figure 4.2.** Molecular structures of the bio-based solvents and organic acids studied in this work.

4.4.2 Experimental procedure

The solubilities of succinic acid and fumaric acid in the bio-based solvents and water were obtained using a gravimetric method, by weighting the solids deposited after the complete evaporation of a saturated solution of [organic acid (1) + solvent (2)]. First, a feed oversaturated solution, i.e., a solution with visible suspended crystals, was prepared at a high temperature (> 60 °C). Then, 2 ml of the feed solution were centrifuged for 3 h in a Sigma 4-16KS refrigerated centrifuge at a controlled fixed temperature of the data point measurement and a relative centrifugal force (RCF) of 23,506g. Lastly, 1 ml of the saturated supernatant was weighed in a Mettler Toledo MS1045/01 analytical scale in a previously weighted glass vial, and let dry overnight in a

vacuum oven at 10 Pa and a temperature set at the boiling point of the solvent. The dry crystallized solid (i.e., just the organic acid) was weighed again to obtain the organic acid mass contained within the saturated supernatant sample. The solubility, expressed as the saturated acid mole fraction, $x_1 / \text{mol mol}^{-1}$, was calculated following Eq. 4.1, where M_{vial} , M_{dry} , and M_{solution} correspond to the vial mass, the dry organic acid plus the vial mass, and the saturated supernatant plus the vial mass, respectively. The mass standard uncertainty is $u(\text{mass}) = 1.48 \cdot 10^{-4} \text{ g}$. Measurements were performed in triplicate, reporting the mean value along with their respective uncertainty of measurement with a confidence level of 95% (LC_{95%}) calculated according to NIST directions (165).

$$x_1 = \frac{M_{\text{dry}} - M_{\text{vial}}}{MW_1} \cdot \left[\frac{M_{\text{dry}} - M_{\text{vial}}}{MW_1} + \frac{M_{\text{solution}} - M_{\text{dry}}}{MW_2} \right]^{-1} \quad (4.1)$$

4.4.3 Solubility correlations

The solid-liquid equilibria of a system composed of a mixture miscible in the liquid phase but completely immiscible in the solid phase can be expressed throughout Eq. 4.2. According to it, two main factors are relevant in the compound solubility: the saturated solute activity coefficient in the liquid phase, $\gamma_1 / \text{mol mol}^{-1}$, to quantify the non-ideality within the system; and the solute enthalpy of fusion, $\Delta H_m / \text{kJ mol}^{-1}$, a temperature-dependent property, which is integrated between the system temperature, T / K , and the solute melting point, T_m / K . Eq. 4.2 also utilizes the gas constant, $R / \text{kJ mol}^{-1} \cdot \text{K}^{-1}$. Different correlations have been proposed in the literature for an easier approach to expressing the solubility data. These correlations are derived from the analysis and simplifications of Eq. 4.2, employing empirical parameters (p) fitted from experimental data.

$$\ln(x_1 \cdot \gamma_1) = \int_T^{T_m} \frac{\Delta H_m(T)}{R} d\left(\frac{1}{T}\right) \quad (4.2)$$

The **van't Hoff equation** (Eq. 4.3) is one of the more broadly thermodynamic models used to correlate solubility with temperature (166). It has two non-dependent temperature empirical parameters, named p_1 and p_2 in this work, respectively related to the entropy and enthalpy of solution, hence giving a good overview of the system non-ideality.

$$\ln(x_1) = p_1 + \frac{p_2}{T} \quad (4.3)$$

The **Modified Apelblat equation** (Eq. 4.4) uses two empirical parameters, p_1 and p_2 , to describe the non-ideality as the van't Hoff equation, but additionally, it includes a third term with an extra parameter, p_3 , to take into account the temperature effect into the enthalpy of solution (167).

$$\ln(x_1) = p_1 + \frac{p_2}{T} + p_3 \cdot \ln(T) \quad (4.4)$$

The **Buchowski-Ksiazaczak λh model** (Eq. 4.5) is a two-parameter solubility correlation that also includes the solute melting point, T_m / K. It states λ as the system non-ideality measure (p_1) and h as the enthalpy of solution (p_2). The correlation assumes both parameters as approximately constant with the temperature (168).

$$\ln\left(1 + \frac{p_1 \cdot (1 - x_1)}{x_1}\right) = p_1 \cdot p_2 \left(\frac{1}{T} - \frac{1}{T_m}\right) \quad (4.5)$$

To fit the experimental solubilities of organic acids reported in this work to the above-described correlations, the minimization of the root mean squared deviation, $\delta(x_1)$, of the N-data points was used as the objective function (OF), showed in Eq. 4.6, where x_1^{exp} and x_1^{cal} correspond to the experimental data and the data calculated from each solubility correlation, respectively. A MatLab® script has been developed to obtain the respective fitted values of the correlation parameters.

$$OF: \min[\delta(x_1)] = \min \left[\sqrt{\frac{1}{N} \sum (x_1^{exp} - x_1^{cal})^2} \right] \quad (4.6)$$

4.4.4 COSMO-RS approach

Thermodynamic phase equilibria can be modelled from the screening charge density, $\sigma / e \text{ nm}^{-2}$, on the molecular surface by the quantum chemical COnductor-like Screening Model for Real Solvents (COSMO-RS) method (107). Through this property, the model can compute the chemical potential of the organic acid (1) as a pure compound, $\mu_1 / \text{kJ mol}^{-1}$, and mixed in the α -phase, $\mu_1^{\alpha} / \text{kJ mol}^{-1}$. For a multi-component system, the solid-liquid equilibrium (SLE) is determined by Eq. 4.7, considering the free energy of the specie in each phase. Herein, the $\Delta G_{fus} / \text{kJ mol}^{-1}$ denotes the compound Gibbs free energy of fusion which can be estimated or provided. To enhance the model predictions, ΔG_{fus} might be obtained from the experimental data given the saturated molar concentration, $x_1 / \text{mol mol}^{-1}$, at a fixed temperature, T / K .

$$\mu_1 + \Delta G_{fus}(T) = \mu_1^{\alpha} + RT \ln(x_1) \quad (4.7)$$

By combining the COSMO-RS method and the experimental results, the equilibria of the system can be solved, allowing to determine the solute activity coefficient, $\gamma_1^{\alpha} / \text{mol mol}^{-1}$, of the saturated solution by Eq. 4.8. Additionally, it is possible to identify specific molecular interactions, i.e., attractive or repulsive forces within the mixtures, by computing the saturated mixture excess energies: excess Gibbs free energy, $G^E / \text{kJ mol}^{-1}$, excess enthalpy, $H^E / \text{kJ mol}^{-1}$, and excess entropy expressed as $-TS^E / \text{kJ mol}^{-1}$, according to Eq. 4.9. Furthermore, a deeper understanding of these interactions can be obtained from the contributions to H^E . These energies are divided into electrostatic energy (MF), hydrogen bonding (HB), and van der Waals forces (vdW), according to Eq. 4.10.

$$RT \ln(\gamma_i^{\alpha}) = \mu_i^{\alpha} - \mu_i \quad (4.8)$$

$$G^E = H^E - TS^E \quad (4.9)$$

$$H^E = H^E(\text{MF}) + H^E(\text{HB}) + H^E(\text{vdW}) \quad (4.10)$$

Computational calculations were performed using the *COSMOtherm* software, version C30, release 18.0.2, at the parametrization BP_TZVP_18.

4.5 Results and discussion

4.5.1 Methodology validation

The experimental methodology proposed in this work was validated by comparing the solubility of organic acids in water measured herein with the data found in the literature for both succinic acid (147,160,176–181,167,169–175) and fumaric acid (147,172,177,182,183) within a temperature range of [283 – 333] K. Compiled literature data for each acid were treated as single data sets and fed into the van't Hoff equation (Eq. 4.3). Experimental data, $\ln(x_1^{exp})$, was compared with the mean literature values, $\ln(x_1^{lit})$, evaluated at the corresponding temperature, by the root mean squared deviation, $\delta[\ln(x_1)]$. Deviation between the values obtained in this work and those reported in literature are $\delta[\ln(x_1)] = 0.19$ and $\delta[\ln(x_1)] = 0.20$, for succinic acid and fumaric acid, respectively. Hence, the proposed methodology is in good agreement with the previously reported data. The validation results details can be found in [Appendix B](#).

4.5.2 Experimental organic acid solubilities

Experimental results obtained in this work for the solubility of succinic acid and fumaric acid using the gravimetric methodology described in [section 4.4.2](#) are exhibited in [Figure 4.3](#). The reported data is expressed as the saturated solute mole fraction with the respective data point uncertainty of measurement: $(x_1 \pm U_{Comb,95\%}(x_1)) / \text{mol mol}^{-1}$. Succinic and fumaric acids display solubilities ranging [0.0025 – 0.0439] mol mol⁻¹ and [0.0005 – 0.0290] mol mol⁻¹, respectively. Succinic acid shows a greater solubility than fumaric acid in water, EtOAc, and 2-MeTHF. As will be discussed later, the solubility phenomenon is driven by enthalpic and entropic processes, where the broken and formed molecular interactions define the system behaviour. Although both organic acids have two carboxyl groups (see [Figure 4.2](#)) to form interactions with the solvent molecules, the molecular structure of succinic acid presents three rotatable bonds, making it more flexible. In contrast, fumaric acid has a carbon–carbon double bond in its chain, resulting in a more

rigid molecule. The molecular capability to rotate might favour the formation of solute-solvent interactions, hence increasing the solubility.

Saturated succinic acid mole fractions in water and bio-based solvents measured in this work at temperatures in the range [283 – 313] K are plotted in [Figure 4.3.a](#), along with the solubility in water data compiled from the literature. The solubility values show an overall trend following: EtOAc \approx CPME < Cineole \approx Water < 2-MeTHF. Likewise, [Figure 4.3.b](#) displays the solubility values for fumaric acid, which exhibits greater solubility in 2-MeTHF, CPME, and cineole than in water, following the trend: EtOAc \approx Water < CPME < Cineole < 2-MeTHF. Note that similar trends were obtained in our previous work for the experimental liquid-liquid extraction of both organic acids from model aqueous solutions using the bio-based solvents studied herein (3).

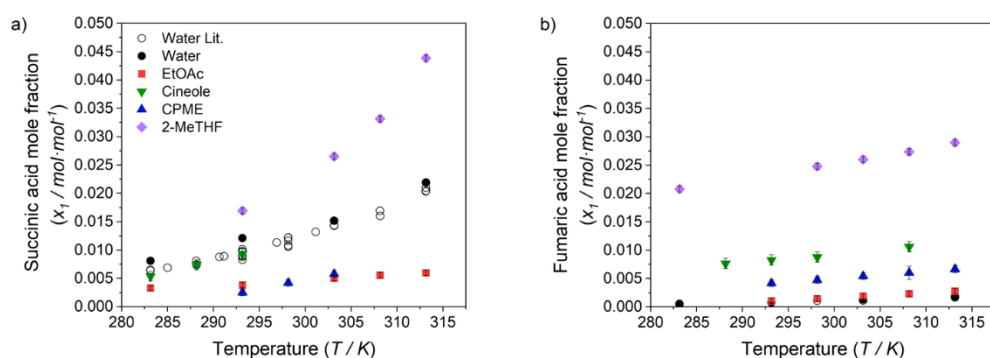


Figure 4.3. Experimental and literature (147,160,176–183,167,169–175) solubilities of organic acids in water and bio-based solvents at temperatures ranging [283 – 313] K: a) Succinic acid; b) Fumaric acid. Average combined expanded uncertainty of measurement $U_{\text{Comb},95\%}(x_1) = 5.2 \cdot 10^{-4} \text{ mol mol}^{-1}$.

Experimental error is composed of uncertainties arising from random and systematic effects. The first one can be related to the variability of the results, while the second one is related to the measurement procedure. Its proper determination by statistical methods is a subject of discussion in literature, and nonstatistical approaches, such as the mathematical gnostic, have been proposed for the estimation of thermophysical/chemical properties uncertainty (184). Due to the complexity of the methodology procedure, no more replicate experiments by data point were possible to measure. This results in large confidence bounds given by the basic statistical methods

estimation of the random variable, which do not reflect the experimental precision, and the uncertainty should be estimated from other scientific judgment. Since the proposed methodology is based on reliable independent measurements under highly controlled conditions, the reported errors for the organic acid solubility values are expressed as the combined expanded uncertainty of measurement, $U_{\text{Comb},95\%}(x_1) / \text{mol mol}^{-1}$.

The reported errors for the organic acid solubility values are expressed as the combined expanded uncertainty, $U_{\text{Comb},95\%}(x_1) / \text{mol mol}^{-1}$. They were estimated from the measured variables and the error propagation with a confidence level of 95% (165). The respective variable standard uncertainties and the expression for the combined uncertainty of the organic acid saturated mole fraction derived from Eq. 3.1 are available in Appendix B. Solubilities of succinic acid and fumaric acid have an $U_{\text{Comb},95\%}(x_1) < 8.7 \cdot 10^{-4} \text{ mol mol}^{-1}$ and $U_{\text{Comb},95\%}(x_1) < 9.3 \cdot 10^{-4} \text{ mol mol}^{-1}$ respectively, where the average relative error, $100 \cdot U_{\text{Comb},95\%}(x_1)/x_1$, is 11%. Experimental solubility results and uncertainty estimation details can be found in Appendix B.

4.5.3 Correlation of organic acid solubility data

The following thermodynamic models for solubility i) the van't Hoff equation (Eq. 4.3), ii) the modified Apelblat equation (Eq. 4.4), and iii) the Buchowski-Ksiazaczak λh model (Eq. 4.5) were used to correlate the solid-liquid equilibria data as a function of the temperature. The empirical parameters were obtained by fitting the equation to the experimental data points and minimizing the objective function (Eq. 4.6). Table 4.2 presents the fitted parameters for each [organic acid (1) + solvent (2)] system along with their root mean square deviation, $\delta(x_1)$. Although the modified Apelblat equation shows a slightly better fit, this might be due to overfitting, considering the few data points available within the system. Moreover, the few measurements obtained for the systems [succinic acid + cineole] and [succinic acid + CPME], undermine the Apelblat equation and are presented just for a comparative purpose.

Table 4.2. Fitted values of parameters for the van't Hoff equation (Eq. 4.3), modified Apelblat equation (Eq. 4.4), and Buchowski-Ksiazaczak λh model (Eq. 4.5) for the organic acid solubilities in water and bio-based solvents.

| Eq. | Succinic acid | | | Fumaric acid | | | | |
|-------------------|---------------|---------|--------|-------------------|---------|--------|--------|-------------------|
| | p_1 | p_2 | p_3 | $100 \delta(x_1)$ | p_1 | p_2 | p_3 | $100 \delta(x_1)$ |
| <i>Water</i> | | | | | | | | |
| van't Hoff | 5.407 | -2894 | | 0.025 | 6.408 | -3973 | | 0.002 |
| Apelblat | -179.1 | 5371 | 27.52 | 0.023 | 317.7 | -17950 | -46.40 | 0.002 |
| λh model | 0.3419 | 8220 | | 0.024 | 0.5147 | 7707 | | 0.002 |
| <i>EtOAc</i> | | | | | | | | |
| van't Hoff | 0.8937 | -1880 | | 0.005 | 7.545 | -4202 | | 0.003 |
| Apelblat | -110.6 | 3095 | 16.64 | 0.005 | 1079 | -52749 | -159.5 | 0.001 |
| λh model | 0.0227 | 68940 | | 0.005 | 1.074 | 3909 | | 0.003 |
| <i>Cineole</i> | | | | | | | | |
| van't Hoff | 10.64 | -4485 | | 0.008 | 0.2407 | -1477 | | 0.006 |
| Apelblat* | 2240 | -101101 | -334.4 | 0.003 | -330.5 | 13292 | 49.35 | 0.003 |
| λh model | 2.236 | 2012 | | 0.008 | 0.0602 | 21451 | | 0.005 |
| <i>CPME</i> | | | | | | | | |
| van't Hoff | 17.71 | -6927 | | 0.010 | 1.839 | -2145 | | 0.002 |
| Apelblat* | 2895 | -135500 | -429.3 | 0.010 | 201.7 | -11170 | -29.77 | 0.002 |
| λh model | 12.41 | 559.3 | | 0.010 | 0.1158 | 17683 | | 0.002 |
| <i>2-MeTHF</i> | | | | | | | | |
| van't Hoff | 11.26 | -4509 | | 0.037 | -0.4378 | -972.8 | | 0.004 |
| Apelblat | -485.3 | 18036 | 73.89 | 0.017 | -12.82 | -421.7 | 1.849 | 0.003 |
| λh model | 4.410 | 1045 | | 0.039 | 0.0424 | 14738 | | 0.003 |

*Correlation fit for this equation does not fulfil the required data size.

The percentage of the individual relative deviations, $\varepsilon_i / \%$ (Eq. 4.11), for each data point and the predicted saturated solute mole fraction obtained using the solubility correlations can be found in Appendix B. Succinic acid systems show an average relative deviation of 4.4%, with a maximum of 6.6% in the CPME solution correlated with the Buchowski-Ksiazaczak λh model. On the other hand, the fumaric acid solubilities present an overall better fit, with an average relative deviation of 3.4%. The largest data point deviations are found for the fumaric acid in EtOAc with the van't Hoff equation and Buchowski-Ksiazaczak λh model, where their respective maximum relative deviations are 9.1% and 9.2%.

$$\varepsilon_i = 100 \cdot (x_{1,i}^{exp} - x_{1,i}^{cal}) / x_{1,i}^{exp} \quad (4.11)$$

4.5.4 Thermodynamic analysis of organic acid – solvent systems using COSMO-RS

The observed solubility behaviour depends on the molecular interactions present within the system. Such interactions can be quantified from the chemical potential of the species determining the solid-liquid equilibria. To estimate the chemical potential of the compounds, the COSMO-RS method uses the charge density probability distribution of a molecular surface segment, defined as the σ -profile, as the main descriptor. The molecular charge density, or σ -surface, and the respective σ -profile of the compounds used in this work are depicted in Figure 4.4. Three core regions are recognized: two polar-nature regions, hydrogen bond donor (HBD) at $\sigma < -0.82 \text{ e nm}^{-2}$ and hydrogen bond acceptor (HBA) at $\sigma > 0.82 \text{ e nm}^{-2}$, and a non-polar region within. Based on the experimental data and the σ - profiles of the organic acid solutes and the solvents, the solid-liquid equilibria of each studied system were determined along with their intermolecular affinities.

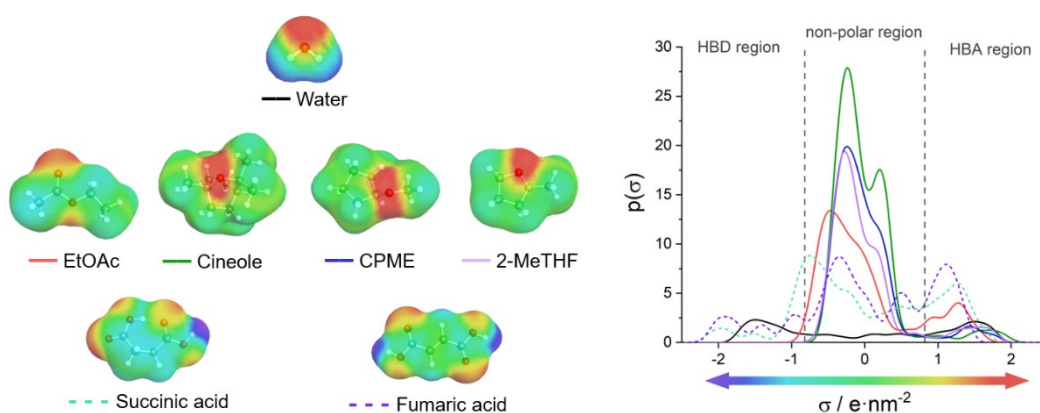


Figure 4.4. Representation of the σ - surfaces (left) and σ - profiles (right) of the bio-based solvents and organic acids studied in this work.

As one of the main thermodynamic properties of a multicomponent solution, the activity coefficient of each specie provides key insights into the molecular affinity, $\ln(\gamma_1) < 0$, or repulsion, $\ln(\gamma_1) > 0$, i.e., to understand the non-ideal behaviour of a solution. The activity coefficients of the organic acids at the saturated liquid condition are presented in Figure 4.5 as a temperature function. Note that the organic acid solubility increases with the temperatures,

so the γ_1 -values are not at the same concentration. However, the infinite dilution activity coefficients of each acid present similar trends with the temperature than the saturated mixtures. The details of the computed activities coefficients results can be found in [Appendix B](#). The activity coefficients of both organic acids are lower in the bio-based solvents than in water, supporting bio-based solvents as good extractants for the recovery of the acids from fermentation broths. From the solvents σ - profiles can be inferred that molecules with a greater non-polar area provide a relatively lower solubility, while those showing greater HBA capacity enhance the solubility of the target solutes. As mentioned above, the molecular rotation capacity of succinic acid allows the breaking of the internal hydrogen bond depicted in [Figure 4.4](#) hence promoting interactions with the solvent molecules. The computed γ_1 -values results do not follow the experimental solubility, suggesting that more complex interactions are present in the solid solvation phenomena. Regarding the solubility of organic acids in aqueous solutions, the molecule of water presents both hydrogen bond donor and acceptor capacities, which can promote strong interactions with the carboxyl groups of the organic acids. Nevertheless, the limited solubility of fumaric acid in water is explained by the “hydrophobic effect”; this is an entropic phenomenon (148) where the water molecules can form complex tetrahedral networks with water-water interactions stronger than acid-water interactions, requiring high energy to disturb them (150).

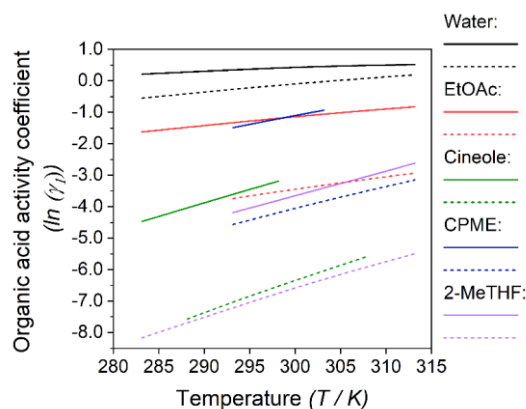


Figure 4.5. Natural logarithm activity coefficient, $\ln(\gamma_1)$, of saturated succinic acid (solid lines) and fumaric acid (dashed lines) in water and bio-based solvents computed by COSMO-RS method within the experimental temperature range of each [organic acid (1) + solvent (2)] system.

At the solid-liquid equilibria, the specific interactions of the saturated liquid phase can be described through an excess energies analysis. Figure 4.6 shows the saturated organic acid-solvent mixtures' excess energies and their respective contributions to the H^E -value, according to Eq. 4.9 and Eq. 4.10, respectively. Within each system, the temperature dependence of the H^E and $-TS^E$ determining the excess G^E remained relatively constant. Thus, the analysis was made at a fixed temperature of 293.15 K to allow a proper comparison. Overall results demonstrate that it is possible to establish a proportional trend between G^E values and the solubility results for each organic acid.

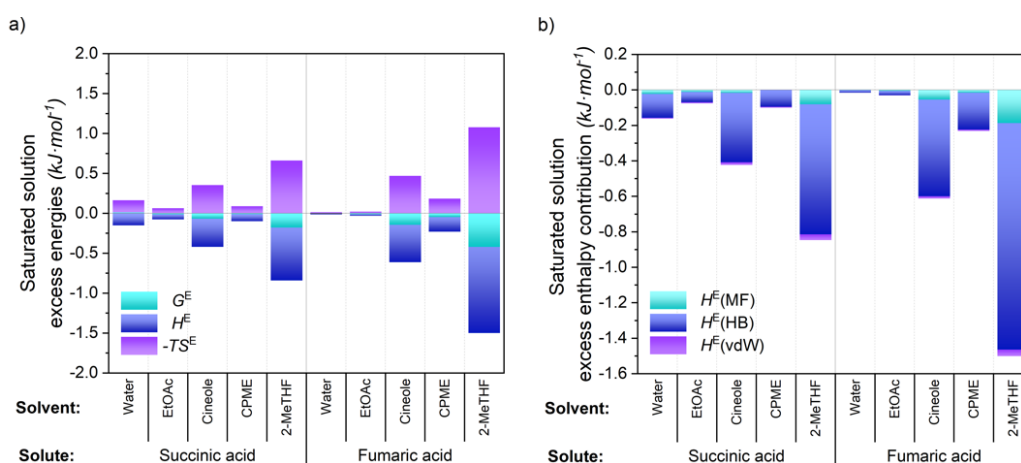


Figure 4.6. Analysis of the excess mixing energies of saturated organic acid - bio-based solvent systems computed by the COSMO-RS method at 293.15 K. a) Excess Gibbs free energy (G^E / kJ mol⁻¹), Excess enthalpy (H^E / kJ mol⁻¹), and Excess entropy ($-TS^E$ / kJ mol⁻¹); b) Excess enthalpy contributions (kJ mol⁻¹): electrostatic energy (MF), hydrogen bonding (HB), and van der Waals forces (vdW).

Except for succinic acid in water, G^E values are negative, reflecting the spontaneity of the solvation process. This agrees with the $\ln(\gamma_1)$ -value > 0 for the former system, evidencing its low unlike-molecules affinities. Succinic acid tends to form internal hydrogen bonds, exposing the non-polar surface charges which repulse the water molecules. Most systems show a proportional $-TS^E$ compensation effect with the H^E , suggesting an increasing order within the system due to the new interactions formed. Such compensation effect is predominant for aqueous systems where G^E values tend to zero, denoting the hydrophobic effect described above. In general, the main H^E contribution corresponds to hydrogen bonding interactions between the carboxyl groups

of the solutes and the solvents; this is followed by a slight contribution of electrostatic interactions and a negligible influence of the van der Waals forces. Solute-solvent interactions are stronger for succinic acid than fumaric acid in water and EtOAc, while stronger for fumaric acid in Cineole, CPME, and 2-MeTHF. Both solvent groups differ mainly in the non-polar region and the HBD/HBA capacity. Notably, for the systems composed of CPME with both acids, greater ratios of HB/MF and HB/vdW contributions are observed. This might explain the low affinity identified from the activity coefficient analysis, yet the similar HBA capacity than other bio-based solvents, such as cineole and 2-MeTHF. The low MF contribution suggests a poor molecular interstitial accommodation, reducing the interaction capacity and thus limiting the solubility of both acids in CPME. The energetic analysis revealed the complex interaction network that can be formed between the target organic acids and the bio-based solvents, which is critical to consider for the appropriate selection of the extraction media. The results details of the computed excess energies can be found in [Appendix B](#).

4.5.5 Energies of solution of organic acid – solvent systems

Given the solubility data and the van't Hoff equation ([Eq. 4.3](#)) is possible to estimate the energies of solution from the variation of the equilibrium constants with the temperature following the modification proposed by Krug et al. ([185,186](#)). The method normalizes the temperature by accounting for the harmonic temperature, i.e., the harmonic mean of the N experimental temperature data points, according to [Eq. 4.12](#). This results in a solubility function in the form of $\ln(x_1) = f(1/T-1/T_{hm})$, as shown in [Figure 4.7](#), where the Gibbs free energy of solution, $\Delta G_{soln} / \text{kJ mol}^{-1}$, corresponds to the function intercept times the gas constant, $R / \text{kJ mol}^{-1} \cdot \text{K}^{-1}$, and the harmonic temperature, as shown in [Eq. 4.13](#); the enthalpy of solution, $\Delta H_{soln} / \text{kJ mol}^{-1}$, is related to the function slope times the gas constant, as per [Eq. 4.14](#); and the entropy of solution, $\Delta S_{soln} / \text{kJ mol}^{-1} \cdot \text{K}^{-1}$, is derived from the Gibbs free excess energy equation ([Eq. 4.15](#)). Uncertainties of the energies of solution are derived from the respective intercept and slope confident bounds of the van't Hoff

equation linear regression. The full derivation of the linear regression parameters, as well as the energies of solution uncertainties, can be found in [Appendix B](#).

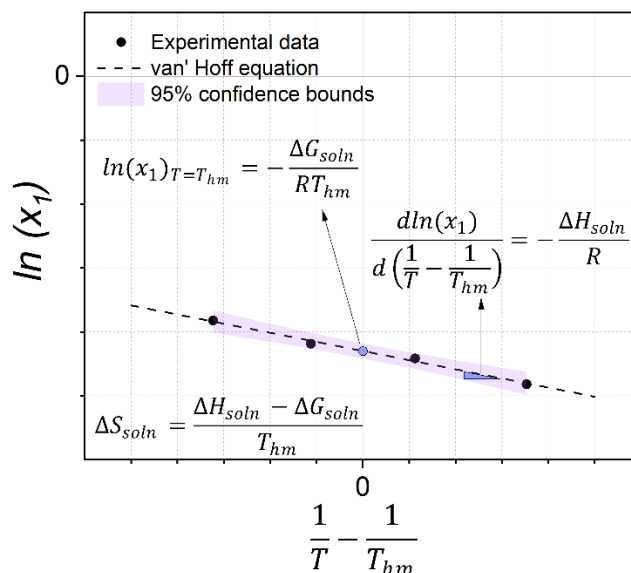


Figure 4.7. Schematic representation of energies of solution estimation from the solubility experimental data in the van't Hoff plot modified by Krug et al. (185,186). The free energy of solution, ΔG_{soln} / kJ mol^{-1} , is proportional to the function intercept, i.e., the function evaluated at $T = T_{hm}$, the enthalpy of solution, ΔH_{soln} / kJ mol^{-1} , to the function slope. The entropy of solution is obtained from the Gibbs free energy relationship: $\Delta G = \Delta H - T\Delta S$.

$$T_{hm} = \frac{N}{\sum 1/T} \quad (4.12)$$

$$\Delta G_{soln} = -R \cdot T_{hm} \cdot \ln(x_1)_{T=T_{hm}} \quad (4.13)$$

$$\Delta H_{soln} = -R \frac{d \ln(x_1)}{d \left(\frac{1}{T} - \frac{1}{T_{hm}} \right)} \quad (4.14)$$

$$\Delta S_{soln} = \frac{\Delta H_{soln} - \Delta G_{soln}}{T_{hm}} \quad (4.15)$$

The energies of solution of the organic acids in water and the bio-based solvents studied in this work were estimated at a fitted temperature of $T_{hm} = 299$ K, i.e., the harmonic mean of the temperature of all data reported, to allow for a proper comparison between the systems. The estimated energies of solution for succinic acid and fumaric acid are presented in [Table 4.3](#). As expected, the dissolution of the organic acids is an endothermic process

($\Delta H_{\text{soln}} > 0$) in all solvents. Gibbs free energy results follow a similar trend to that of the overall organic acid solubilities: the higher the solubility values, the lower the Gibbs free energy. Positive values of the entropy of solution in all cases, except for fumaric acid in 2-MeTHF, suggest a possible contribution of this factor to the dissolution. Note that due to the few points measured for the systems [succinic acid + cineole] and [succinic acid + CPME], the uncertainty of the linear regression parameter causes a large estimated uncertainty of their respective energies of solution. Thus, those data points are presented only as a qualitative insight into the energy trend.

To corroborate the predominant driving force in the organic acid dissolution process within the studied solvents, the relationship between the enthalpy and entropy of solution was assessed. A slope of the enthalpy respect to the entropy variation (Eq. 4.16) bigger than one denotes an enthalpy-driven dissolution process, and otherwise an entropy-driven process (187). The results demonstrate an enthalpy-entropy compensation effect where a proportional linear trend is found between those factors for both organic acids, as depicted in Figure 4.8. The slopes of the enthalpy to the entropy are 1.01 and 1.30 for succinic acid and fumaric acid, respectively. This indicates an enthalpy-driven process for fumaric acid, while no predominated effect can be observed for succinic acid, i.e., its dissolution mechanism is based on the absorbed energy required to break the molecular structure over the entropy change, which agrees with the observed low solubilities. On the other hand, no predominated effect can be observed for succinic acid, as both enthalpy and entropy mechanisms are balanced.

$$\text{Slope} = \frac{d(\Delta H_{\text{soln}})}{d(T_{\text{hm}} \cdot \Delta S_{\text{soln}})} \quad (4.16)$$

Table 4.3. Estimated Gibbs free energy (ΔG_{soln}), enthalpy (ΔH_{soln}), and entropy ($T_{\text{hm}} \cdot \Delta S_{\text{soln}}$) of solution, and their respective uncertainty with a confidence limit of 95% ($U_{\text{Comb},95\%}$), for succinic acid and fumaric acid in water and the bio-based solvents studied in this work. Estimations were performed following the methodology detailed in section 4.5.5 at $T_{\text{hm}}=299$ K.

| Solvent | ΔG_{soln} kJ mol ⁻¹ | | ΔH_{soln} kJ mol ⁻¹ | | $T_{\text{hm}} \cdot \Delta S_{\text{soln}}$ kJ mol ⁻¹ | |
|----------------------|--|-------|--|--------|--|--------|
| <i>Succinic acid</i> | | | | | | |
| Water | 10.62 | ±0.20 | 23.77 | ±6.97 | 13.15 | ±7.17 |
| EtOAc | 13.41 | ±0.09 | 15.46 | ±3.41 | 2.05 | ±3.49 |
| Cineole | 10.81 | ±1.83 | 38.70 | ±45.51 | 27.89 | ±47.34 |
| CPME | 13.59 | ±1.14 | 61.35 | ±61.30 | 47.76 | ±62.44 |
| 2-MeTHF | 9.48 | ±0.13 | 35.81 | ±7.46 | 26.33 | ±7.59 |
| <i>Fumaric acid</i> | | | | | | |
| Water | 17.14 | ±0.49 | 34.65 | ±7.13 | 17.51 | ±0.52 |
| EtOAc | 16.23 | ±0.37 | 37.06 | ±6.42 | 20.83 | ±6.06 |
| Cineole | 11.69 | ±0.17 | 12.04 | ±3.35 | 0.36 | ±3.18 |
| CPME | 13.25 | ±0.11 | 18.45 | ±1.05 | 5.20 | ±0.94 |
| 2-MeTHF | 9.18 | ±0.06 | 8.08 | ±0.54 | -1.10 | ±0.48 |

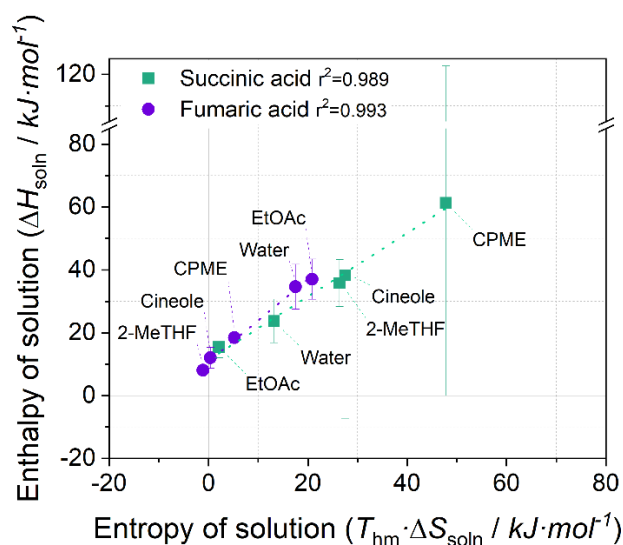


Figure 4.8. Enthalpy-entropy compensation effect for organic acids in water and bio-based solvents at a mean harmonic temperature of $T_{\text{hm}} = 299$ K and $T_{\text{hm}} = 300$ K for succinic acid and fumaric acid. Dotted lines represent the linear regression for each organic acid.

4.6 Conclusions

The saturated succinic acid and fumaric acid mole fraction solubility in water and bio-based solvents were measured in the temperatures range of [283 - 313] K, with an experimental uncertainty of measurement less than $9.3 \cdot 10^{-4}$ mol mol⁻¹. Succinic acid shows to be the most soluble in 2-MeTHF, while fumaric acid also presents high solubility in 2-MeTHF, followed by cineole and CPME, rather than EtOAc and water. Except for the systems composed of succinic acid in cineole and CPME, results were successfully correlated with three solubility models, i.e., the van't Hoff equation, the modified Apelblat equation, and the Buchowski-Ksiazaczak λh model, with relative deviations of less than 10%. However, considering the number of data points, the two-parameter van't Hoff equation provides a proper description of the reported data, allowing for further energetic interpretation of the dissolution phenomenon. The saturated liquid mixture interactions were analysed by computing the solid-liquid equilibria using the COSMO-RS method. Results reveal a complex unlike molecule interactions, where hydrogen bonding dominates the organic acid dissolution process. The Gibbs free energy, enthalpy, and entropy of solution were estimated for all systems at a mean harmonic temperature of the experimental data. While the dissolving process of the organic acids is endothermic, the thermodynamic analysis shows an enthalpy-entropy compensation effect for both solutes within the bio-based solvents studied in this work, providing insights into the predominant driving force for organic acid dissolution. This work provides new experimental data and insights into the bio-organic acid solubility in green hydrophobic solvents. Overall, these findings will promote the design of more benign biorefinery downstream processes for organic acids recovery.

Part III

Maturing the Liquid Membrane technology as a clean separation alternative.

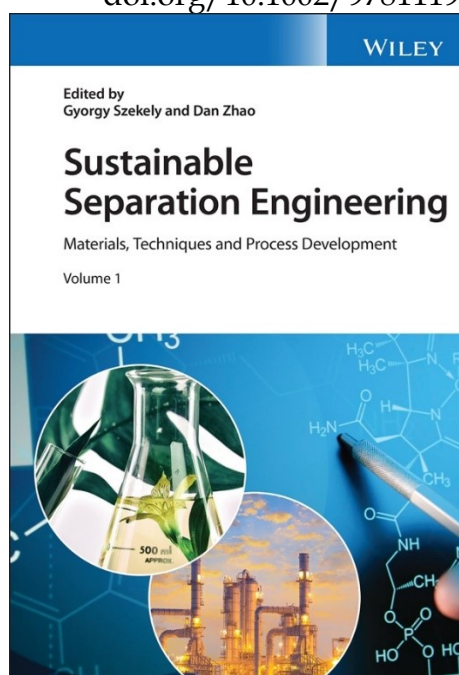
"I question this picture and ask if we ever reach a final steady state of science and technology. At no time in the 10,000 years or so since the last Ice Age has the human race been in a state of constant knowledge and fixed technology."

— Stephen Hawking, *Brief Answers to the Big Questions*

Chapter 5. Liquid membrane technology for sustainable separations

This chapter relates to the second pillar in the establishment of green separation routes for bio-based organic acid production. The liquid membrane technology has been reviewed as an alternative to liquid-liquid extraction. The work was published as a chapter contribution in *Sustainable Separation Engineering: Materials, Techniques and Process Development* book, Wiley 2022 (2). The fundamental basis and the state-of-the-art research of liquid membranes are presented, highlighting their potential for sustainable applications.

| | |
|--------------------------|---|
| Authors: | Pablo López-Porfiri María González-Miquel Patricia Gorgojo |
| Book (Edition): | Sustainable Separation Engineering (First Edit) |
| Publisher: | Wiley |
| Editors: | Gyorgy Szekely Dan Zhao |
| Pages: | 297-341 |
| Status: | Published |
| Publication Date: | Mach 29, 2022 |
| Doi: | doi.org/10.1002/9781119740117.ch8 |



5.1 Foreword

This thesis pursues to contribute to the development of green production routes of fundamental building blocks in the biorefinery industry. Despite the broad research on new extraction solvents, discussed in the previous chapters, conventional separation methods might not be the optimal option to accomplish such a goal. In addition to producing environmentally compatible materials and compounds, the biorefinery industry needs to find more efficient extraction methods. Reducing and recycling the extraction media is key to warrant the sustainability of separation processes. Liquid membranes have been developed, in different configurations, to target these objectives. They are based on the selective separation of solutes from a feed solution by a thin layer containing an extraction solvent.

Within the next pages, a comprehensive state-of-the-art review of such technology and its current limitations for sustainable separations is presented. The concepts, definitions, and operational aspects of liquid membrane technology are summarized, as well as its potential to replace commercial liquid-liquid extraction systems for several applications. The solute-diffusion approach for the transport models is examined, setting the ground for an improved approach proposed in the next chapter.

5.2 Introduction to liquid membrane (LM) technology

Chemical Engineering is continuously evolving to improve process efficiencies, considering not only economic aspects but also major global social concerns. In order to enhance competitiveness and sustainability, chemical industries must advance toward green practices, reducing energy consumption, using renewable fuels and raw materials, and looking at sustainable synergies with the environment. Separation operations, the core stage of chemical processes, are often the bottleneck in process development, due to their high energy demand and use of toxic substances. Among several avenues of separation engineering research, membrane technology, has gained great interest over the past few decades. Membrane-based separation methods can be an order of magnitude more energy-efficient than heat-driven separations as they do not involve phase-change (188).

A membrane is a semipermeable barrier that allows the selective transport of substances between two streams. Membranes are typically thin polymer films fabricated on highly porous substrates, although other materials such as inorganic ceramics, zeolites, metal-organic frameworks (MOFs), and metals are often used. Novel materials such as polymer/graphene nanocomposite membranes are currently being investigated with promising results (189–191). It is worth noting the extended use of membranes in the following processes: micro/ultrafiltration (MF/UF), water treatment, desalination, gas purification, pervaporation (PV), and dialysis. Membranes can be classified according to the operational pressures they work at or pore size (113). Reverse osmosis (RO) has been widely implemented for water desalinization with extremely dense membranes (equivalent pore size of 1–5 Å), at pressures ranging from 20 to 100 bar, which are required to overcome the osmotic pressure. Nanofiltration (NF) membranes, on the other hand, work at lower pressures of 5–15 bar with pores below 1 nm, for the separation of species larger than monovalent ions. Filtration of larger bodies, e.g., micro-organics,

lipids, and proteins, can be done by UF with membranes of 2-100 nm pore size, as well as MF for suspended solids and bacteria bigger than 0.1 μm at a pressure below 1 bar. Amongst other membrane techniques, electro-membranes are used for ion separation; in gas separation (GS) membranes the permeating species are gases, while PV and membrane distillation (MD) allow for volatile components separation.

A noteworthy membrane type is the so-called liquid membrane (LM), where the semipermeable barrier is composed of a liquid instead of a solid medium. Taking advantage of the liquid immiscibility, LMs can still separate two streams and transfer target solutes in a diffusional process. Thus, they combine two processes in one stage: liquid-liquid extraction (LLX) and stripping altogether. LMs do not need pressure or temperature gradient to accomplish the separation, which means a low energy consumption. The reduction in solvents requirements as compared to other processes such as LLX, simplicity of operation, and energy-efficiency", make LM technology stand as a competitive alternative to traditional separation operations (192). As discussed in detail further in this chapter, LMs have been applied in bio-refinery, GS, wastewater treatment processes, the recovery of amino acids, metal ions, and rare earths (REs), as well as the removal of nuclear waste and heavy metals, as illustrated in Figure 5.1.

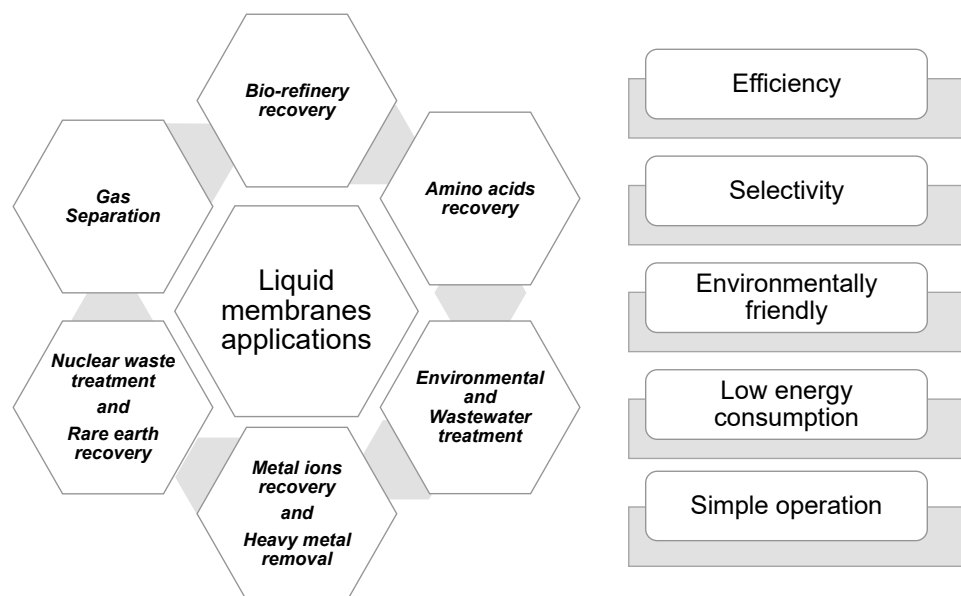


Figure 5.1. Fields where liquid membranes (LMs) are applied and main features.

This chapter gives a comprehensive overview of the LM technology applied for sustainable separations. The basic concepts and definitions of LMs are presented, along with a selection of the most relevant applications for the development of sustainable processes. Fundamental aspects inherent to the liquid membrane operation are given as well to help the reader understand the scope of the technology and its current limitations.

5.2.1 Components of a liquid membrane

A LM is an immiscible liquid that acts as a barrier, allowing compounds to move from one stream to another while keeping them separated. The target solute to be recovered or removed is extracted from a concentrated feed stream, and transferred into a receiving stream, the stripping phase, as represented in [Figure 5.2](#). Both streams can be in a gaseous or liquid phase, according to the nature of the process. The diffusional pathways that compounds follow across the membrane depend on thermodynamic affinities and hydrodynamic parameters, which contribute to the overall transport rate. The selectivity of an LM is related to the difference in velocity at which different compounds move through the membrane. In comparison to polymer matrices, diffusion coefficients are higher in liquids, within a range of $10^{-6} - 10^{-5} \text{ cm}^2 \cdot \text{s}^{-1}$, which translates into larger solute flux [\(193\)](#). For the membranes process, this transport velocity is known as solute permeation. Still, other operational variables, such as temperature, and pressure or electric field gradients, can be tailored to improve the membrane performance [\(192\)](#).

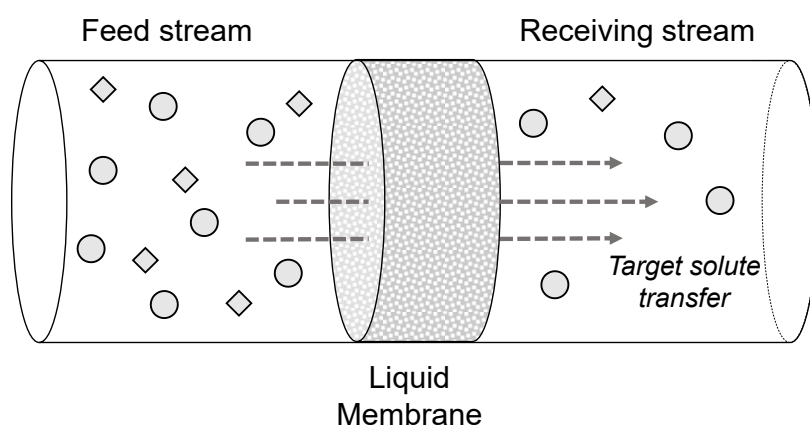


Figure 5.2. Liquid membrane system scheme.

From a phenomenological perspective, LMs share more similarities with LLX than filtration processes. Solutes permeate from the feed to the receiving side of the membrane (the stripping phase) following a concentration gradient. Nevertheless, in LM the permeation ratio is not governed by thermodynamics equilibrium, but by the chemical potential gradient in a constant diffusional phenomenon. Thus, extraction against the concentration gradient could be achieved given the appropriate conditions. LMs allow for accomplish reactive extraction and its back extractions comprising the extraction and stripping in a sole process stage, continuously recycling the extractant agent. Furthermore, LM can attain a larger mass transfer area per unit volume in comparison to LLX columns (194). This process simplification, in both step number and solvent requirements, leads to a reduction of operational costs. Since LM can accomplish the liquid stream separation by solute-phase affinity gradients, operation conditions found in the literature are often atmospheric pressure and room temperature, which means no extra energy requirement. On the other hand, both parameters become critical in gas stream separations.

The simplest LMs are conformed of a single solvent to separate the phases, transporting the target solute by diffusion. This solvent can be a pure compound, though mixtures of solvents plus modifiers are often adopted to tailor the membrane properties, e.g., the viscosity. Nonetheless, mixtures composed of a diluent solvent and a carrier or extractant agent are the most promising alternative. While in membranes without a carrier, the solute transport is just driven by intermolecular affinities; in those where a carrier is present, there is a reversible reaction that leads to a carrier-solute complex that enhances the solubility and diffusivity. The presence of carriers enhances not only the mass transfer but the selectivity as well. Moreover, carriers can accomplish high chiral resolution for enantiomer separations with LMs (195,196). However, carrier selection and its reaction kinetics must be carefully considered for the process design in order to find a suitable candidate. Acid carriers, di(2-ethylhexyl)phosphoric acid (D2EHPA), for example, and basic carriers, such as trioctylamine (TOA), tributylphosphate (TBP),

and Aliquat[®] 336, are widely found in the literature, yet neutral carriers might be employed as well (197). Water-immiscible solvents are required to extract compounds from aqueous matrices, and aqueous solutions are required to extract substances from organic solutions. Kerosene and n-heptane are highly hydrophobic solvents used as a diluent on LM for the extraction of organic compounds, phenol, REs, and metal ions from aqueous solutions. Novel solvents such as ionic liquids (ILs) are escalating in popularity for LM, the so-called IL-membranes (198–202), which find their use in organic acids recovery (203–205), removal of phenols (206–209), and heavy metals (210), as well as bio-alcohol PV separations (211). Moreover, hydrophobic deep eutectic solvents (DESs) have been recently investigated for the preparation of LM and applied in biorefinery (212) and amino acid recovery (213), and bio-based vegetable oils can be found in LM to enhance their performance; coconut oil (214), sunflower oil (215,216), rice oil (217,218), corn oil (219), palm oil (220–222), and even waste vegetable oil (223) have been incorporated as a diluent for LMs using TOA or D2EHPA as the carriers. Vegetable oils are mainly mixtures of tri-, di-, and mono-glycerides, with a non-polar nature. However, due to their natural sources, vegetable oils can vary in their composition, which compromises the reproducibility of LMs.

5.2.2 Liquid membrane configurations

LMs are classified into three main configurations as shown in Figure 5.3: a) bulk liquid membrane (BLM), which uses relatively large amounts of extraction solvent within the membrane; b) emulsion liquid membrane (ELM), also called double emulsion membrane, where the membrane is emulsified as globules in the feed, thus maximizing the exchange area; and c) supported liquid membrane (SLM), where a small amount of liquid is used to impregnate a thin porous layer, reducing the mass transfer resistance from the feed to the product stream.

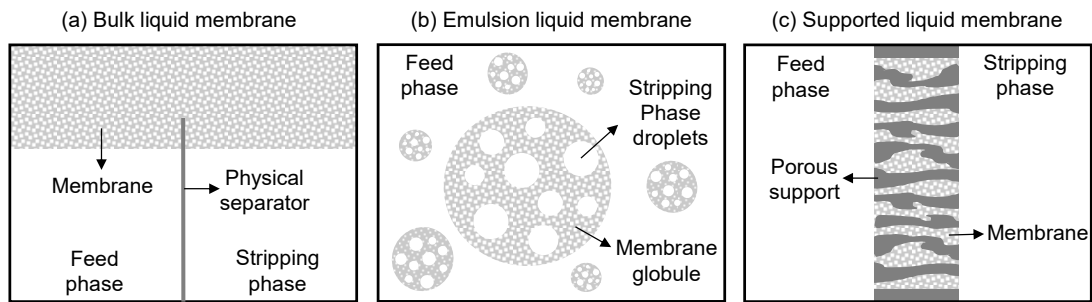


Figure 5.3. Main liquid membranes configurations. (a) Bulk liquid membrane; (b) Emulsion liquid membrane; (c) Supported liquid membrane.

There are advantages and limitations for each membrane configuration, as summarized in [Table 5.1](#), and its selection depends on the specific applications and the whole process design. Further details on operational aspects will be presented in [Section 5.3](#).

Table 5.1. Strengths and limitations of the three main liquid membrane configurations.

| | Strengths | Limitations |
|------------|--|---|
| BLM | <ul style="list-style-type: none"> • Simple construction and operation • High membrane stability • Allows to determine mass transfer and kinetic parameters at laboratory scale | <ul style="list-style-type: none"> • Low mass transfer surface area and flux • A large amount of solvent requirement • Not feasible on an industrial scale |
| ELM | <ul style="list-style-type: none"> • Simple equipment • Largest surface-to-volume area ratio. • High concentration factors (i.e., stripping phase results in more concentrate than the feed phase) • Can be broadly applied | <ul style="list-style-type: none"> • The addition of surfactants required • Requires extra emulsification and de-emulsification stages • Numerous operational variables • Emulsion stability issue by breakage and swelling phenomena • Risk of feed and stripping mix |
| SLM | <ul style="list-style-type: none"> • Low solvent requirement • Thin layers reduce mass transfer resistance • Large surface area per unit volume may be obtained using hollow fibre or spiral wound arrays • No loading and floating issues • Simple to scale up | <ul style="list-style-type: none"> • Support capacity to retain the solvent determines its stability, operational life, and overall performance • The support matrix adds extra mass resistance • Membrane instability leads to low mass flux or poor selectivity |

5.2.2.1 *Bulk liquid membranes:*

BLM configurations contain three bulk liquid phases, where the feed and the stripping streams are kept separated by an immiscible solvent. Specific arrangements have been proposed to avoid the mixture of the feed and receiving phases, often by physical barriers and profiting from density differences, at the same time they are continuously stirring (224). In more elaborate designs, semi-permeable barriers have been used in layered BLM to hold the membrane phase between streams. BLM stands out by its easy setup at a laboratory scale, allowing to determine mass transfer and kinetic parameters. Nonetheless, this configuration is not particularly attractive for industrial applications due to the low mass transfer area-to-bulk volume ratio. Another important limitation is the difficulty in ensuring liquid immiscibility with both feed and receiving phases, and carrier leaching throughout the extraction process.

5.2.2.2 *Emulsion liquid membranes:*

While in BLMs phase mixing must be completely prevented, EMLs use surfactants to emulsify the stripping phase within the LM and then disperse the emulsion inwards the feed phase. Although it may be the other way around: the feed phase inward the membrane globule and the stripping phase outside. First proposed by Li in 1968 (225), depending on the streams and the membrane nature, ELMs are typically classified as water in oil in water (W/O/W) for aqueous feed/stripping phases and an organic membrane process, or oil in water in oil (O/W/O) when the membrane is an aqueous solution. Besides the diluent and extracting solvents, the procedure requires a surfactant to form the membrane globules. Kumar et al. have published comprehensive reviews on ELM developments (226) and on sustainable solvents to form them (227). ELMs take advantage of the different component permeation rates through the membrane globules, separating the target solute into a stripping immiscible solvent. The resulting double emulsion configuration provides a large total surface area-to-volume ratio of 1000–3000 $\text{m}^2 \cdot \text{m}^{-3}$, and small membrane average thickness, favouring the mass flux (193).

The process involves stages of emulsification, extraction, separation, and finally a de-emulsification to recover the stripping phase together with the target solute. The emulsification may be done by mechanical agitation or ultrasounds. Among the de-emulsification mechanisms, heat or an electrostatic field are applied to the mixtures to achieve the internal phase coalescence, and lastly the membrane – stripping phase separation by density difference (228). The simplicity of each stage offers simple operation with low equipment investment, up to 40% less, plus the possibility to regenerate the membrane phase. The opportunity to recover the extracting solvent reduces waste production, as well as improving the energy efficiency, turning the ELM into a highly sustainable separation process. Nonetheless, despite the simple operational procedures of ELMs, the degrees of freedom during process design increase due to the growth in operating variable numbers.

Due to the above reason, most of the ELM studies are focused on statistical analyses of the operating variable effect contributions, in order to find an optimum recovery point. Streams concentrations and emulsion composition affect directly not only in the process hydrodynamics but also in the overall extraction performance. Moreover, due to its heterogeneous mixture nature, its stability becomes another crucial factor in its optimization. The more stable mixtures are harder to break in the downstream process, requiring more energy-demanding processes that hinder the final solute back-extraction stage.

5.2.2.3 Supported liquid membranes:

In supported liquid membranes the solvent media is immobilized within a nano or microporous matrix, which together composes the semipermeable barrier between the phases. Common supports are polymeric matrix, among them: polypropylene (PP), polyethylene sulfide (PES), polyvinylidene fluoride (PVDF), and polytetrafluoroethylene (PTFE), as well as inorganic materials, such as ceramics and metal matrices.

SLM dated from the late 1960s. Since then, continuous developments in both membrane phase and supporting materials have been researched and their applications at an industrial scale broadened (229). Due to their high selectivity, as well as the low investment and operational costs, SLMs have captured the attention of several separation processes. Depending on the nature of the process extraction from an aqueous or organic stream, hydrophobic and hydrophilic matrix alternatives may be adopted, respectively. The LM impregnation on the support for the SLM preparation may be done by simple immersion or application of pressure/vacuum methods. Although they provide similar outcomes, the proper procedure is chosen according to the supporting material and the liquid properties, viscosity being one of the most relevant.

The matrix parameters that characterize a porous membrane are its thickness, pore size, porosity, and pore tortuosity. Typical SLM supports present high porosity and low thickness, usually of 100 and 200-300 μm for flat sheet and hollow fibre (HF), respectively (230). This allows a significant reduction of solvent requirement and improves the solute flux. Nevertheless, it is important to consider the reduction in mechanical stability as well as its loss of LM retention capacity. Contrary to conventional membrane filtration processes, SLM separation is not carried out by the solute size relative to the pore diameter, but by the solute-membrane phase affinity. Nonetheless, the pore size helps retain the LM inside them by capillary forces. For viscous solvents such as ILs, the suitable pore size in polymer supports is within 100-200 nm (198). SLMs are commonly studied as flat sheet configurations, allowing to determine their transport properties and stabilities. However, to ensure their feasibility at an industrial scale, other configurations with the better surface area-to-volume ratios, such as HF or spiral wound, must be adopted. HF geometry, solution physicochemical properties, stream velocity, and solute diffusion coefficients affect the mass transfer rate. Dimensionless correlations for mass transfer coefficient in specific HF geometries can be found in the work published by Gabelmana and Hwang (231).

5.2.2.4 *Other liquid membrane configurations:*

More complex configuration designs can be found in the literature. In an attempt to increase the mass transfer rate on BLM, arrangements as a continuous liquid membrane (CLM) have been adopted, where the membrane phase is bubbled into the feed and stripping phases, mixed, and then recirculated (223). In a bulk flow liquid membrane (BFLM) the carrier solution is fed into a pressurized feed side which is kept separated from the stripping side by means of a UF membrane, permeates through the porous barrier, releases the solute, and is recirculated back to the feed chamber (232).

Using an electric field, electrostatic pseudo-liquid membranes (ESPLIM) aim at stabilizing and dispersing the ELM (233). Instead of common surfactants, pickering ELM (PELM) uses magnetic nanoparticles, chitin nanocrystals, cellulose microfibrils, polymer particles, or starch to form the emulsion globules. This improves membrane stability and aids in the deemulsification stage (228). Pérez and Fontalvo (234) developed an ELM in a Taylor flow liquid membrane (TFLM), where the aqueous phases (feed and stripping), are injected at specific intervals as droplets into a membrane phase flowing through a pipe. As shown in Figure 5.4a, the continuous flow causes toroidal vortexes within the droplets and in the LM filling the space within them. The design allows natural stirring in each phase due to the turbulent regime and increases the interfacial area, increasing mass transfer. The Taylor-Couette flow was previously proposed in a similar arrangement, using a rotary vertical cylinder to create the vortexes within the feed phase and the emulsion (235). ELM can also be carried out as a spray column, dispersing the membrane globules into the feed solution at countercurrent flow, as represented in Figure 5.4b (236). In order to reduce the organic membrane required, a similar arrangement was proposed as a bubbling organic liquid membrane (BOLM) (237). A gas stream is fed altogether with the organic phase forming bubbles that support a layer of organic LM. An aqueous-to-oil ratio greater than 600:1 can be reached maintaining the surface area and the

solute mass flux. Afterwards, the loaded LM is treated in a stripping tank to recover the solute.

In an attempt to avoid solvent losses from the pores in the SLM configuration, gelled and polymer inclusion membranes (PIM), also known as plasticized polymer membrane (PPM) or fixed site membrane (FSM) have been developed. They are produced by adding a gelator agent into the extraction solution or polymerizing it into a dense matrix, to ensure adherence to the support. This allows reducing the extractant agent required, giving it an eco-friendly feature (201,202,238).

New materials are currently developing to profit from novel solvent features in membrane separations. Porous IL polymers are a porous matrix composed of the IL itself (239). The fluidic IL is solidified forming a polymer of tuneable physicochemical properties with high porosity and surface area. Thanks to the electrostatic field and ionic density inside the pores, the material is expected to improve separation processes.

At an industrial scale, HF (240), Figure 5.4c, and spiral-wound modules (241) have been adopted to build SLM and increase the effective exchange surface up to $104 \text{ m}^2 \cdot \text{m}^{-3}$ (242). Hollow fibre renewal liquid membrane (HFRLM), shown in Figure 5.4d, is based on the surface renewal theory; the feed circulates outside the fibres, whose pores are previously filled with the solvent, while a mixture of the stripping phase with low solvent content is pumped into the lumen side of the fibre (243,244). The arrangement creates a thin LM layer that covers the inside of the fibre, being continually renewed by the stripping-membrane stream that flows through it. A combination of ELM with a hollow fibre contactor allows the separation of the emulsion from the feed, reducing its breakage (245,246). Furthermore, pseudo-emulsion hollow fibre strip dispersion (PEHFSD), Figure 5.4e, has been developed, having the feed flowing inside the HFs impregnated with LM while a mixture of LM and the stripping phase flows from the outside. It is called “pseudo-emulsion” since the LM is supported into the HF matrix as well as dispersed into the

stripping phase. The arrangement overcomes the SLM stability issues, as the LM losses become part of the pseudo-emulsion (247–249).

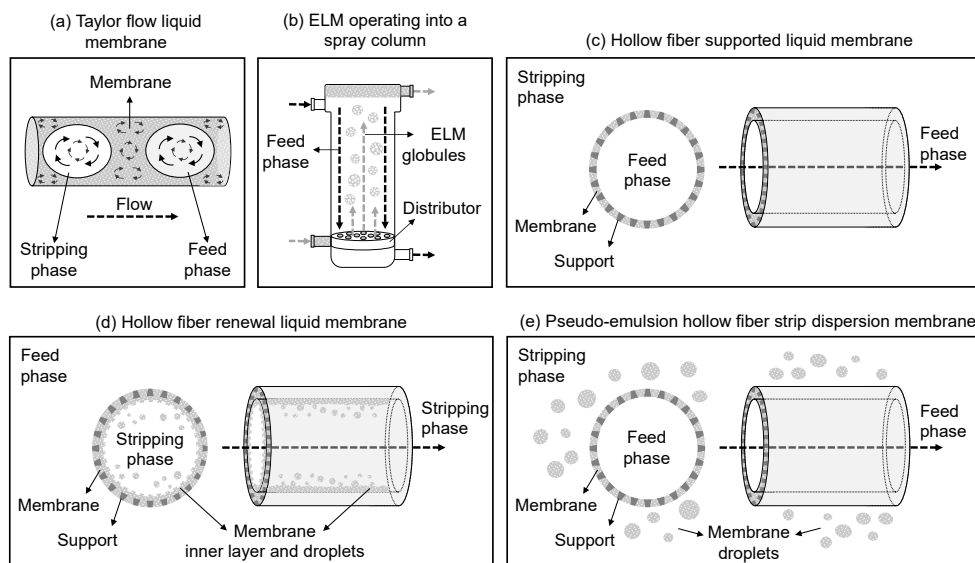


Figure 5.4. Other liquid membrane arrangement schemes: (a) Taylor flow LM; (b) ELM operating into a spray column; (c) Hollow fibre SLM; (d) Hollow fibre renewal liquid membrane; (e) Pseudo-emulsion hollow fibre strip dispersion membrane.

5.3 Fundamental aspects of liquid membranes

5.3.1 Theoretical background

A range of mathematical transport models for LMs can be found in the literature. Although the derivation of transport models depends strongly on the specific system constituents and LM configuration, i.e., physical phases and contactor arrangement, the solute-diffusion approach is their common starting point (192). These models can be divided into two main groups according to their transport mechanism: simple transport and facilitated transport. In the simple transport model, the solute mass transfer rate is governed only by its respective phase affinity, which can be quantified by the species chemical potential in the solution. In the facilitated transport, also known as reactive extraction, the solute undergoes a chemical reaction to enhance the molecule movement toward the stripping phase.

As with other spontaneous phenomena, the movement of solutes in LMs occurs when the Gibb's free energy of the system is minimized. In this case, the system is a set of different components and the free energy is the

summation of all the chemical potentials for each component in the mixture. In LM, the solute moves across the solvent (membrane phase), from a high to a low chemical potential. In traditional LLX, the solute chemical potential in each phase converges to an equilibrium state, at which point the mass transfer ceases. Contrariwise, in an LM process, the difference of chemical potential between the feed and the membrane, and the membrane and the stripping phase is maintained, for both simple and reactive extraction modes. This enhances the mass transfer, allowing solute movement even against concentration gradients.

The chemical potential of a solution containing solute “*i*”, μ_i ($\text{J}\cdot\text{mol}^{-1}$), is given by its chemical potential as a pure component, μ_i^p , and its activity, a_i ($\text{mol}_i\cdot\text{mol}^{-1}$), which is defined as the solute concentration, c_i ($\text{mol}_i\cdot\text{mol}^{-1}$) times its activity coefficient, γ_i (-). Both μ_i^p and γ_i can be lumped together into a standard chemical potential term (μ_i^{std}), therefore the solute chemical potential contribution can be expressed by [Eq. 5.1](#):

$$\mu_i = \mu_i^p + RT\ln(a_i) = \mu_i^p + RT\ln(\gamma_i c_i) = \mu_i^{\text{std}} + RT\ln(c_i) \quad (5.1)$$

In a one-dimensional frame, considering the mass transfer occurs in only one-dimension trough the x-axis, the driving force corresponds to the chemical potential gradient, $-d\mu_i/dx$. The solute chemical potential across an LM barrier is represented in [Figure 5.5](#); the solute movement can be divided into seven steps from the feed down to the stripping stream:

- i*) from the bulk feed solution to the proximity of the membrane;
- ii*) transport to the surface of LM;
- iii*) interface adsorption into the LM;
- iv*) inner movement within LM;
- v*) desorption from LM interface;
- vi*) transport in the proximity of the LM on the stripping side;
- vii*) transport to the bulk stripping phase.

At the feed and stripping phases, i.e., steps *i)*, *ii)*, *vi)* and *vii)*, the mass transfer resistance is increased due to a concentration polarization effect, reducing the solute movement at the bulk streams and widening the interface film thickness at both membrane sides. The aforementioned effect may be minimized by increasing turbulent mixing at the membrane surface.

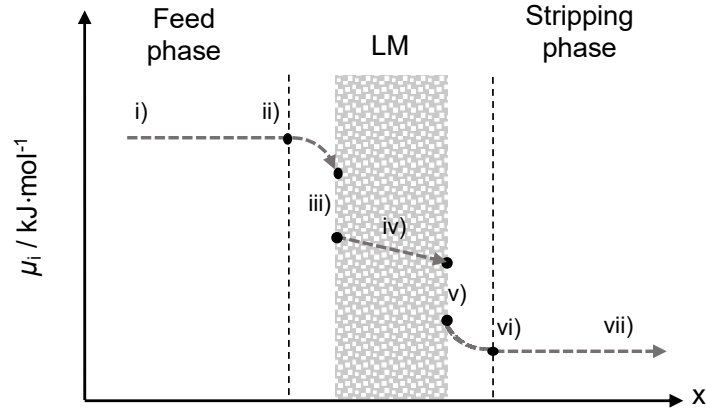


Figure 5.5. Solute chemical potential, $\mu_i / \text{kJ}\cdot\text{mol}^{-1}$, profile through a liquid membrane.

If a negligible influence of activity coefficient and molar density variations along the x -axis is assumed, i.e., they are constant values, the chemical potential gradient result in Eq. 5.2, as a function only of the concentration profile, C_i ($\text{mol}_i\cdot\text{m}^{-3}$). According to the Nernst-Planck equation, without considering an electrostatic potential, the solute mass flow per unit area, J_i ($\text{mol}_i\cdot\text{m}^{-2}\cdot\text{s}^{-1}$), can be determined by the solute concentration times the molecular mobility, u_i , and the driving force (197). The result resembled Fick's law of diffusion as shown in Eq. 5.3, where D ($\text{m}^2\cdot\text{s}^{-1}$) is the solute diffusion coefficient.

$$\frac{d\mu_i}{dx} = \frac{RT}{c_i} \frac{dc_i}{dx} = \frac{RT}{C_i} \frac{dC_i}{dx} \quad (5.2)$$

$$J_i = C_i u_i \left(-\frac{d\mu_i}{dx} \right) = -u_i RT \frac{dC_i}{dx} = -D \frac{dC_i}{dx} \quad (5.3)$$

In the bulk phases, the diffusion coefficient is given by the Stokes-Einstein correlation, Eq. 5.4, based on the Boltzmann constant, $k_{\text{Boltzmann}} = 1.38 \cdot 10^{-23}$ (J·K⁻¹), temperature, T (K), phase dynamic viscosity, η (Pa·s), and molecule radius, r (m), (250).

$$D = \frac{k_{\text{Boltzmann}}T}{6\pi\eta r} \quad (5.4)$$

Considering a steady-state mass transfer without chemical reaction and a membrane phase totally immiscible, the concentration profile may be simplified as shown in Figure 5.6, and Eq. 5.3 simplified into Eq. 5.5, where the solute flux, J_i , depends only on the membrane thickness δ (m), the diffusion coefficient D (lumped together into a new mass transfer coefficient, k_{phase} (m·s⁻¹)), and the difference in solute concentration (ΔC_i). In this approach, the films and solvent diffusion resistances are included as a whole membrane resistance, as well as the pore diffusion resistance for the supported membranes cases. C_{Fi}^* and C_{Si}^* are hypothetical solute concentrations at their respective “whole-barrier” side in the feed and the stripping phases, respectively. The overall process results in three stages: *i*) feed to membrane extraction, also called pertraction; *ii*) membrane diffusion; and *iii*) membrane to stripping recovery, as shown in Eq. 5.6.

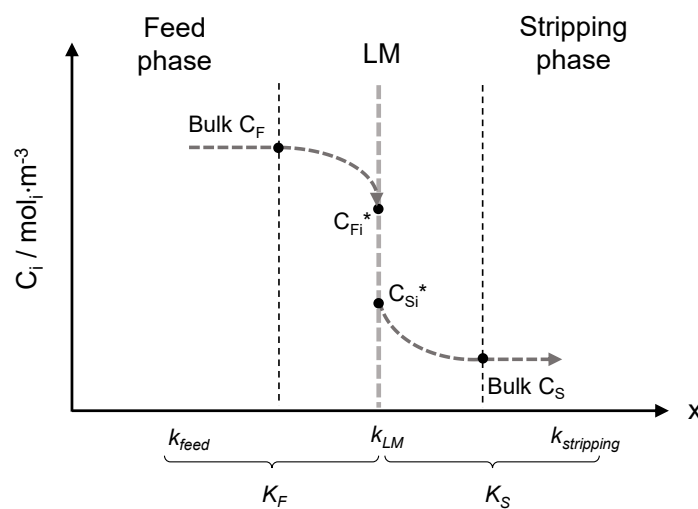


Figure 5.6. Solute concentration, $C_i / \text{mol} \cdot \text{m}^{-3}$, profile through a liquid membrane.

$$J_i = \frac{D}{\delta} \Delta C_i = k_{phase} \Delta C_i \quad (5.5)$$

$$J_i = k_F(C_{BF} - C_{Fi}) = k_{LM}(C_{Fi} - C_{Si}) = k_S(C_{Si} - C_{SB}) \quad (5.6)$$

The global mass transfer coefficient at the feed and stripping phase, K_F and K_S , is obtained by Eq. 5.7 and Eq. 5.8, respectively, where the solute distribution coefficient, m , assumed constant over the concentration range, is expressed by Eq. 5.9 (242).

$$\frac{1}{K_F} = \frac{1}{k_F} + \frac{1}{m \cdot k_{LM}} + \frac{1}{m \cdot k_S} \quad (5.7)$$

$$\frac{1}{K_S} = \frac{m}{k_F} + \frac{1}{k_{LM}} + \frac{1}{k_S} \quad (5.8)$$

$$m = \frac{C_{Si}^*}{C_{FB}} = \frac{C_{Si}}{C_{Fi}} = \frac{C_{SB}}{C_{Fi}^*} \quad (5.9)$$

If no solute accumulation in the film is assumed, i.e., when a steady-state is reached, the total mass flux is defined by the membrane permeability, P ($\text{m} \cdot \text{s}^{-1}$), resulting in Eq. 5.10.

$$J_i = K_F \cdot (C_{FB} - C_{Fi}^*) = K_S \cdot (C_{Si}^* - C_{SB}) = -P \cdot (C_{SB} - C_{FB}) \quad (5.10)$$

For multi-component mixture separation, where two or more solutes are present, the membrane selectivity for an a -component with respect to a b -component, $S_{a,b}$, is determined by the ratio of their respective permeabilities, as shown in Eq. 5.11:

$$S_{a,b} = \frac{P_a}{P_b} \quad (5.11)$$

Since temperature affects the solute chemical potential in each phase, the membrane permeability is sensible to temperature changes. Permeability temperature dependence, $P_i = P_i(T)$, can be described according to an Arrhenius-form equation, Eq. 5.12, where $R = 8.314 \text{ (J}\cdot\text{mol}^{-1}\cdot\text{K}^{-1})$ is the gas constant and $E_a \text{ (J}\cdot\text{mol}^{-1})$ the activation energy, which is a fitting parameter usually obtained using experimental data (198).

$$\frac{P_i(T_2)}{P_i(T_1)} = \exp\left[-\frac{E_a}{R}\left(\frac{1}{T_2} - \frac{1}{T_1}\right)\right] \quad (5.12)$$

5.3.2 Transport mechanisms in liquid membranes

The commonly accepted solute transport mechanism in an LM is solution-diffusion, where transport is governed by the chemical potential gradient as explained in Section 5.3.1. This corresponds to the so-called simple transport model (Figure 5.7a); the solute diffusion depends only on the intermolecular interactions, such as van der Waals forces, electrostatics, and hydrogen bonding.

However, in order to overcome the trade-off behaviour in solution-diffusion membranes, reaction-activated transport mechanisms can be found, where the mechanism grows in complexity and variable number, yet the mass transfer rate is increased due to a resistance reduction either at the interfaces or within the LM. The stripping phase reaction-facilitated transport, Figure 5.7b, allows compensating for the lack of spontaneity on the solute back-extraction from the LM. Since a high solute solubility in the membrane phase improves the extraction from the feed solution, desorption into the stripping phase may be an important resistance. Solute saturation in the membrane reduces, even to an endpoint, the solute flow rate. To diminish this effect, an agent (B) dissolved in the stripping stream continuously reacts with the solute (A) to decrease the concentration at the interface, promoting the solute desorption and the overall solute flux. Likewise, buffers, strong acid or base solutions, are used to reach an optimum extraction yield by controlling the pH.

If the main resistance is at the membrane phase, a third agent may be included to reinforce its internal movement, and this is known as a carrier-facilitated transport mechanism, see [Figure 5.7c](#). The carrier, a complexing agent, must be soluble only in the LM to ensure membrane stability without leaching to the other streams. Solute (A) reacts with the carrier (C) at the feed-membrane interface to form the complex (AC) that diffuses through the LM. Then the reaction is reverted at the membrane-stripping interface, allowing the solute desorption and recycling of the carrier. The flow rate increases with the complexing agent concentration in the diluent, which acts as a barrier with no significant extraction role.

The formation of complexes may also involve more compounds from the feed or stripping phases. In couple facilitated transport, [Figure 5.7d](#), two or more substances are transported through the membrane along with the target solute as a sole complex molecule. A couple-counter-facilitated transport, [Figure 5.7e](#), can be used to maintain the osmotic pressure or the solution electroneutrality, exchanging substances between the feed and stripping phases. Carrier selection thoroughly depended on the complexation and decomplexation rates balance. On one hand, weak carriers do not reach suitable fluxes due to the slow extraction rate at the feed-membrane interface but offer a spontaneity decomplexation to release the solutes toward the stripping phase. On the other hand, strong carriers result in a high initial solute flux at the feed-membrane interface, but they quickly saturate the membrane phase, reducing the concentration gradient within the membrane and thereby the flux rate. The carrier strength is determined by its bond energy, where a suggested range is $1 \cdot 10^4 - 5 \cdot 10^4 \text{ kJ} \cdot \text{mol}^{-1}$ (250).

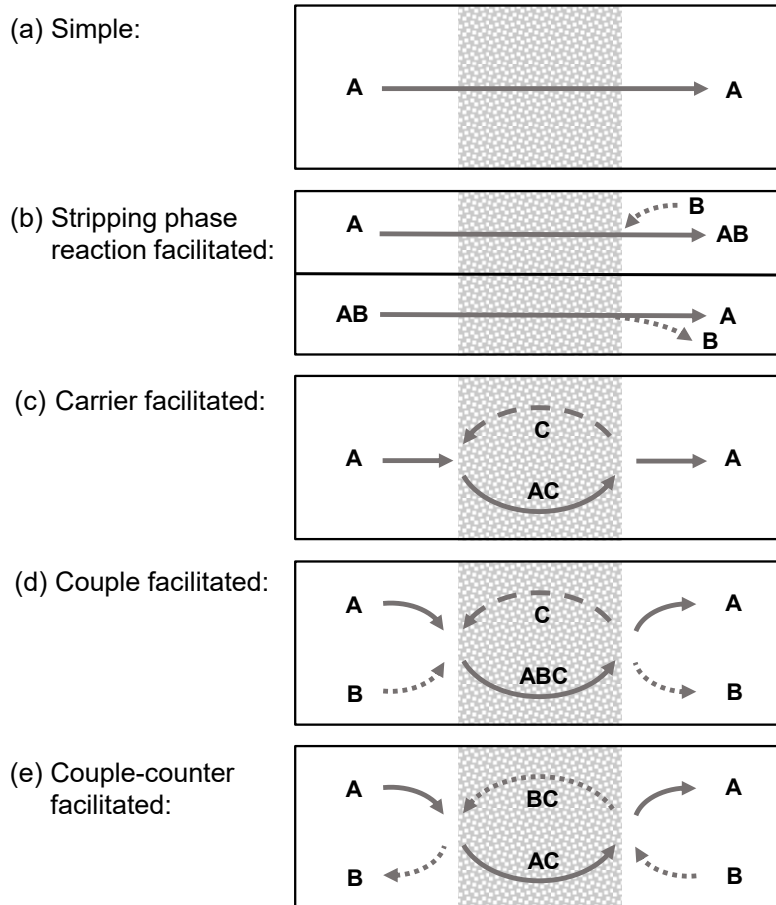


Figure 5.7. Transport mechanisms in liquid membrane: (a) simple transport; (b) stripping phase reaction reaction-facilitated transport; (c) carrier-facilitated transport; (d) couple-facilitated transport; (e) couple-counter-facilitated transport.

5.3.3 Extraction and recovery efficiencies

Despite LMs being described as single-step processes, they effectively work in two stages: i) solute extraction from feed to membrane, and ii) solute recovery from the membrane to the stripping stream. [Figure 5.8a](#) schematized the typical phase concentration behaviour observed in LM processes. As the extraction progresses, the solute concentration decreases in the feed phase and increases in both membrane and stripping phases, surpassing the concentration in the feed under favourable conditions. If the membrane phase volume is enlarged with respect to the other phases, a greater solute extraction occurs, but this does not imply a greater recovery to the stripping phase. In the first stage, the larger membrane volume enhances the flux due to a lower solute concentration in the LM, but flux gets reduced at the stripping stage due to solute accumulation halfway through the process.

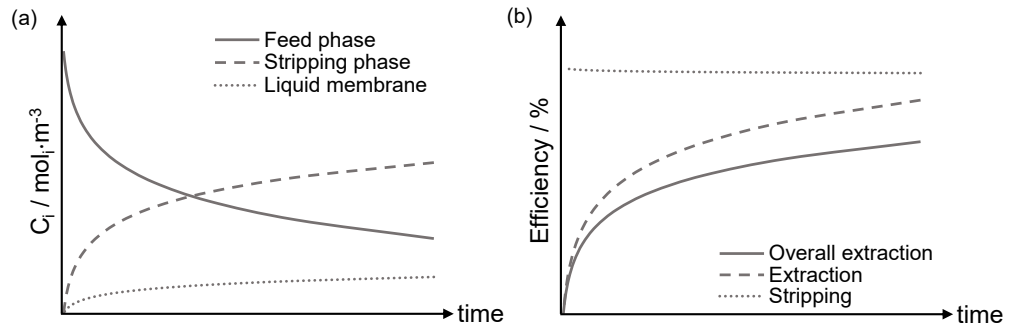


Figure 5.8. Schematic typical behaviour in the LM extraction process: (a) phase concentration profile; (b) extraction efficiency parameters.

The performance of an LM is typically described by the capacity to transport the target solute in terms of extracting percentage or permeation ratios. Although the terminology used to report it varies among works. The overall extraction, recovery, or yield (Ex) is expressed by the total solute recovery in the stripping phase with respect to the initial feed, according to Eq. 5.13, where $C_{i,S}$ and C_{i,F_0} are the solute concentration in the stripping phase and the solute initial concentration in the feed phase, respectively.

$$Ex = \frac{C_{i,S}}{C_{i,F_0}} \quad (5.13)$$

Generally, there are two extraction efficiencies to consider in the process, the extraction of solute from the feed stream (Ex_F) and the solute recovery to the strip stream, the so-called stripping efficiency (Ex_S). The extraction efficiency (Eq. 5.14) is defined as the membrane capacity to extract the solute from the feed phase, while the stripping efficiency (Eq. 5.15) represents the membrane capacity to release the solute into the stripping phase (206). Note that these definitions assume a feed-stripping volume ratio equal to 1. Otherwise, a mass-based relationship must be adopted to properly describe the extraction performance.

$$Ex_F = 1 - \frac{C_{i,F}}{C_{i,F_0}} \quad (5.14)$$

$$Ex_S = \frac{C_{i,S}}{C_{i,F_0} - C_{i,F}} \quad (5.15)$$

Typical Ex (solute recovery), Ex_F , and Ex_S profiles are illustrated in [Figure 5.8b](#). Due to membrane solute retention, the expected recovery is lower than the extraction from the feed phase. On the other hand, Ex_S depends on the membrane-stripping capacity to accomplish the solute back-extraction.

5.3.4 Liquid membrane stability

As aforementioned, the main limitation of LMs is membrane stability, i.e., their capacity to stay as a separate phase, avoiding leaching of one or more components from it. Membrane losses within the feed and stripping phases may occur by dispersion (or evaporation in the case of gaseous streams). Losses also imply contamination of the feed and/or stripping streams with the leached LM components, which can negatively affect the separation process such as when toxic diluents or carriers are used [\(194\)](#). Therefore, phase immiscibility is crucial in order to guarantee stability, although the nature and amount of the potential leached components and operational conditions have a great influence as well. For instance, the limited contact area of BLMs results in lower membrane losses and hence, higher stability.

ELM stability may be expressed by two distinct terms: i) the membrane breakage rate (%), which represents the percentage of internal phase losses toward the external phase, and ii) the emulsion swelling rate (%), which measures the increment in the emulsion volume. Usually, high osmotic pressures between the feed and the stripping phase might cause reverse micelles (aqueous solution pockets) transporting water to the internal phase, which leads to globule swelling. Being able to homogenize speed and emulsification time is crucial in the formation of a stable emulsion. Although higher stirring speed contributes to increasing the mass transfer rate, it may cause breakage. Emulsion size, composition, and operational conditions, such as temperature, pH, concentrations, and stirring rate, as well as retention time, might affect the swelling phenomenon [\(228\)](#). Both effects are correlated and determine the overall LM extraction performance: high swelling rates may lead to emulsion breakage.

Droplet size and rheological properties are the main factors in ELM stability. Both emulsion globule and droplet sizes depend on the phase ratios, composition, solvents properties, and emulsification process conditions. Bigger globules that contain more droplets can reach a large internal mass transfer, around $10^6 \text{ m}^2\cdot\text{m}^{-3}$. To ensure good ELM stability without jeopardizing its performance, the inner droplets, usually the stripping phase, should have a small diameter of about 1-3 μm . The whole membrane globule has an average size of less than 2 mm (242). As the diluent is the major component in an LM, its immiscibility ability greatly contributes to better ELM stability. Also, it is worth noting that as discussed in Section 5.3.1, the diffusion coefficient is inversely proportional to the membrane viscosity (see Eq. 4.4); so, the use of common nontoxic diluents with low water solubility and high viscosity, results in greater mass transfer resistance (222).

Phase ratios, i.e., emulsion-to-feed and stripping-to-membrane ratios, play other fundamental roles in ELM stability. The relation between emulsion globule (membrane and stripping phase heterogeneous mixture) and feed phase volume is defined as the treat ratio, $V_{\text{ELM}}/V_{\text{F}}$. At a larger treat ratio or large emulsion volume, the total interface area is increased by the number and dispersibility of membrane globules in the global mixture (220). On the other hand, the internal-to-membrane phase ratio corresponds to the stripping (internal phase) to the membrane phase volume proportion, $V_{\text{int}}/V_{\text{LM}}$. Increasing this ratio causes a reduction of the LM requirements for the process, although the emulsion globules become unstable, leading to breakage or emulsion inversion, i.e., the emulsion might turn from W/O to O/W. When the internal-to-membrane phase ratio is increased, an improvement can be observed, but this might also lead to the internal droplet coalescence. Contrariwise, low internal-to-membrane phase ratios lead to poor inner droplets dispersion and high surface tension, which reduces the overall membrane performance and stability. Since the internal surface area at the membrane-stripping interface is typically several orders of magnitude larger than at the feed-emulsion interface, the major mass transfer resistance is found

at the membrane adsorption stage. Therefore, the treat ratio has a larger influence on the overall process performance. On the contrary, the internal-to-membrane phase ratio has a less significant effect on the performance, and it should be optimized aiming for membrane stability rather than high extraction yields.

In SLMs, the lack of membrane phase within the pores reduces solute flux and its selectivity. Thus, the stability of SLMs, defined as the capacity of the support to hold the membrane phase, becomes their main limitation. As for all the LMs, the stability of the SLM depends on the membrane phase immiscibility with the other streams, although the affinity LM-support and the capillary forces also favour retention. Despite the increase of mass transfer resistance, viscous membranes show higher stabilities due to larger van der Waals forces. Hydrophobic supports retain organic solvents more strongly by strong molecular interactions. Pore size and tortuosity of the support porosity must be tailored to ensure a high solute flux and avoid LM losses. Generally, bigger pore sizes increase the effective surface area but reduce the capillary forces, while higher porosities enhance the mass transfer rate and stability due to hydrostatic pressure (198).

When several extraction cycles are carried out, the membrane performance may be affected by stability issues. Recycling membranes leads to partial compound or total LM losses, changing the membrane physicochemical properties. During the ELM de-emulsification stage, losses of volatile modifiers alter its viscosity and thereby the overall mass transfer coefficient (220). Although PIM shows high stability, a minor drop in solute transport can be observed when it is reused. PIM losses can be evidenced by membrane mass changes or a structural variation on the surfaces in scanning probe microscopy images (238). Still, proper membrane setup has been shown to reduce the losses over the cycles, preserving an extraction yield nearly to the original one (213,251).

5.3.5 Compounds interaction within liquid membranes

In a steady-state process, the overall mass transfer from the feed to the stripping phases is controlled by the step with greater resistance. As stressed in [Section 5.3.1](#), the extraction in LM can be subdivided into internal streams, surface interface films, and interfaces transport steps. By implementing proper stirring at each phase, the concentration polarization effect and thereby the film resistances can be minimized. Including a carrier to the membrane phase and a stripping agent to the receiving phase, i.e., adopting facilitated transport, the inner LM movement is considerably improved. The above arrangements leave the major resistance at the interface mass transfer. Nevertheless, complexation kinetics become dominant. The mass transfer is not limited by the bulk feed to membrane resistance, but by the interface transport. Likewise, solute desorption is limited by decomplexation. Higher carrier concentrations increase chances for complex formation, while higher stripping agent concentrations favour carrier regeneration, both improving the mass flux within the membrane phase. Nevertheless, this increment has a limit; when the ionic strength of the stripping solution becomes a significant resistance to the solute mass transfer, complex carrier-solute accumulates at the membrane-stripping interface.

Emulsion surfactants have an important effect on the membrane performance as well as the carrier. To form the emulsion globules, ionized or non-ionic surfactants must be included either in W/O/W or O/W/O systems, although the selection depends on the respective phase solubility. The hydrophilic-lipophilic balance value (HLB) is used to represent the surfactant molecule percentage of hydrophilic functional groups. At higher HLB (> 8), i.e., more hydrophilic surfactant, the mixture tends to form an O/W/O system, and vice versa, when $HLB < 6$, W/O/W emulsions take place. A common environmentally friendly surfactant found in the literature is sorbitan monooleate, Span[®] 80, ($HLB = 4.3$) ([226](#)). Nevertheless, under certain conditions, Span 80 have been reported to permit water transport, causing swelling, and being susceptible to hydrolysis reactions ([252](#)). Besides

contributing to the emulsion drop formation and its stability, surfactants influence the membrane-solute interactions. Better extraction efficiency can be observed at lower surfactant concentrations. The improvement is maintained as far as it is kept at a minimum concentration, above which point the extraction performance suddenly drops due to the membrane instability (215). Furthermore, surfactant agents may act as a carrier as well, forming complexes with the solute. Separations of similar components require careful system optimization. In multicomponent systems, such as fermentation broths, membrane selectivity becomes a paramount factor. For instance, the proper surfactant agent choice has shown to be determinant on the selective separation of acetic acid from succinic acid in an aqueous solution (253).

The extraction performance depends on the specific mechanisms resulting from the solute-membrane interaction. This effect is particularly evident in dissociable solutes, where adjusting the solution pH, the molecular acid form, i.e., dissociated, undissociated, mono- or di-anionic forms, can be controlled. Pratiwi et al. (203) compared the extraction of succinic acid with an IL-based SLM and PIM. For the first case, the solute permeability improves at a feed pH of 6.5, coincident with the fermentation broth pH range (22). At such pH, the dissociated form of the acid reacts by an ion-exchange mechanism with the LM and diffuses as an IL-solute complex. On the other hand, for the PIM tests, better permeability was found at pH lower than the pKa of succinic acid, suggesting less membrane-succinic anion interactions, and the solute was extracted by simple transport mechanisms (see Figure 5.7a). The same dependence was observed in an amino acid extraction study, where authors found an increase in the extraction efficiency directly proportional to the stripping phase pH and inversely proportional to feed acidity. Results identify pH as one of the most important variables in the extraction operation (213).

5.4 Sustainable separations with liquid membranes

LM technology has proved to be a sustainable separation method at a laboratory scale, which could potentially replace commercial LLX systems for several applications. As observed in Figure 5.9 throughout the last decades, there has been a sustained increase in LM research.

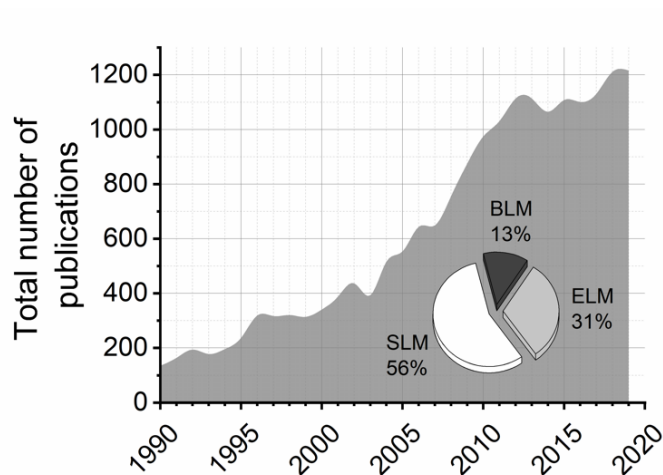


Figure 5.9. Total liquid membrane publications number per year given by the search engine Google Scholar using the keywords “*bulk liquid membranes*”, “*emulsion liquid membranes*”, and “*supported liquid membranes*.”

This section presents a comprehensive recompilation of recent studies published on the topic, focusing on liquid stream separations. In the last decade, good progress has been made on LM technology for the recovery of value-added substances. Organic LMs have been extensively studied for the recovery of organic compounds from aqueous solutions in the biorefinery industry. ELMs have been successfully used for the recovery of metal ions, such as copper, lithium, bismuth, cadmium, silver, vanadium, palladium, and high-value RE elements. LMs have also proved useful for wastewater remediation. For instance, removal of pullulans such as by-product organic compounds, pharmaceutical residues, lignin from pulping waste, heavy metals, and nuclear radioactive waste have been accomplished. Extracted solutes reported in the last 10 years using LMs are discussed in detail in this review.

For more specific details on LMs and their applications, readers are referred to the textbook by Kislik et al. (192) where LM model derivations and their progress in separation processes are discussed, and chapters of other books regarding LM basic concepts (242,250), industrial developments (193,197), and novel IL-based membranes (202,254). Likewise, literature offers LM chapters dedicated to specific applications, such as pharmaceutical and biotechnology (195), GS (255,256), radioactive waste and metal separation (257), organic acids recovery (203), and dyes removal (258).

5.4.1 Recovery of biomolecules in bio-refinery

Biorefineries are an emerging industry conceived for the conversion of biomass into a range of valuable bio-based compounds as alternatives to conventional commodities such as polymers, organic acids, alcohols, composites, surfactants, paintings and coatings, lubricants; binders; plasticizers; and solvents. It is well known that the production of biomolecules by fermentation routes often presents challenges in the downstream purification stages. Fermentation broths contain mainly water and a small concentration of valuable biomolecules, which often involves very high energy consumption for their extraction. For instance, nonvolatile organic acids, high-value building blocks for a wide variety of industrial sectors (16), require separation processes such as precipitation or liquid extraction using volatile organic compounds (VOCs). Moreover, throughout the bio-organic acid production process, the separation cost can represent more than two-thirds of the total production cost (23,259). In order to overcome the high energy requirement and the use of toxic compounds, LMs have been extensively investigated. They have been successful in the extraction of organic acids exploiting the properties of novel solvents such as ILs (203). In this section, recent research on LMs application for bio-based organic acids and other essential biomolecules is presented and summarized in Table 5.2.

Table 5.2. Summary of recent liquid membrane studies for the recovery of compounds in biorefinery.

| Solute | Membrane | Results | Ref. |
|-----------------------|---|--|-----------|
| Lactic acid | TOA in n-heptane ELM | 95% extraction and 80% stripping efficiencies | (260) |
| | Aliquat 336 in sunflower oil ELM | 99% extraction efficiency | (215) |
| | Aliquat 336 in rice oil ELM | 96% extraction efficiency | (217) |
| | Aliquat 336 in rice oil ELM | 95% extraction efficiency | (218) |
| | TOA in dodecanol and dodecane TFLM | 27% in productivity increase | (234,261) |
| Succinic acid | TOA or Amberlite LA-2 in kerosene ELM | 98% extraction efficiency | (262) |
| | Palm oil ELM | Complete recovery | (220) |
| Levulinic acid | TBP in imidazolium-based ILs BLM | 99% extraction and 95% stripping | (204) |
| Benzoic acid | Isooctane or dodecane BLM | Diffusive transport model | (263) |
| Gibberellic acid | Aliquat 336 in n-heptane ELM | Recovery of 88% for model solution and for broths 68% for real solution with a concentration factor of 2.2 | (264) |
| Acetic acid | C9232, TOA or Amberlite LA-2 in kerosene ELM | >92% extraction efficiency | (253) |
| | TBP in ([C ₄ min][Tf ₂ N], [C ₄ min][PF ₆], [C ₆ min][Tf ₂ N], and [C ₆ min][PF ₆]) BLM | 92% extraction and 81% stripping efficiencies | (205) |
| | TBA in oleyl alcohol BLM | >75% extraction efficiency | (265) |
| Formic acid | TBA in oleyl alcohol BLM | >57% extraction efficiency | (265) |
| Propionic acid | TBA in oleyl alcohol BLM | >75% extraction efficiency | (265) |
| Butyric acid | TBA in oleyl alcohol BLM | >75% extraction efficiency | (265) |
| Ethanol | n-Hexane ELM | 95% extraction efficiency | (266) |
| ABE | Gelled [C ₄ min][PF ₆] in PTFE hollow fibres-supported liquid membrane (HF-SLM) | Trans-membrane fluxes and selectivity | (211) |
| Penicillin G | HFRLM | Concentration factor of 4.4 | (243) |
| Catechin (\pm C) | TBP in vegetable-based solvent BLM | 70% extraction and 40% stripping efficiencies | (216) |
| Furfural | DES-based in polymeric SLM | Permeability > 3.3·10 ⁻⁴ m·s ⁻¹ | (212) |
| Hydroxymethylfurfural | DES-based in polymeric SLM | Permeability > 0.2·10 ⁻⁴ m·s ⁻¹ | (212) |

Lactic acid is one of the smallest organic acids and a high-value building block used for chemical, food, cosmetic, textile, biomedical, and bioplastic industries. It can be produced from renewable sources, such as biomass and food wastes and a range of separation technologies have been thoroughly researched for its extraction (267). The extraction of lactic acid by ELM was studied using a membrane composed of TOA as carrier diluted in n-heptane and a solution of sodium carbonate as a stripping phase (260). The membrane interchanged the lactate–amine complex with carbonate–amine complex from one phase to another in a couple-counter-facilitated transport regimen (see Figure 5.7e). The authors evaluated the effect of Na₂CO₃ concentration, phase ratios (strip-to-membrane and feed-to-emulsion), and contact time into the lactic acid pertraction (extraction from feed to membrane), and recovery (extraction from membrane to strip) efficiencies. The study determined an optimal operation zone where pertraction efficiency is above 95% and the recovery efficiencies over 80%. Vegetable diluents were also studied for the recovery of lactic acid with green ELMs. Under optimal operation conditions, ELMs based on sunflower oil (215) and rice oil (217,218), using Aliquat 336 as a carrier, proved to reach as high lactic acid recovery values as those obtained in petrochemical-derived solvents-based ELM. As a way to improve extraction yields of lactic acid from fermentation broths, Pérez et al. (234,261) proposed a novel LM configuration (TFLM shown in Figure 5.4a) using a membrane composed of dodecanol and dodecane as diluent plus TOA as the carrier, and sodium carbonate solution as the stripping phase. Feed and stripping droplets were injected into the membrane phase, which improved the phase internal agitation due to the turbulent flow created inside the droplets as well as in the LM within them. Lactic acid removal was done in situ to minimize acidification, thus increasing the fermentation yield. The hybrid fermentation–extractor operation reached a lactic acid productivity 27% greater than that obtained in a conventional fermenter.

Succinic acid is used as a starting material in the production of a wide range of commodities, including 1-4-butanediol, γ -butyrolactone, tetrahydrofuran, and bio-based polymers such as butylene succinic acid. It can be obtained through the fermentation of sugars (e.g. lactose, xylose, arabinose, and cellobiose) from various biomass sources such as whey, cane molasses, straw, corn fibre, crop stalk, wheat, and duckweed (22). Succinic acid extraction yields up to 98% were obtained using TOA or Amberlite® LA-2 (a secondary amine) as extracting agents, in kerosene-based ELM (262). Succinic acid recovery in multiples cycle was assessed using palm oil-based ELM, reaching a complete recovery in the first cycle, dropping to 62% in the second cycle, and lastly, to 43% in the third cycle (220).

Levulinic acid is widely used as a starting material for solvents, biofuels, chemical intermediates, resins, and other products. It can be produced using monosaccharides, HMF, furfural, polysaccharides or starch, and lignocellulosic biomass as raw materials (28). Hydrophobic ILs ($[\text{C}_4\text{min}][\text{Tf}_2\text{N}]$, $[\text{C}_4\text{min}][\text{PF}_6]$, $[\text{C}_6\text{min}][\text{Tf}_2\text{N}]$, and $[\text{C}_6\text{min}][\text{PF}_6]$) were studied for the extraction of levulinic acid using a BLM with TBP and NaOH solution as carrier and stripping phase, respectively (204). Since the ILs employed are denser than the aqueous feed and stripping solutions, the extractions were carried out into a U-tube arrangement. The effect of several operational variables was investigated, although all tested imidazolium-based ILs exhibited similar extraction and stripping efficiencies of up to 99 and 95%, respectively.

Similarly, LMs have been proposed for the recovery of large carboxyl acids. Koter and Szczepański (263) developed a diffusive transport model for aqueous benzoic acid, a food preservative, and precursor of several high-value chemicals, through isooctane or dodecane-based BLM. Considering molecular dissociation and dimerization effects, the authors achieved a successful prediction of the acid concentration profile as a function of time for all three phases. The carrier-surfactant composition of ELMs containing n-heptane, Aliquat 336, and Span 80 was optimized to maximize the recovery from

fermentation broths of gibberellic acid, a vegetal growth promoter (264). The optimization conditions for model solutions resulted in a recovery of 88% and for broths 68% with a concentration factor of 2.2.

Moreover, LMs can be used for the separation of volatile compounds. In carboxylic acid fermentation processes, for instance, acetic acid is a common by-product which leads to product inhibition. C9232-based ELMs showed good performance and high selective acetic acid separation over succinic acid fermentation broth (253). ILs ($[\text{C}_4\text{min}][\text{Tf}_2\text{N}]$, $[\text{C}_4\text{min}][\text{PF}_6]$, $[\text{C}_6\text{min}][\text{Tf}_2\text{N}]$, and $[\text{C}_6\text{min}][\text{PF}_6]$) were studied in BLM for acetic acid removal from aqueous solution using TBP and NaOH solution as the carrier and stripping medium, respectively (205). As a result, extraction and stripping efficiencies of 92 and 81%, respectively, were obtained. In this work, it was found a significant effect of carrier and stripping concentrations on the efficiencies, while the initial feed concentration was not relevant under the operational range. Several other volatile carboxylic acids have been recovered via BLMs from aqueous solutions. Mixtures of oleyl alcohol and tributylamine (TBA) were successfully used for the extraction of acetic, propionic, and butyric acids, with yields over 75%, and yields above 57% for the extraction of formic acid (265). An n-hexane-based ELM was used for ethanol extraction from aqueous matrices (266). The work studied the effect of different salts concentration in the stripping phase and found a drastic reduction in ethanol extraction when salts were present, which was attributed to ions and water co-transport due to osmotic pressure.

LMs have also been used for liquid-gas separations in PV mode. Bio-butanol is a sustainable fuel that is produced via the fermentation of biomass. The resulting broth is an aqueous mixture of acetone, butanol, and ethanol (ABE) that is typically separated via conventional distillation, although research is now geared toward the use of PV membranes, including LMs (268). Hydrophobic HFSLMs based on PTFE filled with $[\text{C}_4\text{min}][\text{PF}_6]$ were prepared and tested for the recovery of butanol from ABE mixtures in aqueous solutions (211). To improve the solvent retention in the pores, the IL was gelled with 12-hydroxystearic acid, and the authors compared the performance of the SLM

in sweep gas PV mode to a membrane evaporation process, using the PTFE HF membrane without IL. Results showed a slight increase in butanol selectivity over the other organic compounds for the SLM with the main mass transfer resistance being the solute diffusion inside the membrane.

Penicillin G is a natural antibiotic and precursor of other semisynthetic ones. Although its recovery from fermentation broths has been industrialized for massive production, gaps remain to improve efficiency and avoid product losses. In this context, the feasibility to recover Penicillin G utilizing HFRLM in a cascade process was studied (243). In this work, hydrophobic PP-based HF supports were filled with di-n-octylamine in iso-octanol and kerosene, and a K_2CO_3 aqueous solution was selected as the stripping phase. The proposed arrangement reached a concentration in the stripping phase of up to 4.4 times higher than that of the feed.

The development of novel green solvents opens an avenue to improve LM technology for sustainable separations (3). In this regard, BLMs containing vegetable-based solvents (sunflower, soybean, and coconut oil) were compared to analogous conventional petrochemical-derived solvents (iso-octane, n-decane, and n-heptane) for the extraction of catechin, a natural substance retrieved from tea leaves with pharmacological applications, from an aqueous solution (216). The selected carrier was TBP, and better extraction performance was obtained when using the bio-based solvents; the BLM with sunflower oil extracted around 70% of catechin and the recovery to the stripping phase was up to 40%.

Alongside ILs, SLM impregnated with DESs have been tested. DESs share many of the features that positioned ILs as promising alternative solvents for several industrial processes. While ILs are composed of a pair of cation-anion, DESs are formed by hydrogen bond donor (HBD) and acceptor (HBA) compounds (72). Recovery of bio-based furfural and hydroxymethylfurfural from model aqueous solutions, starting raw materials in the production of bioplastic monomers, were studied with different polymeric SLMs (212).

Several DESs, based on decanoic acid and thymol as the HBD-component and tetraoctylammonium bromide, thymol, menthol, and lidocaine as the HBA-component, were used as the membrane phases. In such work, authors found larger furfural permeability than hydroxymethylfurfural, attributed to the solute hydrophobicity difference. Moreover, the study showed that bigger pores and lower viscosity improve the permeability but increased solvent losses, pointing out the extraction method limitations besides the importance of its proper optimization.

5.4.2 Amino acid recovery

Amino acids are the fundamental constituents of proteins. Their primary exponents are L-cysteine, L-histidine, L-isoleucine, L-leucine, L-lysine, L-methionine, L-phenylalanine, L-threonine, L-tryptophan, and L-valine. They have an important place in the chemical industry, and proof of this is their rising sustained commercialization, projected to surpass \$35 billions in the coming years (269). They are used as starting material for the synthesis of chiral-active ingredients and bioplastics, as well as food, agricultural, and pharmaceutical products manufacturing. Sustainable amino acid production is mainly carried out by aerobic microbial conversion, attaining growing interest in their synthesis from renewable feedstock, such as lipids, cellulose, hemicellulose, lignin, and chitin. Table 5.3 collects the studies developed for amino acids recovery with LMs.

Table 5.3. Summary of recent liquid membrane studies for the recovery of amino acids.

| Solute | Membrane | Results | Ref. |
|-----------------|--|-----------------------------|-------|
| L-tryptophan | Quaternary ammonium salt-based DESs in polymeric SLM | 86% extraction efficiency | (213) |
| L-cysteine | Dicyclohexyl-18-crown-6 in toluene ELM | > 96% extraction efficiency | (270) |
| L-phenylalanine | Paraffin, sulfonated kerosene, D2EHFA ELM | > 94% extraction efficiency | (271) |

Proteins and amino acids are complex molecules, which are susceptible to be denatured by organic solvents (44). To avoid compounds denaturalization, biocompatible solvents, such as hydrophobic ILs, have been proposed for amino acid extraction (71). Likewise, DESs have shown high biocompatibility. Several polymeric porous supports were impregnated with quaternary ammonium salt-based DESs for amino acid recovery from aqueous solutions (213). Among other common amino acids, the best extraction yield (86%) was achieved for tryptophan, followed by glycine and DL-aspartic acid with yields for both greater than 60%. The optimal SLM, in terms of solute flux, was found for a mixed cellulose support impregnated with DESs composed of choline chloride and *p*-toluene sulfonic acid, at a molar ratio of 1:2. This membrane was reused in extraction cycles up to seven times, with an extraction efficiency drop of less than 20%. The observed decrease was attributed to solvent losses due to membrane instability. L-cysteine extraction from a KCl solution was achieved using a dicyclohexyl-18-crown-6 in toluene (270). The observed transport mechanism was based on the extraction agent and the potassium ion complexation, which acted as the actual carrier for amino acid extraction. Furthermore, the proposed ELM gave a high L-cysteine selectivity over other amino acids. Through a back propagation neural network combined with a genetic algorithm, the extracting of L-phenylalanine using ELM was successfully simulated in real-time (271). Training the simulation with experimental data, the authors found the optimal operational conditions. An extraction efficiency greater than 94% was reached with an ELM composed of paraffin, sulfonated kerosene, D2EHPA, and Span 80.

As with bio-based products, the downstream separation in the amino acid production is a critical stage due to their complexity and energy consumption. Moreover, amino acid production requires a specific chiral orientation. Therefore, the selective separation of amino acid enantiomers from racemic mixtures becomes one of the key concerns. Enantioseparation achieved through LMs has been reported to be comparable to traditional techniques, such as chiral chromatography and diastereoisomeric crystallization. In this

regard, high enantioselectivity of amino acid was reported for HFSLM containing specific chiral carriers, such as N-3,5-dinitrobenzoyl-L-alanine octyl ester, copper(II) N-dodecyl-L-hydroxyproline, and quinidine or quinine derivatives (196). Selective extraction of stereoisomers also can be improved by a previous enzymatic reaction, which converts the target enantiomer into a complex transportable by the LM.

5.4.3 Environmental and wastewater treatment

Water streams from industrial processes contaminated with organic compounds are a growing hazard to population health and aquatic ecosystems. Their treatment is of paramount concern, prompting stricter government regulations. Luckily, many of these pollutants can be removed to meet the discharge requirements while valuable chemicals are recovered. Studies on wastewater remediation with LMs are compiled in Table 5.4.

Table 5.4. Summary of recent liquid membrane studies for wastewater treatment.

| Solute | Membrane | Results | Ref. |
|--------------------------------------|--|--|-------|
| Phenol, tyrosol, and p-coumaric acid | Hostarex A327, Alamine 336, Aliquat 336, and Cyanex 923 in isoparaffinic hydrocarbon ELM | 97–99% recovery efficiency | (272) |
| p-Nitrophenol | n-Hexane, n-heptane, and kerosene ELM | Complete removal | (251) |
| Aniline | n-Hexane, n-heptane, and kerosene ELM | Complete removal | (251) |
| Phenol | Palm oil:kerosene ELM | 83% extraction efficiency | (221) |
| | ([C ₄ min][Tf ₂ N], [C ₄ min][PF ₆], and [C ₄ min][FAP]) BLM | 96% extraction and 98% stripping efficiencies | (206) |
| | [C ₄ min][PF ₆] BLM | 99% removal | (207) |
| Phenol and chlorophenol compounds | [C ₄ min][PF ₆] + TBP kerosene ELM | >99% phenol removal >90% chlorophenol removal | (208) |
| Bisphenol A | ILs supported in PVDF SLM | 44% of solute permeation within 24 hours | (209) |
| | n-Heptane in PP HFSLM | 96% extraction efficiency | (273) |
| Diclofenac | Tetrabutylammonium bromide dichloromethane in ELM | 99% removal | (274) |
| Ibuprofen | TOA in Parleam 4 ELM | Complete removal | (275) |
| Tetracycline | TBP and Fe ₂ O ₃ nanoparticles in n-heptane PELM | 97% removal | (276) |
| (S)-amlodipine | O,O'-dibenzoyl-(2S,3S)-tartaric acid | 78% extraction and 75% recovery efficiencies. Enantiomeric excess of 58% | (277) |
| Ethylparaben | TOA in n-heptane ELM | 90% removal | (278) |
| Propylparaben | TOPO in hexane ELM | Complete removal | (279) |
| Kraft lignin | Aliquat 336 in kerosene and 2-ethyl-1-hexanol ELM | 98% recovery efficiency | (280) |
| Lignosulfonate | TOA in dichloroethane in Nylon 6,6 SLM | 50% removal | (281) |

Phenolic compounds are commonly generated as waste in several industries; however, they are extendedly used as raw material for chemical derivatives' production. Thus, there is substantial research toward the development of sustainable extraction processes. Treatment of olive oil plant wastewater for the removal of phenol and two of its derivatives, tyrosol, and *p*-coumaric acid, was carried out with an ELM, with a recovery of up to 97–99% (272). Several carriers including Hostarex® A327, Alamine® 336, Aliquat 336, and Cyanex® 923 were tested in isoparaffinic hydrocarbon. The effect of adding iso-decanol as a membrane modifier was also studied and showing an enhancement in the extraction efficiency. Removal of *p*-nitrophenol (starting compound for several pesticides) and aniline (pharmaceutical and dye waste) was studied using organic solvent-based ELM (251). Operational variables and membrane composition, such as diluent type, *n*-hexane, *n*-heptane, and kerosene, and surfactant (Span 80) concentration were optimized. The work showed a nearly complete *p*-nitrophenol and aniline removal.

In order to reduce the organic solvent requirement in the ELM conformation, the use of vegetable oils was proposed. The effect of the diluent composition ratio, palm oil–kerosene mixture, on the phenol removal efficiency was studied (221). With a considerable solvent decrease, a palm oil-to-kerosene ratio of 70:30 showed good emulsion stability. Under optimal conditions, phenol extraction using the pure diluents reached 97 and 82% for kerosene and palm oil, respectively, while at 70:30 diluent composition ratio, the removal was nearly 83%. Since no carrier was used, the phenol transport was achieved by simple diffusion through the membrane, reacting with a NaOH solution that constituted the stripping phase (see Figure 5.7b). This suggests that the membrane viscosity, related to the solute diffusivity by Eq. 5.4, is the main factor in the membrane performance.

IL-based LMs have also been investigated for the removal of phenol. Hydrophobic imidazolium-ILs ([C₄min][Tf₂N], [C₄min][PF₆], and [C₄min][FAP]) were used for the preparation of BLM for phenol removal from

aqueous effluents (206). Maximum extraction and stripping efficiencies of 96 and 98%, respectively, were obtained. This work also compared the performance of LMs containing $[C_4min][Tf_2N]$ with analogues made of conventional organic solvents such as dichloromethane. Due to the low viscosity of the organic solvent, higher phenol diffusivity values were expected. However, similar extraction and stripping efficiencies were obtained for both types of solvents. It is worth noting that ILs can be considered for the preparation of facilitated-transport LMs as well. For example, phenol migration was studied in $[C_4min][PF_6]$ in BLMs, where the complex solute-IL was formed and was transported across the membrane by hydrogen bonding interactions (207). Likewise, $[C_4min][PF_6]$ was added to TBP and used as the carrier in the removal of phenolic compounds using kerosene-based ELMs (208). In comparison to pure TBP carrier, the use of the IL mixture improved the emulsion stability as well as the removal efficiency. Given the high viscosity of ILs, they are also suitable candidates for the preparation of SLMs. A range of ILs supported in a PVDF matrix was tested for the removal of bisphenol A, an endocrine disruptor used in plastic production, from aqueous effluents (209). Flat sheet SLMs of 12 cm² were tested and reached a maximum of 44% of solute permeation within 24 hours, and it was suggested that performance could be improved by phase pH control. Moreover, in another work, a maximum bisphenol A extraction of 96% was achieved in a 9-hour cycle using an HFSLM module (273). The membrane was PP fibres impregnated with n-heptane, with a total surface area of 1.4 m². Although a conventional organic solvent was used in the aforementioned study, the results highlight the feasibility of scaling up SLM for industrial processes.

Looking at other types of contaminants in water bodies, the presence of prescribed and unprescribed drugs, such as painkillers and nonsteroidal anti-inflammatories, is a growing field of concern in domestic wastewater treatment plants. Human and animal excretions may carry several substances discharged in faeces and urine in unchanged form or metabolized into

secondary compounds. Nevertheless, due to their toxicity and bioaccumulation, the presence of pharmaceutical waste in household and hospital waste effluents means a risk to aquatic ecosystems with potential hazards to human health. For instance, around 15% of the administered anti-inflammatory drug diclofenac is excreted without chemical changes (274), while 70% of antibiotics are not metabolized (276). As an alternative to conventional separation processes, the removal of pharmaceuticals from wastewater has been carried out with LMs. In a 6-minute process, over 99% removal of diclofenac ions was reached with ELMs (274). The membrane was composed of tetrabutylammonium bromide, Span 80, and dichloromethane as the carrier, surfactant, and diluent, respectively. Similarly, almost complete ibuprofen removal was reached using an ELM prepared with organic solvent Parlean® 4 as a diluent, surfactant Abil® EM90, and extracting agent TOA (275). Another work reported an efficiency of 97% for the removal of tetracycline, an antibiotic drug, using nano-fluid emulsion (276). The PELM was composed of Fe₂O₃ nanoparticles in n-heptane and stabilized with oleic acid, and TBP was used as the extracting agent. The work compared the PELM performance against the ELM technique and results showed that the stability of the membrane was substantially improved by nanoparticle inclusion. In the case of racemic mixtures, the separation process must offer a high chiral resolution to accomplish the recovery target (195,196). Enantioseparation of (R)- and (S)-amlodipine from pharmaceutical wastewater was studied using PP-based HFSLM (277). (S)-amlodipine is a high-value compound used to treat hypertension and as an antianginal agent, while (R)-amlodipine is inactive; hence, the process selectivity becomes essential. The membrane was prepared with the chiral extractant O,O'-dibenzoyl-(2S,3S)-tartaric acid diluted in organic solvents. For the release of (S)-amlodipine into the stripping solution, b-cyclodextrin was added. The process attained a maximum extraction and stripping efficiency of 78 and 75%, respectively, and reached an (S)-amlodipine enantiomeric excess of 58%.

Other dangerous pollutants from plants and urban wastewater have been found in water bodies, becoming a major environmental hazard. Alkyl esters of p-hydroxybenzoic acid, better known as paraben compounds, are used as preservatives in cosmetics, pharmaceuticals, and food products. However, they are also known as endocrine-disrupting chemicals and related to other health issues. Therefore, ELMs have also been proposed for the removal of parabens from aqueous solutions. In a comprehensive emulsion characterization study, 90% of ethylparaben was removed using an n-heptane-based ELM, with TOA as the carrier (278). Similarly, trioctylphosphine oxide (TOPO) in hexane was used for complete propylparaben removal from aqueous solutions (279).

Pulp and paper industries generate millions of metric tons of lignin waste annually. Beyond its enormous impact on the ecosystems, lignin offers the opportunity to be used as a renewable feedstock in the production of high-value compounds. Recovery of up to 98% of kraft lignin from pulping wastewater was reported using Aliquat 336 as the carrier in a kerosene-based ELM and 2-ethyl-1-hexanol as a modifier (280). Moreover, the treatment proved to be as feasible in actual pulp wastewater as the model solution.

5.4.4 Metal ion recovery and heavy metal removal

Metal-contaminated wastewaters are commonly found in industrial processes as well as in natural reservoirs, where groundwater sources can be heavily polluted. Although some metals such as lithium, iron, gold, and bismuth have low toxicity, other heavy metal elements are an undeniable health threat due to their bioaccumulation, toxicity, and carcinogenic effects. Their removal in contaminated waters for human consumption and prior to the discharge of wastewater industrial streams is thus necessary. Copper, silver, vanadium, and palladium are among the highly toxic heavy metals. Yet, arsenic, cadmium, chromium, lead, and mercury are major hazards to both humans and the environment. It is important to note that the development of separation technologies of metal solutions has hoarded a great interest for not only environmental and health reasons but also economic reasons since some

metal ion solutions have great added value potential. Nowadays, their extraction is carried by physicochemical treatments, such as solvent extraction, absorption, precipitation, membrane filtration, and electrocoagulation. And alternatively, biosorption, phytoremediation, and sulphate reducing are other biological remediation techniques (282). Likewise, LM technology has been investigated for this purpose, as Table 5.5 summarizes.

Organic solvent-based BLMs, with carbon tetrachloride, chloroform, and dichloromethane, were studied for mercury removal (283). In this work, extraction and recovery kinetic parameters of Hg (II) using calix[4]arene thioalkyl derivative carriers were determinate. An SLM, composed of TOA in dichloroethane supported in Nylon 6,6, was studied for mercury (II) removal (281). Under optimal conditions, the membrane showed a removal efficiency of 81–88%. In the same work, the SLM was tested for mercury removal from a complex mixture. The model solution, containing mercury chloride and sodium lignosulfonate, emulated wastewater from pulp and paper industries. The extraction efficiency was 53 and 50%, for mercury and lignosulfonate, respectively, which demonstrated the need for testing real mixtures. Treatment of petroleum-produced water using a PP-based HFSLM impregnated with Aliquat 336 in toluene showed a nearly complete mercury extraction (284).

Table 5.5. Summary of recent liquid membrane studies for the removal of heavy metals and recovery of metal ions.

| Solute | Membrane | Results | Ref. |
|--------------------|--|---|-------|
| Mercury | Calix[4]arene thioalkyl derivative in CCl ₄ , CHCl ₃ , and CH ₂ Cl ₂ BLM | Extraction and recovery kinetic parameters | (283) |
| | TOA in dichloroethane in Nylon 6,6 SLM | 81%–88% removal | (281) |
| | Aliquat 336 in toluene PP HFSLM | Nearly complete removal | (284) |
| | TOA in coconut oil supported in PVDF SLM | 95% removal | (214) |
| Lithium | TBP in [Tf ₂ N]-based ILs supported in PVDF SLM | Permeability of 1.2·10 ⁻⁶ m·s ⁻¹ | (285) |
| Copper and Lithium | Cyanex 272 diluted in kerosene HFSLM and SLM | Cu(II) over Li(I) separation factor of 18 and 178 for HFSLM and SLM, respectively | (286) |
| Copper | D2EHPA in kerosene HFRLM | 60% removal | (244) |
| | Acorga M5640 in aliphatic diluent PEHFSD LM | 96%–97% removal | (247) |
| | LIX 984N in kerosene ELM | >99% removal | (287) |
| | D2EHPA in waste-vegetal oil CLM | 96% removal | (223) |
| Bismuth | D2EHPA in n-pentanol ELM | Complete removal | (288) |
| Rhodium | Polyisobutylene and TOA in kerosene ELM | 46% removal | (289) |
| Silver | Cyanex 302 in paraffinic and naphthenic hydrocarbons diluent ELM | 95–99% extraction efficiency | (290) |
| Vanadium | D2EHPA in paraffin ELM | 91% recovery efficiency | (291) |
| Platinum | [P ₈₈₈₁₂][Cl] IL in PVDF-co-hexafluoropropyle and 2-nitrophenyloctyl ether PIM | 96% recovery efficiency | (238) |
| Palladium | [P ₈₈₈₁₂][Cl] IL in PVDF-co-hexafluoropropyle and 2-nitrophenyloctyl ether PIM | 96% recovery efficiency | (238) |
| | Cyanex 302 in kerosene ELM | 97% recovery efficiency | (292) |
| Arsenic | Aliquat 336 and 2-ethyl hexanol in kerosene ELM | 78% and 88% removal, respectively | (293) |
| Chromium | Aliquat 336 in kerosene and decanol ELM, spray column | Volumetric mass transfer coefficient of 0.036–0.074 s ⁻¹ | (236) |
| | TOMAC in [C ₄ min][Tf ₂ N] and kerosene ELM | 97% removal | (210) |
| Lead | Fe ₂ O ₃ magnetic particles and D2EHPA in kerosene PELM | 97% removal | (294) |
| Cadmium | Aliquat 336 in corn oil ELM | >98% removal | (219) |

Since the IL trioctyl(dodecyl) phosphonium chloride, [P₈₈₈₁₂][Cl], has shown high platinum-group metals extraction, their ions recovery with a reduced amount of [P₈₈₈₁₂][Cl] polymerized as PIM was proposed as a greener alternative (238). The membrane was prepared with the polymer PVDF-co-hexafluoropropylene and 2-nitrophenyloctyl ether as the plasticizer. In a two-stage sequential transport cycle, the authors aimed to the selective separation of an aqueous mixture of platinum, palladium, and rhodium. For each sequence, a proper stripping solution was used to enhance the permeation of a single metal, each acting in a specific transport mechanism. The work found the optimum stripping solutions were 0.1 M NaClO₄ in 1 M HCl and 0.1 M KSCN in 1 M HCl for platinum and palladium, respectively. The experiments reached 96% of recovery efficiency for Pt(IV) in the first transport and 96% of Pd(II) in the second. In neither of both sequences Rd(III) was transported. The high selectivity attained by tuning the stripping solution highlights the versatility of LM technology to be tailored in order to efficaciously perform the extraction process.

The recovery of lithium ions from complex aqueous mixtures was studied using SLMs impregnated with TBP in ILs (285). Several [Tf₂N]-based ILs were tested supporting them in PVDF matrices varying the support thickness and pore size. Faster Li(II) permeation than Mg(II), one of the main impurities in lithium brines, was observed. Likewise, the study tested the lithium permeation in presence of Co(II) and Ni(II), by-products obtained from recycle lithium-ion batteries, also showing good selectivity, but reducing the Li(II) permeation coefficient. In a comparative study, separation of copper and lithium ions was carried out using an HFSLM via nondispersive solvent extraction and compared with the use of the membranes in flat sheet configuration and also against the use of a dispersive solvent extraction process (286). LMs in this work were composed of Cyanex 272 diluted in kerosene, and although results showed similar performance for the three methods, the authors outstripped the advantages that HF membranes offer when scaling up the process. Other HF-based configurations have also been

used for the extraction of copper. HFRLMs (see [Figure 5.4d](#)) containing D2EHPA in kerosene were used to remove copper from sulphate solutions ([244](#)). A complete model to describe the mass transfer coefficients and flux rate, which fit the experimental data, was reported. Similarly, a PEHFSD arrangement (see [Figure 5.4e](#)) was proposed for this system ([247](#)); the copper mass transfer coefficients and the effect of having Fe and Zn ions were studied. Comparing the extraction performance, the authors obtained a Cu removal efficiency of 96–97% for PEHFSD versus 91–97% for an equivalent ELM. Besides the lower overall extraction yields, ELMs showed poor copper/iron selectivity, attributed to swelling issues.

Nonetheless, other works have reported effective metal recovery throughout ELMs. A kerosene-based ELM obtained more than 99% of copper removal using LIX[®] 984N as the carrier ([287](#)). Bismuth extraction from nitric solutions was achieved using an ELM based on D2EHPA in n-pentanol and biodegradable surfactant Triton[®] X-100 ([288](#)). Emulsion membranes containing polyisobutylene, TOA, and Span 80 in kerosene were used to reduce the toxicity of rhodium-contaminated wastewater ([289](#)). Using an ELM based on Cyanex 302 in paraffinic and naphthenic hydrocarbon diluent, silver extractions of 95–99% were obtained within 15 minutes of treatment ([290](#)). ELM composed of D2EHPA in paraffin reached 91% of vanadium recovery from a stone coal leaching solution ([291](#)). High palladium recovery from electroplating wastewater was attained using a Cyanex 302 in kerosene ELM ([292](#)). The membrane also showed good Pd over Cr selectivity. Kerosene-based ELMs were used for arsenic (V) removal, with Aliquat 336 and 2-ethyl hexanol as carriers, obtaining a maximum removal of 78 and 88%, respectively ([293](#)).

Other LMs have been proposed as well for the removal of highly toxic heavy metals from wastewater. In order to improve the ELM dispersibility in chromium (VI) removal, a spray column (see [Figure 5.4b](#)) was modified to include a rotator that produced centrifugal acceleration ([236](#)). The work showed that the addition of the rotor resulted in an approximately ten times

higher mass transfer coefficient for chromium using an emulsion conformed of Aliquat 336 in kerosene and decanol. To improve membrane stability, a stabilizer compound can also be included to avoid globule breakage. In a chromium removal study, IL [C₄min][Tf₂N] was added to a kerosene membrane also containing extracting agent tri-n-octylmethylammonium chloride (TOMAC) (210). Despite the slight reduction in the extraction efficiency, high stability was obtained with 3% (w/w) of the IL, reaching 97% of Cr removal. In another work, α -Fe₂O₃ magnetic particles were used as co-stabilizer in a PELM composed of D2EHPA in kerosene, resulting in 97% lead removal, and a significant increase in membrane stability (294).

Aiming to develop more sustainable metal extraction LM technologies, sustainable green-based LMs have been proposed. A waste-vegetable oil membrane was used for copper recovery in a CLM configuration with D2EHPA as the carrier and reached 96% of Cu removal (223). The work compared the effect of replacing the diluent with fresh-vegetable oil or kerosene, and separation performance followed the trend kerosene > fresh oil > waste oil, which was attributed to an improved ion diffusivity due to the reduction in diluent viscosity. More than 98% of cadmium removal was obtained with a corn oil-based ELM which contained extracting agent Aliquat 336 and surfactant Span 80 (219). Using palm oil as the diluent in an ELM, 97–99% of chromium (VI) removal was reached with TOMAC as the carrier (222) [36]. Vegetal oils can be used in SLM configurations as well. A PVDF support was impregnated with TOA in coconut oil for mercury removal (214). The membrane showed great performance, in terms of extraction efficiency and stability, with only slight improvements when the carrier was added, from 91% with no carrier to 95% at a carrier concentration of 4% (v/v). The vegetal-based membrane exhibited similar performance to SLMs with organic solvents, such as dichloroethane or n-heptane, which highlights the sustainability of LM technology as an extraction alternative.

Further applications of ELMs based on organic solvents, such as kerosene or n-heptane, and their operational effects on the removal of heavy metals (copper, nickel, chromium, cobalt, zinc, silver, lead, mercury, cadmium, gold, molybdenum, platinum, and palladium) have been reviewed by Ahmad et al. (295).

5.4.5 Nuclear waste treatment

Nuclear waste treatment is another field of application of LM technology. Nuclear waste is produced at resource extraction, nuclear facilities, and power plants, as well as in nuclear fuel conversion, fabrication, and reprocessing of spent fuel. It can contain: i) actinides, the main source of fissile fuels uranium and plutonium, ii) americium, iii) lanthanides such as cerium, a radioactive poison, which hinders the waste transmutation into short-lived radionuclides, iv) isotopes of molybdenum-99 (^{99}Mo), used in medical imaging procedures, caesium-137 (^{137}Cs), an irradiation source, cobalt-60 (^{60}Co), widely used for sterilization, radiography, and density measurements, and strontium-90 (^{90}Sr), administered for cancer radiotherapy. The traditional technique to recover plutonium and uranium from used nuclear fuels is the PUREX (plutonium uranium reduction extraction) process (296). It is based on dissolving the spent fuel in nitric acid and separation by LLX using a mixture of 20–30% (v/v) of TBP diluted in an organic paraffinic hydrocarbon solvent. The process results in two high-purity uranium and plutonium nitric solutions, which can be further converted into metal oxides, along with solid wastes and a remaining radiative stream, classified into high, intermediated, and low-level waste, that are derivate to further treatments. Several LM systems have been proposed for radioactive waste remediation. Table 5.6 presents a summary of the works discussed in this section.

Table 5.6. Summary of recent liquid membrane studies for nuclear waste treatment.

| Solute | Membrane | Results | Ref. |
|------------|--|--|-------|
| Uranium | 2-Thenoyltrifluoroacetone in kerosene ELM | >99% removal | (297) |
| | TBP in kerosene PE HFSLM | 67% extraction and 40% recovery efficiencies | (298) |
| | Alamine 336 in heavy paraffin ELM | Concentration factor of 6.9 | (299) |
| | D2EHPA and cellulose triacetate PIM | Nearly complete extraction | (299) |
| | D2EHPA, TBP, Cyanex 272, Alamine 336, and Aliquat 336 in polyvinylchloride PIM | Nearly complete extraction with D2EHPA carrier | (299) |
| | TBP in paraffin hydrocarbon PEHFSD LM | >84% recovery efficiency | (299) |
| Plutonium | TBP in dodecane PP HFSLM | >80% extraction efficiency | (299) |
| Americium | Cyanex 301 in cellulose triacetate-TBP PIM | Unirradiated and irradiated (194.4 kGy) permeability greater than $5.1 \cdot 10^{-4}$ and $1.1 \cdot 10^{-4} \text{ m} \cdot \text{s}^{-1}$, respectively | (299) |
| | 2-Ethylhexyl phosphonic acid mono-2-ethylhexyl ester in dodecane ELM | 93% extraction efficiency | (299) |
| Yttrium | Two-stage PTFE SLMs using 2-ethyl hexyl phosphoric acid-mono-2-ethyl hexyl ester and CMPO in dodecane, respectively | 95% removal | (299) |
| Strontium | D2EHPA BLM | 98% removal | (298) |
| Molybdenum | Aliquat 336-based ELM | 85% removal | (298) |
| Caesium | Crown ethers or TBP in calix(4)-bis-2,3-naphtho-crown-6, 2-nitrophenyl octyl ether and dodecane supported in cellulose triacetate-PTFE PIM | Permeability of $8.5 \cdot 10^{-5} \text{ cm} \cdot \text{s}^{-1}$ | (298) |
| | TBP and octyl (phenyl)- <i>N,N</i> -diisobutyl carbamoyl methyl phosphine oxide in dodecane supported in PP SLM | >99% removal | (298) |
| | CMPO or <i>N,N,N,N</i> -tetraoctyl-3-oxapentane diamine in 2-nitrophenyl <i>n</i> -octyl ether supported in cellulose triacetate-PIM | Permeation rates | (298) |
| | TBP in dodecane BLM | 90% removal | (298) |
| | Cobalt dicabollide on phenyl trifluoromethyl sulphone in PTFE SLM | >95% extraction efficiency | (299) |
| | TBP or crown ether carriers in cellulose triacetate PIM | Permeability of $0.2 \cdot 10^{-5}$ – $8.1 \cdot 10^{-5} \text{ cm} \cdot \text{s}^{-1}$ | (299) |
| Neodymium | CMPO in dodecane PVDF SLM | 95% extraction efficiency | (298) |
| | CMPO, <i>N,N</i> -dihexyl octanamide, and <i>N,N,N',N'</i> -tetraoctyl diglycolamide paraffinic hydrocarbon PP HFSLM | Nearly complete extraction | (299) |

Ambashta and Sillanpää (298) published a review on liquid nuclear waste treatment using membrane technology, where advances on the use of RO, MF, MD, and PV techniques are discussed for low-level waste decontamination. However, these methods are unable to treat high-level waste due to their acid nature which compromises the stability of the polymer-based membranes. Several NF membranes have been studied for cobalt species removal. Colloidal solutions of ^{239}Pu , ^{240}Pu , and ^{214}Am were pretreated by seeded UF and flocculation MF, where a suspension solution was formed by “seed particles” that absorbed the solutes or flocculated them to increase its size, respectively. Inorganic membranes, such as ceramic and zeolite-based, are an alternative to polymer-based membranes as they can be operated under a wide pH range. A zeolite NaA membrane in RO mode showed complete rejection of Cs^+ , Sr^{+2} , and MoO_4^{-2} from low-concentration solutions.

As an alternative to membrane filtration processes, the above review also presents the LMs as an emergent approach to radioactive waste remediation. BLM using D2EHPA as the carrier was applied to ^{90}Sr extraction from an alkaline solution to an acid stripping phase, where it was precipitated as SrSO_4 . An Aliquat 336-based ELM was used for ^{99}Mo removal. PIMs composed of plasticized cellulose triacetate and different crown ethers or TBP as the carrier and SLM composed by calix(4)-bis-2,3-naphtho-crown-6 dissolved in 2-nitrophenyl octyl ether and dodecane in a PTFE support showed effective ^{137}Cs transport. Remediation of model low-level waste containing cerium was studied using SLMs. The membrane phases were composed of octyl (phenyl)-*N,N*-diisobutyl carbamoyl methyl phosphine oxide, and TBP as carriers, dissolved in dodecane. Cellulose triacetate plasticized-PIM using octyl-(phenyl)-*N,N*-diisobutyl carbamoyl methyl phosphine oxide (CMPO) or *N,N,N*-tetraoctyl-3-oxapentane diamine carriers in 2-nitrophenyl *n*-octyl ether shows efficient Ce^{+3} transport. TBP in dodecane-based BLM had reached 90% of cerium transport after its electro-oxidation to Ce^{+4} . HFSLMs were developed using mixtures of CMPO in dodecane and TBP in kerosene for the removal of neodymium and uranium, respectively, from nitric acid solutions.

ELMs for waste uranium extraction have been studied since the 1980s. TBP used as a carrier has been shown to improve the distribution ratio on benzoyl acetone and dibenzoyl methane membranes (297). The use of TOPO carriers leads to a uranium extraction above 90%, and Aliquat 336-based membranes surpass conventional process efficiency, reaching a complete uranium extraction. In a recent study, hexavalent uranium extraction from aqueous acid solutions using kerosene-based ELM was evaluated. The membrane included 2-thenoyltrifluoroacetone as the carrier and surfactant Span 80, and an HCl solution was used as the stripping phase. Under optimal conditions, the authors were able to quickly extract the uranyl ions, within 1 minute, which was explained by the pH differences between the feed and stripping phases.

Likewise, another comprehensive review of nuclear waste remediation with LMs was published by Rathore et al. (299). For instance, high selective uranyl ion permeation was reported using an Alamine 336-based ELM. The study found a uranium (VI) concentration factor of 6.9, with remarkable selectivity removal from the leach liquor containing Fe^{+3} , Mg^{+2} , Ca^{+2} , and Mn. Americium (III) transport with Cyanex 301 in a cellulose triacetate-based PIM was researched using TBP as the plasticizer. In a Stripping phase reaction-facilitated transport regime (see Figure 5.7b), alpha-hydroxy iso-butyric acid was added as a stripping extracting agent to drive the Am^{+3} back extraction. Several radionuclides could be removed from PUREX waste employing ELM with 2-ethylhexyl phosphonic acid mono-2-ethylhexyl ester as the carrier in dodecane. More than 93% of the Am(III), Ce(III), Nb(III), and Zr(IV) were extracted from the feed waste stream. In a two-stage process, SLMs using 2-ethyl hexyl phosphoric acid-mono-2-ethyl hexyl ester and CMPO for the first and second stages, respectively, 95% of Yttrium-90 (^{90}Y) removal has been archived. The system also has been able to retain ^{90}Sr , a common second impurity, between the stage membranes, giving a high-purity final product. Caesium (I) removal from nitric acid solutions by cobalt dicabollide in phenyl trifluoromethyl sulphone and PTFE as the support, showing a strong permeability dependence with the feed phase acidity and carrier

concentration. To ensure SLM stability in high-level waste treatments for selective Cs extraction, PIMs have been studied. Likewise, PIM-based on di-tert-butylbenzo-18-crown-6, TBP, and cellulose triacetate as the plasticizer was effectively used for Cs transport from acidic solutions. PIMs were used for uranium removal as well. Through the addition of different plasticizers and scintillants to a D2EHPA and cellulose triacetate PIM, high uranium extraction from nitrate solutions was achieved. Several carriers, such as D2EHPA, TBP, Cyanex 272, Alamine 336, and Aliquat 336, were tested for dioxouranium (II) extraction from acidic sulfate solutions with polyvinylchloride-based PIM. The study showed D2EHPA as the best extracting agent, through an intricate complexation kinetic. Each UO_2^{+2} ion is bonded to two carrier molecules and two carrier conjugated bases. HFSLM had also been used for the removal of trivalent lanthanides and actinide from nitric solutions using CMPO, N,N-dihexyl octanamide, and N,N,N',N'-tetraoctyl diglycolamide as carriers in paraffinic hydrocarbon. Lastly, plutonium (IV) and uranium (IV) removal have been achieved by PEHFSD-based membranes and TBP as the extracting agent.

5.4.6 Rare-earth recovery

REs are a group of elements that comprises scandium, yttrium, and lanthanides. They are used in the production of technological devices, electronic components, rechargeable batteries' manufacturing, as well as on metallurgy, medical, optical, magnets, and catalysis chemistry applications. RE are commonly purified by solvent extraction techniques, such as cation or anion exchangers, solvation – chelating extractants, and synergistic solvent extraction (300). Nonetheless, LMs have been investigated as an alternative to the highly complex solvent extraction processes needed for RE recovery. Recent studies on the RE extraction with LMs are presented in [Table 5.7](#).

Table 5.7. Summary of recent liquid membrane studies for the recovery of RE elements.

| Solute | Membrane | Results | Ref. |
|-------------------------|--|---|-------|
| RE oxides | (RO) ₂ P(O)OPh-COOH in sulfonated kerosene ELM | 83% recovery efficiency | (252) |
| | Primary amine N1923 in sec-caprylic alcohol and kerosene BOLM | RE over Al separation factor of 45 | (237) |
| Gadolinium | D2EHPA in kerosene ELM | 99% extraction and 79% stripping efficiencies | (301) |
| Dysprosium | D2EHPA in kerosene ELM | >99% recovery efficiency | (302) |
| | Cyanex 572 in kerosene ELM | 99% recovery efficiency | (303) |
| | 2-Ethyl hexyl phosphoric acid-mono-2-ethyl hexyl ester in kerosene PEHFSD LM | 96% extraction efficiency | (249) |
| Yttrium | D2EHPA in kerosene PEHFSD LM | 99% extraction and 98% recovery efficiencies | (248) |
| RE radioactive nuclides | Bis(2-ethylhexyl) hydrogen phosphate-decal supported in PTFE SLM | Permeation of 95% cerium, 95% promethium, 80% gadolinium, and 10% ytterbium | (298) |
| Samarium | D2EHPA in cyclohexane ELM | Permeation rates | (298) |
| Neodymium | Thenoyltrifluoroacetone and TOPO in cyclohexane ELM | Permeation rates | (298) |

The production of phosphoric acid by a wet process often carries lanthanide oxides from the phosphate ore. ELMs were used to compare the extraction efficiency of RE oxides: La₂O₃, Ce₂O₃, Y₂O₃, and Nd₂O₃, from a model HNO₃ solution (252). The emulsions were composed of sulfonated kerosene and polyisocrotyl succinimide as the diluent and surfactant, respectively, and an H₃PO₄ solution was used for the stripping phase. In this work, different carriers: D2EHPA, (RO)₂P(O)OPh-COOH, and (RO)₂P(O)OPh, were tested, and results showed a feed phase acidic dependence of the extraction yield; increasing the pH significantly improved the RE oxides' recovery, (RO)₂P(O)OPh-COOH being the carrier with the best performance (83%), attributed to its carboxyl group. The observed trend agreed with previous works, where at greater pH solutions, more RE complexes are formed at the feed-globule interface, enhancing the mass transfer (302,304). Likewise, extraction and stripping yields of 99% and 79%, respectively, were achieved for gadolinium (III) recovery, which is typically used as a contrast in medical procedures and the production of alloys, using an ELM of D2EHPA in kerosene (301). Recovery of dysprosium (III), mainly used in permanent magnets manufacturing, was also studied with D2EHPA in kerosene-based

ELMs with a stripping efficiency above 99% (302). Likewise, a Cyanex 572 in kerosene-based ELM shows an extraction efficiency of 99% with a high Dy (III) selectivity with respect to Nd (III) (303). BOLM composed of primary amine N1923 in sec-caprylic alcohol and kerosene has been proposed as an environmentally friendly alternative to the RE separation from aluminium oxide impurity in leaching solutions (237). The process gives a highly RE to Al selectivity, reaching a separation coefficient of 45.

Successful dysprosium (III) extraction from acidic solution was also carried out using a PEHFSD (see Figure 5.4e), a variation of HFSLM to improve the SLM stability (249). The system resembled a tube and shell exchanger, where the feed phase was pumped into the fibres, while the stripping phase with LM droplets remained in the shell. The composition of the LM was 2-ethyl hexyl phosphoric acid-mono-2-ethyl hexyl ester dissolved in kerosene, and within 170 minutes, the authors reached a transport efficiency of 96%. The recovery of yttrium (III) from mixed oxide ores was also achieved using PEHFSDs in facilitated transport mode, using D2EHPA (carrier) in kerosene (248). The authors reached an extraction yield of 99% and a stripping recovery of 98%, which represents a substantial improvement with respect to HFSLM systems.

During nuclear waste treatments, several lanthanide radioisotopes are removed as a part of the remediation process. Separation of RE radioactive nuclides in acidic solution using a PTFE-based SLM impregnated with bis(2-ethylhexyl) hydrogen phosphate-decalin showed a selective preference for light RE elements (298). The mixture composed of cerium, promethium, gadolinium, and ytterbium in a 0.5 N HCl solution reached a permeation of 95%, 95%, 80%, and 10% for each element respectively, while no transport was observed for other components. In another work, ELMs composed of cyclohexane and Span 80 were studied for RE recovery from nitrate solutions using HNO₃ as a stripping phase. The carriers used for the recovery of samarium (III) and neodymium (III) were D2EHPA and a mixture of thenoyltrifluoroacetone and TOPO, respectively.

5.5 Conclusions and perspectives

Since liquid membranes were first proposed, advances in the field have geared toward improving their scope and suitability as a sustainable alternative to traditional solvent extraction and membrane filtration. Liquid membranes have been successfully applied at laboratory scale in the recovery of compounds in biorefinery, amino acids, metal ions, and RE elements, as well as for the removal of heavy metals, and wastewater, and nuclear waste treatment. Throughout this chapter, recent advances in liquid membranes' research and their fundamental basis have been overviewed. Different liquid membrane configurations have been discussed highlighting their pros and cons. For example, despite their low flux, bulk liquid membranes have proved to be useful to determine membrane performance in terms of extraction kinetics and transport coefficients. ELMs are broadly studied due to the likelihood of being implemented at an industrial scale. However, most studies mainly focus on statistical models of effects contribution and significance due to the larger operational variables involved in this arrangement. Finally, a third category which involves the use of porous supports, i.e., SLMs, can improve the separation performance of bulk and ELMs, minimizing the solvent requirements while avoiding contamination into the feed and stripping phases due to membrane leakage. Furthermore, other novel membrane arrangements, often based on these three main configurations, can help overcome specific limitations, and the most relevant ones have been presented in this chapter.

It is important to note that several aspects of liquid membranes related to their potential as commercial technology remain a challenge. Based on the results found in the literature, future work should focus on improving the mass transfer resistance, membrane stability, and solvent-process compatibility. Moreover, there is a clear need to adopt standard terminology to allow proper evaluation and comparison. Great efforts on process design and integration are also required to understand the feasibility of the new

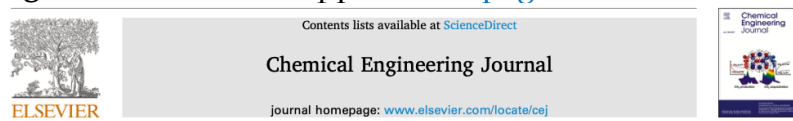
technology for each particular separation. Liquid membranes have been widely presented as an eco-friendly alternative, stressing their environmental applications. Nevertheless, some of the reported membranes discussed in this chapter still use less environmentally friendly compounds where waste membrane management is poorly discussed. Variable optimization, operational costs, and membrane lifecycle should be evaluated by both, simulation and pilot-scale experiments.

The possibility of replacing toxic conventional solvents with greener alternatives such as novel ILs or vegetable-based oils is promising, allowing an enhancement in the sustainability and efficiency of the process. In the near future, industrial applications ranging from the recovery of high-value components to high-risk waste remediation will undoubtedly benefit from current research on liquid membrane technology as a sustainable alternative to conventional processes.

Chapter 6. Green supported liquid membranes: the permeability activity-based linear operation (PABLO) method

The last scientific contribution of this thesis is the combination of green solvents and supported liquid membranes for the recovery of organic acids. Based on the results shown in [Chapter 3](#) and [Chapter 4](#), and the literature review in [Chapter 5](#) of this thesis, a new approach to mass transfer and process design is presented in this chapter. The published permeability activity-based model considers for the first-time solute-phase affinities (1). As an additional contribution, a novel graphical method is proposed for a countercurrent cascade system.

| | |
|--------------------------------|---|
| Authors: | Pablo López-Porfiri María González-Miquel Patricia Gorgojo |
| Journal: | Chemical Engineering Journal |
| Pages: | 137253 |
| Volume: | 446, Part 3 |
| Status: | Published |
| Publication Date: | 28 May 2022 |
| Doi: | doi.org/10.1016/j.cej.2022.137253 |
| Supporting Information: | Appendix C, page 237 |



Green supported liquid membranes: The permeability activity-based linear operation (PABLO) method

Pablo López-Porfiri^{a,*}, María González-Miquel^{a,b}, Patricia Gorgojo^{a,c,d,*}

^a Department of Chemical Engineering, Faculty of Science and Engineering, The University of Manchester, Manchester M13 9PL, UK

^b Departamento de Ingeniería Química Industrial y del Medioambiente, ETS Ingenieros Industriales, Universidad Politécnica de Madrid, C/ José Gutiérrez Abascal 2, 28006, Madrid, Spain

^c Nanoscience and Materials Institute of Aragón (INMA) CSIC-Universidad de Zaragoza, C/ Mariano Esquillor s/n, 50018 Zaragoza, Spain

^d Chemical and Environmental Engineering Department, Universidad de Zaragoza, C/ Pedro Cerbuna 12, 50009 Zaragoza, Spain

ARTICLE INFO

Keywords:
Supported liquid membrane (SLMs)
Green solvent
Organic acid
Biorefinery
Process design
COSMO-RS

ABSTRACT

Supported liquid membranes (SLMs) containing novel green solvents are proposed as a sustainable alternative separation process in the recovery of biomolecules. In this work, succinic acid has been successfully extracted from model fermentation broths through a stripping phase-facilitated transport mechanism with four different green supported liquid membranes: two eutectic solvents (DL-menthol:OctA and N₄₄₄₄Cl:OctA), the bio-based solvent eucalyptol and the ionic liquid [C₄pyrr][TE₂N]. A permeability activity-based model that takes into account for the first time solute-phase affinities has been developed using the quantum chemical COSMO-RS method; the model corrects the mass transfer driving force and allows extraction predictions beyond the concentration equilibrium. The best recovery has been achieved experimentally for the eucalyptol-based SLM (concentration factor of 1.4) using an alkaline aqueous solution (0.5 M NaOH) as the stripping phase. A countercurrent cascade extraction process design is proposed, and a graphical method to determine the stage number, interstage concentrations as well as mass transfer area requirements is presented. This new tool, the Permeability Activity-Based Linear Operation (PABLO) method, will substantially enhance the process design of SLMs technology for the biorefinery industry.

6.1 Foreword

As environmental concerns gain more and more relevance among communities, both industries and political regulators are urged to promote cleaner routes for material and energy production. Several technologies are currently being researched to answer such engineering challenges. Nevertheless, it is common to find redundant lab-scale research and poor signs of effective technology transfer to the industry. Gaps in the process design of these new technics are among the reasons for such drawbacks.

This piece of work aims at building a direct but solidly grounded methodology for green-supported liquid membranes process design, as outlined in Figure 6.1. By taking into account the thermodynamic constraints of the extraction system, this novel method improves the prediction of the system behaviour and, in consequence, enhances process design estimations.

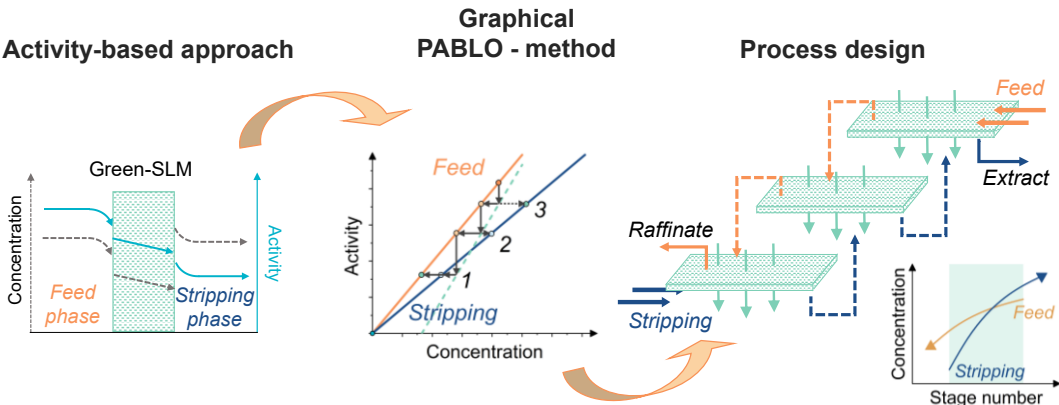


Figure 6.1. Green SLM development is presented in this work. Under an activity-based approach, suitable design methods can be proposed that allow for better process evaluations.

Novel design approaches have shown success in the development of fruitful technology. As B. Linnhoff wrote in his own PhD thesis (305), which set the principles of what would become the *Pinch method of process energy integration*, an approach of thermodynamically feasible targets leads to a "natural driving force conscious" process design. His practical application is nowadays vastly spread throughout the industry, helping to optimize processes by reducing energy consumption.

"In times of rapidly changing costs for many materials and services, such methods might be especially valuable. They might encourage the designer to clarify the physical constraints on a system and to explore as many feasible alternatives as possible that would comply with these constraints. Thus, his view would be restricted by limits of feasibility rather than by economic criteria which are subject to change."

— B. Linnhoff, *Thermodynamic Analysis in the Design of Process Networks*. PhD thesis

6.2 Abstract

Supported liquid membranes (SLMs) containing novel green solvents are proposed as a sustainable alternative separation process in the recovery of biomolecules. In this work, succinic acid has been successfully extracted from model fermentation broths through a stripping phase-facilitated transport mechanism with four different green supported liquid membranes: two eutectic solvents (DL-menthol:OctA and N₄₄₄₄Cl:OctA), the bio-based solvent eucalyptol and the ionic liquid [C₄pyrr][Tf₂N]. A permeability activity-based model that takes into account for the first time solute-phase affinities has been developed using the quantum chemical COSMO-RS method; the model corrects the mass transfer driving force and allows extraction predictions beyond the concentration equilibrium. The best recovery has been achieved experimentally for the eucalyptol-based SLM (concentration factor of 1.4) using an alkaline aqueous solution (0.5M NaOH) as the stripping phase. A countercurrent cascade extraction process design is proposed, and a graphical method to determine the stage number, interstage concentrations as well as mass transfer area requirements is presented. This new tool, the Permeability Activity-Based Linear Operation (PABLO) method, will substantially enhance the process design of SLMs technology for the biorefinery industry.

6.3 Introduction

Nowadays, concerns over climate change have led to stricter environmental regulations in the manufacturing processes, emphasizing the need to develop green chemistry alternatives (130). However, green processes are often hard to implement at industrial scale due to the lack of technical maturity as well as economic, organizational, and even cultural barriers (306). Examples of successful green processing facilities are the biorefineries, that transform biomass into value-added products, yet most downstream separations in the industry still rely on the use of conventional processes to reach a competitive product quality and production cost.

For instance, the production of succinic acid and other bio-based organic acids, highlighted as strategic platform chemicals by the United States Department of Energy (16), through green routes has shown economically competitive in comparison to the conventional analogues (128). However, the need to improve the downstream processes is also stressed. In fact, the purification of the bio-succinic acid produced by fermentation of lignocellulose-derived sugars is carried out by highly energy consuming precipitation processes or using harmful volatile organic compounds (VOCs), such as organophosphorus compounds or aliphatic amines, in liquid-liquid extractions (LLX) (129).

Novel technologies and materials are being proposed as sustainable alternatives or process intensification. Several ionic liquids (IL), i.e., liquid salts at room temperature, eutectic solvents (ES), i.e., hydrogen bond donor (HBD) and acceptors (HBA) eutectic mixtures, and bio-based solvents (BS), i.e., solvents produced from renewable sources, have shown to be suitable alternatives in LLX of bio-based organic acids (3). Other energy efficient separation processes in the biorefinery industry can benefit from including the use of membranes, which are up to an order of magnitude more efficient than their phase change-based counterparts (188).

Liquid Membrane (LM) technology has been presented as an innovative approach for the selective extraction of diluted species from liquid or gaseous matrices, including the recovery of biomolecules, amino acids, metal ions, and rare earths, as well as the treatment of wastewater, nuclear waste, and removal of heavy metals (2). By including an immiscible solvent within the porosity of an inert thin substrate in the so-called supported liquid membranes (SLM), allows to reduce the extraction media requirement and thereby the mass transfer resistance (200). Furthermore, they can be coupled with green solvents to guarantee the sustainable requirements by the biorefinery industry. By comprising the extraction and back-extraction in a single stage, SLMs offer higher efficiency and simplest operation than LLX (192), even reaching a large mass transfer area per equipment volume (194).

Notwithstanding, despite the large number of published studies on LMs and the well acknowledged advantages, the technology is far from reaching industrial scale. In a separation roadmap report, formulated in the year 2000 by the American Institute of Chemical Engineers, the need for the development of alternative technologies was brought forward, highlighting the bio-separations as one of the highest priority key research needs (19). Moreover, they specifically mentioned the importance of focusing on the development of membranes and extractants, as well as generating better predictive models to boost the separation technologies. The same conclusion was given in 2019 by the ACS Green Chemistry Institute® in a Sustainable Separation Processes Roadmap report (307).

The state of these separation methods can be overviewed from a technology maturity perspective. In order to visualize and compare different separation technologies, Figure 6.2 shows their position with respect to each other, in terms of use maturity (antiquity) and from less sophisticated ones up to more sophisticated and well-established processes (technical sophistication, estimated from the wane in their respective patent activity). It is noted that LMs is a relatively young technology with a still high invention rate, which explains the poor industrial-scale development but leaves room for

improvement and developing the solutions the biorefinery industry is aiming for.

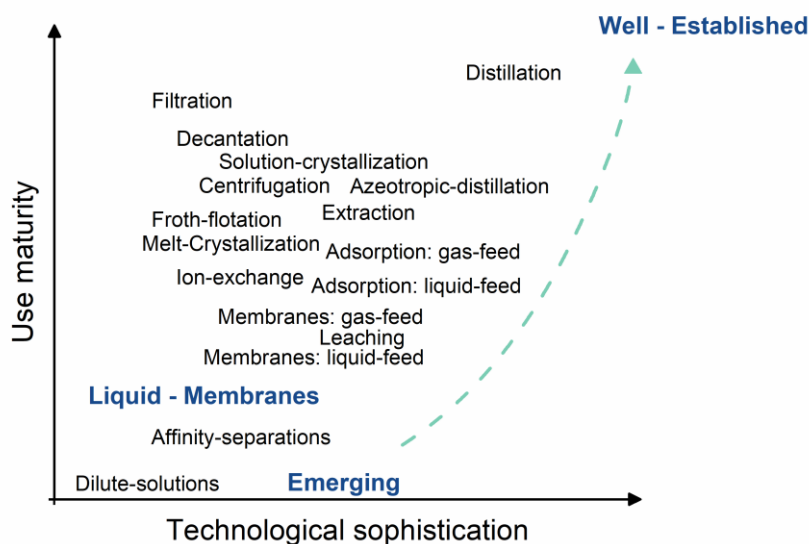


Figure 6.2. Maturity of the separation process technology. Technological sophistication as the patent activity wane (x -axis); Use maturity as the antiquity in the last century (y -axis). Reconstructed from Vision 2020: 2000 Separation Roadmap, Center for Waste Reduction Technologies of the AIChE, 2000 (19).

Under the proper conditions, several studies have shown that it is possible to push the LM extraction yields beyond the equilibria, i.e., to reach in the stripping phase a greater concentration than in the feed phase. For instance, it was reported that LMs based on Aliquat 336[®] could reach concentration factors of 2.2 and 6.9 in the gibberellic acid recovery (264) and uranium removal (299), respectively. In another work, lithium extraction from complex aqueous mixtures with IL-based SLM at an initial Li concentration of 619 mg l⁻¹ showed to reach final concentrations of ca. 180 and 400 mg l⁻¹, in the feed and stripping phase, respectively (285). This is possible due to reactive-facilitated mechanisms or specific solute-phase solvent affinities, and generally explained by the solute thermodynamic activity. However, discussions lack further insight or quantification, possibly due to time and cost constrains for the determination of thermodynamic properties.

In this work, we propose the use of computational quantum chemical methods to have a preliminary insight into such interaction effects. More

precisely, the COnductor-like Screening MOdel for Real Solvents (COSMO-RS), which provides good predictions of compounds chemical potentials from the screening charge density on the molecular surface (106). This unveils a potential improvement in the LM mass transfer description based on intermolecular interactions within the system and, in consequence, promoting further process modelling and design. The model will be validated with experimental data from the extraction of succinic acid using four SLMs based on four different green solvents: DL-menthol:OctA (eutectic solvent), N₄₄₄₄Cl:OctA (eutectic solvent), eucalyptol (bio-based solvent) and [C₄pyrr][Tf₂N] (ionic liquid).

In order to reach technological maturity, it is necessary to develop tools that allow preliminary SLMs-based extraction process design (as those used for conventional separation technologies). In this work, a graphical method is proposed for the preliminary countercurrent configurations sizing.

6.4 Permeability activity-based model

In order to impulse LMs from an emerging to a well-established technology, descriptive models and process design methodologies must be improved. In LMs, the well-accepted mass transfer driving force is the concentration difference (284,286). Assuming no solute accumulation within the membrane, the solute *i* flux, J_i (mol_{*i*} m⁻²·s⁻¹), is driven by the difference in concentration, C_i^a (mol m⁻³), between both phases (*a*: feed (*F*) or stripping (*S*)), and also depends on the permeability, P (m·s⁻¹). Thus, J_i can be calculated with Eq. 6.1 (201).

$$J_i = P \cdot (C_i^F - C_i^S) \quad (6.1)$$

The above approach is limited to describing the mass transfer only until both phase concentrations are equalized. Therefore, a new model needs to be developed to account for higher extraction efficiencies that can be found in the literature and go beyond the expected equilibrium.

In this work, the solute mass flux is expressed as a modified version of the Nernst-Planck equation, according to Eq. 6.2. The electrostatic potential is dismissed, resulting in a driving force along with a one-dimensional frame through the x -axis given by the chemical potential, μ_i ($\text{J}\cdot\text{mol}^{-1}$), gradient. The other two terms in the equation are the solute activity, a_m ($\text{mol}_i \text{ m}^{-3}$), that accounts for molecular interactions within the mixture, and the molecular mobility u .

$$J_i = a_m \cdot u \left(-\frac{d\mu_i}{dx} \right) \quad (6.2)$$

Based on the chemical potential relationship with the molar activity, a_i ($\text{mol}_i \text{ mol}^{-1}$), shown in Eq. 6.3 (308), and substituting $a_m = C_i \cdot \gamma_i$ as $a_m = c_i \cdot \rho \cdot \gamma_i$, where C_i ($\text{mol}_i \text{ m}^{-3}$), c_i ($\text{mol}_i \text{ mol}^{-1}$), γ_i (-), and ρ ($\text{mol} \text{ m}^{-3}$) are the solute molar concentration, the molar fraction, the activity coefficient, and the solution molar density, respectively, Eq. 6.2 can be rewritten as Eq. 6.4. The factor uRT , molecular mobility times the gas constant, R ($\text{J}\cdot\text{mol}^{-1}\cdot\text{K}^{-1}$), and temperature, T (K), is redefined as the solute diffusion coefficient, D ($\text{m}^2\cdot\text{s}^{-1}$), resembling a Fick's law of diffusion based on the solute activity differential.

$$d\mu_i = RT d\ln(a_i) = RT d\ln(c_i \cdot \gamma_i) \quad (6.3)$$

$$J_i = -a_m \cdot uRT \frac{d\ln(a_i)}{dx} = -\frac{a_m}{a_i} \cdot D \frac{da_i}{dx} = -D \frac{d(C_i \cdot \gamma_i)}{dx} \quad (6.4)$$

Finally, the solute flux through the LM is obtained from the difference in each phase of the solute concentration times the activity coefficient and the permeability, P ($\text{m}\cdot\text{s}^{-1}$), defined as the quotient of the diffusion coefficient over membrane thickness, δ (m), as shows Eq. 6.5. Is important to note that this approach considers no solute accumulation in the membrane and condenses all mass transfer resistances as a single empirical parameter P .

$$J_i = P \cdot (C_i^F \cdot \gamma_i^F - C_i^S \cdot \gamma_i^S) \quad (6.5)$$

Throughout the proposed permeability activity-based model, [Eq. 6.5](#), the description of the LM process extraction is substantially improved. Wherever the separation process is, the final concentrations that it might reach are governed by the thermodynamic equilibria. In other words, when the activity of the compounds in each phase are equalized, also are the mass flow in both directions, meaning a zero-net mass transfer rate. For instance, if both feed and stripping phases are composed of the same solvent, e.g., water, no difference in the solute activity is observed, and the system will follow an ideal approach as per [Eq. 6.1](#). In this case, both solute concentration trajectories, in feed and stripping phases, are constrained to meet over the same path, as shown the [Figure 6.3.I](#). In such figure, the *a*-point and *b*-point represent the initial feed and stripping concentrations, respectively, while the *c*-point is the final concentration of both phases obtained from the solute mass balance. Since the driven force of the ideal approach is the concentration gradient, the mass transfer is equilibrated at the *c*-point, as [Figure 6.3.II](#) depicts.

On the other hand, under the activity-based approach, the solute trajectories are dependent on the specific solute-phase affinity. It is possible to attain equilibrium with different final concentrations, if different feed and stripping phases are adopted, such as water and a solution of 0.1 M NaOH, respectively. This case is illustrated in [Figure 6.3.III](#), where starting concentrations (*a*-point and *b*-point) are the same as in the above example, but the final feed concentration, *d*-point, is lower than the final stripping concentration, *e*-point, where the activities are balanced. In consequence, the observed concentration profiles behaviour will match the one represented in [Figure 6.3.IV](#), agreeing with the results found in the literature.

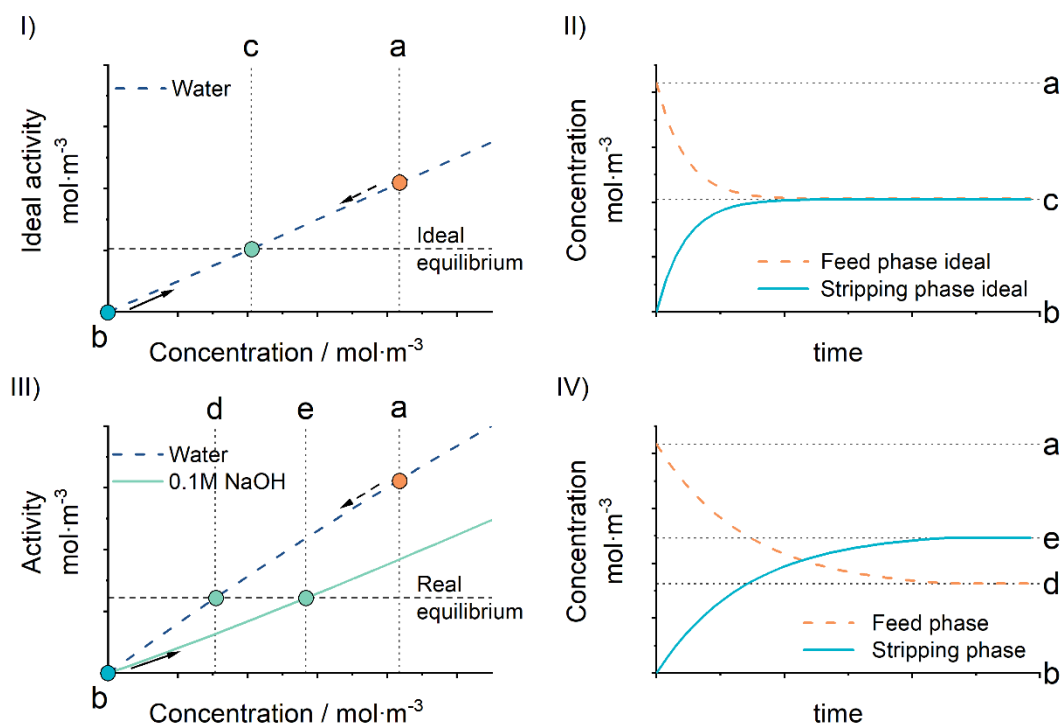


Figure 6.3. Schematic comparison of the liquid membrane behaviour predicted from a concentration-based approach (Eq. 6.1) and an activity-based approach (Eq. 6.5). I) Ideal trajectories for the solute concentration with the same affinity with the feed and stripping phases; II) Concentration profile obtained from the concentration-based approach; III) Activity trajectories for the solute concentration with different affinity with the feed and stripping phases; IV) Concentration profile obtained from the activity-based approach. a-point: initial feed concentration; b-point: initial stripping concentration; c-point: final ideal feed and ideal stripping concentration; d-point: final activity-based feed concentration; e-point: final activity-based stripping concentration.

6.5 Bio-organic acid recovery with green-SLM

6.5.1 Materials

Succinic acid ($\geq 99.0\%_{w/w}$), octatonic acid ($\geq 98\%_{w/w}$), tetrabutylammonium chloride ($>98\%_{w/w}$), 1,8-cineole ($99\%_{w/w}$), and [C₄pyrr][Tf₂N] ($\geq 98.5\%_{w/w}$) were purchased from Sigma-Aldrich. DL-menthol ($\geq 97.0\%_{w/w}$) and NaOH ($98\%_{w/w}$) were purchased from Alfa Aesar. Chemicals were used without further purification. Milli-Q type 1 water was produced in the laboratory. Millipore Durapore PVDF support was acquired from Merck. Nominal support characteristics are thickness: 125 μm , pore size: 0.22 μm , and porosity: 75%.

6.5.2 Preparation of green-SLMs

For the preparation of the SLMs, four green solvents (shown in Table 6.1) were selected based on their separation performance for the recovery of succinic acid through conventional LLX reported in our previous work (3): two eutectic solvents (ESs) (DL-menthol:OctA and N₄₄₄₄Cl:OctA), the bio-based solvent eucalyptol, and the ionic liquid (IL) [C₄pyrr][Tf₂N]. They were introduced into hydrophobic polyvinylidene fluoride (PVDF) porous supports by impregnation (Figure 6.4.I and preparation details in Appendix C). Table 6.1 also contains the SLM impregnation ratio, $\varepsilon = V_{\text{solvent}}/V_{\text{SML}}$ (%), and stability in water for each of the prepared membranes (more details on these tests can be found in Appendix C).

Table 6.1. Green-SLMs and their properties studied in this work.

| Green solvent | Family | Abbreviation | ε % | Stability ^b % at 96 h |
|---|--------|--|--------------------|-------------------------------------|
| DL-menthol : Octanoic acid {1:1} ^a | ES | DL-menthol:OctA | 66.0±2.7 | 94.29±1.12 |
| Tetrabutylammonium chloride: Octanoic acid {1:2} ^a | ES | N ₄₄₄₄ Cl:OctA | 66.1±2.0 | 90.34±1.28 |
| 1,8-Cineole | BS | Eucalyptol | 66.5±0.6 | 98.18±3.15 |
| 1-butyl-1-methylpyrrolidinium bis(trifluoromethylsulfonyl)imide | IL | [C ₄ pyrr][Tf ₂ N] | 49.3±1.8 | 63.09±2.80 |

^a ES {HBA:HBD} molar ratio.

^b Full stability data available in Appendix C.

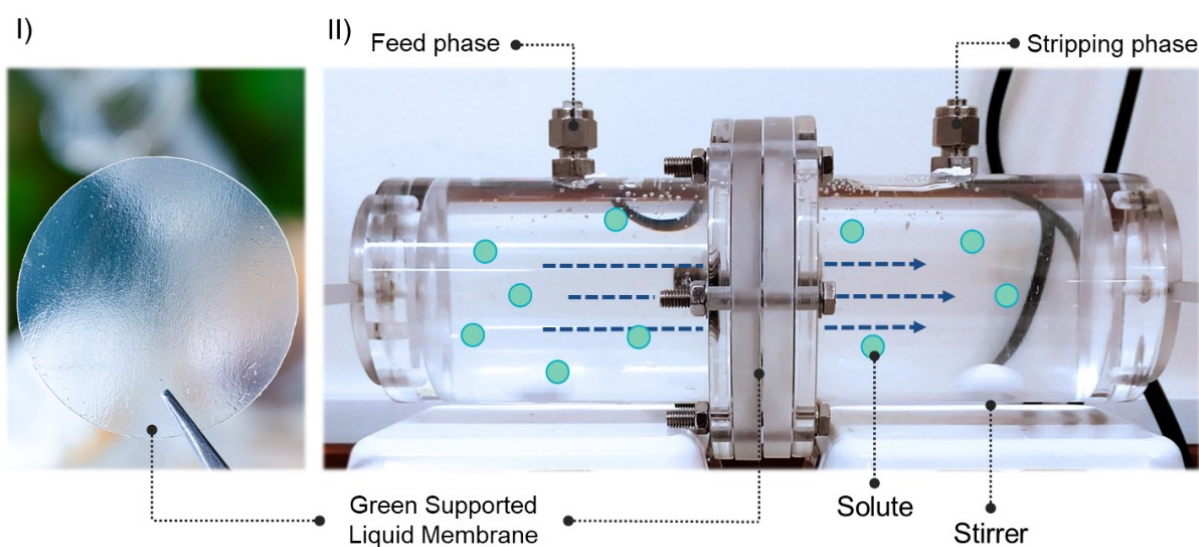


Figure 6.4. Experimental setup used in this work for the succinic acid recovery with green-SLMs. I) SLM prepared by immersing a PVDF porous support in a green solvent; II) Diffusion cell and SLM module.

6.5.3 Methodology for the extractions with SLMs

Succinic acid was used as representative bio-based organic acid for the green-SLM extraction assays. Experimental extractions were carried out at room temperature in the diffusion cell depicted in [Figure 6.4.II](#); volume of 325 ml for the feed and stripping phase chambers and an effective mass transfer area of $30.19 \pm 0.01 \text{ cm}^2$. A model succinic acid aqueous solution of $40\text{-}50 \text{ g l}^{-1}$, within the typical average concentration in the fermentation broths ([22](#)), was used as the feed phase. Pure water, 0.1 M NaOH, and 0.5 M NaOH were used for the stripping phase. Both feed and stripping phases were continually stirred to reduce polarization effects. The organic acid concentration of the stripping phase was measured in time intervals up to 100 h to ensure equilibrium was reached. The succinic acid concentration was analysed by HPLC.

6.5.4 Modelling procedure

To give a continuous description of the succinic acid concentration profile in time, the experimental data were modelled with the permeability activity-based model proposed in this work. Since the approach is based on the solute-phase affinity, the succinic acid activity coefficients in water and NaOH solutions were preliminary computed with COSMO-RS method at $20 \text{ }^\circ\text{C}$. The method has been successfully applied in the separation process design of complex systems ([309](#)) and in predicting the non-ideal carboxylic acids' aqueous solubilities ([136](#)). By computing the compounds chemical potential within a mixture, COSMO-RS method can estimate the γ -values through [Eq. 6.6](#), where μ_i^a and μ_i are the solute i chemical potential in the a -phase and as a pure compound, respectively ([107](#)). Computational calculations were performed using the COSMOtherm software, version C30, release 18.0.2, at the parametrization of BP_TZVP_18.

$$RT \ln(\gamma_i^a) = \mu_i^a - \mu_i \quad (6.6)$$

The SLM configuration gives a negligible membrane phase volume in comparison with the feed and stripping phases. Therefore, the solute mass balance in the system described in Figure 6.4.II can be expressed by Eq. 6.7. V^a , n^a , A , and t are the a -phase volume (m^3), solute mass (mol), membrane effective area (m^2), and extraction time (s), respectively.

$$J_i \cdot A = V^S \cdot \frac{dC_i^S}{dt} = -V^F \cdot \frac{dC_i^F}{dt} = \frac{dn_i^S}{dt} = -\frac{dn_i^F}{dt} \quad (6.7)$$

Assuming constant solute permeability throughout the concentration range (i.e., solute accumulation in the membrane is neglected), the permeability can be estimated from the mass balance formulated as Eq. 6.7, with experimental extraction data. With the boundary conditions of $0 < C^S(t) < C_i^{S,eq}$ and $t^{st} < t < t^{eq}$, the mass balance (Eq. 6.7) and the permeability activity-based model (Eq. 6.5) can be rearranged in the form: $Y=b \cdot X+a$, as shown in Eq. 6.8. The linearized form establishes an independent variable $X=t$ and arises a dependent variable $Y=\psi$. The initial condition is given at $C_i^S(t^{st})=0$ and $t = t^{st}$, the mass transfer steady-time (st), i.e., the time that the solute needs to fully permeate the SLM and start to desorb into the stripping phase. The final condition is reached when the system is equilibrated (eq), at $C_i^{S,eq}$ and t^{eq} , and the mass transport rate is ceased. The effective succinic acid permeability throughout the green-SLMs is determined from the function slope.

$$\frac{P \cdot A}{V^S} \cdot (t - t^{st}) = \frac{1}{V^S} \int_0^{C^S} \frac{dn^S}{\left(\frac{n_{t=0}^F - n^S}{V^F} \cdot \gamma^F - \frac{n^S}{V^S} \cdot \gamma^S \right)} = \psi \quad (6.8)$$

12 systems (1 solute x 4 green-SLM x 3 stripping phase) have been measured. To fit Eq. 6.8 to each experimental k dataset of j data-point number, both feed and stripping solute affinities must be corrected from COSMO-RS predictions. In total, there are three parameters to be fitted: γ_i^{Water} , $\gamma_i^{0.1M NaOH}$, and $\gamma_i^{0.5M NaOH}$. Since the parameter values must meet the Eq. 6.8 linearization, the objective function was established as the inverse sum of the squared Pearson correlation coefficient (r^2), according to Eq. 6.9. A MatLab® algorithm has been

developed to obtain the solute activity coefficients (Eq. C.3 to Eq.C.12 in the Appendix C).

$$OF: \min \left[\sum_k \left\{ \left(\frac{\sum_j \{(t_{j,k} - \bar{t}_k) \cdot (\psi_{j,k} - \bar{\psi}_k)\}}{\sqrt{\sum_j \{(t_{j,k} - \bar{t}_k)^2\} \cdot \sum_j \{(\psi_{j,k} - \bar{\psi}_k)^2\}}} \right)^2 \right\} \right]^{-1} \quad (6.9)$$

Finally, the goodness of the model fit was determined by the root mean squared deviations from all experimental datasets, according to Eq. 6.10, where N is the total experimental data points.

$$RSM D = \sqrt{\frac{1}{N} \sum_k \sum_j (C_{j,k}^{exp} - C_{j,k}^{cal})^2} \quad (6.10)$$

6.5.5 Results and discussion

Extraction of succinic acid from aqueous model solutions with green-SLM composed of DL-menthol:OctA, N₄₄₄₄Cl:OctA, eucalyptol, or [C₄pyrr][Tf₂N] in PVDF supports were performed at room temperature. The measured concentrations over time have an average combined expanded uncertainty of $U_{comb,95\%}(C_i) = 1.67 \text{ g l}^{-1}$, estimated following the directions of Chirico et al. (140) and Miller and Miller (141) with a confidence level of 95%.

According to the preliminary COSMO-RS computational results, the succinic acid activity coefficient in NaOH solutions remains constant in neutral and low pH solutions, and significantly decreases for pH values over 12 (activity coefficient vs pH for succinic acid and other organic acids in Figure C.0.4). The succinic acid concentration profile over time for the eucalyptol green-SLM with three different stripping phases (Figure 6.5) reveals the expected behaviour, i.e., greater concentrations as the pH of the receiving phase increases. Indeed, the average concentration factors resulted in 1.0, 1.1, and 1.4 for the membranes whose stripping solutions were water (pH 6-7), 0.1 M NaOH (pH 13.0-13.2), and 0.5 M NaOH (pH 13.5-13.7), respectively. The same behaviour is observed for all green-SLM systems studied in this work

(shown in Figure C.0.5). This suggests that solute-phase affinities have a greater influence on the maximum process extraction capacity, while the solute-membrane affinity determines the mass transfer rate and therefore, the time needed to reach equilibrium.

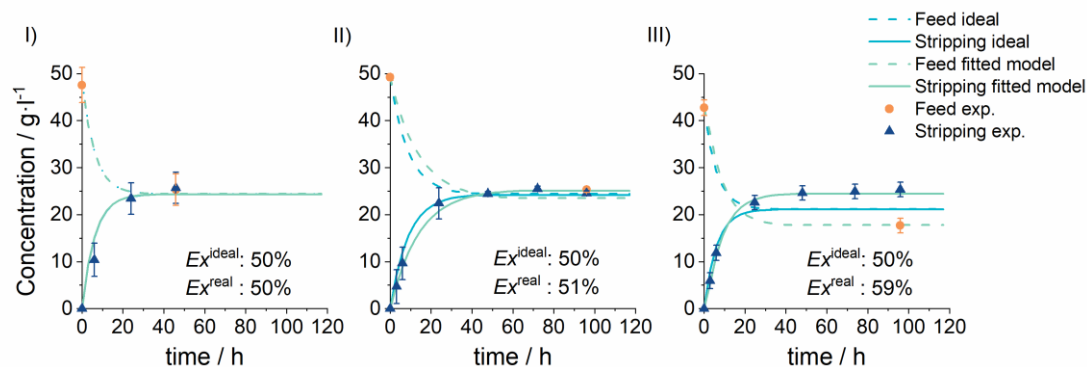


Figure 6.5. Experimental, ideal (Eq. 6.1), and fitted permeability activity-based (Eq. 6.5) models concentration profile and extraction yields (Ex) for succinic acid extraction with a eucalyptol-based green-SLM and three different stripping solutions. I) pure water; II) 0.1 M NaOH; III) 0.5 M NaOH. The same behaviour is observed for all green-SLM studied in this work.

Alkaline stripping solutions are commonly used to aid in the extraction of acid compounds from the membrane phase, due to the solute dissociation at a high pH that overcomes concentration gradients (203,213). Moreover, the use of stripping phases of different nature allows tailoring the extraction selectivity in multistage separation processes, as demonstrated elsewhere for the separation of platinum and palladium from an aqueous mixture of the two components plus rhodium in a two-step process (238). In such work, a stripping solution of 0.1 M NaClO₄ in 1 M HCl was first used to extract 96% of Pt(IV), and then a stripping solution of 10 mM thiourea and 0.1 M KSCN in 1 M HCl to extract 6% of Pd(II), with no Rd(III) extracted from the feed in neither of the two steps.

Graphs in Figure 6.5 also show the ideal (Eq. 6.1) and activity-based (Eq. 6.5) models fitted to the experimental data. For the permeability activity-based model, the succinic acid activity coefficients were fitted following the procedure described in section 6.5.4. Fitted results, Figure 6.6.I, indicates that the COSMO-RS method overestimates the differences in affinity but provides

a correct trend prediction. When solute-phase affinities are alike, i.e., feed and stripping solution are the same (i.e., water in both phases), the ideal and the activity-based approaches, converge to equivalent trajectories. However, as the affinity gradient is increased, the concentration-based model keeps predicting the same ideal behaviour, disagreeing with the experiment data. The RMSD (Eq. 6.10) of both models are compared with the root mean squared deviations of the experimental uncertainty, as shown in Figure 6.6.II. It is noted that the ideal model has a significant difference from the experimental measurements, while the fitted activity-based model shows better agreement to each data point.

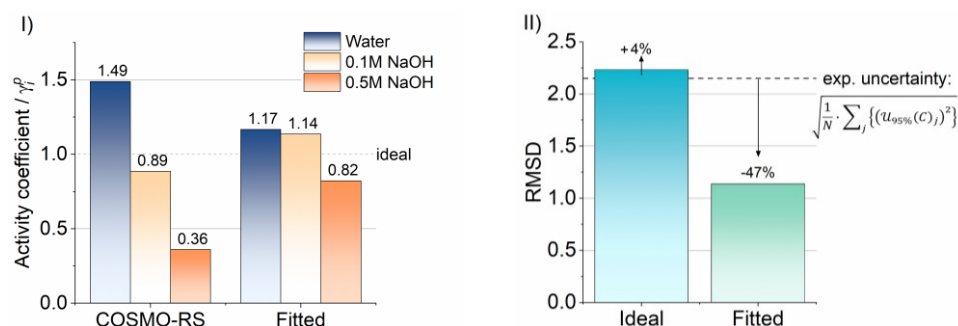


Figure 6.6. I) Succinic acid activity coefficient in water and alkaline solutions predicted by the COSMO-RS method at 20 °C and fitted to the experimental extraction data with green-SLM and the permeability activity-based model proposed in this work; II) Root mean squared deviation comparison of the ideal and fitted permeability activity-based models. The goodness of the models is also evaluated through the root mean squared deviations of the experimental uncertainty with a confidence level of 95%.

Estimations of succinic acid permeabilities from both approaches are depicted in Figure 6.7. The average combined expanded uncertainties are $U_{\text{comb},95\%}(P^{\text{ideal}}) = 1.5 \times 10^{-7} \text{ m} \cdot \text{s}^{-1}$ and $U_{\text{comb},95\%}(P^{\text{activity-based}}) = 6.9 \times 10^{-8} \text{ m} \cdot \text{s}^{-1}$, respectively. Despite slightly better succinic extractions for the SLMs with 0.1 M NaOH as the stripping solution, the permeability in those systems tends to be smaller than with pure water. The addition of NaOH leads to an increase in the osmotic pressure of the receiving phase, and therefore, an extra mass transfer resistance for the solute desorption from the membrane. However, at higher NaOH concentrations of 0.5 M the succinic acid affinity gradient becomes the predominant effect over the osmotic pressure. Indeed, the most favourable extraction system for the succinic acid recovery is the eucalyptol-based SLM, despite its low permeability in comparison to other systems.

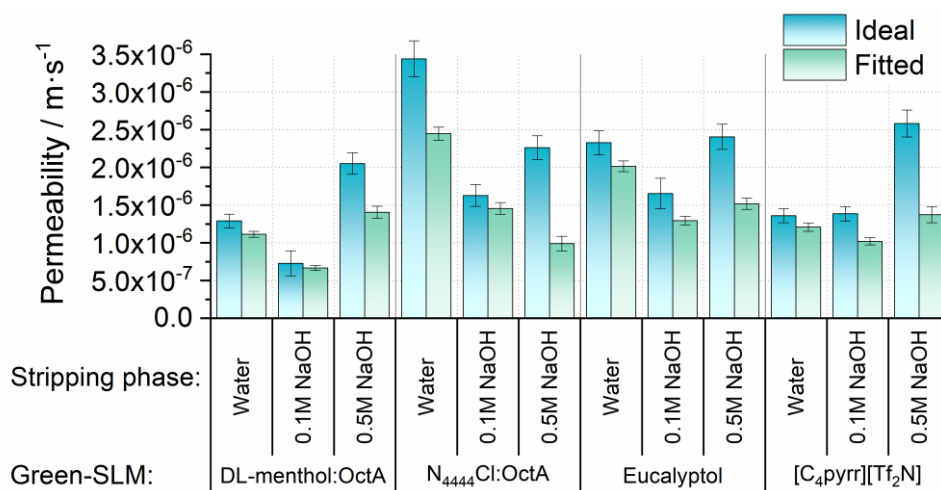


Figure 6.7. Succinic acid permeability ($\text{m}\cdot\text{s}^{-1}$) for the green-SLM studied in this work with water and two alkaline aqueous solutions (0.1 and 0.5 M NaOH) as stripping phase obtained from the ideal and fitted permeability activity-based models. Error bars considered the value uncertainties with a confidence level of 95%.

The above results highlight the importance of not treating complex interactions as an ideal system for the proper process description. Moreover, a misleading approach can have major consequences in the technology scale-up. Since the ideal model does not consider the activity correction in the concentration gradients, the permeability is overestimated. This might result in smaller equipment sizing that will not reach the expected extraction yields.

6.6 Cascade extraction process theoretical design

The extraction effectiveness in a separation process is governed by the thermodynamic equilibrium of the system. Given enough time and mass transfer area, the maximum possible solute extraction in a two-phase system is determined by the solute distribution coefficient, K'_D . The solute distribution coefficient establishes the solute concentration ratio in equilibrium between the feed (F) and the stripping (S) phase, each defined as the saturated solute mass over the solute-free solvent mass, $X_i^{S,eq}$. Rearranging it by the equilibria criteria, $a_m^{F,eq} = a_m^{S,eq}$, the distribution coefficient can be obtained from the ratio of the phase solvent density (ρ) times the solute activity coefficient (γ) in it, as shown in Eq. 611.

$$K'_D = \frac{X_i^{S, eq}}{X_i^{F, eq}} = \frac{\rho^{Solvent S} \cdot \gamma_i^S}{\rho^{Solvent F} \cdot \gamma_i^F} \quad (6.11)$$

Separation processes require K'_D above 1 to keep the mass transfer rate towards the extracting phase. Although operating with a large stripping to feed ratio allows to improve the extraction for systems with low K'_D , this implies a low final concentration in the extract. In practice, a single extraction stage often is not sufficient to reach process specifications, and multistage extraction processes are typically used (310). There are several cascade separation process arrangements, e.g., cocurrent, countercurrent, and crosscurrent, being the countercurrent configuration the preferred one for liquid stream separations due to its high efficiency and lower number of stages required. In fact, multi-stage LM processes have shown high selectivity and extraction yields in a range of applications including the racemic amino acid enantioseparation (311), penicillin G recovery (243), and 2-chlorophenol removal (312).

Therefore, to improve the extraction capacity of SLMs, a countercurrent configuration of N -stages (Figure 6.8) is proposed. The design is based on the equilibrium-stage model, considering the thermodynamic limitations discussed in previous sections. The feed (F) and stripping (S) streams, with initial solute concentrations C_F and C_S , respectively, are fed to each end of the process. It is assumed that the area and time within every stage are sufficient for the mass transfer to reach the equilibrium, i.e., solute activities in each stream are equalized. In an intermediate stage n , the raffinate stream coming out from the above stage (R_{n+1}) is treated with the extract of the stage below (E_{n-1}), helping to hold the mass transfer driving force.

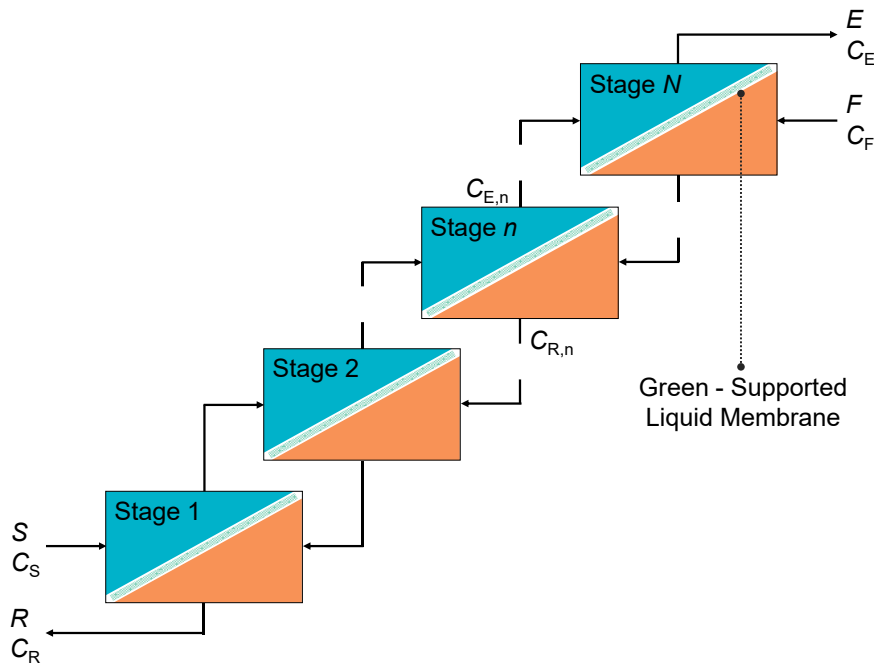


Figure 6.8. Cascade green-SLM extraction process in a countercurrent flow diagram. F , feed stream; S , stripping stream; R , raffinate stream; E , extract stream; N , total stages number; n , stage number; C_F , initial solute concentration in the feed stream; C_S , initial solute concentration in the stripping stream; $C_{R,n}$, solute concentration in the raffinate for stage n ; $C_{E,n}$, solute concentration in the extract for stage n ; C_R , final solute concentration in the raffinate stream; C_E , final solute concentration in the extract stream.

6.6.1 Graphical activity-based process design

To determine the total number of stages (N) required in the proposed green-SLM countercurrent cascade process, a graphical method is derived from the permeability activity-based model seen in previous sections. The method, denoted as PABLO (Permeability Activity-Based Linear Operation) method, includes the following assumptions:

- i)* Constant activity coefficients and permeability within the concentration range.
- ii)* Equilibrium is reached in each stage.
- iii)* Negligible solute retained within the LM phase.
- iv)* Negligible water and pH-modifier transport.
- v)* Negligible phase volume changes.
- vi)* Isothermic process.

The following operating parameters were selected for assessing the accuracy of the graphical method: concentration of succinic acid in the feed $C_F = 50 \text{ g l}^{-1}$, an alkaline 0.5 M NaOH stripping solution with no solute ($C_S = 0 \text{ g l}^{-1}$), and a feed to stripping phase ratio $S/F = 0.5$ (Table 6.2). The activity coefficient values were fitted from the permeability activity-based model and experimental green-SLM extraction measurements (see Figure 6.6) presented in section 6.5.5. Nevertheless, feeding the model with purely empirical solute activity coefficients values might improve its capacity to predict the extraction behaviour and thus the process design.

Table 6.2. Operating conditions and target final concentrations for the succinic acid recovery with green-SLM in a countercurrent cascade process.

| | Phase: | Feed | Stripping |
|--|-----------------------------------|-------|-----------|
| | Solvent: | Water | 0.5M NaOH |
| Solute Activity coefficient (γ) | - | 1.17 | 0.82 |
| Solvent density ($\rho^{Solvent}$) | $\text{mol}_s \text{ m}^{-3}$ | 55396 | 55896 |
| Flow rate | $\text{m}^3 \text{ h}^{-1}$ | 1.0 | 0.5 |
| Initial concentration (C) | g l^{-1} | 50 | 0.0 |
| Solute free-based concentration (X) | $\text{mol}_i \text{ mol}_s^{-1}$ | 0.008 | 0.000 |
| Target final concentration (C) | g l^{-1} | 16.5 | 67.0 |

The extraction factor, E_f (%), is defined as the distribution coefficient times the initial solvent mass flow ratio, M^S/M^F (Eq. 6.12). The theoretical maximum possible concentration in the extract stream (C_E^{max}) is calculated with Eq. 6.13. In a process design, the target final concentration in the extract stream must be set below the theoretical maximum in order to obtain a reasonable stage number and mass transfer area. The solute i recovery (X_i^R/X_i^F) in a countercurrent cascade with N -stages can be obtained from the process mass balance and the E_f value, according to Eq. 6.14, (310).

$$E_f = K'_D \cdot \frac{M^S}{M^F} = K'_D \cdot \frac{S \cdot (1 - X_i^S)}{F \cdot (1 - X_i^F)} \cdot \frac{\rho^{\text{Solvent } S}}{\rho^{\text{Solvent } F}} \quad (6.12)$$

$$C_E^{\text{max}} = \frac{F}{S} \cdot C_F \cdot E_f \quad (6.13)$$

$$\frac{X_i^R}{X_i^F} = \frac{1}{\sum_{n=0}^N (E_f)^n} \quad (6.14)$$

The distribution coefficient (Eq. 6.11) and the extraction factor (Eq. 6.12) for the system under the selected operating conditions results in $K'_D = 1.4$ and $E_f = 71.5\%$, respectively. According to Eq. 6.13, a maximum possible final concentration in the extract stream of $C_E^{\text{max}} = 71.5 \text{ g l}^{-1}$ could be obtained. The solute recovery vs total number of stages is shown in Figure 6.9. It can be seen that extra stages do not lead to significant improvements when the recovery approaches the E_f value. Therefore, an optimum target value must be determined from the specific process objectives and constraints. When the target final solute concentration in the extract is set as $C_E = 67 \text{ g l}^{-1}$ five stages are needed, and the final concentration in the raffinate (calculated from the global mass balance) results in $C_R = 16.5 \text{ g l}^{-1}$.

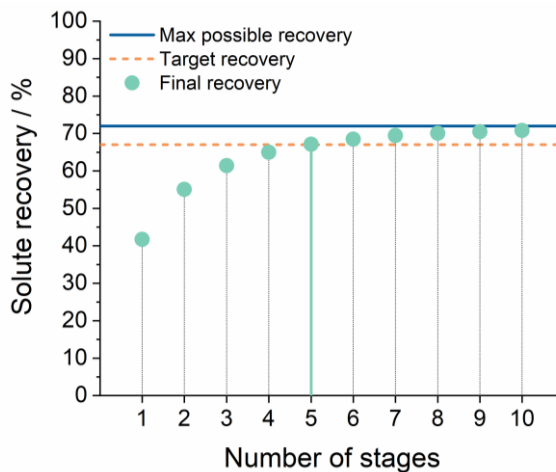


Figure 6.9. Solute (succinic acid) recovery as a function of the number of stages in a countercurrent cascade at operating conditions listed in Table 6.2 (analytical resolution). The solute recovery converges to an upper limit given by the system thermodynamic equilibrium. To reach a target final concentration $C_E = 67 \text{ g l}^{-1}$, a five-stage extraction process is required.

Intermediate concentrations (C_{Rn} and C_{En}) are given by the operating solute activity trajectory a_m^{op} : the stripping phase solute trajectory corrected by the flowrate ratio as well as the initial and target concentrations. The operating line is defined as a linear function of the operating concentration (C_i^{op}), as expressed in Eq. 6.15. Operating line slope (b^{op}) and intercept (a^{op}) are given by Eq. 6.16 and Eq. 6.17, respectively.

$$a_m^{op} = C_i^{op} \cdot b^{op} + a^{op} \quad (6.15)$$

$$b^{op} = \gamma_i^S \cdot \frac{F}{S} \quad (6.16)$$

$$a^{op} = \gamma_i^S \cdot \left(C_E - \frac{F}{S} \cdot C_F \right) \quad (6.17)$$

Figure 6.10 shows the graphical algorithm to obtain the required number of stages and interstage solute concentrations for the countercurrent cascade process with green-SLM coupled with the permeability activity-based model proposed in this work. The activity trajectories and operating line plot is built from the solute activity coefficients in the feed and stripping phases (Figure 6.10.I). C_F is the starting point, from which to descend vertically until the operating line is reached; the intersections of an horizontal line from that point with the feed and stripping phases trajectories give the raffinate and extract concentrations, respectively, for that stage (Figure 6.10.II). The same procedure is repeated starting from the new C_{Rn} until reaching the final C_R concentration. The total number of stages is given by the number of steps taken to complete the algorithm (Figure 6.10.III).

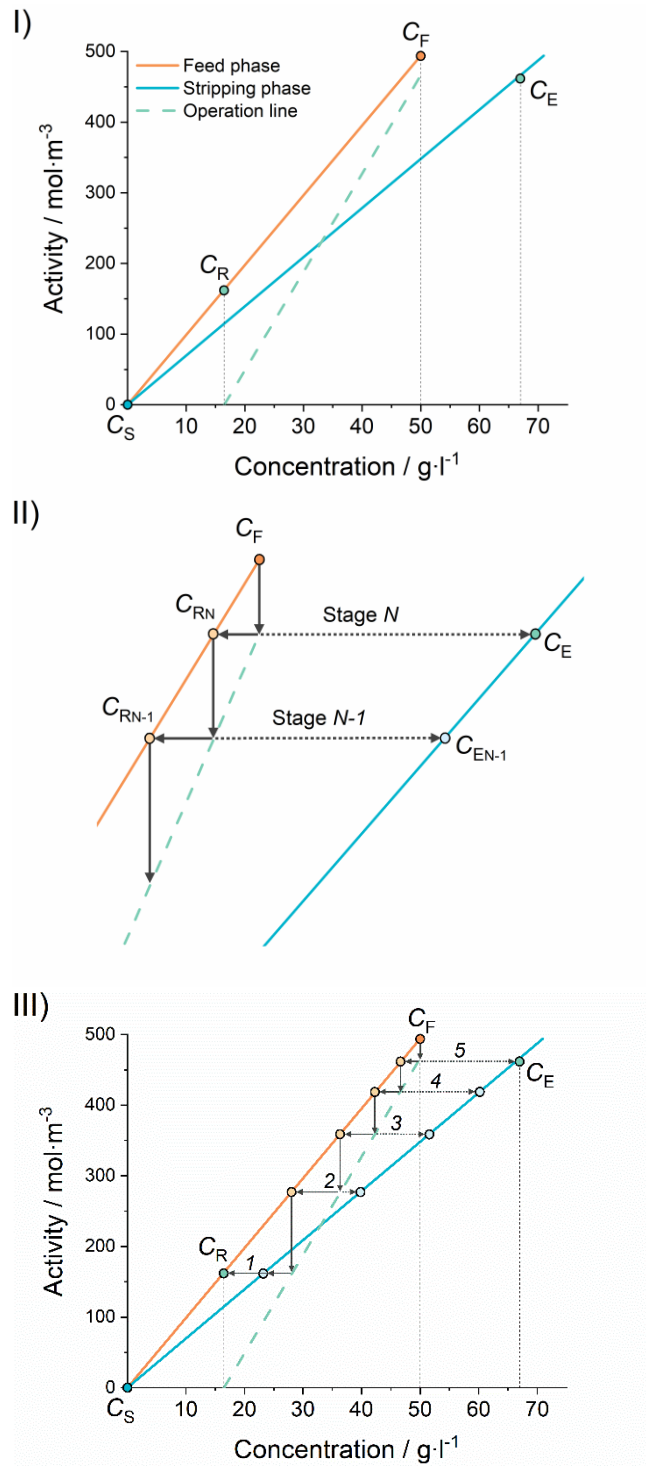


Figure 6.10. Green-SLM countercurrent cascade extraction process graphical algorithm (PABLO) to determine the number of stages required to reach the target final concentration by the permeability activity-based linear operation. I) Activities trajectories of the solute in the feed and stripping phases as well as the operating line obtained from the respective solute activity coefficient in each phase and the process operating conditions through Eq. 6.15 to Eq. 6.17; II) Stage number determination procedure: vertically descending from the initial feed concentration, C_F , to the operation line, then spitted horizontally towards the feed, C_{Rn} , and stripping, C_E , lines. Repeat the procedure from C_{Rn} , until reaching the final concentration in the raffinate, C_R ; II) Total number stages as the step number required to reach the final raffinate concentration, obtained under the operational condition listed in Table 6.2.

The proposed graphical activity-based procedure predicts 5 stages for the conditions defined in Table 6.2 (see Figure 6.10.III), which agrees with the calculated from of the analytical method (Eq. 6.14). The overall succinic acid recovery results in 67%. The graphical method is capable of determining the interstage activity profile. The driving force for the mass transfer, i.e., the activity gradient between the feed and the stripping phases, is maintained along the process as seen in Figure 6.11.I. This enhances the extraction going in an uphill concentration flux, where the final extract concentration is greater than the initial feed stream, as it is shown in the interstage concentration profile in Figure 6.11.II.

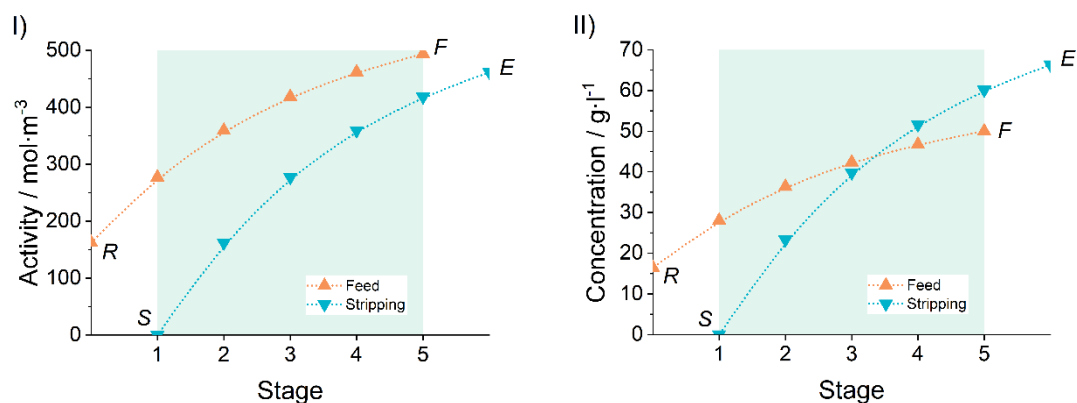


Figure 6.11. I) Activity profile and II) concentration profile of the succinic acid throughout a counter-current cascade five-stages green-SLM extraction obtained from the permeability activity-based model proposed in this work. A solution of 0.5 M NaOH is used as stripping phase. *F*: feed stream; *S*: stripping stream; *R*: raffinate stream; *E*: extract steam. Lines were included to guide the eye.

6.6.2 Required green-SLM area estimation

Equipment sizing is a key aspect in process design to perform both technical and economic evaluations. For SLM separation technology, this means to determine the effective mass transfer surface area to assess material, solvent, and apparatus costs.

In order to estimate the required mass transfer area to carry out the extraction with the green-SLM counter-current cascade design described above, the following procedure is proposed. The transported solute flow, q (mol s⁻¹), throughout a membrane section, A (m²), is described by Eq. 6.18. If a rectangular green-SLM geometry is assumed, the area section is defined as

$dA=y \cdot dz$, where the section width (y) is constant and the activity gradient, Δa_m (mol m^{-3}), only vary in the z -axis. Thus, the total transported solute within a fixed length (L) is determined by Eq. 6.19. A general expression of the Δa_m dependence along the z -axis is given by Eq. 6.20, as the activity gradient logarithmic mean, $\Delta a_{m \text{ LM}}$ (mol m^{-3}), it is based on the initial ($z=0$) and final ($z=L$) extraction stage conditions. The formal $\Delta a_{m \text{ LM}}$ derivation is found in Appendix C.

$$\frac{\partial q}{\partial A} = P \cdot (a_m^F - a_m^S) = P \cdot \Delta a_m \quad (6.18)$$

$$q = P \int_{z=0}^{z=L} \Delta a_m \cdot y dz \quad (6.19)$$

$$\Delta a_{m \text{ LM}} = \frac{(a_m^F - a_m^S)_{z=0} - (a_m^F - a_m^S)_{z=L}}{\ln \left(\frac{(a_m^F - a_m^S)_{z=0}}{(a_m^F - a_m^S)_{z=L}} \right)} \quad (6.20)$$

The required stage green-SLM area (A), is determined from Eq. 6.21, where the activity values can be obtained from the activity profile (see Figure 6.11.I) derived from the graphical permeability activity-based method described in section 6.6.1. The total area, A_T (m^2), of an n -stages countercurrent cascade extraction process is given by Eq. 6.22.

$$A = \frac{q}{P \cdot \Delta a_{m \text{ LM}}} \quad (6.21)$$

$$A_T = \frac{1}{P} \sum_{n=1}^N \frac{q_n}{\Delta a_{m \text{ LM},n}} \quad (6.22)$$

The required area (total and for each of the countercurrent cascade stages) with the four different green-SLM studied in this work is shown in Figure 6.12. The total area is inversely proportional to the solute permeability throughout the green-SLM (see Figure 6.7). For the same operating conditions and number of extraction stages, values of equipment size show significant differences. Although experimental results exhibited others succinic acid extraction

systems with larger permeability, e.g., using pure water as the stripping phase, their final concentration factor capacity was reduced, meaning smaller equipment but lesser final extract concentration. This evidences the importance to consider the systems thermodynamic capacity to extract the target solute and the SLM mass transport performance as a coupled effect in the process development.

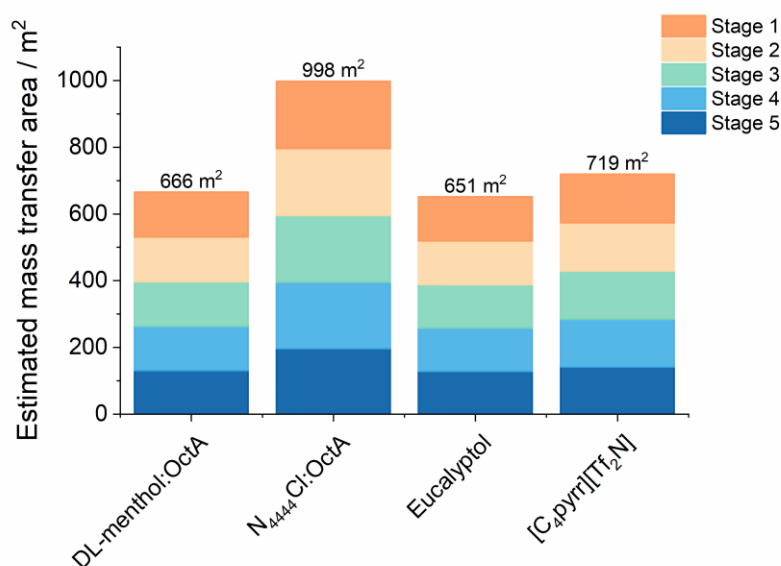


Figure 6.12. Estimated total and by stage mass transfer area for the extraction of succinic acid in a five-stage countercurrent cascade extraction process using an alkaline aqueous solution (0.5 M NaOH) as the stripping phase and four different green-SLM.

6.6.3 Temperature-driven green SLM extraction

In previous sections it has been modelled and demonstrated experimentally that adding a pH modifier can favour the extraction of an organic acid through SLMs. However, in some cases, this strategy might not be possible due to incompatibilities with the process or interferences in further purification stages.

The solute activity coefficient is not only a property dependent on the system conformation but on the temperature as well. This presents an opportunity for further studies on the SLM technology process design based on temperature gradients as an alternative way to control the solute affinity within the system. Temperature-driven processes are well known in

membrane separation technologies. One examples is membrane distillation (MD), another emerging separation method that benefits from stream temperature differences to enhance the trans-membrane vapour flux in water recovery (313,314).

The affinity temperature dependency can be reliably described by empirical activity coefficient models, such as the Non-Random Two Liquid model (NRTL) (97). Based on the system excess Gibbs energy calculations, the NRTL model allows the activity coefficients determination as a function of the temperature and mixture composition. Figure 6.13.I shows the succinic acid activity in pure water represented by the NRTL model computed by COSMO-RS method. At high acid concentration and temperature, greater activity is observed with a non-linear dependency. Thus, a counterflow extraction process of a hot feed stream and a cold stripping stream will effectively promote the solute mass transfer.

In this arrangement, the mass and heat transfer are coupled phenomena. On the one hand, both the mass transfer resistances, ab/desorption rates and solute diffusion, as well as the driving force, solute chemical potential, are temperature-dependent factors. Thus, permeability must be corrected along with the heat exchange. The permeability as a temperature function is expressed in an Arrhenius-form equation (Eq. 6.23), based on an empirical parameter, E_a (J mol⁻¹), representing the activation energy (198). On the other hand, given a membrane area and temperature gradient, ΔT (K), the heat transfer, Q (kJ kg⁻¹), throughout the membrane is determined from Eq. 6.24. The heat flow is dependent on the convective heat transfer coefficient, h (kW m⁻² K⁻¹), of each stream, the membrane thickness, δ (m), and membrane thermal conductivity, k (kW m⁻¹ K⁻¹). For membrane conductive heat transfer, an isostrain model can be used to estimate the two-phase composite material SLM thermal conductivity, according to Eq. 6.25, weighing the support and solvent thermal conductivity by the SLM impregnation ratio, ε (%) (315).

$$\frac{P_i(T_2)}{P_i(T_1)} = \exp \left[-\frac{E_a}{R} \left(\frac{1}{T_2} - \frac{1}{T_1} \right) \right] \quad (6.23)$$

$$Q = \left[\frac{1}{h^F} + \frac{\delta}{k} + \frac{1}{h^S} \right]^{-1} \cdot A \cdot \Delta T \quad (6.24)$$

$$k = (1 - \varepsilon) \cdot k_{support} + \varepsilon \cdot k_{solvent} \quad (6.25)$$

Figure 6.13.II presents a schematic two-stage countercurrent cascade extraction process driven by the solute activity dependence on the temperature and concentration gradients. As both mass and heat are transferred from one stream to another, the temperature gradient is reduced after each extraction stage. Thus, to enhance the process efficiency, interstage heaters and coolers can be implemented to overcome the mass transfer rate drop. Despite the increased energy consumption, this effect can be efficiently managed through process energy integration methods between the cold and heat streams (316). Note that this temperature-enhanced approach can be coupled with the facilitated transport mechanisms to reach an optimum extraction process design, opening up avenues to impulse the LM technology towards becoming one of the predominant separation methods among other well-established industrial processes.

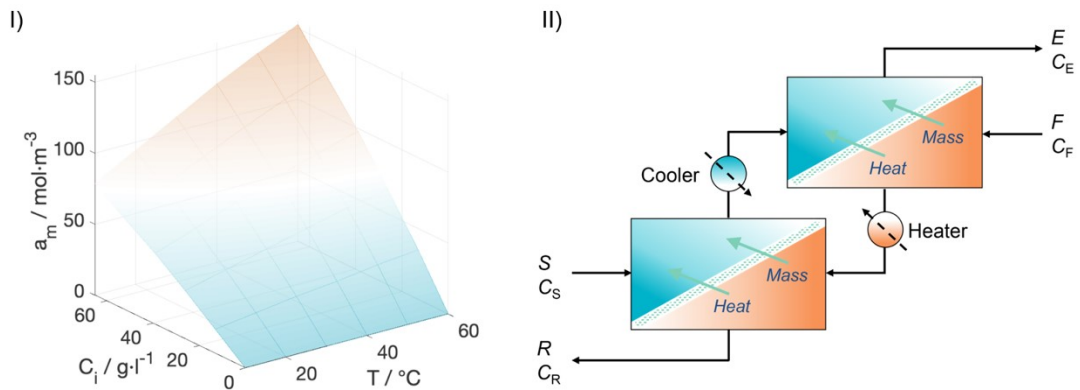


Figure 6.13. I) Succinic acid activity dependence with concentration and temperature computed with COSMO-RS method and represented by the NRTL model; II) Schematic two-stage countercurrent cascade extraction process with intermediate cooler/heater auxiliary processes.

6.7 Conclusions

The new permeability activity-based approach presented in this work fulfils a fundamental gap in the SLM process modelling. It allows overcoming the concentration-based models' limitations, as it predicts the final equilibrium state by accounting for the solute activity effect. Experimental succinic acid recovery with four different green-SLM (DL-menthol:OctA and N₄₄₄₄Cl:OctA eutectic solvents, the bio-based solvent eucalyptol and the ionic liquid [C₄pyrr][Tf₂N]) confirmed that extraction yields are determined by the solute-phase affinities, being the stripping phase pH the most relevant factor. Thus, a selective-oriented design can be performed establishing favourable compound affinities. On the other hand, the SLM conformation has a major influence on the solute permeability, determining the mass transfer rate. Both effects are key for a proper SLM process design.

A graphical method, PABLO (Permeability Activity-Based Linear Operation), for calculating the theoretical number of stages required for the extraction of organic acids in a multistage countercurrent cascade design has been developed. The mass transfer area requirement, a critical parameter for assessing the techno-economic feasibility of the process, can be also calculated. Additionally, coupling mass and heat transfer phenomena into the green-SLM extraction process has been proposed.

The developed approach will allow researchers to address preliminary system selection for further studies and will help in the feasibility assessment of green solvents and SLMs for sustainable separation processes. Especially, it is foreseen as a tool for the biorefinery industry to implement competitive green routes into chemical manufacturing and work towards technological maturity.

Part IV

Contribution to knowledge.

"If you really want truth, you need to escape the black hole of power, and allow yourself to waste a lot of time wandering here and there on the periphery. Revolutionary knowledge rarely makes it to the centre, because the centre is built on existing knowledge."

— Yuval Noah Harari, *21 Lessons for the 21st Century*

Chapter 7. Thesis conclusions and further research

In this chapter, the main contributions are summarized, and future work that is still required to achieve a competitive sustainable separation technology is outlined.

7.1 Conclusions

Advanced sustainable separation alternatives have been suggested to overcome the main bottleneck in bio-based organic acid production from renewable sources. As fundamental building blocks for the chemical industry, organic acids have attracted immense interest among researchers. A broad range of chemical engineering solutions has been proposed for their efficient production and further purification. Downstream separation processes are the core of the chemical industry and usually the ones with higher operating costs. In the biorefinery industry, current recovery methods might involve the use of petrochemical-derived substances or intensive energy-demanding processes for the production of compounds that are contradictory to the intended reduction of petroleum dependence. From the need to find alternatives to such processes, the use of *novel green solvents* and *liquid membrane technology* was systematically assessed.

Ionic liquids, eutectic solvents, and bio-based solvents are among the ecological candidates suggested in the literature to improve bioseparations. In this thesis, the thermodynamic assessments of the molecular interactions within the systems [organic acid + water], [organic acid + green solvent] and [water + green solvent] revealed the complexity of the biomolecules extraction from aqueous solutions. The green solvent extraction capacity is governed by hydrogen bonds formed with the solute. However, solute and water molecules compete to form such interactions with the solvent. High interactions mean better extraction but poor process selectivity. As the number of extraction

media specifications grows for a target process, the suitability of preliminary solvents becomes diffuse. Nevertheless, it was possible to identify patterns to classify the performance of green solvents for the recovery of structurally different organic acids considering three key aspects: extraction performance, water affinity, and spontaneity. On this basis, solvent recommendations for further empirical studies were provided.

Besides the evidence of the green solvent suitability, the separation process design requires to be fed with the physicochemical properties of the system. New data on the temperature dependence of organic acids solubilities and activity coefficients were reported. Solid-liquid equilibria measurements and modelling of organic acids in water and bio-based solvents give deeper comprehension of the aforementioned interactions as well as the energetic contributions leading to their formation. Although the dissolution of the organic acids is an endothermic process, the observed enthalpy-entropy compensation effect indicates the tendency of the systems to increase their order as the new complex interactions are formed.

Following the principles of green chemistry, not only replacing harmful compounds but also reducing the amount of solvent is required. Thus, is imperative to develop more sustainable bio-based organic acid separations. Liquid membranes, with minimum solvent requirement and the ability to generate large separation yields, are an excellent separation alternative to conventional processes. The technology has proved its applicability in several fields, including a broad range of biomolecules recovery from their fermentation matrices. Moreover, green solvents, such as those studied in this work, have been successfully used in different liquid membrane configurations. However, despite its potential and having been proposed several decades ago, the technological maturity is far to compete with the commercial systems. Several operational issues remain a challenge. Among them, membrane stability, solvent-process compatibility, and process integration are highlighted as research priorities. Moreover, improved phenomenological descriptions and modelling are needed. Liquid membranes

promise to enhance bioseparations in the near future, yet there is still abundant research and field tests to do.

In this thesis, green solvents and liquid membranes were combined and applied for succinic acid recovery. Green-supported liquid membranes were successfully prepared with ionic liquids, eutectic solvents, and bio-based solvents in polymeric porous supports. The empirical assays demonstrated that the final extraction yield is governed by the thermodynamic equilibrium, i.e., the solute-phase affinities, while the solute permeability rate on the membrane conformation. A new permeability activity-based approach is presented that overcomes the limitations of the current concentration-based models by accounting for the effect of the solute activity in each phase. A graphical method to determine the theoretical number of stages and membrane mass transfer area requirement in a cascade extraction process design was built. The *Permeability Activity-Based Linear Operation* (PABLO) method, contributes to estimating both fundamental parameters required to assess the techno-economic feasibility of the process. Further guidelines to address future developments are also given. The presented mass transfer approach opens opportunities to exploit thermal gradients as the mass transfer driving force in supported liquid membrane separations.

Insights derived from this work will help to promote the development of clean chemical manufacturing. As discussed in this thesis, current barriers to adopting entire green production routes can be overcome by investing research resources on a deep understanding of the underlying separation mechanism, and how they define the outcome of new technology proposals. Yet, novel solutions need to be rethought and polished to reach their full applicability. The presented approaches to improve the extraction systems selection and supported liquid membranes process design sets a fresh and robust groundwork from where to start walking towards sustainable industries.

7.2 Further research

Throughout this thesis, new research questions on green production routes for bio-based organic acids were raised. They open new opportunities to complement this project by generating approaches from other points of view and delivering new contributions to knowledge on this topic.

7.2.1 On green solvents

By-products and impurities effect

Bio-based organic acid production has an inevitable by-product formation. These compounds and their final concentration depend on the starting raw materials, fermentation pathway, and operational conditions. Bio-succinic acid production typically presents the formation of formic acid, acetic acid, pyruvic acid, lactic acid and small amounts of ethanol (22–27). For bio-levulinic acid, formic acid and furfural are the most common side products (28–31). Finally, bio-fumaric acid production usually involves ethanol and glycerol as by-products (32–35).

On the one hand, fermentation yield depends on the broth composition, where the product or by-products accumulation might cause inhibition issues. Thus, optimal removal is necessary. On the other hand, as the recovery process lacks selectivity, downstream product purification stages become complex and expensive. The process design must balance the trade-off between the production, extraction, and purification stages. In consequence, research on selective recovery will be required to evaluate the real advantages of the proposed extracting media.

Organic acid interaction with IL/ES

The main feature that defines both IL and ES is the strong molecular interactions within its constituents. Such interactions allow for effective extraction of the organic acids from the fermentation broths, yet forming new bonds may prevent its back-extraction. Carboxylic groups in the organic acids act as HBD, which interacts with the HBA component of the ES (72,79).

Depending on the specific interactions formed, the presence of the organic acid within the ES might cause a molecular migration, resulting in the original HBA leaching out of the solvent. Therefore, further molecular and ES stability studies are needed to identify their long-run applicability.

7.2.2 On supported liquid membranes

Solvent - Support chemical compatibility

Although several hydrophobic green solvents have proved their capacity to extract organic acids, they might not be suitable for an SLM separation process due to material incompatibility. As presented in [Chapter 3](#), the bio-based solvents CPME and 2-MeTHF, as well as EtOAc, showed high recovery yields of organic acids. Nevertheless, those components can dissolve the polymers of the porous support, such as the PVDF. This might cause operational issues from a reduction of the effective surface area to stream contamination. The chemical compatibility of the extraction media and support should be assessed to address the SLM conformation, allowing to benefit of the solvent advantages with proper inert material.

Supported Liquid membrane stability

As was stressed in [Chapter 5](#), membrane stability is one of the major challenges in this technology development. Interactions between the extraction solvent and the material support determine the SLM capacity to retain the solvent in time. Membrane stability can be improved by optimizing the support pore size to the solvent physicochemical properties ([198](#)). Other LM arrangements have been proposed to overcome this issue (see [Section 5.2.2.4](#)). Nevertheless, LM stability should be demonstrated in the long run under real operational conditions to guarantee its feasibility for large-scale applications.

7.2.3 On extraction process feasibility

Techno-economic evaluation

Emergent technologies often display a solid background in both theoretical and lab-scale testing aspects. The growing number of publications on LMs development demonstrates their exciting properties. Nevertheless, to prove its competitiveness against conventional technics, the efforts of researchers and engineers must focus also on large-scale implementation. Technology transfer from academic to industry needs to be sustained with detailed techno-economic evaluation in order to identify barriers to its implementation and, in this way, optimize the research resources.

Process lifecycle assessment

Keeping in mind the original motivation of this thesis, the proposed separation method must be assessed as a whole, aiming to demonstrate that the production route meets the green chemistry principles (12) and environmental regulations across each one of its stages. Cradle-to-cradle assessment of the used compounds and materials, as well as the whole separation process, are required to evaluate the environmental impact and the benefits that the technology aims for.

7.3 Closing words

During the four years that this PhD took to deliver the present document, the project's main subject shaped itself. From the direct measurement of novel green solvent for bio-based organic extraction to membrane technology assessment to thermodynamic and mass transfer modelling, the project was polished several times pursuing making a real impact. The presented outcome is the raffinate of all that work as well as the priceless insights attained from the academic environment, most importantly from the colleagues I worked with. I really hope the contributions this work made will help to grow a sustainable society as much as I had on a professional and personal level.

References

1. López-Porfiri P, González-Miquel M, Gorgojo P. Green supported liquid membranes: The permeability activity-based linear operation (PABLO) method. *Chem Eng J* [Internet]. 2022 Oct;446:137253. Available from: <https://linkinghub.elsevier.com/retrieve/pii/S1385894722027425>
2. López-Porfiri P, González-Miquel M, Gorgojo P. Liquid Membrane Technology for Sustainable Separations. In: Szekely G, Zhao D, editors. *Sustainable Separation Engineering* [Internet]. First Edit. Wiley; 2022. p. 297–341. Available from: <https://onlinelibrary.wiley.com/doi/10.1002/9781119740117.ch8>
3. López-Porfiri P, Gorgojo P, Gonzalez-Miquel M. Green Solvent Selection Guide for Biobased Organic Acid Recovery. *ACS Sustain Chem Eng* [Internet]. 2020 Jun 22;8(24):8958–69. Available from: <https://pubs.acs.org/doi/10.1021/acssuschemeng.0c01456>
4. López-Porfiri P, Gorgojo P, Gonzalez-Miquel M. Solubility Study and Thermodynamic Modelling of Succinic Acid and Fumaric Acid in Bio-based Solvents (Under review). 2022;
5. López-Porfiri P, Ramos-Paredes S, Núñez P, Gorgojo P. The Missing Links in the Technological Maturity of Membrane Distillation (Under review). 2022;
6. Cotroneo-Figueroa VP, Gajardo-Parra NF, López-Porfiri P, Leiva Á, Gonzalez-Miquel M, Garrido JM, et al. Hydrogen bond donor and alcohol chain length effect on the physicochemical properties of choline chloride based deep eutectic solvents mixed with alcohols. *J Mol Liq* [Internet]. 2022 Jan;345:116986. Available from: <https://doi.org/10.1016/j.molliq.2021.116986>
7. Villablanca-Ahues R, López-Porfiri P, Canales RI, de la Fuente JC. High-pressure vapor+liquid equilibria for the binary system CO₂ + (E)-2-hexenal. *J Supercrit Fluids* [Internet]. 2020 Oct;105027. Available from: <https://linkinghub.elsevier.com/retrieve/pii/S0896844620302783>
8. Vicencio LA, López-Porfiri P, de la Fuente JC. Vapour pressure and vaporisation enthalpy for two key apple odorants, ethyl butyrate and ethyl hexanoate, at pressures from (15 to 105) kPa. *J Chem Thermodyn* [Internet]. 2020 Jan 1;142:105982. Available from: <https://linkinghub.elsevier.com/retrieve/pii/S0021961419306457>
9. López-Porfiri P, Villablanca-Ahues R, Bejarano A, de la Fuente JC. High-pressure (vapor + liquid) equilibria for binary systems containing carbon dioxide and key apple odorants, hexanal and ethyl-2-methylbutyrate. *J Chem Thermodyn*. 2017;115.
10. López-Porfiri P, Brennecke JF, Gonzalez-Miquel M. Excess molar enthalpies of deep eutectic solvents (DESs) composed of quaternary ammonium salts and glycerol or ethylene glycol. *J Chem Eng Data*. 2016;61(12):4245–51.
11. Bejarano A, López PI, Del Valle JM, De La Fuente JC. High-pressure (vapor + liquid) equilibria for ternary systems composed by {(E)-2-hexenal or hexanal + carbon dioxide + water}: Partition coefficient measurement. *J Chem Thermodyn*. 2015;89:79–88.
12. Anastas P, Eghbali N. Green Chemistry: Principles and Practice. *Chem Soc Rev* [Internet]. 2010;39(1):301–12. Available from: <http://xlink.rsc.org/?DOI=B918763B>
13. Annevelink B, Chavez LG, van Ree R, Vural Gursel I. Global biorefinery status report 2022 [Internet]. 2022. Available from: <https://task42.ieabioenergy.com/wp-content/uploads/sites/10/2022/07/IEA-Bioenergy-Task-42-Global-biorefinery-status-report-2022-220712.pdf>
14. Cherubini F. The biorefinery concept: Using biomass instead of oil for producing energy and chemicals. *Energy Convers Manag* [Internet]. 2010 Jul;51(7):1412–21. Available from: <http://dx.doi.org/10.1016/j.enconman.2010.01.015>
15. de Jong E, Stichnothe H, Bell G, Jørgensen H. Bio-Based Chemicals: A 2020 Update

- [Internet]. IEA Bioenergy Task 42 Biorefinery. IEA Bioenergy; 2020. 1–79 p. Available from: <https://task42.ieabioenergy.com/wp-content/uploads/sites/10/2020/02/Bio-based-chemicals-a-2020-update-final-200213.pdf>
16. Werpy TA, Holladay JE, White JF. Top Value Added Chemicals From Biomass: I. Results of Screening for Potential Candidates from Sugars and Synthesis Gas [Internet]. Richland, WA; 2004 Nov. Available from: <http://www.osti.gov/servlets/purl/926125-eeUkhS/>
 17. Grand View Research. Bio-based Platform Chemicals Market Size, Share & Trends Analysis Report By Product (1,3-Propanediol, Dodecanedioic Acid, Lactic Acid, Succinic Acid, Fumaric Acid, Malic Acid, Glucaric Acid), And Segment Forecasts, 2019 - 2025 [Internet]. 2019 [cited 2019 May 27]. Available from: <https://www.grandviewresearch.com/industry-analysis/bio-based-platform-chemicals-market>
 18. de Jong E, van Ree R. Biorefineries: adding value to the sustainable utilisation of biomass [Internet]. London; 2009. Available from: http://link.springer.com/10.1007/978-1-349-06888-3_42
 19. Adler S, Beaver E, Bryan P, Robinson S, Watson J. Vision 2020: 2000 Separations Roadmap [Internet]. 2000 Jan. Available from: <http://www.osti.gov/servlets/purl/1218701/>
 20. Huang H-J, Ramaswamy S. Overview of Biomass Conversion Processes and Separation and Purification Technologies in Biorefineries. In: Separation and Purification Technologies in Biorefineries [Internet]. Chichester, UK: John Wiley & Sons, Ltd; 2013. p. 1–36. Available from: <https://onlinelibrary.wiley.com/doi/10.1002/9781118493441.ch1>
 21. Kirchherr J. Bullshit in the Sustainability and Transitions Literature: a Provocation. *Circ Econ Sustain* [Internet]. 2022 May 20;(0123456789). Available from: <https://doi.org/10.1007/s43615-022-00175-9>
 22. Jiang M, Ma J, Wu M, Liu R, Liang L, Xin F, et al. Progress of succinic acid production from renewable resources: Metabolic and fermentative strategies. *Bioresour Technol* [Internet]. 2017 Dec;245(30):1710–7. Available from: <https://doi.org/10.1016/j.biortech.2017.05.209>
 23. Song H, Lee SY. Production of succinic acid by bacterial fermentation. *Enzyme Microb Technol* [Internet]. 2006 Jul;39(3):352–61. Available from: <https://linkinghub.elsevier.com/retrieve/pii/S0141022906001190>
 24. Lin SKC, Du C, Koutinas A, Wang R, Webb C. Substrate and product inhibition kinetics in succinic acid production by *Actinobacillus succinogenes*. *Biochem Eng J*. 2008;41(2):128–35.
 25. Liu YP, Zheng P, Sun ZH, Ni Y, Dong JJ, Zhu LL. Economical succinic acid production from cane molasses by *Actinobacillus succinogenes*. *Bioresour Technol*. 2008;99(6):1736–42.
 26. Bechthold I, Bretz K, Kabasci S, Kopitzky R, Springer A. Succinic acid: A new platform chemical for biobased polymers from renewable resources. *Chem Eng Technol*. 2008;31(5):647–54.
 27. Orjuela A, Orjuela A, Lira CT, Miller DJ. A novel process for recovery of fermentation-derived succinic acid: Process design and economic analysis. *Bioresour Technol* [Internet]. 2013;139:235–41. Available from: <http://dx.doi.org/10.1016/j.biortech.2013.03.174>
 28. Morone A, Apte M, Pandey RA. Levulinic acid production from renewable waste resources: Bottlenecks, potential remedies, advancements and applications. *Renew Sustain Energy Rev*. 2015;51:548–65.
 29. Bozell JJ, Moens L, Elliott DC, Wang Y, Neuenschwander GG, Fitzpatrick SW, et al. Production of levulinic acid and use as a platform chemical for derived products 10.1016/S0921-3449(99)00047-6 : Resources, Conservation and Recycling | ScienceDirect.com. *Resour Convers Recycl* [Internet]. 2000;28:227–39. Available from: <http://www.sciencedirect.com.proxy->

- ub.rug.nl/science/article/pii/S0921344999000476
30. Rackemann DW, Doherty WOS. The conversion of lignocellulosics to levulinic acid. *Biofuels, Bioprod Biorefining*. 2011;5:198–214.
 31. Brouwer T, Blahusiak M, Babic K, Schuur B. Reactive extraction and recovery of levulinic acid, formic acid and furfural from aqueous solutions containing sulphuric acid. *Sep Purif Technol*. 2017;
 32. Wei L, Liu J, Qi H, Wen J. Engineering *Scheffersomyces stipitis* for fumaric acid production from xylose. *Bioresour Technol*. 2015;
 33. Cao N, Du J, Gong CS, TSAO GT. Simultaneous Production and Recovery of Fumaric Acid from Immobilized RO with RBC and Adsorption Column. *Appl Environ Microbiol* [Internet]. 1996;62(8):2926–31. Available from: <http://aem.asm.org/>
 34. Xu Q, Li S, Huang H, Wen J. Key technologies for the industrial production of fumaric acid by fermentation. *Biotechnol Adv* [Internet]. 2012;30(6):1685–96. Available from: <http://dx.doi.org/10.1016/j.biotechadv.2012.08.007>
 35. Roa Engel CA, Van Gulik WM, Marang L, Van der Wielen LAM, Straathof AJJ. Development of a low pH fermentation strategy for fumaric acid production by *Rhizopus oryzae*. *Enzyme Microb Technol* [Internet]. 2011;48(1):39–47. Available from: <http://dx.doi.org/10.1016/j.enzmictec.2010.09.001>
 36. Oliveira FS, Araújo JMM, Ferreira R, Rebelo LPN, Marrucho IM. Extraction of l-lactic, l-malic, and succinic acids using phosphonium-based ionic liquids. *Sep Purif Technol* [Internet]. 2012;85:137–46. Available from: <http://dx.doi.org/10.1016/j.seppur.2011.10.002>
 37. Brouwer T, Blahusiak M, Babic K, Schuur B. Reactive extraction and recovery of levulinic acid, formic acid and furfural from aqueous solutions containing sulphuric acid. *Sep Purif Technol* [Internet]. 2017;185:186–95. Available from: <http://dx.doi.org/10.1016/j.seppur.2017.05.036>
 38. Djas M, Henczka M. Reactive extraction of carboxylic acids using organic solvents and supercritical fluids: A review. *Sep Purif Technol*. 2018;201(September 2017):106–19.
 39. Orjuela A, Yanez AJ, Peereboom L, Lira CT, Miller DJ. A novel process for recovery of fermentation-derived succinic acid. *Sep Purif Technol* [Internet]. 2011;83(1):31–7. Available from: <http://dx.doi.org/10.1016/j.seppur.2011.08.010>
 40. Roa Engel CA, Straathof AJJ, Zijlmans TW, Van Gulik WM, Van Der Wielen LAM. Fumaric acid production by fermentation. *Appl Microbiol Biotechnol*. 2008;78(3):379–89.
 41. Pazmiño-Mayorga I, Jobson M, Kiss AA. Conceptual design of a dual reactive dividing wall column for downstream processing of lactic acid. *Chem Eng Process - Process Intensif* [Internet]. 2021 Jul;164(March):108402. Available from: <https://linkinghub.elsevier.com/retrieve/pii/S0255270121001045>
 42. Winterton N. The green solvent: a critical perspective. *Clean Technol Environ Policy* [Internet]. 2021 Nov 30;23(9):2499–522. Available from: <https://doi.org/10.1007/s10098-021-02188-8>
 43. Clarke CJ, Tu W-C, Levers O, Bröhl A, Hallett JP. Green and Sustainable Solvents in Chemical Processes. *Chem Rev* [Internet]. 2018 Jan 24;118(2):747–800. Available from: <https://pubs.acs.org/doi/10.1021/acs.chemrev.7b00571>
 44. Gonzalez-Miquel M, Esteban J. Novel Solvents for Biotechnology Applications. In: Moo-Young M, editor. *Comprehensive Biotechnology*. 3rd ed. Elsevier: Pergamon; 2019. p. 790–806.
 45. Cañadas R, González-Miquel M, González EJ, Díaz I, Rodríguez M. Overview of neoteric solvents as extractants in food industry: A focus on phenolic compounds separation from liquid streams. *Food Res Int* [Internet]. 2020 Oct;136(July):109558. Available from: <https://doi.org/10.1016/j.foodres.2020.109558>
 46. Schuur B, Brouwer T, Smink D, Sprakel LMJ. Green solvents for sustainable separation processes. *Curr Opin Green Sustain Chem* [Internet]. 2019 Aug;18:57–65.

- Available from: <https://doi.org/10.1016/j.cogsc.2018.12.009>
47. Schuur B, Brouwer T, Sprakel LMJ. Recent Developments in Solvent-Based Fluid Separations. *Annu Rev Chem Biomol Eng* [Internet]. 2021 Jun 7;12(1):573–91. Available from: <https://www.annualreviews.org/doi/10.1146/annurev-chembioeng-102620-015346>
 48. Brennecke JF, Maginn EJ. Ionic Liquids- Innovative Fluids for Chemical Processing. 2001;47(3).
 49. Fabre E, Murshed SMS. A review of the thermophysical properties and potential of ionic liquids for thermal applications. *J Mater Chem A* [Internet]. 2021;9(29):15861–79. Available from: <http://xlink.rsc.org/?DOI=D1TA03656D>
 50. Kaur G, Kumar H, Singla M. Diverse applications of ionic liquids: A comprehensive review. *J Mol Liq* [Internet]. 2022 Apr;351:118556. Available from: <https://doi.org/10.1016/j.molliq.2022.118556>
 51. Miao L, Song Z, Zhu D, Li L, Gan L, Liu M. Ionic Liquids for Supercapacitive Energy Storage: A Mini-Review. *Energy & Fuels* [Internet]. 2021 May 20;35(10):8443–55. Available from: <https://pubs.acs.org/doi/10.1021/acs.energyfuels.1c00321>
 52. Zhu S, Wu Y, Chen Q, Yu Z, Wang C, Jin S, et al. Dissolution of cellulose with ionic liquids and its application: A mini-review. *Green Chem*. 2006;8(4):325–7.
 53. Curreri AM, Mitragotri S, Tanner EEL. Recent Advances in Ionic Liquids in Biomedicine. *Adv Sci* [Internet]. 2021 Sep 10;8(17):2004819. Available from: <https://onlinelibrary.wiley.com/doi/10.1002/advs.202004819>
 54. de Jesus SS, Maciel Filho R. Are ionic liquids eco-friendly? *Renew Sustain Energy Rev* [Internet]. 2022 Apr;157(December 2021):112039. Available from: <https://linkinghub.elsevier.com/retrieve/pii/S1364032121013010>
 55. Amde M, Liu JF, Pang L. Environmental Application, Fate, Effects, and Concerns of Ionic Liquids: A Review. *Environ Sci Technol*. 2015;49(21):12611–27.
 56. Viboud S, Papaiconomou N, Cortesi A, Chatel G, Draye M, Fontvieille D. Correlating the structure and composition of ionic liquids with their toxicity on *Vibrio fischeri*: A systematic study. *J Hazard Mater* [Internet]. 2012;215–216:40–8. Available from: <http://dx.doi.org/10.1016/j.jhazmat.2012.02.019>
 57. Weyhing-Zerrer N, Kalb R, Oßmer R, Rossmannith P, Mester P. Evidence of a reverse side-chain effect of tris(pentafluoroethyl)trifluorophosphate [FAP]-based ionic liquids against pathogenic bacteria. *Ecotoxicol Environ Saf*. 2018;148(October 2017):467–72.
 58. Santiago R, Díaz I, González-Miquel M, Navarro P, Palomar J. Assessment of bio-ionic liquids as promising solvents in industrial separation processes: Computational screening using COSMO-RS method. *Fluid Phase Equilib* [Internet]. 2022 Sep;560:113495. Available from: <https://linkinghub.elsevier.com/retrieve/pii/S0378381222001182>
 59. Ventura SPM, e Silva FA, Quental M V., Mondal D, Freire MG, Coutinho JAP. Ionic-Liquid-Mediated Extraction and Separation Processes for Bioactive Compounds: Past, Present, and Future Trends. *Chem Rev* [Internet]. 2017 May 24;117(10):6984–7052. Available from: <https://pubs.acs.org/doi/10.1021/acs.chemrev.6b00550>
 60. Absalan G, Akhond M, Sheikhan L. Extraction and high performance liquid chromatographic determination of 3-indole butyric acid in pea plants by using imidazolium-based ionic liquids as extractant. *Talanta*. 2008;77(1):407–11.
 61. Pei Y, Wang J, Kun Wua XX, Lu X. Ionic liquid-based aqueous two-phase extraction of selected proteins. *Sep Purif Technol*. 2009;64:288–295.
 62. Matsumoto M, Mochiduki K, Fukunishi K, Kondo K. Extraction of organic acids using imidazolium-based ionic liquids and their toxicity to *Lactobacillus rhamnosus*. *Sep Purif Technol*. 2004;40(1):97–101.
 63. Pratiwi AI, Yokouchi T, Matsumoto M, Kondo K. Extraction of succinic acid by aqueous two-phase system using alcohols/salts and ionic liquids/salts. *Sep Purif Technol* [Internet]. 2014;155:127–32. Available from:

- <http://dx.doi.org/10.1016/j.seppur.2015.07.039>
64. Smirnova S V., Torocheshnikova II, Formanovsky AA, Pletnev I V. Solvent extraction of amino acids into a room temperature ionic liquid with dicyclohexano-18-crown-6. *Anal Bioanal Chem.* 2004;378(5):1369–75.
 65. Larriba M, Salama Omar, Navarro P, Garcia J, Francisco Rodriguez, Gonzalez-Miquel M. Recovery of tyrosol from aqueous streams using hydrophobic ionic liquids: a first step towards developing sustainable processes for olive mill wastewater (OMW) management. *RSC Adv.* 2016;6:18751–18762.
 66. Florindo C, Branco LC, Marrucho IM. Development of hydrophobic deep eutectic solvents for extraction of pesticides from aqueous environments. *Fluid Phase Equilib* [Internet]. 2017;448:135–42. Available from: <http://dx.doi.org/10.1016/j.fluid.2017.04.002>
 67. Kurnia KA, Quental M V., Santos LMNBF, Freire MG, Coutinho JAP. Mutual solubilities between water and non-aromatic sulfonium-, ammonium- and phosphonium-hydrophobic ionic liquids. *Phys Chem Chem Phys.* 2015;17(6):4569–77.
 68. Yao C, Pitner W, Anderson J. (Pentafluoroethyl) Trifluorophosphate Anion: a New Class of Highly Selective and Ultra Hydrophobic Solvents for the Extraction of Polycyclic Aromatic Hydrocarbons Using. *Anal Chem* [Internet]. 2009;81(12):5054–63. Available from: <http://www.ncbi.nlm.nih.gov/pubmed/19419149><http://pubs.acs.org/doi/abs/10.1021/ac900719m>
 69. Andersen SJ, Berton JKET, Naert P, Gildemyn S, Rabaey K, Stevens C V. Extraction and esterification of low-titer short-chain volatile fatty acids from anaerobic fermentation with ionic liquids. *ChemSusChem.* 2016;9(16):2059–63.
 70. Araya-López C, Contreras J, Merlet G, Cabezas R, Olea F, Villarroel E, et al. [Tf2N]-based ionic liquids for the selective liquid-liquid extraction of levulinic acid/formic acid: COSMO-RS screening and ternary LLE experimental data. *Fluid Phase Equilib* [Internet]. 2022 Oct;561(May):113518. Available from: <https://linkinghub.elsevier.com/retrieve/pii/S0378381222001418>
 71. Tomé LIN, Catambas VR, Teles ARR, Freire MG, Marrucho IM, Coutinho JAP. Tryptophan extraction using hydrophobic ionic liquids. *Sep Purif Technol* [Internet]. 2010 Apr;72(2):167–73. Available from: <https://linkinghub.elsevier.com/retrieve/pii/S1383586610000584>
 72. Smith EL, Abbott AP, Ryder KS. Deep Eutectic Solvents (DESs) and Their Applications. *Chem Rev* [Internet]. 2014 Nov 12;114(21):11060–82. Available from: <https://pubs.acs.org/doi/10.1021/cr300162p>
 73. Van Osch DJGP, Zubeir LF, Van Den Bruinhorst A, Rocha MAA, Kroon MC. Hydrophobic deep eutectic solvents as water-immiscible extractants. *Green Chem* [Internet]. 2015;17(9):4518–21. Available from: <http://dx.doi.org/10.1039/c5gc01451d>
 74. Peyrovedin H, Haghbakhsh R, Duarte ARC, Shariati A. Deep Eutectic Solvents as Phase Change Materials in Solar Thermal Power Plants: Energy and Exergy Analyses. *Molecules* [Internet]. 2022 Feb 20;27(4):1427. Available from: <https://www.mdpi.com/1420-3049/27/4/1427>
 75. Yu D, Xue Z, Mu T. Eutectics: formation, properties, and applications. *Chem Soc Rev* [Internet]. 2021;50(15):8596–638. Available from: <http://xlink.rsc.org/?DOI=D1CS00404B>
 76. Van Osch DJGP, Kollau LJBM, Van Den Bruinhorst A, Asikainen S, Rocha MAA, Kroon MC. Ionic liquids and deep eutectic solvents for lignocellulosic biomass fractionation. *Phys Chem Chem Phys.* 2017;19(4):2636–65.
 77. González EJ, González-Miquel M, Díaz I, Rodríguez M, Fontela C, Cañadas R, et al. Enhancing aqueous systems fermentability using hydrophobic eutectic solvents as extractants of inhibitory compounds. *Sep Purif Technol* [Internet]. 2020 Nov;250(December 2019):117184. Available from: <https://doi.org/10.1016/j.seppur.2020.117184>

78. Van Osch DJGP, Parmentier D, Dietz CHJT, Van Den Bruinhorst A, Tuinier R, Kroon MC. Removal of alkali and transition metal ions from water with hydrophobic deep eutectic solvents. *Chem Commun*. 2016;52(80):11987–90.
79. Ribeiro BD, Florindo C, Iff LC, Coelho MAZ, Marrucho IM. Menthol-based eutectic mixtures: Hydrophobic low viscosity solvents. *ACS Sustain Chem Eng*. 2015;3(10):2469–77.
80. Zhu S, Zhou J, Jia H, Zhang H. Liquid–liquid microextraction of synthetic pigments in beverages using a hydrophobic deep eutectic solvent. *Food Chem* [Internet]. 2018;243(April 2017):351–6. Available from: <http://dx.doi.org/10.1016/j.foodchem.2017.09.141>
81. Cañadas R, González-Miquel M, González EJ, Núñez de Prado A, Díaz I, Rodríguez M. Sustainable Recovery of High Added-Value Vanilla Compounds from Wastewater Using Green Solvents. *ACS Sustain Chem Eng* [Internet]. 2021 Apr 5;9(13):4850–62. Available from: <https://pubs.acs.org/doi/10.1021/acssuschemeng.1c00168>
82. Cao J, Yang M, Cao F, Wang J, Su E. Tailor-made hydrophobic deep eutectic solvents for cleaner extraction of polyprenyl acetates from Ginkgo biloba leaves. *J Clean Prod* [Internet]. 2017;152:399–405. Available from: <http://dx.doi.org/10.1016/j.jclepro.2017.03.140>
83. Cao J, Yang M, Cao F, Wang J, Su E. Well-Designed Hydrophobic Deep Eutectic Solvents As Green and Efficient Media for the Extraction of Artemisinin from *Artemisia annua* Leaves. *ACS Sustain Chem Eng*. 2017;5(4):3270–8.
84. Cañadas R, González-Miquel M, González EJ, Díaz I, Rodríguez M. Hydrophobic eutectic solvents for extraction of natural phenolic antioxidants from winery wastewater. *Sep Purif Technol* [Internet]. 2021 Jan;254(January 2020):117590. Available from: <https://doi.org/10.1016/j.seppur.2020.117590>
85. Lomba L, Zuriaga E, Giner B. Solvents derived from biomass and their potential as green solvents. *Curr Opin Green Sustain Chem* [Internet]. 2019 Aug;18:51–6. Available from: <https://doi.org/10.1016/j.cogsc.2018.12.008>
86. Vovers J, Smith KH, Stevens GW. Bio-Based Molecular Solvents [Internet]. *The Application of Green Solvents in Separation Processes*. Elsevier Inc.; 2017. 91–110 p. Available from: <http://dx.doi.org/10.1016/B978-0-12-805297-6.00004-8>
87. Zirahi A, Sadeghi Yamchi H, Haddadnia A, Zirrahi M, Hassanzadeh H, Abedi J. Ethyl acetate as a bio-based solvent to reduce energy intensity and CO₂ emissions of in situ bitumen recovery. *AIChE J* [Internet]. 2020 Feb 12;66(2). Available from: <https://onlinelibrary.wiley.com/doi/10.1002/aic.16828>
88. Moity L, Durand M, Benazzouz A, Pierlot C, Molinier V, Aubry J-M. Panorama of sustainable solvents using the COSMO-RS approach. *Green Chem* [Internet]. 2012;14(4):1132. Available from: <http://xlink.rsc.org/?DOI=c2gc16515e>
89. Wan Mahmood WMA, Theodoropoulos C, Gonzalez-Miquel M. Enhanced microalgal lipid extraction using bio-based solvents for sustainable biofuel production. *Green Chem* [Internet]. 2017;19(23):5723–33. Available from: <http://dx.doi.org/10.1039/c7gc02735d>
90. Cañadas R, González-Miquel M, González EJ, Díaz I, Rodríguez M. Evaluation of bio-based solvents for phenolic acids extraction from aqueous matrices. *J Mol Liq* [Internet]. 2021 Sep;338:116930. Available from: <https://linkinghub.elsevier.com/retrieve/pii/S0167732221016548>
91. Cañadas R, Díaz I, Rodríguez M, González EJ, González-Miquel M. An integrated approach for sustainable valorization of winery wastewater using bio-based solvents for recovery of natural antioxidants. *J Clean Prod* [Internet]. 2022 Feb;334(August 2021):130181. Available from: <https://linkinghub.elsevier.com/retrieve/pii/S0959652621043468>
92. Ozturk B, Winterburn J, Gonzalez-Miquel M. Orange peel waste valorisation through limonene extraction using bio-based solvents. *Biochem Eng J* [Internet]. 2019 Nov;151:107298. Available from:

- <https://linkinghub.elsevier.com/retrieve/pii/S1369703X19302347>
93. Redlich O, Kwong JNS. On the thermodynamics of solutions. V. An equation of state. Fugacities of gaseous solutions. *Chem Rev* [Internet]. 1949 Feb 1;44(1):233–44. Available from: <https://pubs.acs.org/doi/abs/10.1021/cr60137a013>
 94. Soave G. Equilibrium constants from a modified Redlich-Kwong equation of state. *Chem Eng Sci* [Internet]. 1972 Jun;27(6):1197–203. Available from: <https://linkinghub.elsevier.com/retrieve/pii/0009250972800964>
 95. Peng D, Robinson DB. A New Two-Constant Equation of State. *Ind Eng Chem Fundam* [Internet]. 1976 Feb 1;15(1):59–64. Available from: <https://pubs.acs.org/doi/abs/10.1021/i160057a011>
 96. Gross J, Sadowski G. Perturbed-Chain SAFT: An Equation of State Based on a Perturbation Theory for Chain Molecules. *Ind Eng Chem Res* [Internet]. 2001 Feb 1;40(4):1244–60. Available from: <https://pubs.acs.org/doi/10.1021/acs.iecr.9b01515>
 97. H. R, J.M. P. Local Compositions in Thermodynamic Excess Functions for Liquid Mixtures. *AIChE J*. 1968;14(1):135–44.
 98. Wilson GM. Vapor-Liquid Equilibrium. XI. A New Expression for the Excess Free Energy of Mixing. *J Am Chem Soc*. 1964;86(2):127–30.
 99. Abrams DS, Prausnitz JM. Statistical thermodynamics of liquid mixtures: A new expression for the excess Gibbs energy of partly or completely miscible systems. *AIChE J* [Internet]. 1975 Jan;21(1):116–28. Available from: <https://onlinelibrary.wiley.com/doi/10.1002/aic.690210115>
 100. Orbey H, Sandler SI. Analysis of excess free energy based equations of state models. *AIChE J* [Internet]. 1996 Aug;42(8):2327–34. Available from: <https://onlinelibrary.wiley.com/doi/10.1002/aic.690420822>
 101. Friesner RA. Ab initio quantum chemistry: Methodology and applications. *Proc Natl Acad Sci* [Internet]. 2005 May 10;102(19):6648–53. Available from: <https://pnas.org/doi/full/10.1073/pnas.0408036102>
 102. Schrödinger E. An Undulatory Theory of the Mechanics of Atoms and Molecules. *Phys Rev* [Internet]. 1926 Dec 1;28(6):1049–70. Available from: <https://link.aps.org/doi/10.1103/PhysRev.28.1049>
 103. Das RN, Roy K. Advances in QSPR/QSTR models of ionic liquids for the design of greener solvents of the future. *Mol Divers* [Internet]. 2013 Feb 17;17(1):151–96. Available from: <http://link.springer.com/10.1007/s11030-012-9413-y>
 104. Glasser L, Jenkins HDB. Volume-Based Thermodynamics: A Prescription for Its Application and Usage in Approximation and Prediction of Thermodynamic Data. *J Chem Eng Data* [Internet]. 2011 Apr 14;56(4):874–80. Available from: <https://pubs.acs.org/doi/10.1021/je100683u>
 105. Izgorodina EI, Seeger ZL, Scarborough DLA, Tan SYS. Quantum Chemical Methods for the Prediction of Energetic, Physical, and Spectroscopic Properties of Ionic Liquids. *Chem Rev* [Internet]. 2017 May 24;117(10):6696–754. Available from: <https://pubs.acs.org/doi/10.1021/acs.chemrev.6b00528>
 106. Eckert F, Klamt A. Fast Solvent Screening via Quantum Chemistry: COSMO-RS Approach. *AIChE J*. 2002;48(2):369–85.
 107. Klamt A, Eckert F. COSMO-RS: a novel and efficient method for the a priori prediction of thermophysical data of liquids. *Fluid Phase Equilib*. 2000;172(1):43–72.
 108. Diedenhofen M, Klamt A. COSMO-RS as a tool for property prediction of IL mixtures—A review. *Fluid Phase Equilib*. 2010;294(1–2):31–8.
 109. Jeliński T, Cysewski P. Application of a computational model of natural deep eutectic solvents utilizing the COSMO-RS approach for screening of solvents with high solubility of rutin. *J Mol Model*. 2018;24(7):1–17.
 110. Bezold F, Weinberger ME, Minceva M. Assessing solute partitioning in deep eutectic solvent-based biphasic systems using the predictive thermodynamic model COSMO-RS. *Fluid Phase Equilib*. 2017;437:23–33.
 111. González-Miquel M, Díaz I. Green solvent screening using modeling and simulation.

- Curr Opin Green Sustain Chem [Internet]. 2021 Jun;29:100469. Available from: <https://doi.org/10.1016/j.cogsc.2021.100469>
112. Zapata-Boada S, Gonzalez-Miquel M, Jobson M, Cuéllar-Franca RM. Integrating Technoeconomic, Environmental, and Safety Criteria in Solvent Screening for Extraction Processes: The Case of Algae Lipid Extraction. ACS Sustain Chem Eng [Internet]. 2022 Jan 10;10(1):472–85. Available from: <https://pubs.acs.org/doi/10.1021/acssuschemeng.1c06756>
 113. Baker RW. Membrane Technology and Applications. 3rd ed. Chichester: John Wiley & Sons Ltd; 2012.
 114. Iulianelli A, Drioli E. Membrane engineering: Latest advancements in gas separation and pre-treatment processes, petrochemical industry and refinery, and future perspectives in emerging applications. Fuel Process Technol [Internet]. 2020;206(March):106464. Available from: <https://doi.org/10.1016/j.fuproc.2020.106464>
 115. Suwaileh W, Johnson D, Hilal N. Membrane desalination and water re-use for agriculture: State of the art and future outlook. Desalination [Internet]. 2020;491(June):114559. Available from: <https://doi.org/10.1016/j.desal.2020.114559>
 116. Basile A, Pereira Nunes S, editors. Advanced membrane science and technology for sustainable energy and environmental applications. Advanced membrane science and technology for sustainable energy and environmental applications. Cambridge ; Woodhead Pub.; 2011. (Woodhead Publishing series in energy, no. 25).
 117. Daufin G, Escudier J-P, Carrère H, Bérot S, Fillaudeau L, Decloux M. Recent and Emerging Applications of Membrane Processes in the Food and Dairy Industry. Food Bioprod Process [Internet]. 2001 Jun;79(2):89–102. Available from: <https://linkinghub.elsevier.com/retrieve/pii/S0960308501702441>
 118. Charcosset C. Membrane processes in biotechnologies and pharmaceuticals. Membrane processes in biotechnologies and pharmaceuticals. Amsterdam ; Elsevier; 2012.
 119. Jhaveri JH, Murthy ZVP. A comprehensive review on anti-fouling nanocomposite membranes for pressure driven membrane separation processes. Desalination [Internet]. 2016 Feb;379:137–54. Available from: <http://dx.doi.org/10.1016/j.desal.2015.11.009>
 120. Gohil JM, Choudhury RR. Introduction to Nanostructured and Nano-enhanced Polymeric Membranes: Preparation, Function, and Application for Water Purification. In: Nanoscale Materials in Water Purification [Internet]. Elsevier; 2019. p. 25–57. Available from: <http://dx.doi.org/10.1016/B978-0-12-813926-4.00038-0>
 121. Alberto M, Skuse C, Tamaddondar M, Gorgojo P. Immobilized graphene oxide-based membranes for improved pore wetting resistance in membrane distillation. Desalination [Internet]. 2022 Sep;537(March):115898. Available from: <https://doi.org/10.1016/j.desal.2022.115898>
 122. Mohsenpour S, Ameen AW, Leaper S, Skuse C, Almansour F, Budd PM, et al. PIM-1 membranes containing POSS - graphene oxide for CO₂ separation. Sep Purif Technol [Internet]. 2022 Oct;298(April):121447. Available from: <https://doi.org/10.1016/j.seppur.2022.121447>
 123. Ghosh S. Kernel Smoothing: Principles, Methods and Applications [Internet]. First edit. Encyclopedia of Statistics in Behavioral Science. Oxford, UK: John Wiley & Sons, Ltd; 2017. Available from: <http://doi.wiley.com/10.1002/9781118890370>
 124. Allen DT, Gathergood N, Licence P, Subramaniam B. Expectations for Manuscripts Contributing to the Field of Solvents in ACS Sustainable Chemistry & Engineering. ACS Sustain Chem Eng [Internet]. 2020 Oct 5;8(39):14627–9. Available from: <https://pubs.acs.org/doi/10.1021/acssuschemeng.0c06901>
 125. Bozell JJ, Petersen GR. Technology development for the production of biobased products from biorefinery carbohydrates - The US Department of Energy's "top 10" revisited. Green Chem. 2010;12(4):539–54.
 126. Natrass L, Biggs C, Bauen A, Parisi C, Rodríguez-Cerezo E, Gómez-Barbero M. The EU bio-based industry: Results from a survey [Internet]. 2016. Available from:

- <http://publications.jrc.ec.europa.eu/repository/bitstream/JRC100357/jrc100357.pdf>
127. Sheldon RA. Green and sustainable manufacture of chemicals from biomass: State of the art. *Green Chem.* 2014;16(3):950–63.
 128. Pinazo JM, Domine ME, Parvulescu V, Petru F. Sustainability metrics for succinic acid production: A comparison between biomass-based and petrochemical routes. *Catal Today* [Internet]. 2015;239:17–24. Available from: <http://dx.doi.org/10.1016/j.cattod.2014.05.035>
 129. Sprakel LMJ, Schuur B. Solvent developments for liquid-liquid extraction of carboxylic acids in perspective. *Sep Purif Technol* [Internet]. 2019;211(October 2018):935–57. Available from: <https://doi.org/10.1016/j.seppur.2018.10.023>
 130. Veleva VR, Cue BW. The role of drivers, barriers, and opportunities of green chemistry adoption in the major world markets. *Curr Opin Green Sustain Chem* [Internet]. 2019;19:30–6. Available from: <https://doi.org/10.1016/j.cogsc.2019.05.001>
 131. Marták J, Schlosser Š. Extraction of lactic acid by phosphonium ionic liquids. *Sep Purif Technol.* 2007;57(3):483–94.
 132. Reyhanitash E, Zaalberg B, Kersten SRA, Schuur B. Extraction of volatile fatty acids from fermented wastewater. *Sep Purif Technol* [Internet]. 2016;161:61–8. Available from: <http://dx.doi.org/10.1016/j.seppur.2016.01.037>
 133. Reyhanitash E, Fufachev E, Van Munster KD, Van Beek MBM, Sprakel LMJ, Edelijn CN, et al. Recovery and conversion of acetic acid from a phosphonium phosphinate ionic liquid to enable valorization of fermented wastewater. *Green Chem.* 2019;21(8):2023–34.
 134. Ozturk B, Esteban J, Gonzalez-Miquel M. Deterpenation of Citrus Essential Oils Using Glycerol-Based Deep Eutectic Solvents. *J Chem Eng Data.* 2018;63(7):2384–93.
 135. Ozturk B, Gonzalez-Miquel M. Alkanediol-based deep eutectic solvents for isolation of terpenoids from citrus essential oil: Experimental evaluation and COSMO-RS studies. *Sep Purif Technol.* 2019;227(June):115707.
 136. Schröder B, Santos LMNBF, Marrucho IM, Coutinho JAP. Prediction of aqueous solubilities of solid carboxylic acids with COSMO-RS. *Fluid Phase Equilib.* 2010;289(2):140–7.
 137. Zhou T, Chen L, Ye Y, Chen L, Qi Z, Freund H, et al. An overview of mutual solubility of ionic liquids and water predicted by COSMO-RS. *Ind Eng Chem Res.* 2012;51(17):6256–64.
 138. Esteban J, Vorholt AJ, Leitner W. An overview of the biphasic dehydration of sugars to 5-hydroxymethylfurfural and furfural: a rational selection of solvents using COSMO-RS and selection guides. *Green Chem.* 2020;22.
 139. Gonzalez-Miquel M, Massel M, Desilva A, Palomar J, Rodriguez F, Brennecke JF. Excess enthalpy of monoethanolamine + ionic liquid mixtures: How good are COSMO-RS predictions? *J Phys Chem B.* 2014;118(39):11512–22.
 140. Chirico RD, Frenkel M, Diky V V., Marsh KN, Wilhoit RC. ThermoML-An XML-based approach for storage and exchange of experimental and critically evaluated thermophysical and thermochemical property data. 2. Uncertainties. *J Chem Eng Data.* 2003;48(5):1344–59.
 141. Miller JN, Miller JC. *Statistics and Chemometrics for Analytical Chemistry.* Gosport, UK: Prentice Hall; 2010.
 142. Burghoff B, Goetheer ELV, De Haan AB. COSMO-RS-based extractant screening for phenol extraction as model system. *Ind Eng Chem Res.* 2008;47(12):4263–9.
 143. González EJ, Díaz I, Gonzalez-Miquel M, Rodríguez M, Sueiras A. On the behavior of imidazolium versus pyrrolidinium ionic liquids as extractants of phenolic compounds from water: Experimental and computational analysis. *Sep Purif Technol* [Internet]. 2018;201(March):214–22. Available from: <https://doi.org/10.1016/j.seppur.2018.03.006>
 144. Egorov VM, Smirnova S V., Pletnev I V. Highly efficient extraction of phenols and aromatic amines into novel ionic liquids incorporating quaternary ammonium cation.

- Sep Purif Technol. 2008;63(3):710–5.
145. Sprakel LMJ, Schuur B. Improving understanding of solvent effects on intermolecular interactions in reactive liquid–liquid extraction with Isothermal Titration Calorimetry and molecular modeling. *J Ind Eng Chem* [Internet]. 2019;72:364–73. Available from: <https://doi.org/10.1016/j.jiec.2018.12.038>
 146. Freire MG, Carvalho PJ, Gardas RL, Santos LMNBF, Marrucho IM, Coutinho JAP. Solubility of Water in Tetradecyltriethylphosphonium-Based Ionic Liquids: Journal of Chemical & Engineering Data. *J Chem & Eng Data*. 2008;53(10):2378–82.
 147. Yalkowsky SH, He Y, Jain P. *Handbook of Aqueous Solubility Data*. 2nd ed. Boca Raton, Fla: CRC.; 2010.
 148. Liu K, Cruzan JD, Saykally RJ. Water clusters. *Science* (80-). 1996;271(5251):929–33.
 149. Sun Q. The physical origin of hydrophobic effects. *Chem Phys Lett* [Internet]. 2017;672:21–5. Available from: <http://dx.doi.org/10.1016/j.cplett.2017.01.057>
 150. Lazaridis T. *Hydrophobic Effect*. eLS John Wiley Sons, Ltd Chichester. 2013;
 151. Choudhury B, Basha A, Swaminathan T. Study of lactic acid extraction with higher molecular weight aliphatic amines. *J Chem Technol Biotechnol*. 1998;72(2):111–6.
 152. Sabolová E, Schlosser S, Marták J. Liquid-liquid equilibria of butyric acid in water + solvent systems with trioctylamine as extractant. *J Chem Eng Data*. 2001;46(3):735–45.
 153. Matsumoto M, Otono T, Kondo K. Synergistic extraction of organic acids with tri-n-octylamine and tri-n-butylphosphate. *Sep Purif Technol*. 2001;24(1–2):337–42.
 154. Matsumoto M, Takahashi T, Fukushima K. Synergistic extraction of lactic acid with alkylamine and tri-n-butylphosphate: Effects of amines, diluents and temperature. *Sep Purif Technol*. 2003;33(1):89–93.
 155. Huddleston JG, Visser AE, Reichert WM, Willauer HD, Broker GA, Rogers RD. Characterization and comparison of hydrophilic and hydrophobic room temperature ionic liquids incorporating the imidazolium cation. *Green Chem*. 2001;3(4):156–64.
 156. O'Mahony AM, Silvester DS, Aldous L, Hardacre C, Compton RG. Effect of water on the electrochemical window and potential limits of room-temperature ionic liquids. *J Chem Eng Data*. 2008;53(12):2884–91.
 157. Davey RJ, Mullin JW, Whiting MJL. Habit modification of succinic acid crystals grown from different solvents. *J Cryst Growth* [Internet]. 1982 Jul;58(2):304–12. Available from: <https://linkinghub.elsevier.com/retrieve/pii/0022024882902779>
 158. Jiang X, Hu Y, Meng Z, Yang W, Shen F. Solubility of succinic acid in different aqueous solvent mixtures: Experimental measurement and thermodynamic modeling. *Fluid Phase Equilib* [Internet]. 2013 Mar;341(30):7–11. Available from: <http://dx.doi.org/10.1016/j.fluid.2012.12.018>
 159. Sheng X, Luo W, Wang Q. Determination and Correlation for the Solubilities of Succinic Acid in Cyclohexanol + Cyclohexanone + Cyclohexane Solvent Mixtures. *J Chem Eng Data* [Internet]. 2018 Mar 8;63(3):801–11. Available from: <https://pubs.acs.org/doi/10.1021/acs.jced.7b00956>
 160. Bancroft WD, Butler FJC. Solubility of Succinic Acid in Binary Mixtures. *J Phys Chem* [Internet]. 1932 Sep 1;36(9):2515–20. Available from: <https://pubs.acs.org/doi/10.1021/j150339a013>
 161. Dang L, Du W, Black S, Wei H. Solubility of Fumaric Acid in Propan-2-ol, Ethanol, Acetone, Propan-1-ol, and Water. *J Chem Eng Data* [Internet]. 2009 Nov 12;54(11):3112–3. Available from: <https://pubs.acs.org/doi/10.1021/je9001637>
 162. Padászyński K. An overview of the performance of the COSMO-RS approach in predicting the activity coefficients of molecular solutes in ionic liquids and derived properties at infinite dilution. *Phys Chem Chem Phys* [Internet]. 2017;19(19):11835–50. Available from: <http://xlink.rsc.org/?DOI=C7CP00226B>
 163. Klamt A, Diedenhofen M. Blind prediction test of free energies of hydration with COSMO-RS. *J Comput Aided Mol Des* [Internet]. 2010 Apr 10;24(4):357–60. Available from: <http://link.springer.com/10.1007/s10822-010-9354-4>
 164. Linstrom PJ, Mallard WG, editors. *NIST Chemistry WebBook*, NIST Standard

- Reference Database Number 69. Gaithersburg MD, 20899: National Institute of Standards and Technology;
165. Taylor BN, Kuyatt CE. Guidelines for Evaluating and Expressing the Uncertainty of NIST Measurement Results [Internet]. NIST Technical Note 1297. Gaithersburg, MD; 1994. Available from: <http://physics.nist.gov/TN1297>
 166. Prausnitz JM, Lichtenthaler RN, de Azevedo EG. Molecular Thermodynamics of Fluid-Phase Equilibria. 3rd ed. NJ: Prentice-Hall: Englewood Cliffs; 1999.
 167. Apelblat A, Manzurola E. Solubility of oxalic, malonic, succinic, adipic, maleic, malic, citric, and tartaric acids in water from 278.15 to 338.15 K. J Chem Thermodyn [Internet]. 1987 Mar;19(3):317-20. Available from: <https://linkinghub.elsevier.com/retrieve/pii/002196148790139X>
 168. Buchowski H, Ksiazczak A, Pietrzyk S. Solvent activity along a saturation line and solubility of hydrogen-bonding solids. J Phys Chem [Internet]. 1980 May 1;84(9):975-9. Available from: <https://pubs.acs.org/doi/10.1021/j100446a008>
 169. Dawson RM. Data for Biochemical Research. Oxford: Clarendon Press; 1959.
 170. Doosaj SS, Bhagwat WV. Solubilities of weak acids in salts of weak acids at very high concentrations. J Indian Chem Soc. 1933;10:225-232.
 171. Forbes GS, Coolidge AS. Relations between distribution ratio, temperature and concentration in system: water, ether, succinic acid. J Am Chem Soc [Internet]. 1919 Feb 1;41(2):150-67. Available from: <https://pubs.acs.org/doi/abs/10.1021/ja01459a004>
 172. Freier RK. Aqueous Solutions Volume 1: Data for Inorganic and Organic Compounds. New York: Walter de Gruyter; 1976.
 173. Hyvärinen A-P, Lihavainen H, Gaman A, Vairila L, Ojala H, Kulmala M, et al. Surface Tensions and Densities of Oxalic, Malonic, Succinic, Maleic, Malic, and cis - Pinonic Acids. J Chem Eng Data [Internet]. 2006 Jan 1;51(1):255-60. Available from: <https://pubs.acs.org/doi/10.1021/je050366x>
 174. Lamouroux F. Sur la solubilité dans l'eau des acides normaux de la série oxalique. Comptes Rendus Hebd des Seances l'Academie des Sci. 1899;128:998-1000.
 175. Linderstrom-Lang K. Solubility of hydroquinone. Comptes Rendus des Trav du Lab Carlsberg. 1924;15:4-28.
 176. Marshall H, Bain D. Sodium succinates. J Chem Soc. 1910;97:1074- 1085.
 177. Mullin JW. Crystallisation. London: Butterworths; 1972. 425-426 p.
 178. Massol G, Lamouroux F. Sur la solubilité dans l'eau des acides maloniques substitués. Comptes Rendus Hebd des Seances l'Academie des Sci. 1899;128:1000-1002.
 179. Mullin JW, Whiting MJL. Succinic Acid Crystal Growth Rates in Aqueous Solution. Ind Eng Chem Fundam [Internet]. 1980 Feb 1;19(1):117-21. Available from: <https://pubs.acs.org/doi/abs/10.1021/i160073a020>
 180. Merckel JHC. Die Löslichkeit der dicarbonsäuren. Recl des Trav Chim des Pays-Bas. 1937;56:811-814.
 181. Wright R. CLXXXVII. — Selective solvent action. Part VI. The effect of temperature on the solubilities of semisolutes in aqueous alcohol. J Chem Soc [Internet]. 1927;1334-7. Available from: <http://xlink.rsc.org/?DOI=JR9270001334>
 182. Dawson RMC, Elliott DC, Elliott WH, Jones KM. Data for Biochemical Research. Pergamon: Oxford University Press; 1969.
 183. Weiss JM, Downs CR. The physical properties of maleic, fumaric and malic acids. J Am Chem Soc [Internet]. 1923 Apr 1;45(4):1003-8. Available from: <https://pubs.acs.org/doi/abs/10.1021/ja01657a018>
 184. Wagner Z, Bendová M, Rotrekl J, Sýkorová A, Čanji M, Parmar N. Density and sound velocity measurement by an Anton Paar DSA 5000 density meter: Precision and long-time stability. J Mol Liq. 2021;329.
 185. Krug RR, Hunter WG, Grieger RA. Enthalpy-entropy compensation. 1. Some fundamental statistical problems associated with the analysis of van't Hoff and

- Arrhenius data. *J Phys Chem* [Internet]. 1976 Oct 1;80(21):2335–41. Available from: <https://pubs.acs.org/doi/abs/10.1021/j100562a006>
186. Krug RR, Hunter WG, Grieger RA. Enthalpy-entropy compensation. 2. Separation of the chemical from the statistical effect. *J Phys Chem* [Internet]. 1976 Oct 1;80(21):2341–51. Available from: <https://pubs.acs.org/doi/abs/10.1021/j100562a007>
 187. Aydi A, Ayadi C, Ghachem K, Al-Khazaal A, Delgado D, Alnaief M, et al. Solubility, Solution Thermodynamics, and Preferential Solvation of Amygdalin in Ethanol + Water Solvent Mixtures. *Pharmaceuticals* [Internet]. 2020 Nov 16;13(11):395. Available from: <https://www.mdpi.com/1424-8247/13/11/395>
 188. Sholl DS, Lively RP. Seven chemical separations to change the world. *Nature* [Internet]. 2016 Apr 26;532(7600):435–7. Available from: <http://www.nature.com/articles/532435a>
 189. Abdel-Karim A, Leaper S, Alberto M, Vijayaraghavan A, Fan X, Holmes SM, et al. High flux and fouling resistant flat sheet polyethersulfone membranes incorporated with graphene oxide for ultrafiltration applications. *Chem Eng J*. 2018;334(October 2017):789–99.
 190. Allen DT, Gathergood N, Licence P, Subramaniam B. Expectations for Manuscripts Contributing to the Field of Solvents in ACS Sustainable Chemistry & Engineering. *ACS Sustain Chem Eng* [Internet]. 2020 Oct 5;8(39):14627–9. Available from: <https://pubs.acs.org/doi/10.1021/acssuschemeng.0c06901>
 191. Leaper S, Abdel-Karim A, Faki B, Luque-Alled JM, Alberto M, Vijayaraghavan A, et al. Flux-enhanced PVDF mixed matrix membranes incorporating APTS-functionalized graphene oxide for membrane distillation. *J Memb Sci* [Internet]. 2018 May;554(March):309–23. Available from: <https://doi.org/10.1016/j.memsci.2018.03.013>
 192. Kislik VS. *Liquid Membranes: Principles and Applications in Chemical Separations and Wastewater Treatment*. 1st ed. Elsevier B.V.; 2010.
 193. Scott K, Hughes R. *Industrial membrane separation technology*. 1st ed. London: Blackie Academic & Professional; 1996.
 194. Parhi PK. Supported Liquid Membrane Principle and Its Practices: A Short Review. *J Chem* [Internet]. 2013;2013:1–11. Available from: <http://www.hindawi.com/journals/jchem/2013/618236/>
 195. Charcosset C. Other membrane processes. In: *Membrane Processes in Biotechnology and Pharmaceuticals* [Internet]. Elsevier; 2012. p. 253–93. Available from: <https://linkinghub.elsevier.com/retrieve/pii/B9780444563347000071>
 196. Dzygiel P, Wieczorek PP. Supported Liquid Membranes and Their Modifications. In: Kislik VS, editor. *Liquid Membranes* [Internet]. Elsevier; 2010. p. 73–140. Available from: <https://linkinghub.elsevier.com/retrieve/pii/B9780444532183000039>
 197. Ghoshal AK, Saha P. Liquid – Membrane Filters. In: *Progress in Filtration and Separation* [Internet]. Elsevier; 2015. p. 155–205. Available from: <http://dx.doi.org/10.1016/B978-0-12-384746-1.00005-7>
 198. Wang J, Luo J, Feng S, Li H, Wan Y, Zhang X. Recent development of ionic liquid membranes. *Green Energy Environ* [Internet]. 2016 Apr;1(1):43–61. Available from: <http://dx.doi.org/10.1016/j.gee.2016.05.002>
 199. Noble RD, Gin DL. Perspective on ionic liquids and ionic liquid membranes. *J Memb Sci* [Internet]. 2011 Mar;369(1–2):1–4. Available from: <http://dx.doi.org/10.1016/j.memsci.2010.11.075>
 200. Malik MA, Hashim MA, Nabi F. Ionic liquids in supported liquid membrane technology. *Chem Eng J* [Internet]. 2011 Jun;171(1):242–54. Available from: <http://dx.doi.org/10.1016/j.cej.2011.03.041>
 201. Lozano LJ, Godínez C, de los Ríos AP, Hernández-Fernández FJ, Sánchez-Segado S, Alguacil FJ. Recent advances in supported ionic liquid membrane technology. *J Memb Sci* [Internet]. 2011 Jul;376(1–2):1–14. Available from:

- <http://dx.doi.org/10.1016/j.memsci.2011.03.036>
202. Crespo JG, Noble RD. Ionic Liquid Membrane Technology. In: *Ionic Liquids Further UnCOILed* [Internet]. Hoboken, NJ, USA: John Wiley & Sons, Inc.; 2014. p. 87–116. Available from: <http://doi.wiley.com/10.1002/9781118839706.ch4>
 203. Pratiwi AI, Matsumoto M. Separation of Organic Acids Through Liquid Membranes Containing Ionic Liquids. In: *Ionic Liquids in Separation Technology* [Internet]. Elsevier; 2014. p. 189–206. Available from: <http://dx.doi.org/10.1016/B978-0-444-63257-9.00005-5>
 204. Baylan N, Çehreli S. Ionic liquids as bulk liquid membranes on levulinic acid removal: A design study. *J Mol Liq* [Internet]. 2018 Sep;266:299–308. Available from: <https://doi.org/10.1016/j.molliq.2018.06.075>
 205. Baylan N, Çehreli S. Removal of acetic acid from aqueous solutions using bulk ionic liquid membranes: A transport and experimental design study. *Sep Purif Technol* [Internet]. 2019 Oct;224(April):51–61. Available from: <https://doi.org/10.1016/j.seppur.2019.05.001>
 206. Ng YS, Jayakumar NS, Hashim MA. Behavior of hydrophobic ionic liquids as liquid membranes on phenol removal: Experimental study and optimization. *Desalination* [Internet]. 2011 Sep;278(1–3):250–8. Available from: <https://linkinghub.elsevier.com/retrieve/pii/S0011916411004607>
 207. Lu S, Pei L. A study on phenol migration by coupling the liquid membrane in the ionic liquid. *Int J Hydrogen Energy* [Internet]. 2016 Sep;41(35):15724–32. Available from: <http://dx.doi.org/10.1016/j.ijhydene.2016.05.008>
 208. Balasubramanian A, Venkatesan S. Removal of phenolic compounds from aqueous solutions by emulsion liquid membrane containing Ionic Liquid [BMIM]+[PF6]– in Tributyl phosphate. *Desalination* [Internet]. 2012 Mar;289:27–34. Available from: <http://dx.doi.org/10.1016/j.desal.2011.12.027>
 209. Panigrahi A, Pilli SR, Mohanty K. Selective separation of Bisphenol A from aqueous solution using supported ionic liquid membrane. *Sep Purif Technol* [Internet]. 2013 Apr;107:70–8. Available from: <https://linkinghub.elsevier.com/retrieve/pii/S138358661300035X>
 210. Goyal RK, Jayakumar NS, Hashim MA. Chromium removal by emulsion liquid membrane using [BMIM]+[NTf2]– as stabilizer and TOMAC as extractant. *Desalination* [Internet]. 2011 Sep;278(1–3):50–6. Available from: <http://dx.doi.org/10.1016/j.desal.2011.05.001>
 211. Plaza A, Merlet G, Hasanoglu A, Isaacs M, Sanchez J, Romero J. Separation of butanol from ABE mixtures by sweep gas pervaporation using a supported gelled ionic liquid membrane: Analysis of transport phenomena and selectivity. *J Memb Sci* [Internet]. 2013 Oct;444:201–12. Available from: <http://dx.doi.org/10.1016/j.memsci.2013.04.034>
 212. Dietz CHJT, Kroon MC, Di Stefano M, van Sint Annaland M, Gallucci F. Selective separation of furfural and hydroxymethylfurfural from an aqueous solution using a supported hydrophobic deep eutectic solvent liquid membrane. *Faraday Discuss* [Internet]. 2018;206:77–92. Available from: <http://xlink.rsc.org/?DOI=C7FD00152E>
 213. Li Z, Cui Y, Shen Y, Li C. Extraction Process of Amino Acids with Deep Eutectic Solvents-Based Supported Liquid Membranes. *Ind Eng Chem Res* [Internet]. 2018 Mar 28;57(12):4407–19. Available from: <https://pubs.acs.org/doi/10.1021/acs.iecr.7b05221>
 214. Chakrabarty K, Saha P, Ghoshal AK. Separation of mercury from its aqueous solution through supported liquid membrane using environmentally benign diluent. *J Memb Sci*. 2010;350(1–2):395–401.
 215. Garavand F, Razavi SH, Cacciotti I. Synchronized extraction and purification of L-lactic acid from fermentation broth by emulsion liquid membrane technique. *J Dispers Sci Technol* [Internet]. 2018 Sep 2;39(9):1291–9. Available from: <https://doi.org/10.1080/01932691.2017.1396225>
 216. Manna MS, Bhatluri KK, Saha P, Ghoshal AK. Transportation of Catechin (\pm C) Using

- Physiologically Benign Vegetable Oil As Liquid Membrane. *Ind Eng Chem Res* [Internet]. 2012 Nov 21;51(46):15207–16. Available from: <https://pubs.acs.org/doi/10.1021/ie3017863>
217. Kumar A, Thakur A, Panesar PS. A comparative study on experimental and response surface optimization of lactic acid synergistic extraction using green emulsion liquid membrane. *Sep Purif Technol* [Internet]. 2019 Mar;211(May 2018):54–62. Available from: <https://doi.org/10.1016/j.seppur.2018.09.048>
 218. Kumar A, Thakur A, Panesar PS. Statistical optimization of lactic acid extraction using Green Emulsion Ionic Liquid Membrane (GEILM). *J Environ Chem Eng* [Internet]. 2018 Apr;6(2):1855–64. Available from: <https://doi.org/10.1016/j.jece.2018.01.037>
 219. Ahmad AL, Shah Buddin MMH, Ooi BS, Kusumastuti A. Utilization of environmentally benign emulsion liquid membrane (ELM) for cadmium extraction from aqueous solution. *J Water Process Eng* [Internet]. 2017 Feb;15:26–30. Available from: <http://dx.doi.org/10.1016/j.jwpe.2016.05.010>
 220. Jusoh N, Sulaiman RNR, Othman N, Noah NFM, Rosly MB, Rahman HA. Development of vegetable oil-based emulsion liquid membrane for downstream processing of bio-succinic acid. *Food Bioprod Process* [Internet]. 2020 Jan;119:161–9. Available from: <https://doi.org/10.1016/j.fbp.2019.11.003>
 221. Othman N, Noah NFM, Shu LY, Ooi Z-Y, Jusoh N, Idroas M, et al. Easy removing of phenol from wastewater using vegetable oil-based organic solvent in emulsion liquid membrane process. *Chinese J Chem Eng* [Internet]. 2017 Jan;25(1):45–52. Available from: <http://dx.doi.org/10.1016/j.cjche.2016.06.002>
 222. Björkegren S, Karimi R, Martinelli A, Jayakumar N, Hashim M. A New Emulsion Liquid Membrane Based on a Palm Oil for the Extraction of Heavy Metals. *Membranes (Basel)* [Internet]. 2015 Apr 23;5(2):168–79. Available from: <http://www.mdpi.com/2077-0375/5/2/168>
 223. Chang SH. Parametric studies on an innovative waste vegetable oil-based continuous liquid membrane (WVCLM) for Cu(II) ion separation from aqueous solutions. *J Ind Eng Chem* [Internet]. 2017 Jun;50:102–10. Available from: <http://dx.doi.org/10.1016/j.jiec.2017.01.037>
 224. Diaconu I, Ruse E, Aboul-Enein HY, Bunaciu AA. Analytical Applications of Transport Through Bulk Liquid Membranes. *Crit Rev Anal Chem* [Internet]. 2016 Jul 3;46(4):332–41. Available from: <http://dx.doi.org/10.1080/10408347.2015.1064759>
 225. Li NN. Separating hydrocarbons with liquid membranes. United States: US Patent; 3,410,794, 1968.
 226. Kumar A, Thakur A, Panesar PS. A review on emulsion liquid membrane (ELM) for the treatment of various industrial effluent streams. *Rev Environ Sci Bio/Technology* [Internet]. 2019 Mar 1;18(1):153–82. Available from: <https://doi.org/10.1007/s11157-019-09492-2>
 227. Kumar A, Thakur A, Panesar PS. Recent developments on sustainable solvents for emulsion liquid membrane processes. *J Clean Prod* [Internet]. 2019 Dec;240:118250. Available from: <https://doi.org/10.1016/j.jclepro.2019.118250>
 228. Hussein MA, Mohammed AA, Atiya MA. Application of emulsion and Pickering emulsion liquid membrane technique for wastewater treatment: an overview. *Environ Sci Pollut Res* [Internet]. 2019 Dec 27;26(36):36184–204. Available from: <http://link.springer.com/10.1007/s11356-019-06652-3>
 229. San Román MF, Bringas E, Ibañez R, Ortiz I. Liquid membrane technology: fundamentals and review of its applications. *J Chem Technol Biotechnol* [Internet]. 2010 Jan;85(1):2–10. Available from: <http://doi.wiley.com/10.1002/jctb.2252>
 230. Ryšavá L, Dvořák M, Kubáň P. The effect of membrane thickness on supported liquid membrane extractions in-line coupled to capillary electrophoresis for analyses of complex samples. *J Chromatogr A* [Internet]. 2019 Jul;1596:226–32. Available from: <https://linkinghub.elsevier.com/retrieve/pii/S0021967319302225>
 231. Gabelman A, Hwang S-T. Hollow fiber membrane contactors. *J Memb Sci* [Internet].

- 1999 Jul;159(1-2):61-106. Available from:
<https://linkinghub.elsevier.com/retrieve/pii/S037673889900040X>
232. Teramoto M, Takeuchi N, Maki T, Matsuyama H. Ethylene/ethane separation by facilitated transport membrane accompanied by permeation of aqueous silver nitrate solution. *Sep Purif Technol* [Internet]. 2002 Aug;28(2):117-24. Available from:
<https://linkinghub.elsevier.com/retrieve/pii/S138358660200045X>
233. Gu Z, Wu Q, Zheng Z, Li Z, Jiang Y, Tang C, et al. Laboratory and pilot plant test of yttrium recovery from wastewater by electrostatic pseudo liquid membrane. *J Memb Sci*. 1994;93(2):137-47.
234. Pérez AD, Fontalvo J. A new concept of liquid membranes in Taylor flow: Performance for lactic acid removal. *Chem Eng Process - Process Intensif* [Internet]. 2019 May;139(March):95-102. Available from:
<https://doi.org/10.1016/j.cep.2019.03.015>
235. Park Y, Forney LJ, Kim JH, Skelland AHP. Optimum emulsion liquid membranes stabilized by non-Newtonian conversion in Taylor-Couette flow. *Chem Eng Sci* [Internet]. 2004 Dec;59(24):5725-34. Available from:
<https://linkinghub.elsevier.com/retrieve/pii/S0009250904003859>
236. Bhowal A, Bhattacharyya G, Inturu B, Datta S. Continuous removal of hexavalent chromium by emulsion liquid membrane in a modified spray column. *Sep Purif Technol* [Internet]. 2012 Oct;99:69-76. Available from:
<http://dx.doi.org/10.1016/j.seppur.2012.08.026>
237. Liu J, Huang K, Wu XH, Liu H. Enrichment of Low Concentration Rare Earths from Leach Solutions of Ion-Adsorption Ores by Bubbling Organic Liquid Membrane Extraction Using N1923. *ACS Sustain Chem Eng*. 2017;5(9):8070-8.
238. Fajar ATN, Hanada T, Firmansyah ML, Kubota F, Goto M. Selective Separation of Platinum Group Metals via Sequential Transport through Polymer Inclusion Membranes Containing an Ionic Liquid Carrier. *ACS Sustain Chem Eng*. 2020;8(30):11283-91.
239. Zhang S, Dokko K, Watanabe M. Porous ionic liquids: Synthesis and application. *Chem Sci*. 2015;6(7):3684-91.
240. Pabby AK, Sastre AM. State-of-the-art review on hollow fibre contactor technology and membrane-based extraction processes. *J Memb Sci* [Internet]. 2013 Mar;430:263-303. Available from: <http://dx.doi.org/10.1016/j.memsci.2012.11.060>
241. Offeman RD, Robertson GH. Spiral-wound liquid membrane module for separation of fluids and gases. United States: US Patent; US7341663B2, 2008.
242. Ho, Winston SW, Sirkar KK. *Membrane Handbook*. New York: Van Nostrand Reinhold; 1992.
243. He L, Li L, Sun W, Zhang W, Zhou Z, Ren Z. Extraction and recovery of penicillin G from solution by cascade process of hollow fiber renewal liquid membrane. *Biochem Eng J* [Internet]. 2016 Jun;110:8-16. Available from:
<http://dx.doi.org/10.1016/j.bej.2016.02.002>
244. Ren Z, Zhang W, Dai Y, Yang Y, Hao Z. Modeling of Effect of pH on Mass Transfer of Copper(II) Extraction by Hollow Fiber Renewal Liquid Membrane. *Ind Eng Chem Res* [Internet]. 2008 Jun;47(12):4256-62. Available from:
<https://pubs.acs.org/doi/10.1021/ie0714798>
245. Hu SB, Wiencek JM. Emulsion-Liquid-Membrane Extraction of Copper Using a Hollow-Fiber Contactor. *AIChE J*. 1998;44(3):570-81.
246. Fouad EA, Bart H-J. Emulsion liquid membrane extraction of zinc by a hollow-fiber contactor. *J Memb Sci* [Internet]. 2008 Jan;307(2):156-68. Available from:
<https://linkinghub.elsevier.com/retrieve/pii/S0376738807006801>
247. Agarwal S, Reis MTA, Ismael MRC, Correia MJN, Carvalho JMR. Application of pseudo-emulsion based hollow fibre strip dispersion (PEHFSD) for the recovery of copper from sulphate solutions. *Sep Purif Technol* [Internet]. 2013 Jan;102:103-10. Available from: <http://dx.doi.org/10.1016/j.seppur.2012.09.026>

248. Pirom T, Arponwichanop A, Pancharoen U, Yonezawa T, Kheawhom S. Yttrium (III) Recovery with D2EHPA in Pseudo-Emulsion Hollow Fiber Strip Dispersion System. *Sci Rep* [Internet]. 2018 Dec 16;8(1):7627. Available from: <http://www.nature.com/articles/s41598-018-25771-4>
249. Pei L, Wang L, Guo W, Zhao N. Stripping dispersion hollow fiber liquid membrane containing PC-88A as carrier and HCl for transport behavior of trivalent dysprosium. *J Memb Sci* [Internet]. 2011 Aug;378(1-2):520-30. Available from: <http://dx.doi.org/10.1016/j.memsci.2011.05.037>
250. Mulder M. *Basic Principles of Membrane Technology*. Dordrecht: Kluwer Academic Publishers; 1991.
251. Chaouchi S, Hamdaoui O. Extraction of Priority Pollutant 4-Nitrophenol from Water by Emulsion Liquid Membrane: Emulsion Stability, Effect of Operational Conditions and Membrane Reuse. *J Dispers Sci Technol* [Internet]. 2014 Sep 2;35(9):1278-88. Available from: <http://www.tandfonline.com/doi/abs/10.1080/01932691.2013.844704>
252. Chen Q, Ma X, Zhang X, Liu Y, Yu M. Extraction of rare earth ions from phosphate leach solution using emulsion liquid membrane in concentrated nitric acid medium. *J Rare Earths* [Internet]. 2018 Nov;36(11):1190-7. Available from: <https://doi.org/10.1016/j.jre.2018.05.006>
253. Lee SC, Hyun K-S. Development of an emulsion liquid membrane system for separation of acetic acid from succinic acid. *J Memb Sci* [Internet]. 2010 Mar 15;350(1-2):333-9. Available from: <https://linkinghub.elsevier.com/retrieve/pii/S0376738810000177>
254. Gubicza L, Nemestóthy N, Bélafi-Bakó K, Findrik Z. The Role of Ionic Liquids in Enzyme-Membrane Integrated Systems. In: *Ionic Liquids in Separation Technology* [Internet]. Elsevier; 2014. p. 235-59. Available from: <https://linkinghub.elsevier.com/retrieve/pii/B9780444632579000079>
255. Bélafi-Bakó K, Nemestóthy N, Bakonyi P. Separation of Gases Using Membranes Containing Ionic Liquids. In: *Ionic Liquids in Separation Technology* [Internet]. Elsevier; 2014. p. 261-73. Available from: <https://linkinghub.elsevier.com/retrieve/pii/B9780444632579000080>
256. Luis P. Gas permeation and supported liquid membranes. In: *Fundamental Modelling of Membrane Systems* [Internet]. Elsevier; 2018. p. 103-51. Available from: <http://dx.doi.org/10.1016/B978-0-12-813483-2.00004-6>
257. Sastre AM. *Handbook of Membrane Separations* [Internet]. second. Pabby AK, Rizvi SSH, Requena AMS, editors. *Handbook of Membrane Separations*. CRC Press; 2015. Available from: <https://www.taylorfrancis.com/books/9781466555587>
258. Othman N, Mili N, Idris A, Zailani SN. Removal of Dyes from Liquid Waste Solution: Study on Liquid Membrane Component Selection and Stability. In: *Sustainable Membrane Technology for Energy, Water, and Environment* [Internet]. Hoboken, NJ, USA: John Wiley & Sons, Inc.; 2012. p. 221-9. Available from: <http://doi.wiley.com/10.1002/9781118190180.ch19>
259. Inci I. Linear solvation energy relationship modeling and kinetic studies on reactive extraction of succinic acid by tridodecylamine dissolved in MIBK. *Biotechnol Prog*. 2007;23(5):1171-9.
260. Chanukya BS, Kumar M, Rastogi NK. Optimization of lactic acid pertraction using liquid emulsion membranes by response surface methodology. *Sep Purif Technol* [Internet]. 2013 Jun;111:1-8. Available from: <http://dx.doi.org/10.1016/j.seppur.2013.03.026>
261. Pérez AD, Rodríguez-Barona S, Fontalvo J. Integration of a liquid membrane in Taylor flow regime with a fermentation by *Lactobacillus casei* ATCC 393 for in-situ lactic acid removal. *Chem Eng Process - Process Intensif* [Internet]. 2019 Jun;140(April):85-90. Available from: <https://doi.org/10.1016/j.cep.2019.05.002>
262. Lee SC. Extraction of succinic acid from simulated media by emulsion liquid membranes. *J Memb Sci* [Internet]. 2011 Sep;381(1-2):237-43. Available from:

- <http://dx.doi.org/10.1016/j.memsci.2011.07.039>
263. Koter S, Szczepański P. Modeling of diffusive transport of benzoic acid through a liquid membrane. *Chem Pap* [Internet]. 2011 Jan 1;65(5):584–95. Available from: <http://www.degruyter.com/view/j/chempap.2011.65.issue-5/s11696-011-0010-9/s11696-011-0010-9.xml>
 264. Berrios J, Pyle DL, Aroca G. Gibberellic acid extraction from aqueous solutions and fermentation broths by using emulsion liquid membranes. *J Memb Sci* [Internet]. 2010 Feb;348(1–2):91–8. Available from: <https://linkinghub.elsevier.com/retrieve/pii/S0376738809007820>
 265. Baylan N, Çehreli S, Özparlak N. Transport and separation of carboxylic acids through bulk liquid membranes containing tributylamine. *J Dispers Sci Technol* [Internet]. 2017 Jun 3;38(6):895–900. Available from: <http://dx.doi.org/10.1080/01932691.2016.1214841>
 266. Bouranene S, Soualmia A, Fievet P, Déon S, Ismail F. Extraction of ethanol from aqueous solutions by emulsion liquid membrane: optimization of operating conditions and influence of salts in the feed phase. *Desalin WATER Treat* [Internet]. 2017;88(November):106–15. Available from: http://www.deswater.com/DWT_abstracts/vol_88/88_2017_106.pdf
 267. Kumar A, Thakur A, Panesar PS. Lactic acid and its separation and purification techniques: A review. *Rev Environ Sci Bio/Technology* [Internet]. 2019 Dec 18;18(4):823–53. Available from: <https://doi.org/10.1007/s11157-019-09517-w>
 268. Alberto M, Bhavsar R, Luque-Alled JM, Prestat E, Gao L, Budd PM, et al. Study on the formation of thin film nanocomposite (TFN) membranes of polymers of intrinsic microporosity and graphene-like fillers: Effect of lateral flake size and chemical functionalization. *J Memb Sci*. 2018;565(August):390–401.
 269. Yan N, Wang Y. Catalyst: Is the Amino Acid a New Frontier for Biorefineries? *Chem* [Internet]. 2019 Apr;5(4):739–41. Available from: <https://doi.org/10.1016/j.chempr.2019.03.016>
 270. Fathi SAM, Yaftian MR, Kargari A. Water-In-oil Emulsion Liquid Membrane Transport of L-Cysteine. *Sep Sci Technol* [Internet]. 2013 Jan;48(1):105–12. Available from: <http://www.tandfonline.com/doi/abs/10.1080/01496395.2012.675001>
 271. Fang Z, Liu X, Zhang M, Sun J, Mao S, Lu J, et al. A neural network approach to simulating the dynamic extraction process of l-phenylalanine from sodium chloride aqueous solutions by emulsion liquid membrane. *Chem Eng Res Des* [Internet]. 2016 Jan;105:188–99. Available from: <http://dx.doi.org/10.1016/j.cherd.2015.11.012>
 272. Reis MTA, Freitas OMF, Agarwal S, Ferreira LM, Ismael MRC, Machado R, et al. Removal of phenols from aqueous solutions by emulsion liquid membranes. *J Hazard Mater* [Internet]. 2011 Sep;192(3):986–94. Available from: <http://dx.doi.org/10.1016/j.jhazmat.2011.05.092>
 273. Gupta S, Chakraborty M, Murthy ZVP. Performance study of hollow fiber supported liquid membrane system for the separation of bisphenol A from aqueous solutions. *J Ind Eng Chem* [Internet]. 2014 Jul;20(4):2138–45. Available from: <http://dx.doi.org/10.1016/j.jiec.2013.09.043>
 274. Seifollahi Z, Rahbar-Kelishami A. Diclofenac extraction from aqueous solution by an emulsion liquid membrane: Parameter study and optimization using the response surface methodology. *J Mol Liq* [Internet]. 2017 Apr;231:1–10. Available from: <http://dx.doi.org/10.1016/j.molliq.2017.01.081>
 275. Razo-Lazcano TA, Stambouli M, González-Muñoz M del P, Pareau D, Ávila-Rodríguez M. Emulsion liquid membranes for recovery of ibuprofen from aqueous solutions. *J Chem Technol Biotechnol* [Internet]. 2014 Jun;89(6):890–8. Available from: <http://doi.wiley.com/10.1002/jctb.4329>
 276. Mohammed AA, Atiya MA, Hussein MA. Removal of antibiotic tetracycline using nano-fluid emulsion liquid membrane: Breakage, extraction and stripping studies. *Colloids Surfaces A Physicochem Eng Asp* [Internet]. 2020 Jun;595(December 2019):124680. Available from: <https://doi.org/10.1016/j.colsurfa.2020.124680>

277. Sunsandee N, Ramakul P, Pancharoen U, Leepipatpiboon N. Enantioseparation of (S)-amlodipine from pharmaceutical industry wastewater by stripping phase recovery via HFSLM: Polarity of diluent and membrane stability investigation. *Sep Purif Technol* [Internet]. 2013 Sep;116:405–14. Available from: <http://dx.doi.org/10.1016/j.seppur.2013.06.014>
278. Kohli HP, Gupta S, Chakraborty M. Extraction of Ethylparaben by emulsion liquid membrane: Statistical analysis of operating parameters. *Colloids Surfaces A Physicochem Eng Asp* [Internet]. 2018 Feb;539(November 2017):371–81. Available from: <https://doi.org/10.1016/j.colsurfa.2017.12.002>
279. Chaouchi S, Hamdaoui O. Extraction of endocrine disrupting compound propylparaben from water by emulsion liquid membrane using trioctylphosphine oxide as carrier. *J Ind Eng Chem* [Internet]. 2015 Feb;22:296–305. Available from: <http://dx.doi.org/10.1016/j.jiec.2014.07.023>
280. Ooi Z-Y, Harruddin N, Othman N. Recovery of kraft lignin from pulping wastewater via emulsion liquid membrane process. *Biotechnol Prog* [Internet]. 2015 Sep;31(5):1305–14. Available from: <http://doi.wiley.com/10.1002/btpr.2129>
281. Chakrabarty K, Saha P, Ghoshal AK. Simultaneous separation of mercury and lignosulfonate from aqueous solution using supported liquid membrane. *J Memb Sci* [Internet]. 2010 Jan 1;346(1):37–44. Available from: <https://linkinghub.elsevier.com/retrieve/pii/S0376738809006541>
282. Rene ER, Sahinkaya E, Lewis A, Lens PNL. Sustainable Heavy Metal Remediation [Internet]. Rene ER, Sahinkaya E, Lewis A, Lens PNL, editors. Cham: Springer International Publishing; 2017. (Environmental Chemistry for a Sustainable World; vol. 8). Available from: <http://link.springer.com/10.1007/978-3-319-58622-9>
283. Minhas FT, Memon S, Bhangar MI. Transport of Hg(II) through bulk liquid membrane containing calix[4]arene thioalkyl derivative as a carrier. *Desalination* [Internet]. 2010 Nov;262(1–3):215–20. Available from: <http://dx.doi.org/10.1016/j.desal.2010.06.014>
284. Chaturabul S, Srirachat W, Wannachod T, Ramakul P, Pancharoen U, Kheawhom S. Separation of mercury(II) from petroleum produced water via hollow fiber supported liquid membrane and mass transfer modeling. *Chem Eng J* [Internet]. 2015 Apr;265:34–46. Available from: <http://dx.doi.org/10.1016/j.cej.2014.12.034>
285. Zante G, Boltoeva M, Masmoudi A, Barillon R, Trébouet D. Lithium extraction from complex aqueous solutions using supported ionic liquid membranes. *J Memb Sci* [Internet]. 2019;580(March):62–76. Available from: <https://doi.org/10.1016/j.memsci.2019.03.013>
286. Swain B, Mishra C, Jeong J, Lee J, Hong HS, Pandey BD. Separation of Co(II) and Li(I) with Cyanex 272 using hollow fiber supported liquid membrane: A comparison with flat sheet supported liquid membrane and dispersive solvent extraction process. *Chem Eng J* [Internet]. 2015 Jul;271:61–70. Available from: <http://dx.doi.org/10.1016/j.cej.2015.02.040>
287. Ma H, Kökkılıç O, Waters KE. The use of the emulsion liquid membrane technique to remove copper ions from aqueous systems using statistical experimental design. *Miner Eng* [Internet]. 2017 Jun;107:88–99. Available from: <http://dx.doi.org/10.1016/j.mineng.2016.10.014>
288. Mokhtari B, Pourabdollah K. Emulsion liquid membrane for selective extraction of Bi(III). *Chinese J Chem Eng* [Internet]. 2015 Apr;23(4):641–5. Available from: <http://dx.doi.org/10.1016/j.cjche.2014.06.035>
289. Moyo F, Tandlich R. *Daphnia pulex* toxicity testing of ethylenediaminetetraacetic acid tetrasodium salt dihydrate and the wastewater effluent from extraction of rhodium using emulsion liquid membranes. *Int J Environ Res*. 2014;8(4):1019–26.
290. Laki S, Kargari A. Extraction of silver ions from aqueous solutions by emulsion liquid membrane. *J Membr Sci Res*. 2016;2(1):33–40.
291. Liu H, Zhang Y, Huang J, Liu T, Xue N, Shi Q. Optimization of vanadium (IV) extraction from stone coal leaching solution by emulsion liquid membrane using

- response surface methodology. *Chem Eng Res Des* [Internet]. 2017 Jul;123(Iv):111–9. Available from: <http://dx.doi.org/10.1016/j.cherd.2017.05.001>
292. Noah NFM, Othman N, Jusoh N. Highly selective transport of palladium from electroplating wastewater using emulsion liquid membrane process. *J Taiwan Inst Chem Eng* [Internet]. 2016 Jul;64:134–41. Available from: <https://linkinghub.elsevier.com/retrieve/pii/S1876107016300293>
 293. Srivastava A, Bhagat A, Sharma U, Dohare RK, Singh K, Upadhyaya S. Comparative study of arsenic(V) removal from aqueous solution using Aliquat-336 and 2-ethyl hexanol through emulsion liquid membrane. *J Water Process Eng* [Internet]. 2017 Apr;16:64–8. Available from: <http://dx.doi.org/10.1016/j.jwpe.2016.12.007>
 294. Salman HM, Mohammed AA. Extraction of lead ions from aqueous solution by co-stabilization mechanisms of magnetic Fe₂O₃ particles and nonionic surfactants in emulsion liquid membrane. *Colloids Surfaces A Physicochem Eng Asp* [Internet]. 2019 May;568(February):301–10. Available from: <https://doi.org/10.1016/j.colsurfa.2019.02.018>
 295. Ahmad AL, Kusumastuti A, Derek CJC, Ooi BS. Emulsion liquid membrane for heavy metal removal: An overview on emulsion stabilization and destabilization. *Chem Eng J* [Internet]. 2011 Jul;171(3):870–82. Available from: <http://dx.doi.org/10.1016/j.cej.2011.05.102>
 296. Herbst RS, Baron P, Nilsson M. Standard and advanced separation: PUREX processes for nuclear fuel reprocessing. In: *Advanced Separation Techniques for Nuclear Fuel Reprocessing and Radioactive Waste Treatment* [Internet]. Elsevier; 2011. p. 141–75. Available from: <http://dx.doi.org/10.1533/9780857092274.2.141>
 297. Zaheri P, Davarkhah R. Rapid removal of uranium from aqueous solution by emulsion liquid membrane containing thenoyltrifluoroacetone. *J Environ Chem Eng* [Internet]. 2017 Aug;5(4):4064–8. Available from: <http://dx.doi.org/10.1016/j.jece.2017.07.076>
 298. Ambashta RD, Sillanpää MET. Membrane purification in radioactive waste management: a short review. *J Environ Radioact* [Internet]. 2012 Feb;105:76–84. Available from: <http://dx.doi.org/10.1016/j.jenvrad.2011.12.002>
 299. Rathore NS, Sastre AM, Pabby AK. Membrane assisted liquid extraction of actinides and remediation of nuclear waste: A review. *J Membr Sci Res*. 2016;2(1):2–13.
 300. Xie F, Zhang TA, Dreisinger D, Doyle F. A critical review on solvent extraction of rare earths from aqueous solutions. *Miner Eng* [Internet]. 2014 Feb;56:10–28. Available from: <http://dx.doi.org/10.1016/j.mineng.2013.10.021>
 301. Davoodi-Nasab P, Rahbar-Kelishami A, Safdari J, Abolghasemi H. Evaluation of the emulsion liquid membrane performance on the removal of gadolinium from acidic solutions. *J Mol Liq* [Internet]. 2018 Jul;262:97–103. Available from: <https://doi.org/10.1016/j.molliq.2018.04.062>
 302. Raji M, Abolghasemi H, Safdari J, Kargari A. Pertraction of dysprosium from nitrate medium by emulsion liquid membrane containing mixed surfactant system. *Chem Eng Process - Process Intensif* [Internet]. 2017 Oct;120(January):184–94. Available from: <http://dx.doi.org/10.1016/j.cep.2017.06.010>
 303. Raji M, Abolghasemi H, Safdari J, Kargari A. Selective extraction of dysprosium from acidic solutions containing dysprosium and neodymium through emulsion liquid membrane by Cyanex 572 as carrier. *J Mol Liq* [Internet]. 2018 Mar;254:108–19. Available from: <https://doi.org/10.1016/j.molliq.2017.11.058>
 304. Hasan MA, Aglan RF, El-Reefy SA. Modeling of gadolinium recovery from nitrate medium with 8-hydroxyquinoline by emulsion liquid membrane. *J Hazard Mater*. 2009;166(2–3):1076–81.
 305. Linnhoff B. *Thermodynamic Analysis in the Design of Process Networks*. University of Leeds; 1979.
 306. Roschangar F, Sheldon RA, Senanayake CH. Overcoming barriers to green chemistry in the pharmaceutical industry-the Green Aspiration Level™ concept. *Green Chem*. 2015;17(2):752–68.

307. Constable DJC, Giraud R, Sehgal A, Sullivan D. Sustainable Separation Processes. A Road Map to Accelerate Industrial Application of Less Energy-Intensive Alternative Separations (AltSep). 2019.
308. Cohen ER, Mills I, Strauss HL, Frey JG, Mills I, Homann K, et al. Quantities, Units and Symbols in Physical Chemistry [Internet]. Third Edit. Cohen ER, Cvitas T, Frey JG, Holström B, Kuchitsu K, Marquardt R, et al., editors. International Union of Pure and Applied Chemistry. Cambridge: Royal Society of Chemistry; 2007. Available from: <http://ebook.rsc.org/?DOI=10.1039/9781847557889>
309. Fallanza M, González-Miquel M, Ruiz E, Ortiz A, Gorri D, Palomar J, et al. Screening of RTILs for propane/propylene separation using COSMO-RS methodology. *Chem Eng J* [Internet]. 2013;220:284–93. Available from: <http://dx.doi.org/10.1016/j.cej.2013.01.052>
310. Seader D, Henley EJ. Separation process principles. 2nd ed. Hoboken, N.J.: Wiley; 2005.
311. Maximini A, Chmiel H, Holdik H, Maier NW. Development of a supported liquid membrane process for separating enantiomers of N-protected amino acid derivatives. *J Memb Sci*. 2006;276(1–2):221–31.
312. Lin SH, Pan CL, Leu HG. Liquid membrane extraction of 2-chlorophenol from aqueous solution. *J Hazard Mater* [Internet]. 1999 Mar;65(3):289–304. Available from: <https://linkinghub.elsevier.com/retrieve/pii/S0304389498002738>
313. Leaper S, Abdel-Karim A, Gad-Allah TA, Gorgojo P. Air-gap membrane distillation as a one-step process for textile wastewater treatment. *Chem Eng J* [Internet]. 2019 Mar;360(August 2018):1330–40. Available from: <https://doi.org/10.1016/j.cej.2018.10.209>
314. Skuse C, Gallego-Schmid A, Azapagic A, Gorgojo P. Can emerging membrane-based desalination technologies replace reverse osmosis? *Desalination* [Internet]. 2021 Mar;500(October 2020):114844. Available from: <https://doi.org/10.1016/j.desal.2020.114844>
315. Curcio E, Drioli E. Membrane Distillation and Related Operations – A Review. *Sep Purif Rev* [Internet]. 2005 Jan;34(1):35–86. Available from: <http://www.tandfonline.com/doi/abs/10.1081/SPM-200054951>
316. Linnhoff B, Townsend DW, Boland D, Hewitt GF, Thomas BEA, Guy AR, et al. Process integration for the efficient use of energy. *The Institution of Chemical Engineers*; 1986.
317. Yara-Varón E, Fabiano-Tixier AS, Balcells M, Canela-Garayoa R, Bily A, Chemat F. Is it possible to substitute hexane with green solvents for extraction of carotenoids? A theoretical versus experimental solubility study. *RSC Adv*. 2016;6(33):27750–9.
318. Dean JA. *Handbook of Organic Chemistry*. NY: NY: McGraw-Hill, Inc.; 1987.
319. Kortum G, Vogel W, Andrussov K. Dissociation constants of organic acids in aqueous solution. London: Butterworths; 1961.
320. Lide DR, editor. *CRC Handbook of Chemistry and Physics*. 76th ed. Boca Raton, Fla: CRC.;
321. Database. NC for BIP. Malic acid [Internet]. Available from: <https://pubchem.ncbi.nlm.nih.gov/compound/525>
322. Patty F. *Industrial Hygiene and Toxicology: Volume II: Toxicology*. 2nd ed. Patty F, editor. New York: Interscience Publishers; 1963.
323. Silva AMN, Kong X, Hider RC. Determination of the pKa value of the hydroxyl group in the α -hydroxycarboxylates citrate, malate and lactate by ^{13}C NMR: implications for metal coordination in biological systems. *BioMetals* [Internet]. 2009 Oct 14;22(5):771–8. Available from: <http://link.springer.com/10.1007/s10534-009-9224-5>

Appendices

Supplementary information of the publications presented in this
work.

Appendix A. SI: Green solvents selection guide for bio-based organic acids recovery

Structures of bio-organic acids

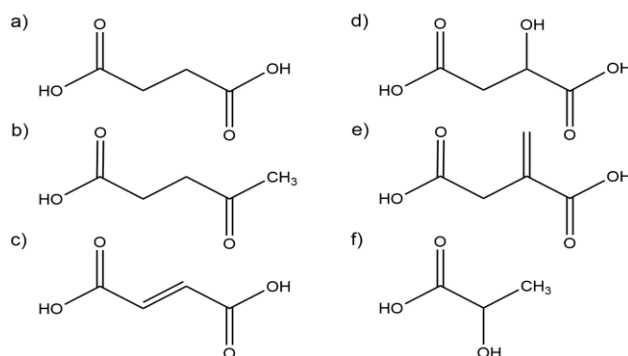


Figure A0.1. Structures of bio-organic acids studied in this work. a) Succinic acid; b) Levulinic acid; c) Fumaric acid; d) Malic acid; e) Itaconic acid; and f) Lactic acid.

Physical characterization of solvents

Solvent properties are summarized in [Table A.0.1](#). Density (ρ) and viscosity (μ) were measured, before the experimental extraction assays, at 25 °C by using an Anton Paar DMA 4500 M density-meter with a Lovis 2000 ME micro viscometer. The saturated water content (wt_w) at 25 °C was measured by Karl Fisher titration using a Metrohm 899 coulometer. Their respective standard uncertainties are: $u(\rho) \leq 5 \cdot 10^{-5} \text{ g mL}^{-1}$; $u(\mu) \leq 0.01 \text{ mPa s}$; and $u(wt_w) \leq 10^{-7} \text{ g g}^{-1}$.

Table A.0.1. Physical properties of green solvents at 25 °C.

| Solvent | Density | Viscosity | Saturated Water Content |
|--|---------------------------|-----------------------|---------------------------------|
| | $\rho / \text{g mL}^{-1}$ | $\eta / \text{mPa s}$ | $\text{wt}_w / \text{g g}^{-1}$ |
| [C ₄ min][Tf ₂ N] | 1.4254 | 31.36 | 0.0142 |
| [C ₄ pyrr][Tf ₂ N] | 1.3859 | 46.91 | 0.0107 |
| [N ₈₈₈₁][Tf ₂ N] | 1.1068 | 440.0 | 0.0026 |
| DL-menthol:OctA (1:1) | 0.9015 | 12.57 | 0.0214 |
| N ₄₄₄₄ Cl:OctA (1:2) | 0.9214 | 280.2 | 0.1379 |
| DL-menthol:DecA (1:1) | 0.8963 | 16.11 | 0.0159 |
| CPME | 0.8585 | 0.55 (317) | 0.0063 |
| 2-MeTHF | 0.8503 | 0.60 (317) | 0.0448 |
| 1,8-Cineol | 0.9204 | 2.75 | 0.0051 |
| EtOAc | 0.8945 | 0.42 (317) | 0.0314 |

Experimental extraction results

Table A.0.2 shows experimental data along with its respective expanded combined uncertainty with a confidence level of 95.45%.

Table A.0.2. Experimental extraction yields of organic acids using green solvents at the temperature of 25 °C and feed:solvent ratio of 1.

| Solvent | Succinic acid | | Levulinic acid | | Fumaric acid | |
|--|---|-------|----------------|-------|--------------|-------|
| | $\%Ex U_{\text{comb}} \pm (\%Ex) / \text{g g}^{-1} \cdot 100\%$ | | | | | |
| [C ₄ min][Tf ₂ N] | 14.1% | ±1.9% | 26.8% | ±0.8% | 8.7% | ±3.1% |
| [C ₄ pyrr][Tf ₂ N] | 12.6% | ±2.3% | 23.4% | ±0.8% | 5.1% | ±3.2% |
| [N ₈₈₈₁][Tf ₂ N] | 0.0% | ±2.6% | 4.8% | ±0.9% | 2.4% | ±3.2% |
| DL-menthol:OctA (1:1) | 8.0% | ±2.4% | 18.8% | ±0.5% | 30.3% | ±2.1% |
| N ₄₄₄₄ Cl:OctA (1:2) | 19.1% | ±2.2% | 36.9% | ±0.4% | 62.0% | ±2.0% |
| DL-menthol:DecA (1:1) | 3.7% | ±2.5% | 17.1% | ±0.5% | 26.3% | ±2.2% |
| CPME | 11.6% | ±2.3% | 19.1% | ±0.5% | 50.3% | ±2.0% |
| 2-MeTHF | 59.3% | ±1.7% | 55.1% | ±0.4% | 91.5% | ±2.2% |
| 1,8-Cineol | 30.0% | ±2.0% | 16.9% | ±0.8% | 63.0% | ±2.2% |
| EtOAc | 25.2% | ±2.1% | 44.5% | ±0.4% | 64.6% | ±2.0% |

pKa and pH-values of bio-based organic acids

Table A.0.3 shows the pKa-values of the bio-based organic acids considered in this work. In addition, Table A.0.4 collects the measured pH-values of the aqueous solutions prepared for the experimental extraction essays, compared to the pH-values predicted by the Henderson–Hasselbalch equation (Eq. A.1), where $[A^-]$ and $[AH]$ correspond to the dissociated and molecular acid concentration, respectively.

$$pH = pK_a + \log_{10} \frac{[A^-]}{[AH]} \quad (\text{A.1})$$

Table A.0.3. pKa-values of bio-based organic acids.

| Acid | | T / °C | pKa | Ref. |
|-----------------|---|--------|------|-------|
| Succinic acid: | 1 | 25 | 4.21 | (318) |
| | 2 | 25 | 5.65 | (318) |
| Levulinic acid: | 1 | 18 | 4.64 | (319) |
| Fumaric acid: | 1 | 25 | 3.03 | (320) |
| | 2 | 25 | 4.54 | (320) |
| Malic acid: | 1 | 20 | 3.51 | (321) |
| | 2 | 20 | 5.03 | (321) |
| Itaconic acid: | 1 | RT | 3.84 | (322) |
| | 2 | RT | 5.55 | (322) |
| Lactic acid: | 1 | RT | 3.86 | (169) |
| | 2 | RT | 15.1 | (323) |

(RT): Room temperature.

Table A.0.4. pH-values of the bio-based organic acid aqueous solutions used for the experimental extraction essays in this work.

| Acid | MW | [acid] ₀ | M | pKa | pH | |
|----------------|---------------------|---------------------|---------------------|------|-------------|----------|
| | g mol ⁻¹ | g l ⁻¹ | mol l ⁻¹ | | Theoretical | Measured |
| Succinic acid | 118.09 | 50 | 0.42 | 4.21 | 2.3 | 2.71 |
| Levulinic acid | 116.11 | 50 | 0.43 | 4.64 | 2.5 | 3.09 |
| Fumaric acid | 116.07 | 5.0 | 0.04 | 3.03 | 2.2 | 2.90 |

Molecular interaction analysis

Figure A.0.2 shows the percentage of non-internal HB organic acid conformer within the different green solvents studied in this work as well as the change respect to the conformer weighting in water.

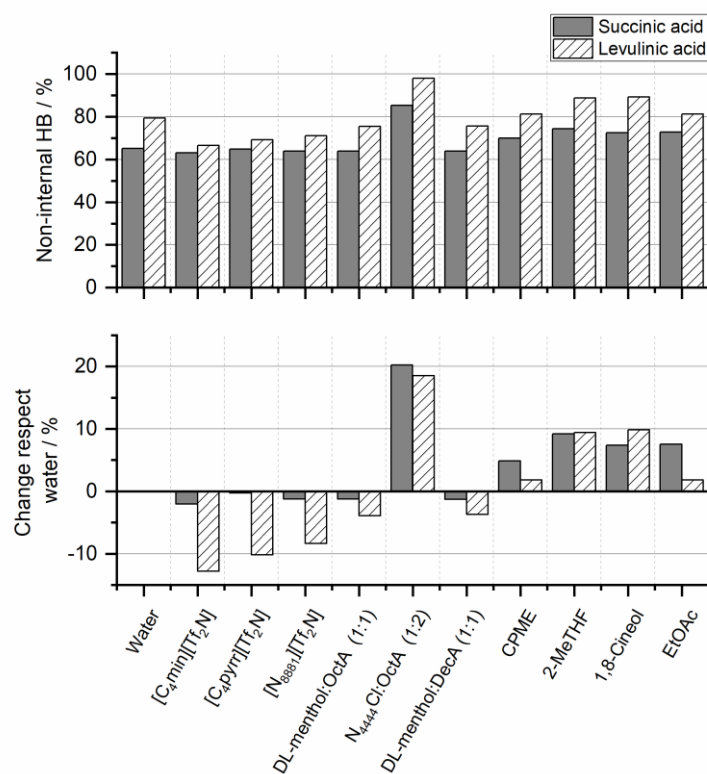


Figure A.0.2. Conformer weighting analysis in terms of the percentage of non-internal HB of organic acid in each solvent (above) and its difference with respect to the percentage in water (below), computed at 25 °C by COSMO-RS method.

Figure A.0.3 shows the correlations found for the excess enthalpy contribution energies (a, b, and c), and the excess entropy (d). HB contribution shows to be the main contribution to the excess enthalpy and directly correlated with the organic acid partition coefficient. Although MF contribution is significant, it has a lower impact than HB and does not show a linear trend respect to $\ln(K_i)$. vdW forces contribution is negligible and does not show a significant correlation with $\ln(K_i)$. On the other hand, excess entropy ($-TS^{\text{ex}}$) shows a significant linear dependence with extraction performance.

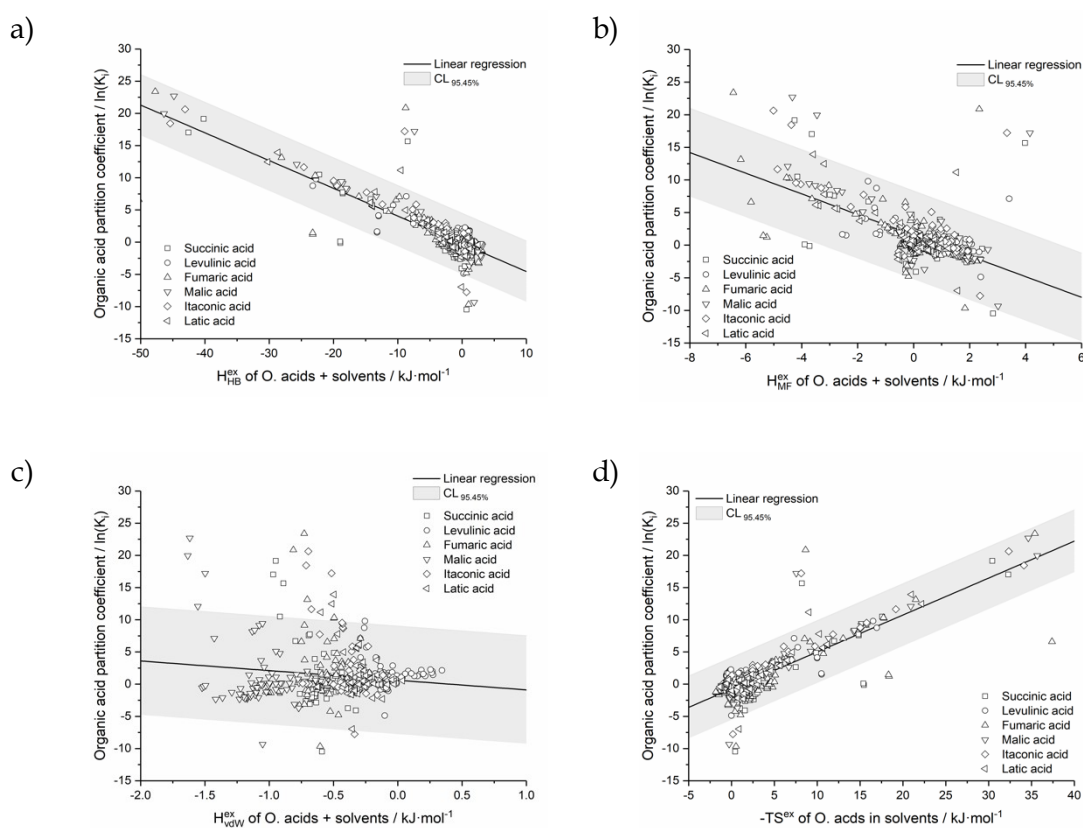


Figure A.0.3. Relationship between organic acid partition coefficients, $\ln(K_i)$, and organic acid – solvent energies contributions: a) hydrogen bonding excess enthalpy contribution ($H_{\text{HB}}^{\text{ex}}$), $r^2 = 0.69$; b) electrostatic excess enthalpy contribution ($H_{\text{MF}}^{\text{ex}}$), $r^2 = 0.36$; c) van der Waals excess enthalpy contribution ($H_{\text{vdW}}^{\text{ex}}$) $r^2 = 0.02$; d) excess entropy ($-TS^{\text{ex}}$), $r^2 = 0.67$. Computed with COSMO-RS at 25 °C.

Solvent-water affinity analysis

Solvent - water affinity was described as the water activity coefficient at infinite dilution, $\ln(\gamma_w^\infty)$, and shown in Figure A.0.4 correlated with the computed partition coefficients of organic acids.

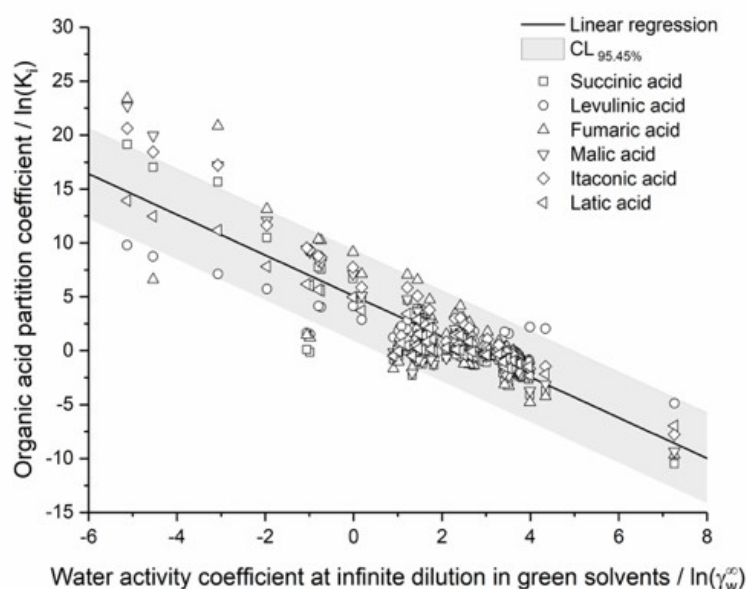


Figure A.0.4. Relationship between organic acid partition coefficients, $\ln(K_i)$, and water activity coefficient at infinite dilution, $\ln(\gamma_w^\infty)$, for screened solvents computed with COSMO-RS at 25 °C. $r^2 = 0.75$.

Based on the proposed methodology, the partition coefficients are estimated considering the affinity of the organic acid for each pure phase, i.e., the partition coefficients are computed from the respective chemical potentials. As a consequence, the water content in the saturated solvents is not included in the calculations. Nevertheless, the organic acid chemical potential at infinite dilution on the water-saturated solvent, can be computed assuming a "pseudo-extract" phase composed of a (water + solvent) mixture, where the composition corresponds to the water saturated content, wt_w , experimentally determined for the green solvents (see Table A.0.1). Based on these computations, partition coefficients of organic acids in the water-saturated solvents were re-calculated as $\ln(K_i)^*$. Figure A.0.5 shows the relationship between the organic acid partition coefficients in the pure solvents, $\ln(K_i)$, and the partition coefficients computed for the water-saturated solvents, $\ln(K_i)^*$.

Due to the lower organic acid–extractant affinities observed if the water content is considered into the extracting solvent, partition coefficients of organic acids for the water-saturated solvents are slightly lower than those computed for pure solvents. Nevertheless, it is possible to observe a direct proportional trend as illustrated in Figure A.0.5. Thus, despite the slight overestimation, the values reported for the partition coefficients of organic acids in pure solvents prove to be a robust descriptor of the overall solvent performance for screening and selection purposes.

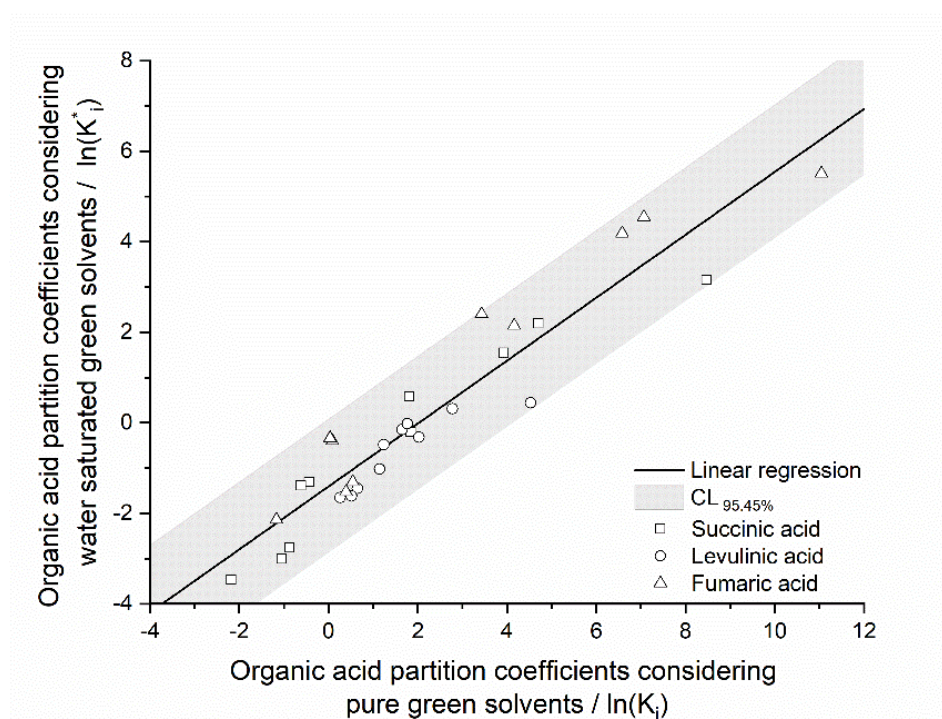


Figure A.0.5. Relationship between the organic acid partition coefficients computed considering pure green solvents, $\ln(K_i)$, (on x -axis) and the organic acid partition coefficients computed considering water saturated green solvents, $\ln(K_i)^*$, (on y -axis). Data was computed for the systems used for the methodology validation, i.e., succinic, levulinic, and fumaric acids with $[\text{C}_4\text{mim}][\text{Tf}_2\text{N}]$, $[\text{C}_4\text{pyrr}][\text{Tf}_2\text{N}]$, $[\text{N}_{8881}][\text{Tf}_2\text{N}]$, DL-menthol:OctA, $\text{N}_{4444}\text{Cl}:\text{OctA}$, DL-menthol:DecA, CPME, 2-MeTHF, 1,8-Cineol, and EtOAc. $r^2 = 0.90$.

Green solvent selection guide methodology

Green solvent recommendations for organic acid recovery were established by employing a quality matrix, [Figure A.0.6](#), assigning to each descriptor (d_i) a score according to its quality: 4-high; 3-moderate; 2-low; and 1-very low. Individual recommendation indexes are determined according to [Eq. A.2](#), where the values were divided following a normal distribution and classified as: [17-64] Highly recommended (in green); [8-16] Moderately recommended (in yellow); and [1-7] Lowly recommended (in red). Quality ranges were determined based on the screening results obtained in this work, using as reference the favourable theoretical values. Descriptor score ranges are shown in [Table A.0.5](#).

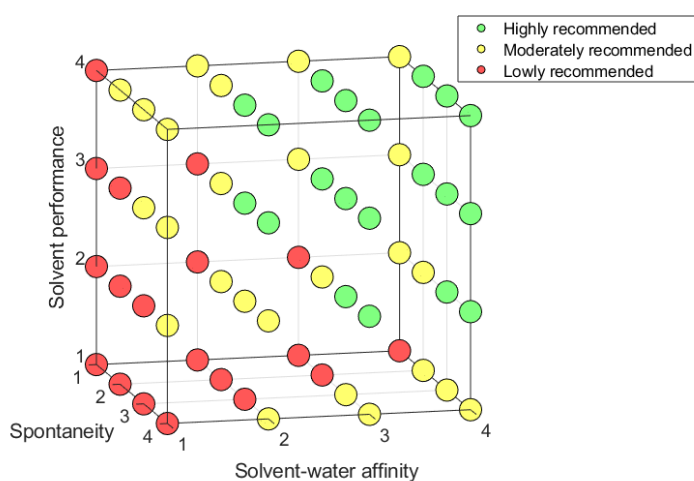


Figure A.0.6. Quality matrix for green solvents recommendation assessment.

$$\text{Recommendation index} = \prod d_i \quad (\text{A.2})$$

Table A.0.5. Quality scores for green solvents recommendation assessment.

| Criteria | Descriptor d_i | Theoretical favourable value | Quality: | | | |
|------------------------|--------------------------------------|------------------------------|----------|----------|---------|------------|
| | | | High | Moderate | Low | Very low |
| | | | Score: 4 | 3 | 2 | 1 |
| Solvent performance | $\ln(K_i) / -$ | > 0 | > 1.7 | > 0.2 | > 0.0 | ≤ 0.0 |
| Solvent-water affinity | $\ln(\gamma_w^\infty) / -$ | > 0 | > 3.4 | > 2.4 | > 0.0 | ≤ 0.0 |
| Spontaneity | $G^{\text{ex}} / \text{kJ mol}^{-1}$ | < 0 | < -0.2 | < 0.0 | < 0.5 | ≥ 0.5 |

Appendix B. SI: Solubility study and thermodynamic modelling of succinic acid and fumaric acid in bio-based solvents

Methodology validation

Solubility data found in the literature for succinic acid (147,160,176–181,167,169–175) and fumaric acid (147,172,177,182,183) in water was used to validate the proposed methodology. Each solubility data set were fed into the van't Hoff equation (Eq. B.1) and compared with the respective correlated data from experimental values by the root mean squared deviation, $\delta[\ln(x_1)]$, according to Eq. B.2. The validation results are shown in Table B.0.1.

$$\ln(x_1) = p_1 + \frac{p_2}{T} \quad (\text{B.1})$$

$$\delta[\ln(x_1)] = \sqrt{\frac{1}{N} \sum \left(\ln(x_1^{\text{exp}}) - \ln(x_1^{\text{lit}}) \right)^2} \quad (\text{B.2})$$

Table B.0.1. Comparison of experimental and mean values found in the literature for aqueous solubility of succinic and fumaric acids for methodology validation. The estimated combined expanded uncertainty for the mean literature values: $U_{\text{comb},95\%}(\ln(x_1^{\text{lit}})) = 0.10$ and 0.14 , for succinic and fumaric acids, respectively.

| | Succinic acid | | Fumaric acid | |
|--------|-------------------------|-------------------------|-------------------------|-------------------------|
| $1/T$ | $\ln(x_1^{\text{exp}})$ | $\ln(x_1^{\text{lit}})$ | $\ln(x_1^{\text{exp}})$ | $\ln(x_1^{\text{lit}})$ |
| 1/K | mol mol ⁻¹ | mol mol ⁻¹ | mol mol ⁻¹ | mol mol ⁻¹ |
| 0.0035 | -4.82 | -5.08 | -7.86 | -7.48 |
| 0.0034 | -4.42 | -4.66 | -7.19 | -7.09 |
| 0.0033 | -4.19 | -4.27 | -6.63 | -6.72 |
| 0.0032 | -3.82 | -3.90 | -6.30 | -6.38 |
| | $\delta[\ln(x_1)]:$ | 0.19 | $\delta[\ln(x_1)]:$ | 0.20 |

Experimental uncertainty

Reported solubility values, \hat{x}_1 , are presented as the measurement result, x_1 , along with the expanded combined uncertainty, $U_{\text{Comb}}(x_1)$, as is shown in Eq. B.3. The saturated acid mole fraction was calculated following Eq. B.4, where M_{vial} , M_{dry} , and M_{solution} correspond to the vial mass, the dry organic acid plus the vial mass, and the saturated supernatant plus the vial mass, respectively. Two approaches were adopted to evaluate $U_{\text{Comb}}(x_1)$, according to the NIST guidelines for expressing results uncertainty (165). First, the type A evaluation by statistical methods of the variability of the results, where the error arising from a random effect on the repeatability of the measurement is obtained assuming a t -distribution and the degree of freedom, ν , according to Eq. B.5. The results standard uncertainty, $u(x_1)$, is obtained from the measurement deviation, while the t -factor, $t_{(N-2)}$, for a level of confidence (LC) of 95% of the measured data in triplicate, i.e., degree freedom $\nu = 1$, results in 12.71. Due to the complexity of the procedure methodology, no more replicate experiments by data point were possible to measure. This results in large confidence bounds given by the basic statistical methods, which do not reflect the experimental precision, and the uncertainty should be estimated from other scientific judgment.

$$\hat{x}_1 = x_1 \pm U_{\text{comb}}(x_1) \quad (\text{B.3})$$

$$x_1 = \frac{M_{\text{dry}} - M_{\text{vial}}}{MW_1} \cdot \left[\frac{M_{\text{dry}} - M_{\text{vial}}}{MW_1} + \frac{M_{\text{solution}} - M_{\text{dry}}}{MW_2} \right]^{-1} \quad (\text{B.4})$$

$$U_{\text{comb}}(x_1) = u(x_1) \cdot t_{(N-2)} \quad (\text{B.5})$$

The type B approach corresponds to the uncertainty of measurement, which comes from the error of the measured properties variation, due to the instruments' resolution and error propagation in the data treatment. Since the proposed methodology is based on reliable independent measurements under highly controlled conditions, a type B approach represents a better

approximation to the experimental uncertainty. Assuming all the variable errors as small and independent, the combined standard uncertainty, $u_{comb}(x_1)$, is determined by the law of propagation of uncertainty: Eq. B.6. The list of the variable uncertainty estimation derived from the organic acid saturated mole fraction measurements (Eq. B.4) is given in Table B.0.2. Then, $U_{Comb}(x_1)$ is calculated by including a coverage factor, k_L , (Eq. B.7) given by the t -distribution for a specific confidence level, p , and effective degrees of freedom, v_{eff} , as shown in Eq. B.8. The effective degrees of freedom are calculated by the Welch-Satterthwaite formula (Eq. B.9), where $v_j = r-1$, is the independent variable j degree of freedom and r is the size of the sample. The mass weight uncertainty was modelled by a normal distribution of the scale resolution ($\pm a = 0.0001$ g) according to the instruments manufacturer's specifications and assuming a 50 per cent probability that the value of the quantity lies in the interval a_- to a_+ , as shown in Eq. B.10. Thus, for the measurement procedure of this work and $r=3$ replicates for the M_{vial} , M_{dry} , and $M_{solution}$ measurements give a $v_{eff} = 4$. Lastly, taking $LC = 95\%$ for $t(4)$ results in a k_L of 2.78.

$$u_{comb}^2(x_1) = \sum_{j=1}^n \left(\frac{\partial x_1}{\partial M_j} \right)^2 \cdot u^2(M_j) \quad (\text{B.6})$$

$$U_{comb}(x_1) = k_L \cdot u_{comb}(x_1) \quad (\text{B.7})$$

$$k_L = t_p(v_{eff}) \quad (\text{B.8})$$

$$v_{eff} = \frac{u_{comb}^4(x_1)}{\sum_{j=1}^n \frac{\left(\frac{\partial x_1}{\partial M_j} \right)^4 \cdot u^4(M_j)}{v_j}} \quad (\text{B.9})$$

$$u(M_j) \approx \frac{a_- - a_+}{2} \cdot 1.48 \quad (\text{B.10})$$

Table B.0.2. Estimation of the combined expanded uncertainty for the saturated organic acid mole fraction in bio-based solvents, $U_{Comb,95\%}(x_1)$, based on the contributions of properties and variables measured and calculated.

| Property, Variable | Type of uncertainty Coverage factor, k_L (CL / %) | Uncertainty |
|--|---|--|
| Water content in bio-based solvent ($10^{-4} \leq wt_w \leq 10^{-2}$) g · g ⁻¹ | Standard | $u(wt_w) = 10^{-7} \text{ g} \cdot \text{g}^{-1}$ |
| Temperature ($283 \leq T \leq 313$) K | Standard | $u(T) = 1 \text{ K}$ |
| Mass ($0.0000 \leq M \leq 10.0000$) g | Standard | $u(M_j) = 1.48 \cdot 10^{-4} \text{ g}$ |
| Saturated mole fraction of organic acid ($0 \leq x_1 \leq 1$) mol · mol ⁻¹ | Combined $k_L = 1.96$ (95%) | $\frac{U_{comb}(x_1)}{k_L} = \left[\left \frac{\partial x_1}{\partial M_{vial}} \right + \left \frac{\partial x_1}{\partial M_{solution}} \right + \left \frac{\partial x_1}{\partial M_{dry}} \right \right] \cdot u(M)$ |
| $\frac{\partial x_1}{\partial M_{vial}} = \frac{M_{dry} - M_{vial}}{(MW_1)^2 \cdot \left[\frac{M_{dry} - M_{vial}}{MW_1} \cdot \frac{M_{solution} - M_{dry}}{MW_2} \right]^2} - \frac{1}{\left[M_{dry} - M_{vial} - \frac{MW_1}{MW_2} (M_{solution} - M_{dry}) \right]}$ $\frac{\partial x_1}{\partial M_{solution}} = \frac{M_{dry} - M_{vial}}{MW_1 \cdot MW_2 \cdot \left[\frac{M_{dry} - M_{vial}}{MW_1} \cdot \frac{M_{solution} - M_{dry}}{MW_2} \right]^2}$ $\frac{\partial x_1}{\partial M_{dry}} = \frac{1}{\left[M_{dry} - M_{vial} - \frac{MW_1}{MW_2} (M_{solution} - M_{dry}) \right]} - \frac{(M_{dry} - M_{vial}) \cdot (1/MW_1 + 1/MW_2)}{\left[M_{dry} - M_{vial} - \frac{MW_1}{MW_2} (M_{solution} - M_{dry}) \right]^2}$ | | |

Experimental solubility data

Table B.0.3 summarizes the experimental data obtained from the proposed methodology along with the respective estimated measurement (type B) and statistical (type A) combined expanded uncertainty, $U_{\text{Comb},95\%}(x_1) / \text{mol mol}^{-1}$.

Table B.0.3. Experimental saturated organic acid mole fraction ($x_1 / \text{mol} \cdot \text{mol}^{-1}$) in water and bio-based solvents and its combined expanded uncertainties.

| Succinic acid | | | | Fumaric acid | | | |
|----------------|-----------------------|---|-----------------------|--------------|-----------------------|---|-----------------------|
| T* | x_1 | $U_{\text{Comb},95\%}(x_1) / \text{mol mol}^{-1}$ | | T* | x_1 | $U_{\text{Comb},95\%}(x_1) / \text{mol mol}^{-1}$ | |
| K | mol mol^{-1} | Type B** | Type A*** | K | mol mol^{-1} | Type B** | Type A*** |
| <i>Water</i> | | | | | | | |
| 283 | 0.0081 | $8.878 \cdot 10^{-5}$ | $4.056 \cdot 10^{-4}$ | 283 | 0.0005 | $9.040 \cdot 10^{-5}$ | $4.130 \cdot 10^{-4}$ |
| 293 | 0.0121 | $9.673 \cdot 10^{-5}$ | $4.419 \cdot 10^{-4}$ | 293 | 0.0008 | $9.129 \cdot 10^{-5}$ | $4.171 \cdot 10^{-4}$ |
| 303 | 0.0152 | $9.849 \cdot 10^{-5}$ | $4.499 \cdot 10^{-4}$ | 303 | 0.0013 | $9.253 \cdot 10^{-5}$ | $4.227 \cdot 10^{-4}$ |
| 313 | 0.0219 | $1.022 \cdot 10^{-4}$ | $4.667 \cdot 10^{-4}$ | 313 | 0.0018 | $9.121 \cdot 10^{-5}$ | $4.167 \cdot 10^{-4}$ |
| <i>EtOAc</i> | | | | | | | |
| 283 | 0.0033 | $4.946 \cdot 10^{-4}$ | $2.260 \cdot 10^{-3}$ | 293 | 0.0010 | $5.018 \cdot 10^{-4}$ | $2.292 \cdot 10^{-3}$ |
| 293 | 0.0038 | $4.927 \cdot 10^{-4}$ | $2.251 \cdot 10^{-3}$ | 298 | 0.0015 | $4.974 \cdot 10^{-4}$ | $2.272 \cdot 10^{-3}$ |
| 303 | 0.0050 | $4.966 \cdot 10^{-4}$ | $2.269 \cdot 10^{-3}$ | 303 | 0.0019 | $5.018 \cdot 10^{-4}$ | $2.292 \cdot 10^{-3}$ |
| 308 | 0.0056 | $4.969 \cdot 10^{-4}$ | $2.270 \cdot 10^{-3}$ | 308 | 0.0023 | $4.956 \cdot 10^{-4}$ | $2.264 \cdot 10^{-3}$ |
| 313 | 0.0060 | $4.814 \cdot 10^{-4}$ | $2.199 \cdot 10^{-3}$ | 313 | 0.0028 | $5.064 \cdot 10^{-4}$ | $2.314 \cdot 10^{-3}$ |
| <i>Cineole</i> | | | | | | | |
| 283 | 0.0054 | $8.577 \cdot 10^{-4}$ | $3.918 \cdot 10^{-3}$ | 288 | 0.0077 | $8.907 \cdot 10^{-4}$ | $4.069 \cdot 10^{-3}$ |
| 288 | 0.0074 | $8.731 \cdot 10^{-4}$ | $3.989 \cdot 10^{-3}$ | 293 | 0.0083 | $9.317 \cdot 10^{-4}$ | $4.256 \cdot 10^{-3}$ |
| 293 | 0.0094 | $8.708 \cdot 10^{-4}$ | $3.978 \cdot 10^{-3}$ | 298 | 0.0088 | $8.908 \cdot 10^{-4}$ | $4.069 \cdot 10^{-3}$ |
| | | | | 308 | 0.0106 | $9.157 \cdot 10^{-4}$ | $4.183 \cdot 10^{-3}$ |
| <i>CPME</i> | | | | | | | |
| 293 | 0.0025 | $5.988 \cdot 10^{-4}$ | $2.736 \cdot 10^{-3}$ | 293 | 0.0042 | $6.105 \cdot 10^{-4}$ | $2.789 \cdot 10^{-3}$ |
| 298 | 0.0042 | $6.086 \cdot 10^{-4}$ | $2.780 \cdot 10^{-3}$ | 298 | 0.0047 | $6.130 \cdot 10^{-4}$ | $2.800 \cdot 10^{-3}$ |
| 303 | 0.0058 | $5.889 \cdot 10^{-4}$ | $2.690 \cdot 10^{-3}$ | 303 | 0.0054 | $6.097 \cdot 10^{-4}$ | $2.785 \cdot 10^{-3}$ |
| | | | | 308 | 0.0060 | $7.568 \cdot 10^{-4}$ | $3.457 \cdot 10^{-3}$ |
| | | | | 313 | 0.0067 | $6.268 \cdot 10^{-4}$ | $2.863 \cdot 10^{-3}$ |
| <i>2-MeTHF</i> | | | | | | | |
| 293 | 0.0169 | $5.421 \cdot 10^{-4}$ | $2.476 \cdot 10^{-3}$ | 283 | 0.0208 | $5.374 \cdot 10^{-4}$ | $2.455 \cdot 10^{-3}$ |
| 303 | 0.0265 | $5.407 \cdot 10^{-4}$ | $2.470 \cdot 10^{-3}$ | 298 | 0.0248 | $5.354 \cdot 10^{-4}$ | $2.446 \cdot 10^{-3}$ |
| 308 | 0.0331 | $5.458 \cdot 10^{-4}$ | $2.494 \cdot 10^{-3}$ | 303 | 0.0260 | $5.463 \cdot 10^{-4}$ | $2.496 \cdot 10^{-3}$ |
| 313 | 0.0439 | $5.712 \cdot 10^{-4}$ | $2.610 \cdot 10^{-3}$ | 308 | 0.0274 | $5.527 \cdot 10^{-4}$ | $2.525 \cdot 10^{-3}$ |
| | | | | 313 | 0.0290 | $5.443 \cdot 10^{-4}$ | $2.487 \cdot 10^{-3}$ |

* Standard uncertainty for temperature, $u(T) = 1 \text{ K}$.

** Combined expanded uncertainty of measurement (type B) estimated with a level of confidence of 95% of saturated organic acid mole fraction in water and bio-based solvents.

*** Statistical combined expanded uncertainty (type A) estimated with a level of confidence of 95% of saturated organic acid mole fraction in water and bio-based solvents.

Correlation relative deviations

Individual relative deviations percentages (Eq. B.11) of the empirical correlation used in this work are presented the Figure B.0.1 below.

$$\varepsilon_i = 100 \cdot (x_{1,i}^{exp} - x_{1,i}^{cal}) / x_{1,i}^{exp} \quad (\text{B.11})$$

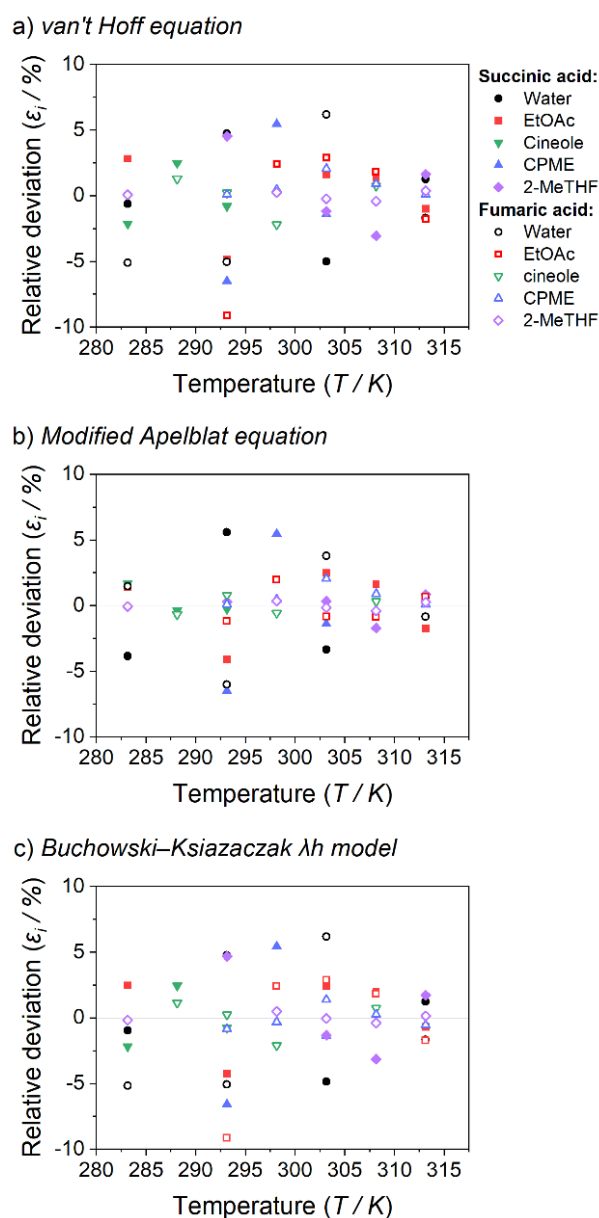


Figure B.0.1. Percentage of the individual relative deviation from a) van't Hoff equation (Eq. 4.3); b) Modified Apelblat equation (eq. 4.4); and c) Buchowski-Ksiazaczak λh model (Eq. 4.5) for experimental organic acid solubility in water and bio-based solvents. Filled symbols: succinic acid; empty symbols: fumaric acid.

Computed organic acid activity coefficients

Table B.0.4 summarizes the organic acid activity coefficients at the saturated solution condition, $\gamma_1 / \text{mol mol}^{-1}$, and at infinite dilution, $\gamma_1^\infty / \text{mol mol}^{-1}$, obtained from solid-liquid equilibria computed by COSMO-RS method within the experimental temperature range.

Table B.0.4. Organic acid activity coefficients at the saturated liquid condition obtained from SLE computed by the COSMO-RS method within the experimental temperature range.

| Succinic acid | | | Fumaric acid | | |
|----------------|-------------------------------------|--|---------------|-------------------------------------|--|
| <i>T</i> K | γ_1 mol mol ⁻¹ | γ_1^∞ mol mol ⁻¹ | <i>T</i> K | γ_1 mol mol ⁻¹ | γ_1^∞ mol mol ⁻¹ |
| <i>Water</i> | | | | | |
| 283 | 1.232 | 1.351 | 283 | 0.5770 | 0.5827 |
| 293 | 1.419 | 1.648 | 293 | 0.7676 | 0.7803 |
| 303 | 1.596 | 1.947 | 303 | 0.9814 | 1.009 |
| 313 | 1.672 | 2.236 | 313 | 1.214 | 1.263 |
| <i>EtOAc</i> | | | | | |
| 283 | 0.1969 | 0.1925 | 293 | 0.0238 | 0.0236 |
| 293 | 0.2657 | 0.2598 | 298 | 0.0296 | 0.0292 |
| 303 | 0.3472 | 0.3387 | 303 | 0.0363 | 0.0358 |
| 308 | 0.3919 | 0.3821 | 308 | 0.0442 | 0.0434 |
| 313 | 0.4386 | 0.4277 | 313 | 0.0533 | 0.0522 |
| <i>Cineole</i> | | | | | |
| 283 | 0.0114 | 0.0104 | 288 | 0.0005 | 0.0004 |
| 288 | 0.0272 | 0.0242 | 293 | 0.0009 | 0.0008 |
| 293 | 0.0413 | 0.0357 | 298 | 0.0015 | 0.0012 |
| | | | 308 | 0.0039 | 0.0032 |
| <i>CPME</i> | | | | | |
| 293 | 0.2251 | 0.2180 | 293 | 0.0104 | 0.0096 |
| 298 | 0.3003 | 0.2857 | 298 | 0.0152 | 0.0140 |
| 303 | 0.3927 | 0.3685 | 303 | 0.0219 | 0.0201 |
| | | | 308 | 0.0308 | 0.0282 |
| | | | 313 | 0.0427 | 0.0388 |
| <i>2-MeTHF</i> | | | | | |
| 293 | 0.0152 | 0.0117 | 283 | 0.0003 | 0.0002 |
| 303 | 0.0332 | 0.0228 | 298 | 0.0012 | 0.0008 |
| 308 | 0.0486 | 0.0312 | 303 | 0.0018 | 0.0012 |
| 313 | 0.0732 | 0.0419 | 308 | 0.0028 | 0.0018 |
| | | | 313 | 0.0041 | 0.0026 |

Saturated organic acid – bio-based solvent excess mixing energies

Table B.0.5 summarizes the excess mixing energies of saturated organic acid – bio-based solvent systems computed by COSMO-RS method at 293.15 K: excess Gibbs free energy (G^E / kJ mol⁻¹), excess enthalpy (H^E / kJ mol⁻¹), and excess entropy ($-TS^E$ / kJ mol⁻¹); electrostatic energy excess enthalpy contribution ($H^E(\text{MF})$ / kJ mol⁻¹), hydrogen bonding energy excess enthalpy contribution ($H^E(\text{HB})$ / kJ mol⁻¹), and van der Waals forces energy excess enthalpy contribution ($H^E(\text{vdW})$ / kJ mol⁻¹).

Table B.0.5. Excess mixing energies of saturated organic acid – bio-based solvent systems and excess enthalpy contributions: electrostatic energy (MF), hydrogen bonding (HB), and van der Waals forces (vdW), computed by COSMO-RS method at 293.15 K.

| Organic acid | Solvent | H^E kJ mol ⁻¹ | G^E kJ mol ⁻¹ | $-TS^E$ kJ mol ⁻¹ | $H^E(\text{MF})$ kJ mol ⁻¹ | $H^E(\text{HB})$ kJ mol ⁻¹ | $H^E(\text{vdW})$ kJ mol ⁻¹ |
|---------------|---------|-------------------------------|-------------------------------|---------------------------------|--|--|---|
| Succinic acid | Water | -0.1514 | 0.0125 | 0.1638 | -0.0223 | -0.1352 | -0.0046 |
| | EtOAc | -0.0758 | -0.0124 | 0.0634 | -0.0111 | -0.0586 | -0.0057 |
| | Cineole | -0.4208 | -0.0661 | 0.3548 | -0.0170 | -0.3910 | -0.0148 |
| | CPME | -0.0990 | -0.0092 | 0.0898 | 0.0005 | -0.0953 | -0.0051 |
| | 2-MetHF | -0.8401 | -0.1783 | 0.6619 | -0.0809 | -0.7333 | -0.0324 |
| Fumaric acid | Water | -0.0156 | -0.0005 | 0.0151 | -0.0016 | -0.0145 | 0.0002 |
| | EtOAc | -0.0314 | -0.0091 | 0.0222 | -0.0054 | -0.0244 | -0.0013 |
| | Cineole | -0.6125 | -0.1439 | 0.4686 | -0.0541 | -0.5452 | -0.0130 |
| | CPME | -0.2307 | -0.0471 | 0.1835 | -0.0152 | -0.2087 | -0.0072 |
| | 2-MetHF | -1.4982 | -0.4201 | 1.0781 | -0.1866 | -1.2772 | -0.0365 |

Energies of solution uncertainties estimation

The van't Hoff equation (Eq. B.1) can be expressed as a linear function $Y=f(X)$ as shown in Eq. B.12. In this way, the parameters can be obtained by the least-squares linear regression method of the N data points (X, Y) (141). The least-squares line intercept, p_1 , as well as slope, p_2 , are determined by the Eq. B.13 and Eq. B.14, respectively, where \bar{X} is average of $1/T$ data point the and \bar{Y} is the average of the $\ln(x_1)$ data points.

$$Y = p_1 + p_2 \cdot X \quad (\text{B.12})$$

$$p_1 = \bar{Y} - p_2 \cdot \bar{X} \quad (\text{B.13})$$

$$p_2 = \frac{\sum_i \{(X_i - \bar{X})(Y_i - \bar{Y})\}}{\sum_i (X_i - \bar{X})^2} \quad (\text{B.14})$$

The standard deviations of the intercept, s_{p1} , and the slope, s_{p2} , are obtained from Eq. B.15 and Eq. B.16, respectively. Both are based on the random errors in the y -direction, $s_{Y/X}$, which is calculated by Eq. B.17. Lastly, the expanded combined uncertainty of each parameter is estimated from the t -distribution with $N-2$ degree of freedom, as Eq. B.18 and Eq. B.19 shows.

$$s_{p_1} = \frac{s_{Y/X}}{\sqrt{\sum_i (X_i - \bar{X})^2}} \quad (\text{B.15})$$

$$s_{p_2} = s_{Y/X} \sqrt{\frac{\sum_i (X_i)^2}{N \cdot \sum_i (X_i - \bar{X})^2}} \quad (\text{B.16})$$

$$s_{Y/X} = \sqrt{\frac{\sum_i (Y_i - \bar{Y})^2}{N - 2}} \quad (\text{B.17})$$

$$U_{comb}(p_1) = s_{p_1} \cdot t_{(N-2)} \quad (\text{B.18})$$

$$U_{comb}(p_2) = s_{p_2} \cdot t_{(N-2)} \quad (\text{B.19})$$

Based on the linear regression of the van't Hoff equation parameters and their respective confidence bounds, the expanded combined uncertainties of the energies of the solution are determined from the [Eq. B.20](#) to [Eq. B.22](#).

$$U_{comb}(\Delta G_{soln}) = R \cdot T_{hm} \cdot U_{comb}(p_1) \quad (\text{B.20})$$

$$U_{comb}(\Delta H_{soln}) = R \cdot U_{comb}(p_2) \quad (\text{B.21})$$

$$U_{comb}(\Delta S_{soln}) = \frac{U_{comb}(\Delta G_{soln}) + U_{comb}(\Delta H_{soln})}{T_{hm}} \quad (\text{B.22})$$

Appendix C. SI: Green supported liquid membranes: the permeability activity-based linear operation (PABLO) method

Eutectic solvent (ES) preparation

DL-menthol : Octanoic acid {1:1} and Tetrabutylammonium chloride: Octanoic acid {1:2} eutectic solvents (ESs) were prepared by mixing the hydrogen bond acceptor (HBA) with the hydrogen bond donor (HBD) components in its specific {HBA:HBD} molar ratio. The mixture was stirred in a heating bath at 50 °C overnight until no solid was observed in the homogeneous liquid fluid. Chemicals were weighted in a Mettler Toledo MS1045/01 analytical scale, with a corresponding standard uncertainty of $u(\text{mass}) = 10^{-4}$ g. The relative errors on molar ratio were lower than 0.11%.

Supported liquid membranes (SLM) preparation and characterization

SLMs were prepared by impregnation. The polymeric support membrane was submerged in 5 ml of solvent in a petri dish and left overnight to allow the solvent penetration through the membrane pores.

SLM impregnation ratio, $\varepsilon = V_{\text{solvent}}/V_{\text{SML}}$ (%) was determined according to the following procedure: Support samples of about 1 x 1 cm were submerged on the green solvent and left overnight at room temperature. The dry W_{dry} (g) and wet W_{wet} (g) SLM were weighted in a Mettler Toledo MS1045/01 analytical scale, with a corresponding standard uncertainty of $u(W) = 10^{-4}$ g. Finally, the impregnation ratio is determined by [Eq. C.1](#), based on the solvent and support densities. Measurements were made in triplicate.

$$\varepsilon = \frac{\frac{W_{wet} - W_{dry}}{\rho_{Solvent}}}{\frac{W_{wet} - W_{dry}}{\rho_{Solvent}} + \frac{W_{dry}}{\rho_{Support}}} \cdot 100\% \quad (C.1)$$

Green-SLM stability was assessed following a gravimetric method. Membrane samples of about 1 x 1 cm were submerged in the green solvent for 1 hour at room temperature. The dry, W_{dry} (g), and wet, W_{wet} (g), membrane were weighted in a Mettler Toledo MS1045/01 analytical scale, with a corresponding standard uncertainty of $u(W) = 10^{-4}$ g. The stability of the SLM is defined as the solvent mass, $W_{s,j}$ (g) remaining in the membrane, according to Eq. C.2. Green-SML samples were weighted and submerged in pure water (Milli-Q type I) in a plastic vial. Vials were placed in a Labnet Accublock dry bath at 25 °C. Independent stability experiments were performed in triplicate for 24, 48, and 96 hours to avoid solvent losses between measurements.

$$SLM \text{ stability} = \left(1 - \frac{W_{s,o} - W_{s,j}}{W_{s,o}} \right) \cdot 100\% \quad (C.2)$$

Stability results are presented in Figure C.0.1. The measurements have an average standard deviation of 2.7%. High liquid membrane stability is observed for DL-Menthol:OctA, N_{4444} :OctA, and eucalyptol, which are maintained above 93.9%, 90.3%, and 97.2%, respectively. For the IL-based SLM case, lower stability is observed with fast solvent losses within the first 24 hours. Nevertheless, the $[C_4pyrr][Tf_2N]$ -SLM stability is relatively maintained at 63.1%, with minor losses.

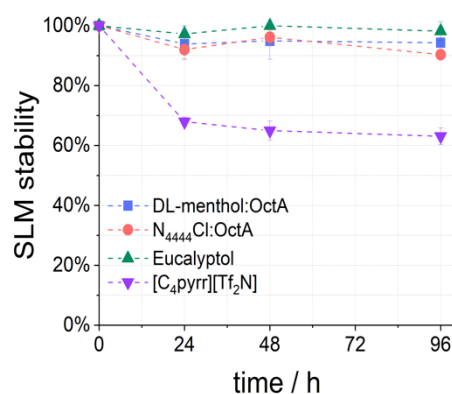


Figure C.0.1. Green-SLM stability in pure water test at 25 °C.

Solute activity coefficients fitting algorithm

In order to correct the activity coefficient computed by the COSMO-RS method, Eq. C.3, the following procedure has been proposed. To solve the system mass balances coupled with the activity-based model, Eq. C.4, the experimental data were treated as k dataset of j data-point number.

$$RT\ln(\gamma_i^a) = \mu_i^a - \mu_i \quad (\text{C.3})$$

$$\frac{P \cdot A}{V^S} \cdot (t - t^{st}) = \frac{1}{V^S} \int_0^{c^S} \frac{dn^S}{\left(\frac{n^{F_{t=0}} - n^S}{V^F} \cdot \gamma^F - \frac{n^S}{V^S} \cdot \gamma^S\right)} = \psi \quad (\text{C.4})$$

Given γ_i^p values for a set of k systems $[C_j, t_j]_k$ and assuming no permeability variation in time, Eq. C.4, might be linearized in the form of $Y = Xb_k + a_k$, where $Y = \psi_k$ and $X = t_k$. From the regression slope, b_k : Eq. C.5, and intercept, a_k : Eq. C.6, the permeability and mass transfer steady-time are determined through Eq. C.7, and Eq. C.8, respectively.

$$b_k = \frac{\sum_i \{(t_{j,k} - \bar{t}_k) \cdot (\psi_{j,k} - \bar{\psi}_k)\}}{\sum_i \{(t_{j,k} - \bar{t}_k)^2\}} \quad (\text{C.5})$$

$$a_k = \bar{\psi}_k - \bar{t}_k \cdot b_k \quad (\text{C.6})$$

$$P_k = \frac{b_k \cdot V^S}{A} \quad (\text{C.7})$$

$$t_k^{ss} = -\frac{a_k}{b_k} = -\frac{\bar{\psi}_k - b_k \cdot \bar{t}_k}{b_k} \quad (\text{C.8})$$

As the parameter $\bar{\psi}_k$ is dependent on the solute activity coefficients, i.e., $\bar{\psi}_k = \bar{\psi}_k(\gamma_F, \gamma_S)$, both values were fitted aiming to meet the linear regression as well as the system mass balance. As the algorithm's constraint, the Pearson correlation coefficient, was set as $r_k^2 > 0.970$. Figure C.0.2 shows an example of the regression output after the activity coefficient fitting to the experimental data.

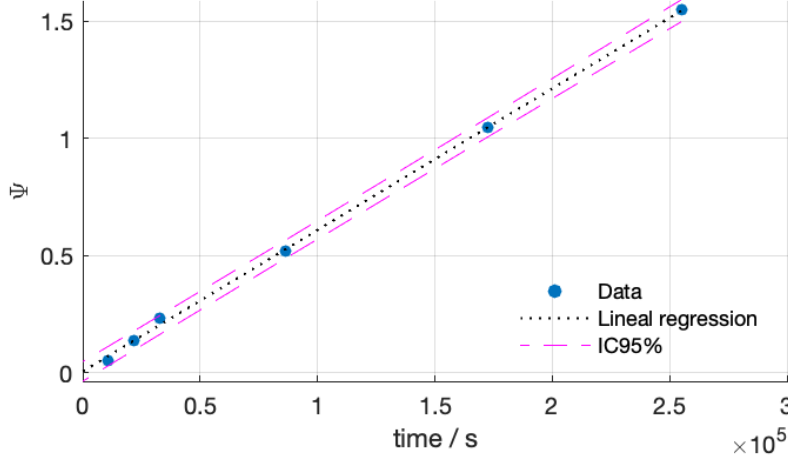


Figure C.0.2. Succinic acid permeability regression of ψ -values of mass balance integration of the extraction with DL-menthol:OctA in PVDF SLM and 0.1 M NaOH stripping solution. $r^2=1$.

The procedure was performed for all k-datasets following the routine depicted in Figure C.0.3. The parameter optimization uses two objective functions (OF): First, the inverse of the sum of each k-dataset Pearson correlation coefficient, according to Eq. C.9, to fulfil the linearity of the system established above; the second objective function, Eq. C.10, ensures the resulted model predictions root square mean deviation, Eq. C.11, are less than the root square mean data uncertainty, Eq. C.12.

$$OF_1: \min \frac{1}{\sum_k r_k^2} = \min \left[\sum_k \left\{ \left(\frac{\sum_i \{(t_{i,k} - \bar{t}_k) \cdot (\psi_{i,k} - \bar{\psi}_k)\}}{\sqrt{\sum_i \{(t_{i,k} - \bar{t}_k)^2\} \cdot \sum_i \{(\psi_{i,k} - \bar{\psi}_k)^2\}}} \right)^2 \right\} \right]^{-1} \quad (C.9)$$

$$OF_2: RSMD_{Fitted} < RSMD_{Exp}. \quad (C.10)$$

$$RSMD_{exp} = \sqrt{\frac{1}{N} \cdot \sum_j \{(\delta C_j)^2\}} = \sqrt{\frac{1}{N} \cdot \sum_j \{(U_{95\%}(C)_j)^2\}} \quad (C.11)$$

$$RSMD_{Fitted} = \sqrt{\frac{1}{N} \cdot \sum_j \{(C_j - \hat{C}_j)^2\}} \quad (C.12)$$

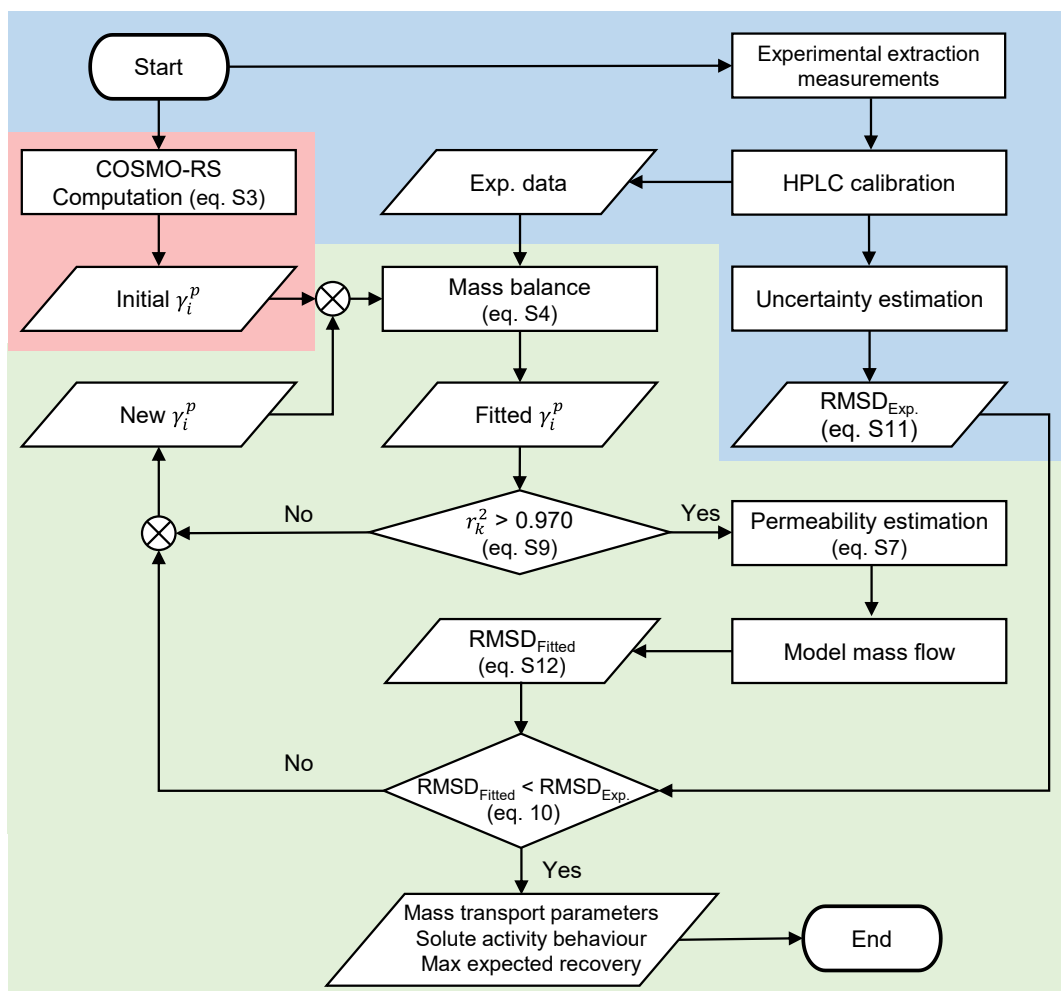


Figure C.0.3. The algorithm developed for the solute activity coefficients fitting to the experimental green-SLM extractions data. In blue, experimental measurement stage; in red, COSMO-RS activity computation stage; in green, MatLab fitting routine stage.

pH effect on the organic acids' activity coefficient

Since the organic acid mass transfer is controlled by the activity gradients between the feed and stripping phases, the recovery might be enhanced by fixing appropriated affinities conditions. In order to understand the effect of the pH in the activity coefficient of several organic acids, such values were computed through the COSMO-RS method at 20 °C. Results are depicted in [Figure C.0.4](#). The solvents were defined as a model mixture of organic acids, water, and pH modifier. Low pH mixtures were modelled as an HCl solution, while high pH as a NaOH solution. No difference was found when using other compounds, such as phosphate buffer solution, to adjust the pH.

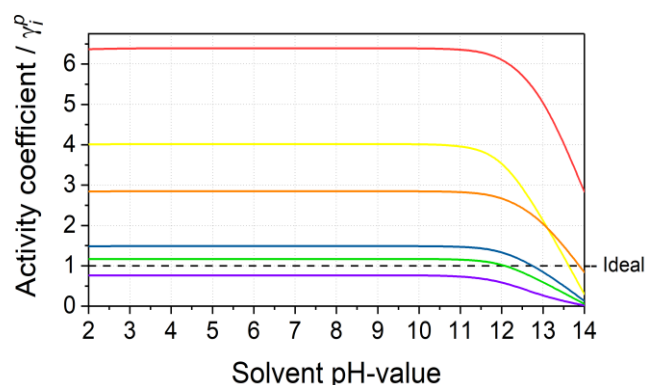


Figure C.0.4. Estimated activity coefficients of different bio-based organic acid in function on the aqueous phase pH-value before mixing for succinic acid (in blue), levulinic acid (in red), fumaric acid (in purple), malic acid (in green), itaconic acid (in yellow), and lactic acid (in orange), computed by COSMO-RS at 20 °C. The model solution is composed of the organic acid at 50 g l^{-1} for all solutes except fumaric acid, with a concentration of 5 g l^{-1} .

Modelled results show a significant effect of the aqueous solvent only at pH-values over 12. Therefore, no effect is expected employing a pH-modifier to reduce the pH-value in the feed phase. Nevertheless, is important to note that to reach high pH values, a concentrated solution of the pH-modifier is needed. This is translated into a greater osmotic pressure, which may increase the solute mass transfer resistance, reducing the overall performance. In this work, a solution of 0.1 M of NaOH was used as the stripping phase, pH = 13, while pure water was used to constitute the model feed solution.

Experimental succinic acid extraction with green-SLM data

Figure C.0.5 summarizes the experimental results for the extraction of succinic acid from a model feed solution of $40 - 50 \text{ g l}^{-1}$ with the studied green-SLM and three stripping solutions. A significant improvement is observed for the activity-based model fitting to the experimental data. The COSMO-RS model (the activity-based model using the coefficients without correction) shows a greater overestimation, while the ideal approach only allows predicting an intermediary concentration.

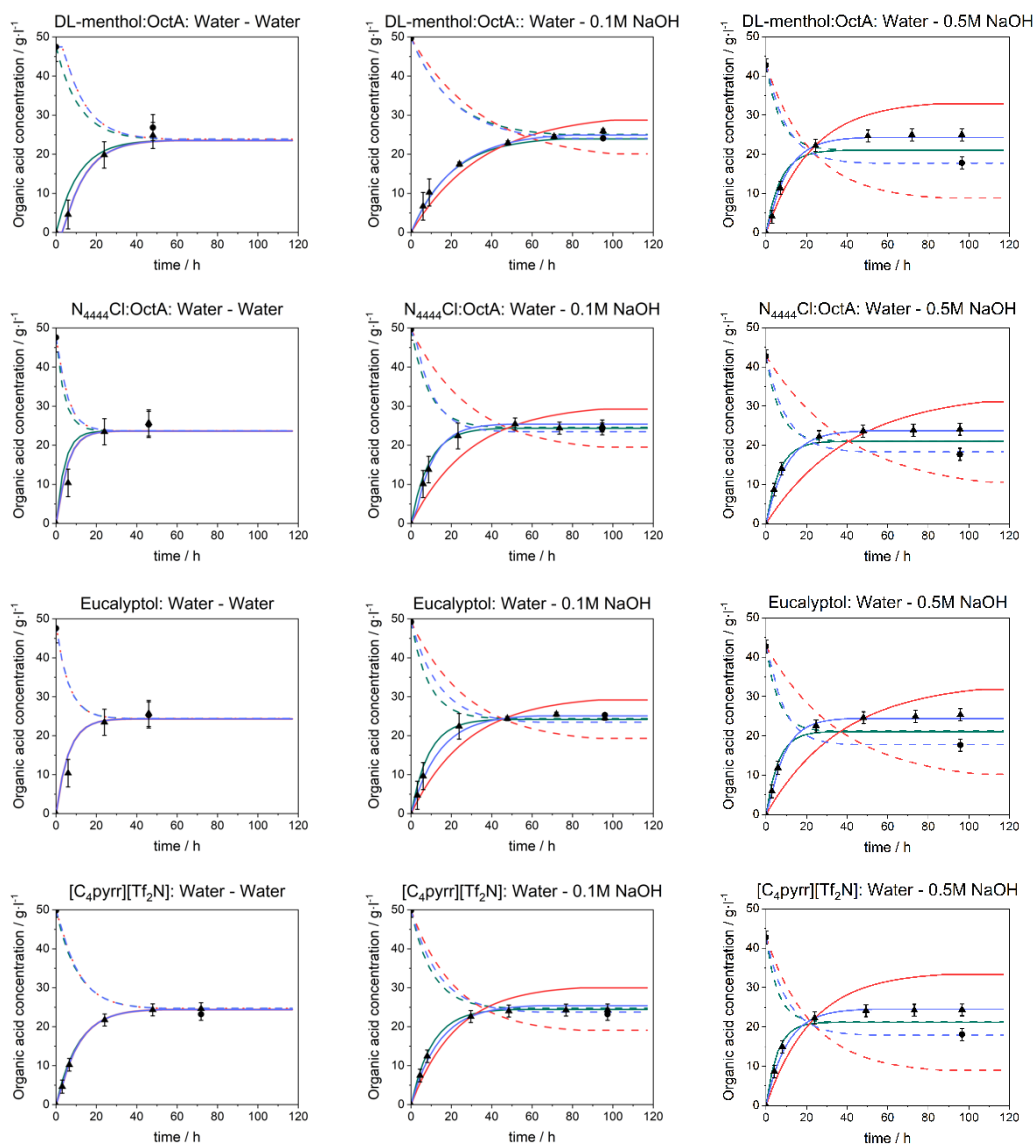


Figure C.0.5. Experimental concentrations (●, feed; ▲, stripping), ideal model prediction (---, feed; —, stripping), COSMO-RS model prediction (---, feed; —, stripping), and fitted permeability activity-based model (— · —, feed; — · —, stripping), concentration profiles for succinic acid extraction with the green-SLM studied in this work using three different alkaline stripping solutions: pure water; 0.1 M NaOH; 0.5 M NaOH. The same behaviour is observed for all systems.

Activity gradient logarithmic mean derivation

To provide a mass transfer area estimation method for the SLM extraction stages, the driven force, i.e., the activity gradient between both phases, Δa_m (mol m⁻³), was defined as the activity gradient logarithmic mean derivation. If parallel streams to the SLM surface are assumed, the Δa_m dependence along the membrane length (z -axis) is illustrated in Figure C.0.6.I.

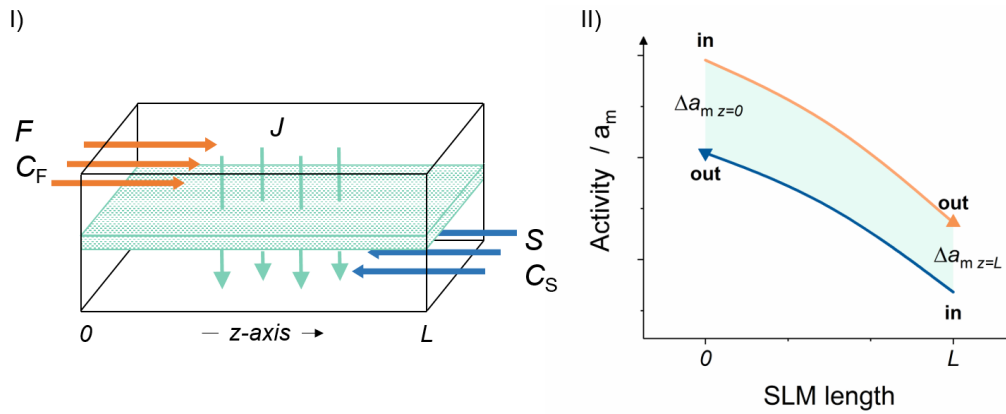


Figure C.0.6. I) Schematic countercurrent green-SLM extraction process. II) Solute activity profile along a countercurrent green-SLM extraction process. (→) Feed stream; (←) Stripping stream; (↔) Transmembrane solute flow.

The solute i mass balance of each α -stream (m³ s⁻¹), feed (F) or stripping (S), is given by the solute concentration, C_i^α (mol _{i} m⁻³), change along the extraction process. The total given/received solute for each stream, q_i^α (mol _{i} s⁻¹), is expressed by Eq. C.13. Assuming the activity coefficients, γ^F and γ^S , as constants within the concentration range, each stream mass balance can be rearranged as the Eq. C.14 and Eq. C.15.

$$q_i^\alpha = \alpha (C_i^{\alpha_{z=0}} - C_i^{\alpha_{z=L}}) \quad (\text{C.13})$$

$$q_i^F = \frac{F}{\gamma^F} (\gamma^F C_i^{F_{z=0}} - \gamma^F C_i^{F_{z=L}}) = \frac{F}{\gamma^F} (a_m^{F_{z=0}} - a_m^{F_{z=L}}) \quad (\text{C.14})$$

$$q_i^S = \frac{S}{\gamma^S} (\gamma^S C_i^{S_{z=0}} - \gamma^S C_i^{S_{z=L}}) = \frac{S}{\gamma^S} (a_m^{S_{z=0}} - a_m^{S_{z=L}}) \quad (\text{C.15})$$

Keeping the left to right z-axis direction as a reference and assuming a negligible solute accumulation within the membrane phase, the mass transported, q_i ($\text{mol}_i \text{ s}^{-1}$), expressed as the membrane flux, J_i ($\text{mol}_i \text{ m}^{-2} \cdot \text{s}^{-1}$), in an area differential, dA (m^2), results in the Eq. C.16. Here both da_m^F and da_m^S are negatives due to the solute activity reduction along the z-axis in both phases, as Figure C.0.6.II depicts.

$$q_i = J_i \cdot dA = -\frac{F}{\gamma^F} da_m^F = -\frac{S}{\gamma^S} da_m^S \quad (\text{C.16})$$

The Eq. C.14 and Eq. C.15 can be rearranged as the Eq. C.17 and Eq. C.18, respectively. If the above equations are coupled to form the Δa_m differential, Eq. C.19, the $d(\Delta a_m)$ factor can be expressed as a function of the stream's flow and activity coefficients, membrane flux, and area differential, according to Eq. C.20.

$$d(\gamma^F C_i^F) = -\frac{\gamma^F}{F} J_i dA \quad (\text{C.17})$$

$$d(\gamma^S C_i^S) = -\frac{\gamma^S}{S} J_i dA \quad (\text{C.18})$$

$$d(\gamma^F C_i^F - \gamma^S C_i^S) = d(\Delta a_m) \quad (\text{C.19})$$

$$d(\Delta a_m) = -\left(\frac{\gamma^F}{F} - \frac{\gamma^S}{S}\right) J_i dA \quad (\text{C.20})$$

In this model, the activity differential is given only in the membrane length (z-axis). Thus, the membrane section results in $dA=ydz$, where y denotes the membrane width. Applying the Eq. C.20 into the new permeability, P ($\text{m}^2 \text{ s}^{-1}$), activity-based approach proposed in this work, Eq. C.21, the activity gradient differential results in Eq. C.22.

$$J_i = P \Delta a_m \quad (\text{C.21})$$

$$d(\Delta a_m) = -\left(\frac{\gamma^F}{F} - \frac{\gamma^S}{S}\right) P \Delta a_m \cdot y dz \quad (\text{C.22})$$

Reordering Eq. C.22 and integrating $d(\Delta a_m)$ within the membrane length boundaries, from $z=0$ to $z=L$, as displayed in Eq. C.23 is possible to obtain an analytical solution, as shown in Eq. C.24.

$$\int_{z=0}^{z=L} \frac{d(\Delta a_m)}{\Delta a_m} = - \left(\frac{\gamma^F}{F} - \frac{\gamma^S}{S} \right) P \cdot \int_{z=0}^{z=L} y dz \quad (\text{C.23})$$

$$\ln \left[\frac{a_m^{F_{in}(z=0)} - a_m^{S_{out}(z=0)}}{a_m^{F_{out}(z=0)} - a_m^{S_{in}(z=L)}} \right] = \left(\frac{\gamma^F}{F} - \frac{\gamma^S}{S} \right) P \cdot A \quad (\text{C.24})$$

From Eq. C.16, the total solute transported, q_{total} ($\text{mol}_i \cdot \text{s}^{-1}$), from and towards the phases are given by Eq. C.25 and Eq. C.26, respectively. Subtracting Eq. C.26 from Eq. C.25 is possible to solve the flow rates/activity coefficients component, according to Eq. C.27.

$$a_m^{F_{in}(z=0)} - a_m^{F_{out}(z=L)} = \frac{q_{total}}{F/\gamma^F} \quad (\text{C.25})$$

$$a_m^{S_{out}(z=0)} - a_m^{S_{in}(z=L)} = \frac{q_{total}}{S/\gamma^S} \quad (\text{C.26})$$

$$\left(\frac{\gamma^F}{F} - \frac{\gamma^S}{S} \right) = \frac{\left(a_m^{F_{in}(z=0)} - a_m^{S_{out}(z=0)} \right) - \left(a_m^{F_{out}(z=L)} - a_m^{S_{in}(z=L)} \right)}{q_{total}} \quad (\text{C.27})$$

Them, replacing this last equation into the Eq. C.24, the total solute transported throughout the membrane is given as a function of only the in and out streams conditions, as Eq. C.24 shows.

$$q_{total} = P \cdot A \cdot \frac{\left(a_m^{F_{in}(z=0)} - a_m^{S_{out}(z=0)} \right) - \left(a_m^{F_{out}(z=L)} - a_m^{S_{in}(z=L)} \right)}{\ln \left[\frac{a_m^{F_{in}(z=0)} - a_m^{S_{out}(z=0)}}{a_m^{F_{out}(z=0)} - a_m^{S_{in}(z=L)}} \right]} \quad (\text{C.28})$$

Therefore, defining the solute mass transfers driven force as the activity gradient logarithmic mean derivation, $\Delta a_{m LM}$ ($\text{mol}_i \text{ m}^{-3}$), according to Eq. C.29, the permeability activity-based model can be simplified as the Eq. C.30.

$$\Delta a_{m LM} = \frac{\left(a_m^{F_{in}(z=0)} - a_m^{S_{out}(z=0)} \right) - \left(a_m^{F_{out}(z=L)} - a_m^{S_{in}(z=L)} \right)}{\ln \left[\frac{a_m^{F_{in}(z=0)} - a_m^{S_{out}(z=0)}}{a_m^{F_{out}(z=L)} - a_m^{S_{in}(z=L)}} \right]} \quad (\text{C.29})$$

$$q_{total} = P \cdot A \cdot \Delta a_{m LM} \quad (\text{C.30})$$

'End page'